Study on α-Glucosidase Inhibitors from *Solanum stramonifolium* Jacq.

Inflorescence and *Neuropeltis racemosa* Wall. Stem

Oraphan Sakulkeo

A Thesis Submitted in Fulfillment of the Requirements for the

Degree of Doctor of Philosophy in Pharmaceutical Sciences

Prince of Songkla University

2022

Study on α-Glucosidase Inhibitors from *Solanum stramonifolium* Jacq. Inflorescence and *Neuropeltis racemosa* Wall. Stem

Oraphan Sakulkeo

A Thesis Submitted in Fulfillment of the Requirements for the Degree of Doctor of Philosophy in Pharmaceutical Sciences Prince of Songkla University 2022

Thesis Title   Study on α-Glucosidase Inhibitors from *Solanum stramonifolium* Jacq. Inflorescence and *Neuropeltis racemosa* Wall. Stem

Author   Miss Oraphan Sakulkeo

Major Program   Pharmaceutical Sciences

Major Advisor

…………………………………

(Asst. Prof. Dr. Sukanya Dej-adisai)

Examining Committee:

………..………..………......Chairperson

(Assoc. Prof. Dr. Kornkanok Ingkaninan)

………………………..……......Committee

(Asst. Prof. Dr. Sukanya Dej-adisai)

Co-advisor

…………………………………

(Asst. Prof. Dr. Chatchai Wattanapiromsakul)

………………….…………......Committee

(Asst. Prof. Dr. Chatchai Wattanapiromsakul)

…………………………………

(Assoc. Prof. Dr. Sanan Subhadhirasakul)

………………….…………......Committee

(Assoc. Prof. Dr. Supinya Tewtrakul)

………………….…………......Committee

(Asst. Prof. Dr. Wandee Udomuksorn)

The Graduate School, Prince of Songkla University, has approved this thesis as fulfillment of the requirements for the Doctor of Philosophy Degree in Pharmaceutical Sciences.

…………………………......................

(Asst. Prof. Dr. Thakerng Wongsirichot)

Acting Dean of Graduate School

This is to certify that the work here submitted is the result of the candidate's own investigations. Due acknowledgement has been made of any assistance received.

………………………….............Signature

(Asst. Prof. Dr. Sukanya Dej-adisai)

Major Advisor

………………………….............Signature

(Asst. Prof. Dr. Chatchai Wattanapiromsakul)

Co-advisor

………………………….............Signature

(Assoc. Prof. Dr. Sanan Subhadhirasakul)

Co-advisor

………………………….............Signature

(Miss Oraphan Sakulkeo)

Candidate

I hereby certify that this work has not been accepted in substance for any degree and is not being currently submitted in candidature for any degree.

…………………………..............Signature

(Miss Oraphan Sakulkeo)

Candidate

ชื่อวิทยานิพนธ์	การศึกษาสารที่มีฤทธิ์ยับยั้งเอนไซม์แอลฟา-กลูโคซิเดสของช่อดอกมะอึก (*Solanum stramonifolium* Jacq.) และลำต้นแส้ม้าทะลาย (*Neuropeltis racemosa* Wall.)
ผู้เขียน	นางสาวอรพรรณ สกุลแก้ว
สาขาวิชา	เภสัชศาสตร์
ปีการศึกษา	2565

บทคัดย่อ

งานวิจัยนี้เป็นงานวิจัยชิ้นแรกที่ศึกษาพฤกษเคมีและฤทธิ์ต้านเบาหวาน ของพืชสมุนไพร 2 ชนิด ซึ่งจัดอยู่ในลำดับ (order) เดียวกันในอนุกรมวิธาน คือ Solanales พืชดังกล่าวได้แก่ช่อดอกมะอึก (*Solanum stramonifolium* Jacq.) และลำต้นแส้ม้าทะลาย (*Neuropeltis racemosa* Wall.) จากการทดสอบฤทธิ์ยับยั้งเอนไซม์แอลฟา-กลูโคซิเดสในสารสกัดพบว่า สารสกัดชั้นเอทธิลอะซีเตทของช่อดอกมะอึก (SSEA) และสารสกัดชั้นเอทานอลของลำต้นแส้ม้าทะลาย (NREO) มีฤทธิ์ยับยั้งเอนไซม์ดีกว่าสารสกัดชั้นอื่น โดยมีค่า IC_{50} เท่ากับ 215.92 µg/ml และ 39.65 µg/ml ตามลำดับ สารสกัดทั้งสองแสดงกลไกการยับยั้งเอนไซม์แบบ mixed-type และจากการศึกษาฤทธิ์ยับยั้งเอนไซม์แอลฟา-กลูโคซิเดสเมื่อใช้สารสกัดร่วมกับสารมาตรฐาน acarbose พบว่าสารสกัด SSEA และ NREO ส่งเสริมฤทธิ์ของ acarbose ในการการยับยั้งเอนไซม์แอลฟา-กลูโคซิเดส

การแยกสกัดสาร โดยใช้ฤทธิ์ยับยั้งเอนไซม์แอลฟา-กลูโคซิเดสชี้นำการแยก พบว่าได้สารบริสุทธิ์ 10 ชนิดและสารผสม 1 ชนิด โดยสารบริสุทธิ์ 5 ชนิดและสารผสม 1 ชนิด แยกได้จากช่อดอกมะอึกเป็นสารกลุ่มฟลาโวนอยด์ คือ myricetin 3, 4′, 5′, 7-tetramethyl ether (SS1), combretol (SS2), kaempferol (SS3), kaempferol-7-*O*-β-glucopyranoside (SS4), 5-hydroxy-3,7,4′,5′ -tetramethoxyflavone-3′-*O*-glucopyranoside (SS5) และสารผสม SS6 ระหว่าง isorhamnetin-3-*O*-glucopyranoside (SS6-1) กับ kaempferol-3-*O*-glucopyranoside (SS6-2) นอกจากนี้เป็นสารบริสุทธิ์ 5 ชนิดจากลำต้นแส้ม้าทะลาย คือ scopoletin (NR1), syringic acid (NR2), methyl 3-methyl-2-butenonoate (NR3), *trans-N*-feruloyltyramine (NR4) และ *trans-N*-coumaroyltyramine (NR5) จากการตรวจสอบพบว่าสารบริสุทธิ์ SS5 เป็นสารที่ยังไม่พบการรายงานมาก่อน

เนื่องจากสารกลุ่มฟลาโวนอยด์จากช่อดอกมะอึกแยกได้ปริมาณน้อย ดังนั้นฤทธิ์ยับยั้งเอนไซม์แอลฟา-กลูโคซิเดสจึงรายงานในรูปแบบร้อยละของความสามารถในการยับยั้ง ส่วนการศึกษากลไกและฤทธิ์ยับยั้งเอนไซม์เมื่อใช้ร่วมกับ acarbose จะใช้สารมาตรฐาน kaempferol และ

สารมาตรฐาน kaempferol-3-*O*-glucopyranoside (astragalin) เป็นตัวแทนในการศึกษา ซึ่งทั้งสาร kaempferol และ astragalin แสดงกลไกการยับยั้งเอนไซม์แอลฟา-กลูโคซิเดสแบบ mixed-type และ พบว่าฤทธิ์ยับยั้งเอนไซม์แอลฟา-กลูโคซิเดสของ acarbose ลดลงเมื่อใช้ร่วมกับ kaempferol หรือ astragalin สำหรับการศึกษาฤทธิ์ยับยั้งเอนไซม์ดังกล่าวของสารจากลำต้นแส้ม้าทะลาย พบว่าสาร NR1, NR2, NR3, NR4 และ NR5 มีค่า IC_{50} เท่ากับ 577.46, >2,523.09, >4,380.59, 95.34 และ 3.25 μM ตามลำดับ ขณะที่ acarbose มีค่า IC_{50} เท่ากับ 424.40 μM โดยสาร NR1 แสดงกลไกการยับยั้ง เอนไซม์แอลฟา-กลูโคซิเดสแบบ mixed-type ส่วนสาร NR4 และ NR5 แสดงกลไกการยับยั้งแบบ uncompetitive ซึ่งมีค่าคงที่การยับยั้ง (Ki′) เท่ากับ 51.81 และ 1.99 μM ตามลำดับ

       นอกจากนี้ในงานวิจัยใช้การจำลองการจับกันระหว่างโมเลกุล (molecular docking) แสดงรูปแบบการยับยั้งเอนไซม์แอลฟา-กลูโคซิเดสของสารที่แยกสกัดได้จากช่อดอก มะอึก พบว่าสารฟลาโวนอยด์ชนิดที่ไม่มีการเกาะของน้ำตาลในโมเลกุล (SS2 และ SS3) มีค่า พลังงานการจับ (binding energy) น้อยกว่าสารอนุพันธ์ของฟลาโวนอยด์ชนิดนั้นที่มีการเกาะของ น้ำตาลในโมเลกุล (SS4, SS5 และ SS6-2) เมื่อเปรียบเทียบค่า binding energy ระหว่าง SS2 กับ SS5 มีค่าเท่ากับ -3.53 และ 63.78 Kcal/mol ตามลำดับ และเมื่อเปรียบเทียบค่า binding energy ระหว่าง SS3 กับ SS4 และ SS6-2 มีค่าเท่ากับ -3.02, -1.29 และ 55.47 Kcal/mol ตามลำดับ ดังนั้นสาร ฟลาโวนอยด์ชนิดที่ไม่มีการเกาะของน้ำตาลในโมเลกุลมีแนวโน้มสามารถยับยั้งเอนไซม์แอลฟา-กลูโคซิเดสได้ดีกว่าสารอนุพันธ์ของฟลาโวนอยด์ชนิดนั้นที่มีการเกาะของน้ำตาล สำหรับสารที่แยก ได้จากลำต้นแส้ม้าทะลายพบว่าสารเอไมด์ชนิดอนุพันธ์ไทรามีน (tyramine-derived amide) คือ สาร NR4 และ NR5 มีค่า binding energy เท่ากับ -5.42 และ -5.15 Kcal/mol ตามลำดับ มีศักยภาพใน การยับยั้งแอลฟา-กลูโคซิเดสได้ดี จากผลการศึกษานี้ทำให้สามารถเชื่อมโยงพฤติกรรมการยับยั้ง เอนไซม์แอลฟา-กลูโคซิเดส ระหว่างผลการศึกษาในห้องปฏิบัติการและการประเมินผ่าน คอมพิวเตอร์ได้ว่ามีความสอดคล้องกัน ซึ่งข้อมูลนี้จะเป็นประโยชน์ในการค้นหาสารออกฤทธิ์ ต่อไปในอนาคต

Thesis Title Study on α-Glucosidase Inhibitors from *Solanum stramonifolium* Jacq. Inflorescence and *Neuropeltis racemosa* Wall. Stem

Author Miss Oraphan Sakulkeo

Major Program Pharmaceutical Sciences

Academic Year 2022

ABSTRACT

This research was the first report, which studied on the phytochemical investigation and potential anti-diabetic effect of two plants from order Solanales, *Solanum stramonifolium* Jacq. inflorescence and *Neuropeltis racemosa* Wall. stem. The plant extracts were evaluated the α-glucosidase inhibitory activity. The ethyl acetate extract of *S. stramonifolium* (SSEA) inflorescence and the ethanol extract of *N. racemosa* (NREO) stem showed better inhibitory activity than other solvent extracts with IC_{50} 215.92 and 39.65 μg/ml, respectively. Both of these extracts performed mixed-type inhibition. The combination study of extracts with acarbose standard suggested that SSEA and NREO extracts promoted the activity of acarbose to inhibit the α-glucosidase enzyme.

The isolation used the α-glucosidase inhibitory activity guided fractionation. Ten compounds and one mixture compound were obtained. The five compounds and a mixture compound from *S. stramonifolium* were identified as flavonoid compounds that were myricetin 3, 4′, 5′, 7-tetramethyl ether (SS1), combretol (SS2), kaempferol (SS3), kaempferol-7-*O*-β-glucopyranoside (SS4), 5-hydroxy-3, 7, 4′, 5′-tetramethoxyflavone-3′-*O*-glucopyranoside (SS5), and a mixture (SS6) of isorhamnetin-3-*O*-glucopyranoside (SS6-1) and kaempferol-3-*O*-glucopyranoside (SS6-2). Other five compounds from *N. racemosa* were defined as scopoletin (NR1), syringic acid (NR2), methyl 3-methyl-2-butenonoate (NR3), *trans-N*-feruloyltyramine (NR4) and *trans-N*-coumaroyltyramine (NR5). From previous survey, the compound of SS5 has not been reported before.

The isolated flavonoid compounds of *S. stramonifolium* were obtained small amount. So, they were preformed the α-glucosidase inhibitory activity as the percent

of inhibition. Kaempferol and kaempferol-3-*O*-glucopyranoside (astragalin) were used as the representative compounds for the study on mechanism of action and enzyme inhibition of the combination with acarbose. Both of kaempferol and astragalin performed mixed-type inhibition with α-glucosidase. Additionally, α-glucosidase inhibitory acitvity of acarbose was decreased when combined with kaempferol or astragalin. The compound NR1, NR2, NR3, NR4 and NR5 of *N. racemosa* showed α-glucosidase inhibitory acitvity with IC_{50} as 577.46, >2,523.09, >4,380.59, 95.34 and 3.25 μM, respectively, whereas the acarbose presented IC_{50} as 424.40 μM. The mechanism of action analysis exhibited that NR1 displayed mixed-type inhibition manner, while NR4 and NR5 exhibited uncompetitive inhibition manner with Ki′ 51.81 and 1.99 μM, respectively.

Moreover, the molecular docking study provided the understanding to α-glucosidase inhibition of isolated compounds. For the flavonoid compounds from *S. stramonifolium*, the non-glycosylated flavonoids (SS2 and SS3) showed lower binding energy than their glycosylated flavonoid derivatives (SS4, SS5 and SS6-2). The binding energy of SS2 showed -3.53 Kcal/mol, while SS5 was 63.78 Kcal/mol. SS3 exhibited the binding energy as -3.02 Kcal/mol, while SS4 and SS6-2 were -1.29 and 55.47 Kcal/mol, respectively. So, non-glycosylated flavonoids exhibited better α-glucosidase inhibitory activity than glycosylated flavonoid derivatives. For the isolated tyramine-derived amides from *N. racemosa*, the binding energy of NR4 and NR5 were -5.42 and -5.15 Kcal/mol, respectively. Both of NR4 and NR5 demonstraded the potential to α-glucosidase inhibition. Fortunately, these findings could be used to relate the accordance between the laboratory and the computer experiments. These results will be the beneficial informations for the furture drug discovery.

ACKNOWLEDGEMENTS

CONTENTS

CONTENTS (continued)

CONTENTS (continued)

CONTENTS (continued)

LIST OF TABLES

LIST OF TABLES (continued)

LIST OF TABLES (continued)

LIST OF TABLES (continued)

LIST OF FIGURES

LIST OF FIGURES (continued)

LIST OF FIGURES (continued)

LIST OF SCHEMES

LIST OF ABBREVIATIONS

Å	Angstrom
br	broad
°C	degree Celsius
COSY	correlation spectroscopy
d	doublet
dd	doublet of doublet
HMBC	heteronuclear multiple bond correlation
HMQC	heteronuclear multiple quantum coherence
HRESIMS	high resolution electrospray ionisation mass spectrometry
IC_{50}	inhibition concentration at 50 percentage
J	coupling constant
Kcal/mol	kilocalorie per mole
K_m	Michaelis-Menten constant
K_i	inhibition constant
m	multiplet
ml	milliliter
mg	milligram
MIC	minimum inhibitory concentration
m/z	mass-over-charge ratio
nm	nanometer
NOESY	nuclear overhauser effect spectroscopy
p	para
q	quartet
s	singlet
t	triplet
α	alpha
β	beta

δ	chemical shift
γ	gamma
λ	lambda
%	percentage
μg	microgram
μl	microliter
μM	micromolar

CHAPTER 1

INTRODUCTION

1.1 Background and rationales

Diabetes mellitus (DM) is metabolic syndrome which was characterized by hyperglycemia (America Diabetes Association [ADA], 2022a). DM was considered as the world health disease due to the high increase rate of DM's patients. The reports showed that numbers of people with diabetes were increasing. The estimation of the DM people in 2021 was 536.6 million. The global estimates of the diabetes prevalence during 2025-2045 will still be increasing (International Diabetes Federation [IDF], 2021). The estimated amount will raise to 578 million in 2030 and to 700 million in 2045 (Saeedi *et al.*, 2019). DM is classified into 2 major types that are type I DM (insulin defection) and type II DM (insulin resistance and/or abnormal insulin secretion). Both of them result to blood glucose uncontrollable condition. To regulate the hyperglycaemia condition, the exogenous insulin or anti-diabetic drugs such as sulphonylureas, biguanides, PPARγ agonists, and α-glucosidase inhibitors are decised to use depend on clinical need (Moller, 2001; ADA, 2022b). Although many types of drug are available to control DM, many patients still suffer from their side effects (Arulselvan *et al.*, 2014). So, the new drugs development is going on.

Thai folk medicines are the alternative treatment for diabetes. So, many herbal medicines are investigated their potential effect. *In vitro* experiment helps to screening the potential of numerous drug candidates. Our preliminary screening of α-glucosidase inhibitory activity showed that *Solanum stramonifolium* Jacq. inflorescence and *Neuropeltis racemosa* Wall. stem methanol extracts exhibited the higher inhibitory activity than α-glucosidase inhibitors drug, acarbose, at our experimental condition. In Thailand, *S. stramonifolium* is used as vegetable for cooking and *N. racemosa* is used as component in traditional Thai recipes. However, the phytochemical investigation of *S. stramonifolium* and *N. racemosa* are still lacking. So, this study aimed to isolate the chemical constituents and determine α-glucosidase inhibitory activity of the isolated compounds from *S. stramonifolium* inflorescence and *N. racemosa* stem which would be the first report. Besides the experimental strategies,

phytochemical investigation and bioactivity determination which are important for the new drug development from natural products. The active compound would be further investigated the mode of inhibition and the molecular docking strategies would be also used for inhibitory mode prediction.

1.2 Objectives

    1.2.1 To isolate and identify the compounds from *S. stramonifolium* inflorescence and *N. racemosa* stem.

    1.2.2 To determine the α-glucosidase inhibitory activity of isolated compounds.

    1.2.3 To propose the mode of inhibition of isolated compounds by experimental and molecular docking method.

CHAPTER 2

LITERRATURE REVIEW

2.1 Diabetes mellitus (DM)

Diabetes mellitus (DM) is a non-returnable syndrome that resulted from the imbalance homeostasis of carbohydrate and lipid metabolism for long time. This syndrome shows hyperglycemia condition. The improperly insulin's regulation is a key point of this disease (Tiwari and Rao, 2002). American Diabetes Association (2022a) devided the etiologic classification of DM into 4 types that are type I DM, type II DM, gestational DM and other specific types. Two main types of this disease are type I DM, an insulin-dependent DM (IDDM) and type II DM, a noninsulin-dependent DM (NIDDM) (Tiwari and Rao, 2002). Type I DM is the absolute insulin deficiency because of non-function of pancreatic β-cell. Although the β-cells are still function in type II diabetes, insulin resistance and inadequate secretion are the problems. Nowadays, many hypoglycemic agents are used for type II DM treatments. They differ from each other due to the mechanisms and targets as (**Figure 2-1**):

1) Exogenous insulin uses for insulin level replacing and hepatic glucose output reduction.

2) Incretin hormone action:

Glucagon-like peptide 1 (GLP-1) agonist is incretin mimetic that use to insulin stimulation and glucagon prohibition.

Dipeptidyl peptidase-IV inhibitors effect to glucagon-like peptide 1 (GLP-1) and glucose-dependent insulinotropic polypeptide (GIP), incretin hormones that involve glucose-dependent insulinotropic properties (Fisman and Tenenbaum, 2021).

3) Insulin secretagogues: sulphonylureas and meglitinides target on the ATP-dependent K^+ (K_{ATP}) channel of pancreatic beta-cells. Potential of the cell alters which lead to induce Ca^{2+} translocation and result to insulin releasing from pancretic β-cells.

4) Insulin sentitiser:

Biguanides regulate glucose and lipid metabolism and cellular energy though adenosine 5′-monophosphate-activated protein kinase (AMPK). Biguanides

stimulation result to hepatic gluconeogenesis reduction, a decrease of glucose absorption and an increase on glucose uptake of skeletal muscle (Krentz and Bailey, 2005).

Thiazolidinediones is peroxisome proliferator-activated receptor-γ (PPARγ) agonists that enhance insulin sensitivity by improving metabolic effect to adipose tissue, muscle and liver (Krentz and Bailey, 2005).

5) Glucose reabsorption inhibitor: sodium-glucose cotransporter 2 (SGLT2) inhibitors involve with glucose reabsorption of renal that result to lowering plasma glucose concentration (Meneses *et al*., 2015).

6) Intestinal glucose absorption inhibitor: α-glucosidase inhibitors effects to reducing the postprandial hyperglycemia (Mollor, 2001; Stumvoll *et al*., 2005).
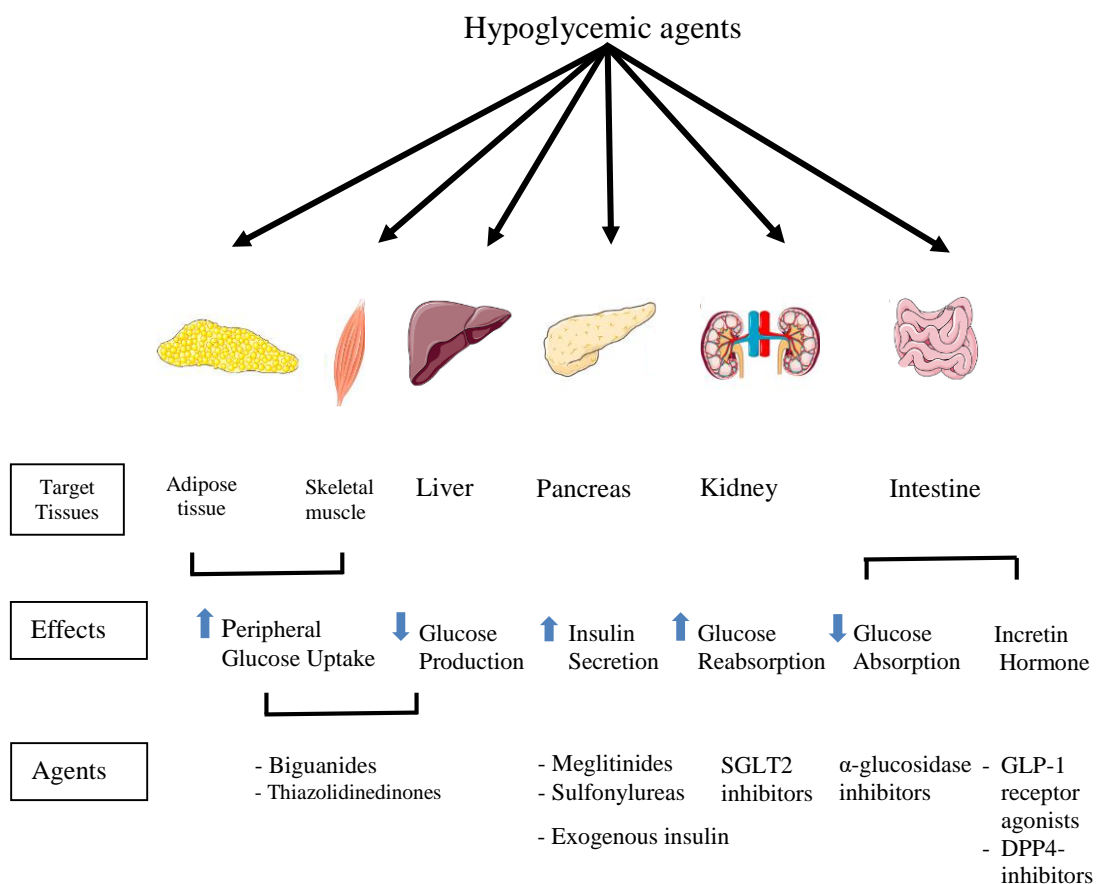
Figure 2-1 Target tissue and mechanism of anti-diabetic drugs (Naimi *et al*., 2017)

2.2 α-Glucosidase

In the digestive tract, the polysaccharide is break-downed into monosaccharaides by digestive enzymes. α-Amylase and α-glucosidase involve in generated glucose process. Starch consists of 20-30% amylose and 70-85% amylopectin. Amylose is glucose molecules linked by α-1,4 glucosidic linkage while amylopectin is glucose molecules linked by α-1,4 glucosidic linkage and bridge α-1,6 glucosidic linkage (Subroto *et al*., 2020). Dhital *et al*. (2013) reported that pancreatic α-amylase just participates in the initiation of starch digestion to hydrolyze the α-1,4 glucosidic linkage. α-Glucosidase belongs to a member of the glycoside hydrolase (GH). However, individually α-glucosidase can hydrolyze starch to be glucoses as showed in **Figure 2-2** (Dhital *et al*., 2013; Dammak *et al*., 2015).

Maltose (R=H)

R = polysaccharide chain

Glucose (R=H)

or polysaccharide chain

Glucose

Figure 2-2 Hydrolytic reaction of α-glucosidase

α-Glucosidase reaction process is the acid base reaction. The reaction used two amino acids. One amino acid acts as acid or electrophile or proton donor, while another acts as base or nucleophile (**Figure 2-3**). The oxocarbenium ion is generated as shown in **Figure 2-3 (B)**. The glucose product is released after the hydroxyl group of water transfer to oxocarbenium ion (**Figure 2-3 C-D**) (Chiba, 1997; Zechel and Withers, 2000). Moreover, α-glucosidase is a calcium containing enzyme that can slow the digestion and adsorption of carbohydrate. The calcium-binding is very tight in crystal structure of yeast α-glucosidase enzyme (Yamamoto *et al*., 2010). The molecular dynamics simulation studies of Azem and his colleagues (2012) also showed the interaction between some compound and calcium ion.

Figure 2-3 Retention mechanism of glucoside hydrolase (Chiba, 1997)

There are various origins of α-glucosidase enzyme such as bacterial, yeast, mold, plant and mammalian. α-Glucosidase enzyme is classified into two families (I and II) based on amino acid sequences similarity. The bacterial, yeast and insect α-glucosidases belong to family I, while mammalian (such as rabbit, rat and human intestine) α-glucosidase belongs to family II (Chiba, 1997 and Kimura *et al*., 2004).

Human α-glucosidase (HAG), maltase (EC 3.2.1.20), is exo-hydrolase that stand in human brush-border of small intestine. It is *N*-terminal of maltase-glucoamylase (MGAM) that used for cleavage the end side of α-1,4 linkage in glucose chain and release α-glucose (Chiba, 1997; Sim, 2010). According to amino acid sequence, it was classified as GH 31 (Sim, 2010). The reported amino acids that involved in the hydrolysis reaction were Asp 542 as electrophile and Asp 443 as nucleophile (Sim, 2010).

Yeast α-glucosidase (YAG) from *Saccharomyces cerevisiae* was used in this research. The yeast α-glucosidase is periplasmic product (Balasundaram *et al*., 2009). It is glucoside hydrolase number 13 (GH13) (Liu *et al*., 2020). The Asp214, Asp349 and Glu276 residues in *S. cerevisiae* enzyme were reported as the catalytic triad (Bharatham *et al*., 2008). Furthermore, the study showed that baker's yeast and rat intestine α-glucosidases can hydrolyze the same substrate (maltose) and can be inhibited by the same inhibitors (acarbose and its derivatives (isoacarbose and acarviosine-glucose)) (Kimura *et al*., 2004).

2.3 α-Glucosidase inhibitors

The α-glucosidase inhibitor is one class of diabetic drugs. It retards the rate of carbohydrate digestion by inhibits the intestinal α-glucosidase enzyme. So, the inhibitor affects to decrease the postprandial glucose. This is the effectiveness for glycemic control. The α-glucosidase inhibitor has been approved for diabetic treatment since 1990s (Derosa and Maffioli, 2012; Alssema *et al*., 2021).

2.3.1 α-Glucosidase inhibitors in clinical use

The clinical available α-glucosidase inhibitors are acarbose, voglibose and migiltol (**Figure 2-4**). They have the nitrogen-containing structures. These drugs were suggested to taken with main meals because their mechanism prevent complex carbohydrate digestion. Among them, acarbose is mostly used in the clinical therapy (Derosa and Maffioli, 2012).
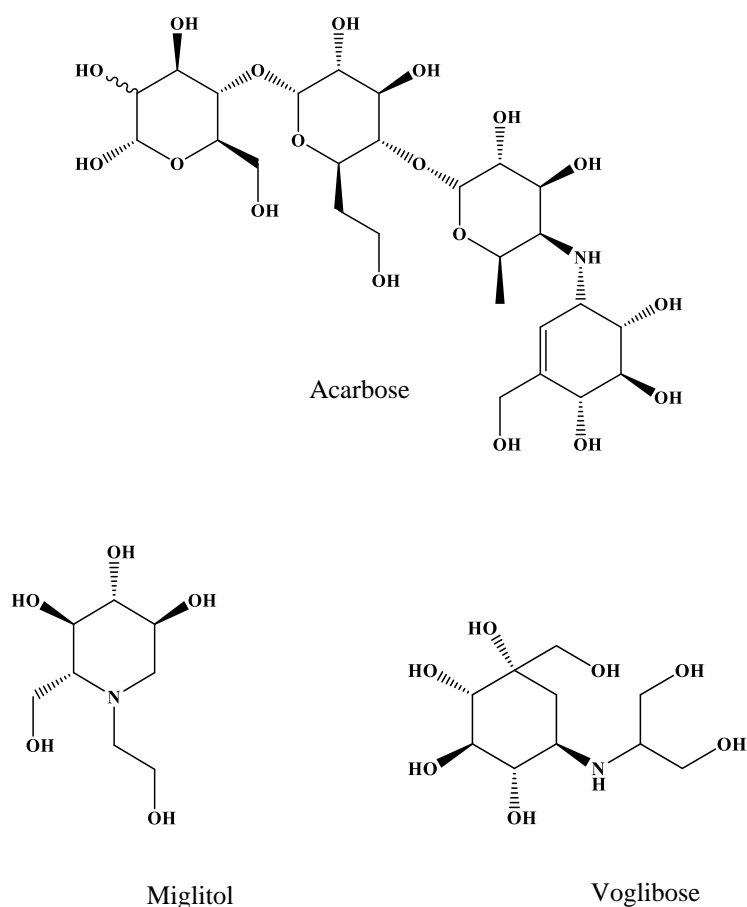
Figure 2-4 Structures of α-glucosidase inhibitors (Sadat-Ebrahimi, 2020)

Acarbose is psudo-tetrasaccharide which has nitrogen atom between the first and second glucose molecule (**Figure 2-4**). The *N*-containing cabasugar of acarbose mimics the oxocarbenium ion-like transition state. This state was generated to inhibit α-glucosidase activity and bind with high affinity (Dinicolantonio *et al*., 2015; Abuelizz *et al*., 2019). Acarbose acts as competitive inhibitor to baker's yeast and rat intestine α-glucosidases (Kimura *et al*., 2004). It usually uses as a standard drug in the experimental study of α-glucosidase inhibition.

The docking study of acarbose binding to HAG showed that the nitrogen atom of acarbose bonds to Asp 542 with a hydrogen bonding. This Asp 542 was determined as proton donor. On the other hand, Asp 443 was defined as nucleophile because the hydrogen bonding was found between hydroxyl group of acarbose and this amino acid (Sim *et al*., 2008). These bindings involve in glucoside hydrolase inhibition of acarbose to HAG (**Figure 2-5**).
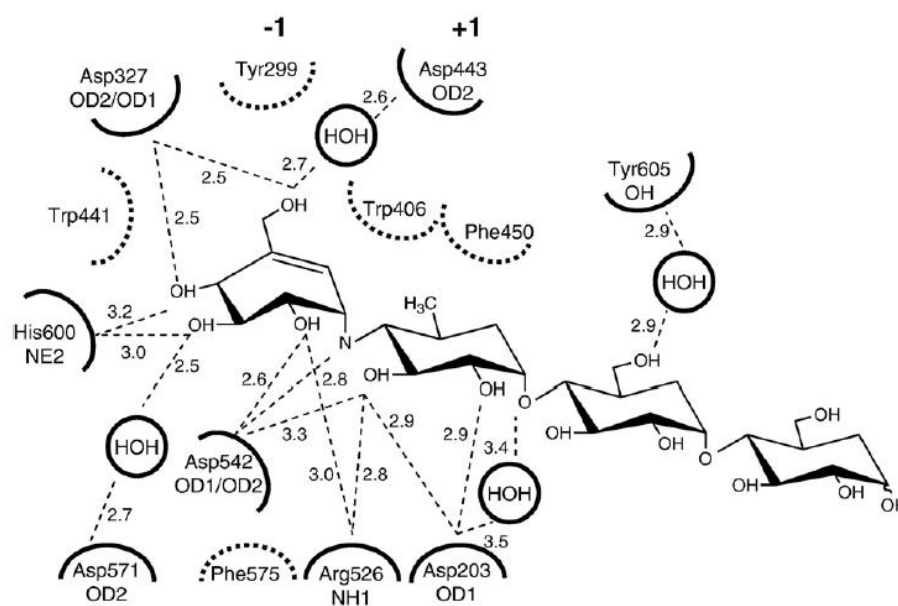
Figure 2-5 Binding of acarbose to HAG, hydrogen bonding presented as dotted lines (Sim *et al*., 2008).

Other study also exhibited the docking study of acarbose binding to YAG. The NH of acarbose formed the hydrogen bonding with Asp349, one of catalytic residues. Beside of this, the terminal hydroxyl group of acarbose also formed hydrogen

9

bonding with Arg212 and His348. The interaction of acarbose to YAG was showed in
Figure 2-6 (Bharatham *et al*., 2008).
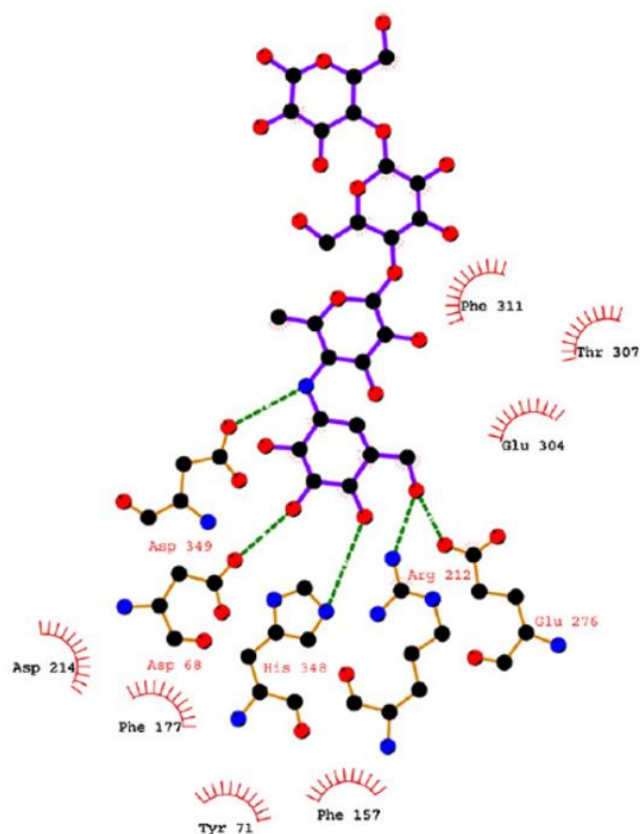
Figure 2-6 Binding of acarbose to YAG, blue cycle exhibited nitrogen atom, red cycle
exhibited oxygen atom and hydrogen bonding presented as dotted line
(Bharatham *et al*., 2008).

2.3.2 α-Glucosidase inhibitors from Solanaceae and Convolvulcaeae plants

There are many reports about α-glucosidase inhibitors from natural
sources that distribute in various classes such as terpenes, alkaloids, quinones,
flavonoids, phenols, phenylpropanoids, steroids and others (Yin *et al*., 2014; Dirir *et
al*., 2022). Our preliminary α-glucosidase study showed that *S. stramonifolium* and *N.
racemosa* methanol extracts have potential to inhibit α-glucosidase enzyme from
Saccharomyces cerevisiae. *S. stramonifolium* and *N. racemosa* belong to Solanaceae
and Convolvulaceae families, respectively. The glucosidase inhibitors present in

Solanaceae and Convolvulaceae families are reviewed as showed in the following **Table 2-1** and **Figure 2-7**.

Table 2-1 The glucosidase inhibitors from Solanaceae and Convolvulaceae plants

Group/Compounds	α-Glucosidase inhibitory activity (IC_{50})	Scientific name, Family	References
Phenylpropanoid derivative [**1**] Methyl caffeate	1.5 mM[a] 2.0 mM[b]	*Solanum torvum*, Solanaceae	Takahashi *et al*., 2010
Quinic acid derivative [**2**] 3,4,5-tricaffeoylquinic acid	4.61±1.00 µM	*Ipomoea batatas*, Convolvulaceae	Zhang *et al*., 2016
Pentasaccharide resin glycoside derivative [**3**] Cairicoside A	25.3±1.6 µM	*Ipomoea cairica*, Convolvulaceae	Pan *et al*., 2015; Jie-Hong *et al*., 2016
[**4**] Cairicoside B	28.5±3.3 µM		
[**5**] Cairicoside I	21.4±2.9 µM		
[**6**] Cairicoside II	26.2±4.6 µM		
[**7**] Cairicoside III	30.4±3.9 µM		
[**8**] Cairicoside IV	28.9±1.4 µM		
Phenolic compounds [**9**] *trans-N-(p-*coumaroyl) tyramine	4.47±0.19 µM	*Solanum melongena*, Solanaceae; *Ipomoea batatas*, Convolvulaceae	Liu *et al*., 2011; Zhang *et al*., 2016
[**10**] *trans-N-*feruloyltyramine	9.04±1.18 µM		
[**11**] *cis-N-*feruloyltyramine	14.35±1.00 µM		
Polyhydroxylated nortropane alkaloids [**12**] Calystegine B_1	2.1 µM[c]	*Ipomoea carnea*, Convolvulaceae	Haraguchi *et al*., 2003
[**13**] Calystegine B_2	0.75 µM[c]		
[**14**] Calystegine C_1	0.84 µM[c]		

[a] against rat intestinal sucrase
[b] against rat intestinal maltase
[c] β-glucosidase inhibitory activity
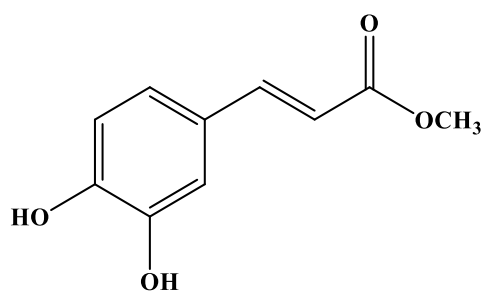
[**1**] Methyl caffeate
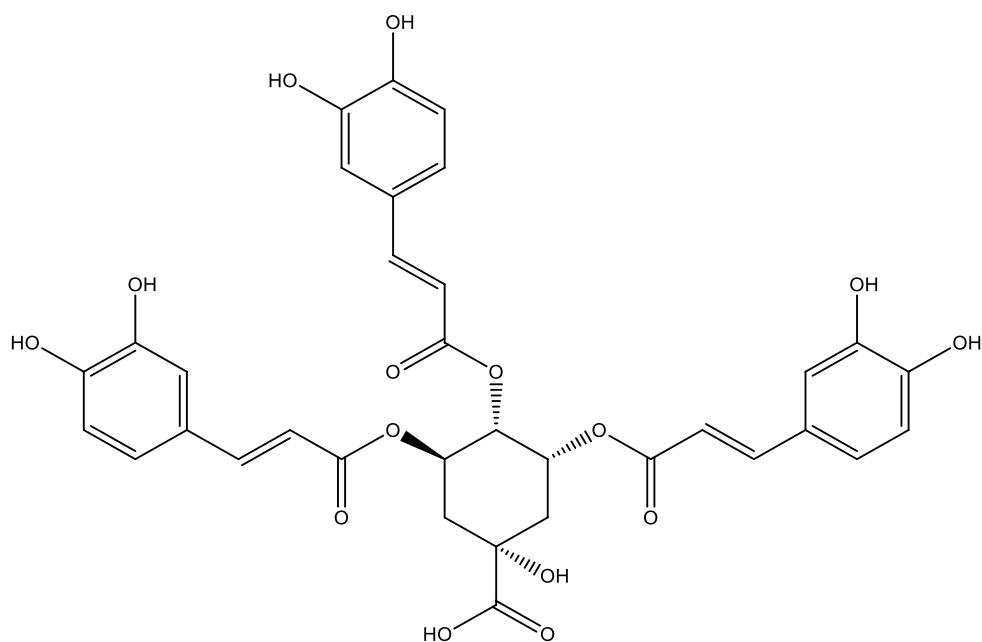
[**2**] 3,4,5-tricaffeoylquinic acid

Figure 2-7 Chemical structures of the isolated compounds from Solanaceae and Convolvulaceae plants
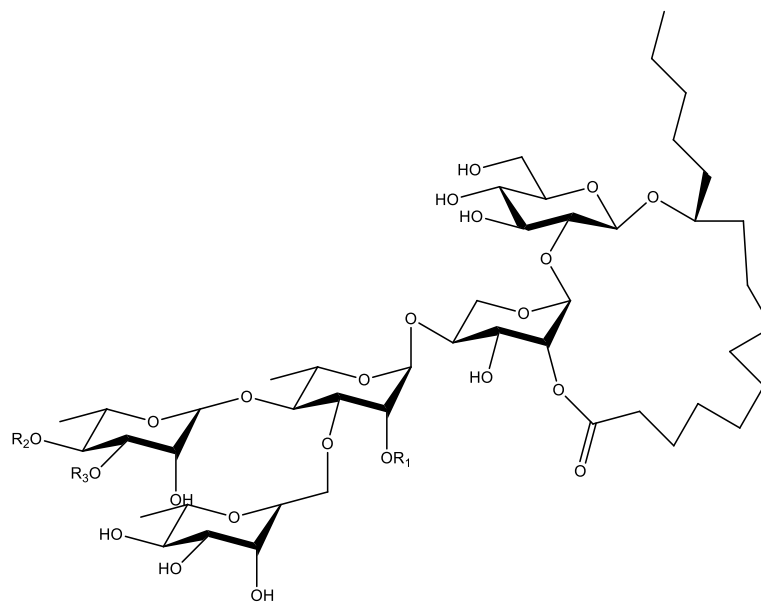
	R₁	R₂	R₃
[3] Cairicoside A	Deca	Iba	Cna
[4] Cairicoside B	Deca	Hexa	Cna
[5] Cairicoside I	Mba	Mba	Cna
[6] Cairicoside II	Bu	Mba	Cna
[7] Cairicoside III	Octa	Mba	Can
[8] Cairicoside IV	Deca	Cna	Mba

Abbreviations: Bu = butyl; Cna = *trans*-cinnamoyl; Deca = *n*-decanoyl;

Hexa = *n*-hexanoyl; Iba = isobutyryl; Oca = n-octanoyl
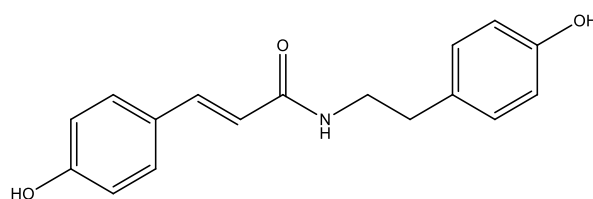
[9] *trans*-*N*-(*p*-coumaroyl) tyramine
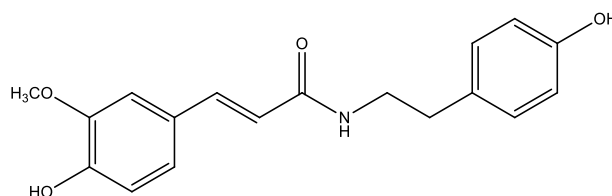
[10] *trans*-*N*-feruloyltyramine

Figure 2-7 Chemical structures of the isolated compounds from Solanaceae and Convolvulaceae plants **(continued)**
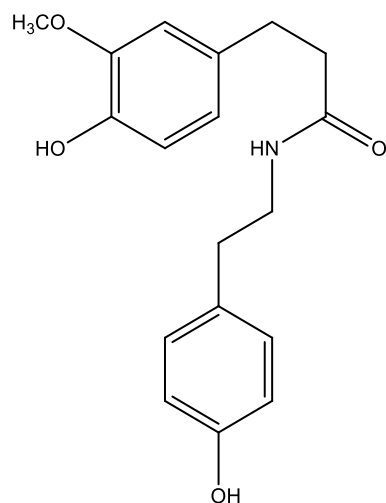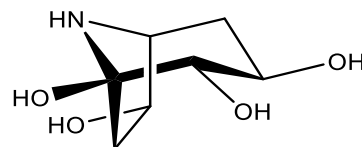
[**11**] *cis-N*-feruloyltyramine　　　　　[**12**] Calystegine B₁
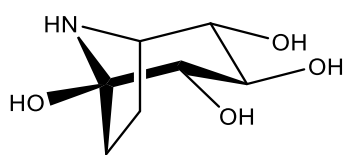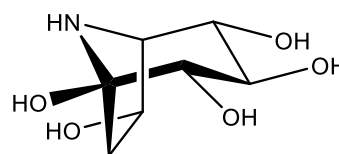
[**13**] Calystegine B₂　　　　　[**14**] Calystegine C₁

Figure 2-7 Chemical structures of the isolated compounds from Solanaceae and
Convolvulaceae plants **(continued)**

2.4 Molecular docking study

Since the 1980s, the molecular docking technique has been used as a tool in drug discovery. It is one of structure-based drug design (SBDD) method. Molecular docking is used for the prediction of molecular interaction between the ligands (compounds) and the receptors (molecular targets) (Ferreira *et al.*, 2015). The ligand-receptor complex bases on the binding affinity including conformational space of binding site and ligand pose. The binding energetic of predicted ligand-receptor

complex involve to the physical-chemical phenomena, including intermolecular interactions, solvation, and entropic effects. The energy is evaluated as scoring functions by the computer programs (*in silico*). The steps which involve in molecular docking are 1) molecular target preparation 2) compound database selection (ligand optimization) 3) molecular docking and 4) post-docking analysis (Ferreira *et al*., 2015).

Many sample algorithms are used for molecular docking including matching algorithms, incremental construction, stochastic method, and molecular dynamic. Matching algorithms map a ligand into an active site and evaluate in term of shape features and chemical information. Incremental construction is fragment-based method. This method divides ligand into small fragments and then incremental fragments. These fragments are mapped into an active site and evaluated the orientated binding. Stochastic method randomly modifies the ligand's conformation and binds into docking site. The typical stochastic methods are Monte Carlo (MC) and Genetic Algorithms (GA). Molecular dynamic moves each atom individually then optimizes energy and provides the results (Meng *et al*., 2011; Ferreira *et al*., 2015).

The scoring function including force-field based, empirical, knowledge-based, and consensus scorings functions are estimated. Force-field-base scoring function consider the ligand-receptor binding energy though the calculation of non-bonded (electrostatics and van der Waals) interaction, hydrogen bonds, solvation, and entropy. Empirical scoring function relies on reproducing binding affinities. This scoring function considers the physical event of the ligand-receptor complex though hydrophobic and entropic effect, hydrogen bond, and ionic interaction. Knowledge-based scoring function considers the scoring though frequency contacts and repulsive interactions between each atom in the ligand under a given cutoff. The last, consensus scoring function is the combine scoring methodologies to improve the prediction of the docking conformations (Serina, 2010; Meng *et al*., 2011; Ferreira *et al*., 2015).

The docking methodologies are classified into rigid ligand and rigid receptor docking, flexible ligand and rigid receptor docking, and flexible ligand and flexible receptor docking. In early, the rigid bodies of both ligand and receptor are considered in the docking methodology. This case limits the binding conformation, so a pre-computed ligand conformation is used. Afterward both flexible ligand and receptor are treated in docking. However, the cost is quite high. Nowadays, the flexible

ligand and rigid receptor docking are used wildly. AutoDock and GOLD, well known docking programs, adopt this methodology (Meng *et al*., 2011).

There are many studies used *in silico* docking method to find out the interaction between compounds and the target α-glucosidase receptor. Moreover, docking strategies can be used for prediction of mode of enzyme inhibition. These studies are reviewed as shown in the following **Table 2-2**.

Table 2-2 *In silico* docking studies of α-glucosidase receptor

Target Protein	Compounds	Molecular Docking Programs	Docking Result	Post Docking Analysis Programs	α-Glucosidase Activity from Experimental	References
Yeast glucose-α-glucosidase (PDB ID: 3A4A)	Rutin (Flavonoid)	AutoDock Vina	BE = -8.2	PostView	IC_{50} = 84.1±4.1 µg/ml; noncompetitive inhibitor	Hyun *et al.*, 2014
	Quercetin (Flavonoid)		BE = -8.0		IC_{50} = 1.0±0.1 µg/ml; competitive inhibitor	
	Myricetin (Flavonoid)		BE = -7.7		IC_{50} = 3.2±0.1 µg/ml; competitive inhibitor	
	1-Naphthyl butyrate		BE = -5.7	NR	NR	
	2,5-Dihydroxybenzoic acid		BE = -5.7			
	2-Hydroxycinnamic acid		BE = -5.5			
	3-Aminobutanoic acid		BE = -3.8			
	3-Hydroxybenzoic acid		BE = -5.1			
	4-Hydroxy-3-methoxybenzoic acid		BE = -5.7			
	4-Hydroxybenzoic acid		BE = -5.0			
	4-Methoxybenzoic acid		BE = -5.0			

Remark: BE = Binding energy in kcal/mol; ΔE = Binding energy estimate in Kcal/mol; IC_{50} = Half-maximal inhibitory concentration;
pIC_{50} = Negative logarithmic values of half-maximal inhibitory concentration; Ki = Inhibition constant;
MOE = Molecular Modeling Environment; NR = Not reported; GLIDE = Grid-Based Ligand Docking with Energetics;
GOLD = Genetic Optimized Ligand Docking

Table 2-2 *In silico* docking studies of α-glucosidase receptor **(continued)**

Target Protein	Compounds	Molecular Docking Programs	Docking Result	Post Docking Analysis Programs	α-Glucosidase Activity from Experimental	References
	5-Sulfosalicylic acid		BE = -5.6			
	Acetylenedicaboxylic acid		BE = -5.1			
	Alpha-humulene		BE = -5.5			
	Benzaldehyde		BE = -4.5			
	Benzoic acid		BE = -4.8			
	Caffeic acid		BE = -5.6			
	Decannoic acid		BE = -3.6			
	Dodecanedionic acid		BE = -4.1			
	Ferulic acid		BE = -5.4			
	Gallic acid		BE = -6.2			
	Glutaric acid		BE = -4.3			
	Hydroquinone		BE = -4.5			
	Indole		BE = -4.9			
	l-Glutamic acid		BE = -4.5			
	Naringenin		BE = -7.3			
	Nobiletin		BE = -6.1			
	p-Coumaric acid		BE = -5.5			
	Phenylacetic acid		BE = -5.0			
	Phloroglucinol		BE = -5.1			

Remark: BE = Binding energy in kcal/mol; ΔE = Binding energy estimate in Kcal/mol; IC_{50} = Half-maximal inhibitory concentration;
pIC_{50} = Negative logarithmic values of half-maximal inhibitory concentration; Ki = Inhibition constant;
MOE = Molecular Modeling Environment; NR = Not reported; GLIDE = Grid-Based Ligand Docking with Energetics;
GOLD = Genetic Optimized Ligand Docking

Table 2-2 *In silico* docking studies of α-glucosidase receptor **(continued)**

Target Protein	Compounds	Molecular Docking Programs	Docking Result	Post Docking Analysis Programs	α-Glucosidase Activity from Experimental	References
	Propionic acid		BE = -4.1			
	Protocatechuic acid		BE = -5.8			
	p-Toluidine		BE = -4.6			
	Scopoletin		BE = -5.9			
	Suberic acid		BE = -3.9			
	Succinic acid		BE = -4.3			
	Syringic acid		BE = -5.3			
	Tangeretin		BE = -6.1			
	trans-3-Hydroxycinnamic acid		BE = -5.5			
	trans-Cinamic acid		BE = -5.1			
Yeast glucose-α-glucosidase (constructed by homology modeling method based on *Bacillus*	Acarbose (positive control)	AutoDock 4	Ki = 0.0024 μM	NR	IC$_{50}$ = 1.7 mM; K$_i$ = 0.26 mM; competitive inhibitor	Esccandón-Rivera *et al*., 2012

Remark: BE = Binding energy in kcal/mol; ΔE = Binding energy estimate in Kcal/mol; IC$_{50}$ = Half-maximal inhibitory concentration; pIC$_{50}$ = Negative logarithmic values of half-maximal inhibitory concentration; Ki = Inhibition constant; MOE = Molecular Modeling Environment; NR = Not reported; GLIDE = Grid-Based Ligand Docking with Energetics; GOLD = Genetic Optimized Ligand Docking

Table 2-2 *In silico* docking studies of α-glucosidase receptor **(continued)**

Target Protein	Compounds	Molecular Docking Programs	Docking Result	Post Docking Analysis Programs	α-Glucosidase Activity from Experimental	References
	6-hydroxyacetyl-5-hydroxy-2,2-dimethyl-2H-chromene		K_i = 13 μM		IC_{50} = 0.42 mM; K_i = 0.13 mM; noncompetitive inhibitor	
	Calein C (sesquiterpene lactone)		K_i = 0.30 μM		IC_{50} = 0.28 mM; K_i = 1.91 mM; mixed-type inhibitor	
	Isorhamnetin (flavonoid)		K_i = 7.9 μM		IC_{50} = 0.16 mM K_i = 0.41 mM; mixed-type inhibitor	
α-glucosidase (PDB ID: 3TOP)	Acarbose (positive control)	MOE	BE = -12.335	NR	IC_{50} = 64.14±0.0033 μM	Abd El-Mohsen *et al*., 2008
	Marrubiin (diterpene)		BE = -12.474		IC_{50} = 16.62±0.0024 μM	
Bacillus cereus oligo 1,6-glucosidase (PDB ID: 1UOK)	Geraldone or 5-deoxyflavone (flavonoid)	GLIDE	BE = -3.53 (Dock score: 61.18)	NR	% inhibition = 93.91±1.21%	Ahmed *et al*., 2014

Remark: BE = Binding energy in kcal/mol; ΔE = Binding energy estimate in Kcal/mol; IC_{50} = Half-maximal inhibitory concentration;
pIC$_{50}$ = Negative logarithmic values of half-maximal inhibitory concentration; Ki = Inhibition constant;
MOE = Molecular Modeling Environment; NR = Not reported; GLIDE = Grid-Based Ligand Docking with Energetics;
GOLD = Genetic Optimized Ligand Docking

Table 2-2 *In silico* docking studies of α-glucosidase receptor **(continued)**

Target Protein	Compounds	Molecular Docking Programs	Docking Result	Post Docking Analysis Programs	α-Glucosidase Activity from Experimental	References
	Isookanin		BE = -3.189 (Dock score: 68.86)		% inhibition = 73.14±1.30%	
	Luteolin		BE = -2.423 (Dock score: 66.91)		% inhibition = 92.59±1.36%	
Sucrose-isomaltase (PDB ID:3LPP)	Acarbose	GOLD	BE = not detected (GOLD score: 56.3)	NR	K_i = 7.8 μM	Jocković *et al.*, 2013
	Calystegine A_3 (nortropane alkaloid)		BE = -49.1 (GOLD score: 51.3)		K_i = 227±47 μM	
	Calystegine B_2 (nortropane alkaloid)		BE = -48.7 (GOLD score: 48.9)		K_i = 55±12 μM	
Maltase-glucoamylase (PDB ID: 3L4X and 2QMJ)	Acarbose (positive control)		BE = not detected (GOLD score: 64.5)		K_i = 4.4 μM	
	Calystegine A_3 (nortropane alkaloid)		BE = -55.0 (GOLD score: 52.7)		K_i = failed	

Remark: BE = Binding energy in kcal/mol; ΔE = Binding energy estimate in Kcal/mol; IC_{50} = Half-maximal inhibitory concentration;
pIC$_{50}$ = Negative logarithmic values of half-maximal inhibitory concentration; Ki = Inhibition constant;
MOE = Molecular Modeling Environment; NR = Not reported; GLIDE = Grid-Based Ligand Docking with Energetics;
GOLD = Genetic Optimized Ligand Docking

Table 2-2 *In silico* docking studies of α-glucosidase receptor **(continued)**

Target Protein	Compounds	Molecular Docking Programs	Docking Result	Post Docking Analysis Programs	α-Glucosidase Activity from Experimental	References
	Calystegine B_2 (nortropane alkaloid)		BE = -53.3 (GOLD score: 49.4)		K_i = 582±144 μM	
Rat-isomaltase (ntSI) (constructed by homology modeling method based on Human-isomaltase PDB ID: 3LPP, identity 73%)	Miglitol	GLIDE	ΔE =- 68.89	NR	pIC_{50} = 4.41 $\log(\mu M^{-1})$	Kato *et al*., 2015
	α-1-C-butyldeoxynojirimycin (α-1-C-butyl-DNJ)		ΔE = -77.11		pIC_{50} = 6.35 $\log(\mu M^{-1})$	
	α-1-C-butyl-1,4-imino-L-arabinitol (α-1-C-butyl LAB)		ΔE = -75.88		pIC_{50} = 5.33 $\log(\mu M^{-1})$	

Remark: BE = Binding energy in kcal/mol; ΔE = Binding energy estimate in Kcal/mol; IC_{50} = Half-maximal inhibitory concentration;
pIC_{50} = Negative logarithmic values of half-maximal inhibitory concentration; Ki = Inhibition constant;
MOE = Molecular Modeling Environment; NR = Not reported; GLIDE = Grid-Based Ligand Docking with Energetics;
GOLD = Genetic Optimized Ligand Docking

2.5 Research plants

From preliminary screening of α-glucosidase inhibitory activity from more than 50 samples that are used as food and composed in traditional Thai anti-diabetic recipes from Solanaceae and Convolvulaceae families. *S. stramonifolium* inflorescence and *N. racemosa* stem methanol extracts showed the potential effects with % inhibition at 2 mg/ml at $96.21 \pm 0.75\%$ and $96.10 \pm 0.75\%$, respectively, while acarbose, a positive control, showed % inhibition at the same concentration at $71.68 \pm 3.48\%$. Due to the highly % inhibition, they were selected for further study on phytochemicals in order to findout the active compounds in these plants.

S. stramonifolium belongs to Solanaceae family and *N. racemosa* belongs to Convolvulaceae family. Solanaceae and Convolvulaceae families are in the same order, Solanales. The Solanales is the flowering plant. It belongs to subclass Asteridae of class Magnoliopsidae (Dicotyledons). Solanaceae plants ranges from herbs, shrubs, small tree to climbers (Zhi-yun *et al.*, 1994). They consist of agricultural crops, medicinal plants, spices, weed and ornamentals. Potato, tomato, chili pepper and eggplant are the member of Solanaceae plants. Many alkaloids (eg. solanine, tropanes, nicotine and capsaicin) are found in this family. Convolvulaceae plants are climbers, herbaceous or woody. The Convolvulaceae stem twins to right but lacks tendrils (Santisuk and Larsen, 2010). They are used as foods and medicinal plants. Tropane alkaloids, lysergic acid type alkaloids, cinnamic acid derivatives and coumarin are reported from Convolvulaceae plants (Bendz and Santesson, 1973).

2.5.1 *Solanum stramonifolium* Jacq. (Figure 2-8)

Family: Solanaceae

Synonyms: มะเขือปู่ ma khuea pu, มะปู่ ma pu (Northern), มะอึก ma uek (Central, Nakhon Ratchasiam), ยั้งคุยดี yang-khui-di (Karen-Mae Hong Son) (เต็ม สมิตินันทน์, 2557), hairy-fruited eggplant, bolo maka, coconilla, tapirillo, groselilierdiable, groseille sauvage (Tropilab®Inc, 2016)

Description: Perennial shrub, 100-200 cm. **Stems** glabrous or copiously prickly, stellate hairs. **Leaves** simple, alternate, ovate-sinuate, 9-13 x 5-10.5 cm, apex acute to obtuse, base obtuse or sinuous, prickles and stellate pubescent on both surfaces, veins green or purple. **Inflorescences** in

paniculate cymes, axillary; peduncles stout, 10-35 mm long. **Flowers** bisexual, 2 cm in diameter; corolla 5, united, white, apex acute; calyx campanulate, divided nearly to base; 5 lobes, green, pubescent. **Stamens** 5, anthers yellow. **Ovary** superior. **Fruits** berry, juicy, globose 8-12 mm in diameter, yellow to orange when ripening, pubescent, calyx persistent. This plant description was written by Neamsuvan (2016a).

Distribution: Widely found in South and South-East Asia (Parmar, 2018)

Ecology: On hill fields and agroforest orchards (Chanmee *et al*., 2013)

Use: As vegetable

Thai traditional use (วุฒิ วุฒิธรรมเวช, 2540):

Leaf: anti-itching and relieve swollen skin

Flower: anti-itching

Fruit: expectorant and anti-cough

Root: expectorant, analgesics, anti-pyretic and diuretic

Seed: relieve toothache

Chemical constituents and biological activities of *S. stramonifolium*:

Carpesterol and linoleic acid were isolated from fruits of *S. stramonifolium*. Lipase inhibitory activities of both compounds exhibited IC_{50} values as 56.0 and 43.6 µg/ml, respectively while orlistat, a positive control, exhibited IC_{50} value as 0.0035 µg/ml. Capesterol was a competitive lipase inhibitor but linoleic acid was a noncompetitive lipase inhibitor (Chanmee *et al*., 2013).

Aqueous extract of *S. stramonifolium* seed showed antibacterial activity against gram positive bacteria (*Staphylococcus aureus*, *Bacillus licheniformis*, *Bacillus subtilis* and *Xanthomonas* sp.) and negative bacteria (*Pseudomonas aeruginosa* and *Salmonella typhi*) at concentration 100 µg/disc (Sarnthima and Khannuang, 2012).

Ethanol extract of *S. stramonifolium* fruits exhibited anti-leishmanicidal activity. *In vitro* against amastigote stage (the growing form in macrophages) of *Leshmania amazonensis* showed IC_{50} value as 56.9 µg/ml, while amphotericine B and glucantime, positive controls,

showed IC$_{50}$ values as 0.2 and 30 µg/ml, respectively (Estevez *et al.*, 2007).
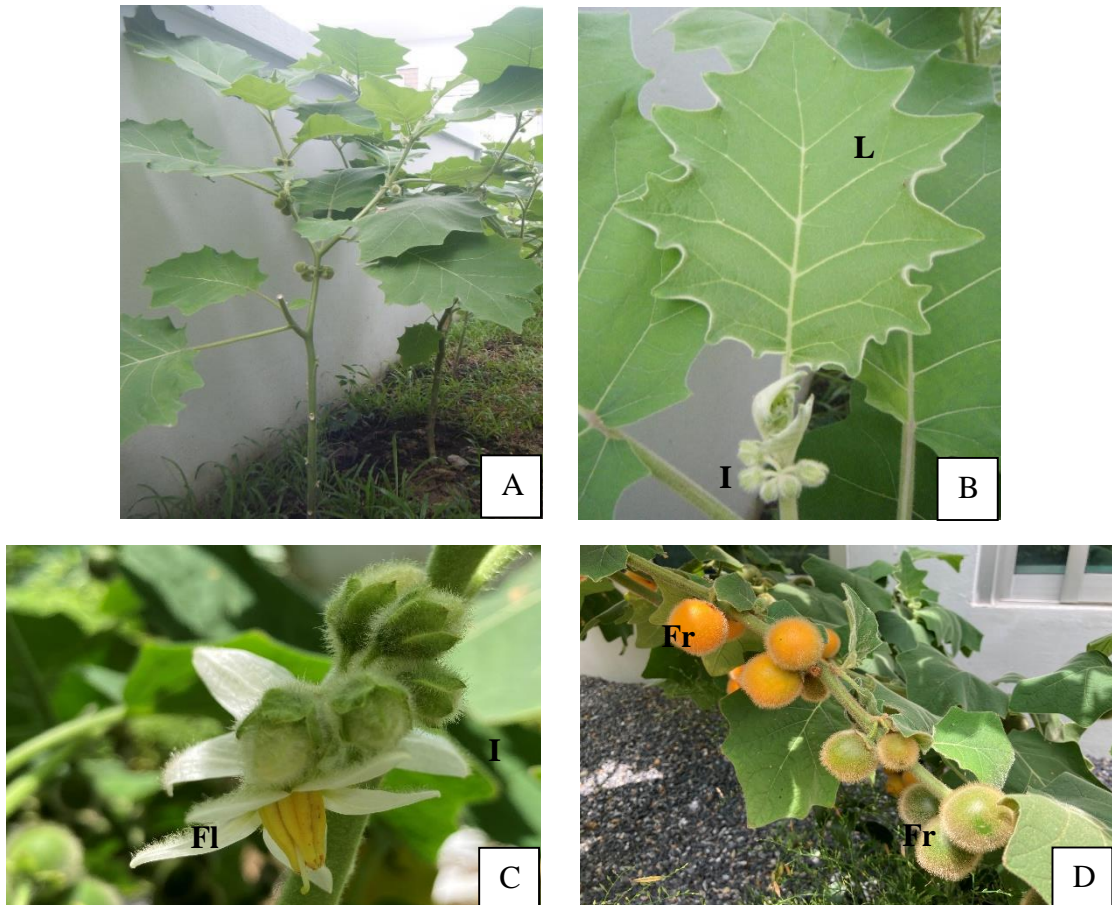
Figure 2-8 *S. stramonifolium* Jacq.;

A = whole plant, B = leaves (L) and inflorescence (I),

C = flowers (Fl) and I, D = fruits (Fr)

2.5.2 *Neuropeltis racemosa* **Wall.** (**Figure 2-9**)

Family: Convolvulaceae

Synonyms: กาโร karo (Ranong), นอนหลับ non lap, พญานอนหลับ phaya non lap (Nakhon Sawan), มันฤาษี man ruesi (Central), มาดพล้ายโรง mat plai rong (Nakhon Ratchasima), ม้ากระทืบโรง ma kra thuep rong, ม้าทลายโรง ma thalai rong (General), ย่านขี้ไก่ yank hi kai (Nakhon Si Thammarat) (เต็ม สมิตินันทน์, 2557)

Description: Woody climber. **Stems** terete, young parts appressed densely by rust colored tomentose, older ones sparsely short thorny. **Leaves** simple, alternate, elliptic to elliptic-oblong, 5-15 by 2-4.5 cm, papery, glabrous, glabrescent, abaxially glossy, base acute, margin entire, apex abruptly short acuminate, lateral veins 8-9 per side, curved near margin, midrib and veins prominent beneath; petiole 10-15 mm long, rust colored tomentose. This plant description was written by Neamsuvan (2016b).

Distribution: Myanmar, China, Malaysia, Indonesia (Santisuk and Larsen, 2010)

Ecology: Edge of evergreen forest or seasonal rain forest, along streams (Santisuk and Larsen, 2010)

Thai traditional use (กองการประกอบโรคศิลปะ, 2541):

          Stem: a component of Thai traditional recipes for relieve skin disorder eg. rash iching and atropic dermatitis

Chemical constituents and biological activities of *N. racemosa*.:

          In the present study, it has not been reported concerning of chemicals and biological activities.
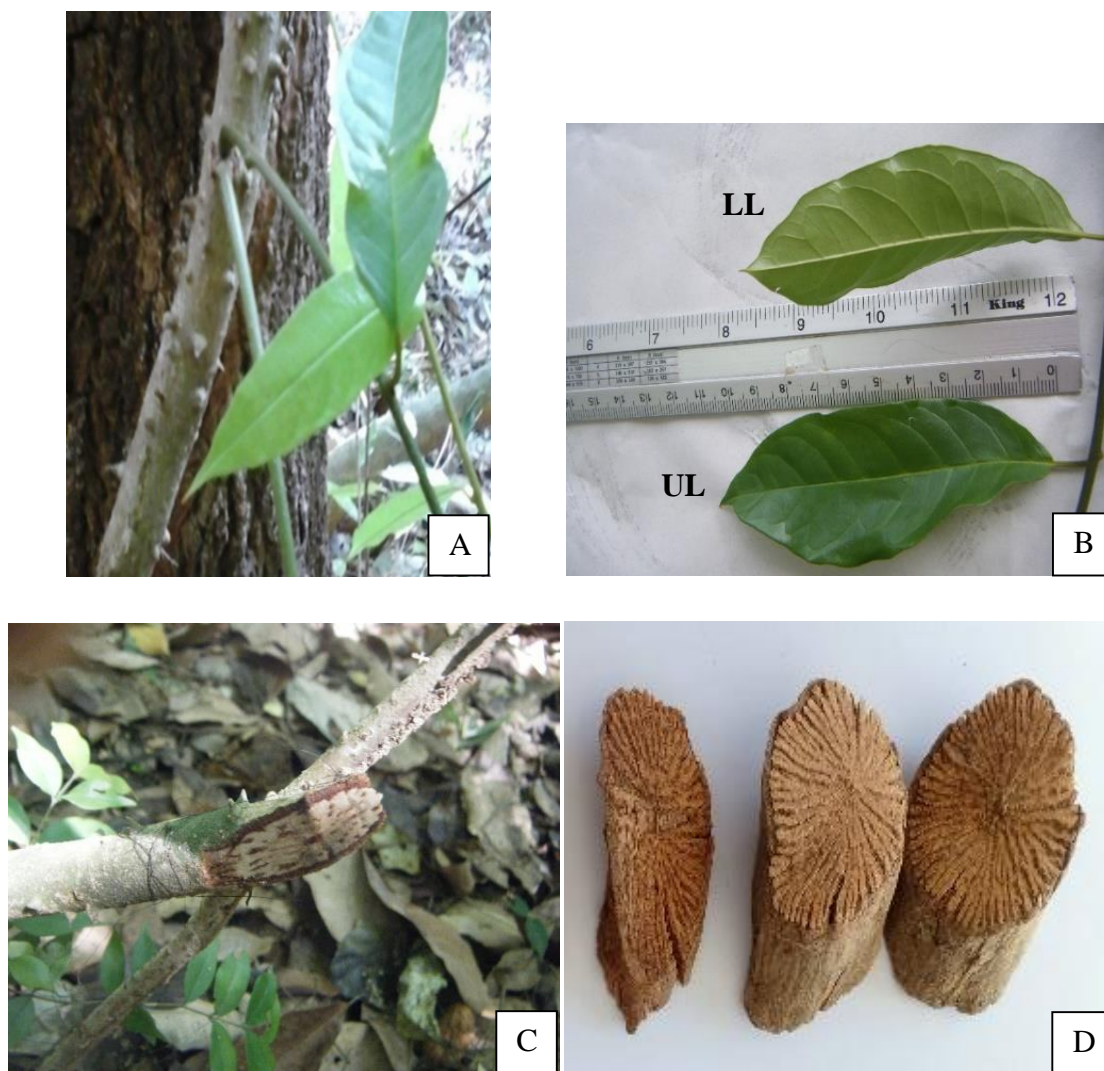
Figure 2-9 *N. racemosa* Wall.;

A = *N. racemosa* in forest, B = upper (UL) and lower (LL) surface leaves,
C = cross section of fresh stem, D = cross section of dried stem

From the literatures review of both plants, *S. stramonifolium* inflorescence and *N. racemosa* stem, they have not been reported of phytochemicals and α-glucosidase inhibition. So, this study will be the first report of their active compounds and mode of α-glucosidase inhibition.

CHAPTER 3

MATERIALS AND METHODS

3.1 Plant materials

3.1.1 *Solanum stramonifolium* **Jacq. inflorescence**

The inflorescence of *S. stramonifolium* was collected from Songkhla province, Thailand. The specimens were identified by Ms. Ramrada Meeboonya, botanist of Forest Herbarium, and are deposited as reference at Forest Herbarium, Department of National Park Wildlife and Plant Conservation, Thailand with herbarium number as BKF No. 189326 and BKF No. 189327.

3.1.2 *Neuropeltis racemosa* **Wall. stem**

The stem of *N. racemosa* was collected from Songkhla province, Thailand. The specimens were identified by Assoc.Prof.Dr. Orathai Neamsuvan, lecturer and botanist of Faculty of Traditional Thai Medicine, Prince of Songkla University, Thailand and are deposited as reference at Department of Pharmacognosy and Pharmaceutical Botany, Faculty of Pharmaceutical Sciences, Prince of Songkla University, Thailand with herbarium number as SKP 054 14 18 01.

3.2 Chemicals, materials and instruments

3.2.1 Chemicals and materials for extraction and isolation

The chemicals and materials for extraction and isolation are shown in **Table 3-1**.

Table 3-1 Chemicals and materials for extraction and isolation, and its source

Chemicals and materials	Source
Chloroform	RCI Labscan Limited, Thailand
Dichloromethane	RCI Labscan Limited, Thailand
Ethanol	Thaioil Co. Ltd., Thailand
Ethyl acetate	Thaioil Co. Ltd., Thailand

Table 3-1 Chemicals and materials for extraction and isolation, and its source **(continued)**

Chemicals and materials	Source
Hexane	Thaioil Co. Ltd., Thailand
Methanol	Thaioil Co. Ltd., Thailand
Sephadex® LH-20	GE Healthcare life sciences, UK
Silica gel 60	Merck, Darmstadt, Germany
LiChroprep®RP-18	Merck, Darmstadt, Germany
Sulphuric acid	Fluka, Sigma-Aldrich, USA
TLC sheet plate (Silica gel GF254)	Merck, Darmstadt, Germany
TLC sheet plate (Silica gel RP-18)	Merck, Darmstadt, Germany

3.2.2 Chemicals and materials for α-glucosidase inhibitory activity determination

The chemicals and materials for α-glucosidase inhibitory activity determination are shown in **Table 3-2**.

Table 3-2 Chemicals and materials for α-glucosidase inhibitory activity determination and its source

Chemicals and materials	Source
α-Glucosidase enzyme (*Saccharomyces cerevisieae*)	Sigma, Sigma-Aldrich, Germany
p- Nitrophenyl-α-D-glucopyranoside (*p*NPG)	Sigma, Sigma-Aldrich, Germany
Bovine serum albumin	Sigma, Sigma-Aldrich, Germany
Sodium azide	Sigma, Sigma-Aldrich, Germany
Dimethylsulfoxide (DMSO)	Sigma, Sigma-Aldrich, Germany
$NaH_2PO_4.2H_2O$	MAY&BAKER Limited Dagen, England
Na_2HPO_4	MAY&BAKER Limited Dagen, England
Acarbose	Sigma, Sigma-Aldrich, Germany
Kaempferol	Chem Face, China

Table 3-2 Chemicals and materials for α-glucosidase inhibitory activity determination and its source **(continued)**

Chemicals and materials	Source
Astragalin	Chem Face, China

3.2.3 General instruments

The instruments for phytochemical investigation and α-glucosidase inhibitory activity determination are shown in **Table 3-3**.

Table 3-3 Instruments for phytochemical investigation and α-glucosidase inhibitory activity determination, and its source

Instruments	Source
Hot air oven	Memmert, Schwabach, Germany
Micropipettes : 1-10 μl, 20-200 μl, 100-1000 μl	Socorex, Ecublens, Switzerland
Microplate 96 wells	Nunc, Roskilde, Denmark
Multichannel micropipette	BiotekInstruments, Cyber scan 510, Nijkerk, Netherland
pH meter	Biotek Power, BioTek Instruments, Vermont, USA
Rotary evaporator	Heidolph, Germany
UV-cabinet : 254 and 365 nm.	CAMAG, North Carolina, USA
Vortex G560E	VTX-3000L, LMS Co., Ltd., Tokyo, Japan
Water bath	WB-14, Memmert, Schwabach, Germany

3.2.4 Spectroscopic instruments

3.2.4.1 Ultraviolet (UV) spectroscopy

The Genesys 6 UV-Visible instrument (Thermo Scientific, Thermo Electron Corporations) at Department of Pharmacognosy and Pharmaceutical Botany, Faculty of Pharmaceutical Sciences, Prince of Songkla University was used to performed the UV absoption character of the isolated compounds.

3.2.4.2 Infrared (IR) spectroscopy

The Perkin Elmer FT-IR Spectrum One Spectrometer at Department of Pharmaceutical Chemistry, Faculty of Pharmaceutical Sciences, Prince of Songkla University was used to measure the IR spectra of the isolated compounds. The used IR technique was neat technique with sodium chloride (NaCl) plates.

3.2.4.3 Mass spectrometer (MS)

The Liquid Chromatograph-Quadupole Time-of-Flight Mass Spectrometer, LC-QTOF MS, (1290 Infinity II LC-6545 Quadrupole-TOF, Agilaent Technologies, USA) at Office of Scientific Instrument and Testing (OSIT), Prince of Songkla University was used to determine the molecular mass of the obtained compounds. The mass spectrometric technique was direct injection negative electrospray ionization (ESI) – high resolution mass spectrometry.

3.2.4.4 Nuclear magnetic resonance (NMR) spectroscopy

Two NMR instrument were performed to the signal spectra of isolated compounds. The first instrument is Fourier Transform NMR Spectrometer (^{1}H-NMR 500 MHz and ^{13}C-NMR 125 MHz), Unity Inova, Varian, Germany at OSIT, Prince of Songkla University. The second instrument is 500 MHz NMR Spectrophotometer (^{1}H-NMR 500 MHz and ^{13}C-NMR 125 MHz), BRUKER/AVANCE^{TM} *NEO*, ASCEND^{TM}, Switzerland at Scientific Equipment Technology, Walailuk University.

The samples were dissolved in deuterated solvent including deuterated methanol (CD$_3$OD), deuterated chloroform (CDCl$_3$) and deuterated dimethyl sulfoxide (DMSO-d_6). The NMR spectra exhibited the chemical shift in ppm scale.

3.2.5 Other instruments

3.2.5.1 High performance liquid chromatography (HPLC)

The high performance liquid chromatography, Algilant Technologies 1200 series (HPLC-Agro) at OSIT, Prince of Songkla University was used to define the purification of selected sample. HPLC-Diode array (DAD) with hypersil ODS column (250×4.0 mm, 5 μm particle size detected the peak at 260, 292, 370 nm. Mobile phase consisted of 0.3% (v/v) acetic acid in water (A) and methanol (B) with a gradient elution at 0-100 min. The flow rate of mobile phase was 1.0 ml/min^{-1} and the injection volume was 50 μl.

3.2.5.2 Microplate reader

The SPECTROstar Nano BMG Labtech microplate reader at Pharmaceutical Sciences Laboratory Service Center, Faculty of Pharmaceutical Sciences, Prince of Songkla University was performed at 405 nm to monitoring an enzyme reaction.

3.3 Plant extraction

Fresh plant material of *S. stramonifolium* inflorescence (800 g) was washed and dried in the oven at temperature 50ºC until dryness. In the other way, fresh plant material of *N. racemosa* stem (10 kg) was washed, chopped and dried in the oven at temperature 50ºC until dryness, respectively. Then, each dried plant materials were blended into small pieces and macerated with distillated solvents. The extraction was started by using the lower polarity solvent and followed by increasing the solvent polarity until obtained 4 extracts. First, the plant materials were macerated with hexane at room temperature 3 days and repeated 3 times. The marc and filtrated were separated by course filter paper. The marc was macerated at room temperature 3 days and repeated 3 times again with ethyl acetate and ethanol, respectively. For final extraction, the marc was boiled with filtrated water at 70 ºC for 4 hours. Each filtrated solvent was pooled and evaporated under reduced pressure at temperature not exceeding 60 ºC by rotary evaporator to obtain the hexane extract, ethyl acetate extract, ethanol extract and water extract. The extraction scheme was shown as **Scheme 3-1**. All extracts were kept at 4 ºC.

```
                    ┌─────────────────────┐
                    │  Dry plant material │
                    └─────────────────────┘
                              │ + Hexane (3 times)
            ┌─────────────────┴─────────────┐
 ┌──────────────────────┐          ┌──────────┐
 │   Hexane extract      │          │   Marc   │
 │  (SSHX or NRHX)       │          └──────────┘
 └──────────────────────┘               │ + Ethyl acetate (3 times)
                        ┌────────────────┴─────────────┐
          ┌──────────────────────────┐       ┌──────────┐
          │   Ethyl acetate extract   │       │   Marc   │
          │     (SSEA or NREA)        │       └──────────┘
          └──────────────────────────┘            │ + Ethanol (3 times)
                            ┌──────────────────────┴─────────────┐
              ┌──────────────────────┐              ┌──────────┐
              │   Ethanol extract     │              │   Marc   │
              │   (SSEO or NREO)      │              └──────────┘
              └──────────────────────┘                   │ + Boiled water (3 times)
                                ┌────────────────────────┴─────────────┐
                  ┌──────────────────────┐                 ┌──────────┐
                  │   Water extract       │                 │   Marc   │
                  │   (SSWT or NRWT)      │                 └──────────┘
                  └──────────────────────┘
```
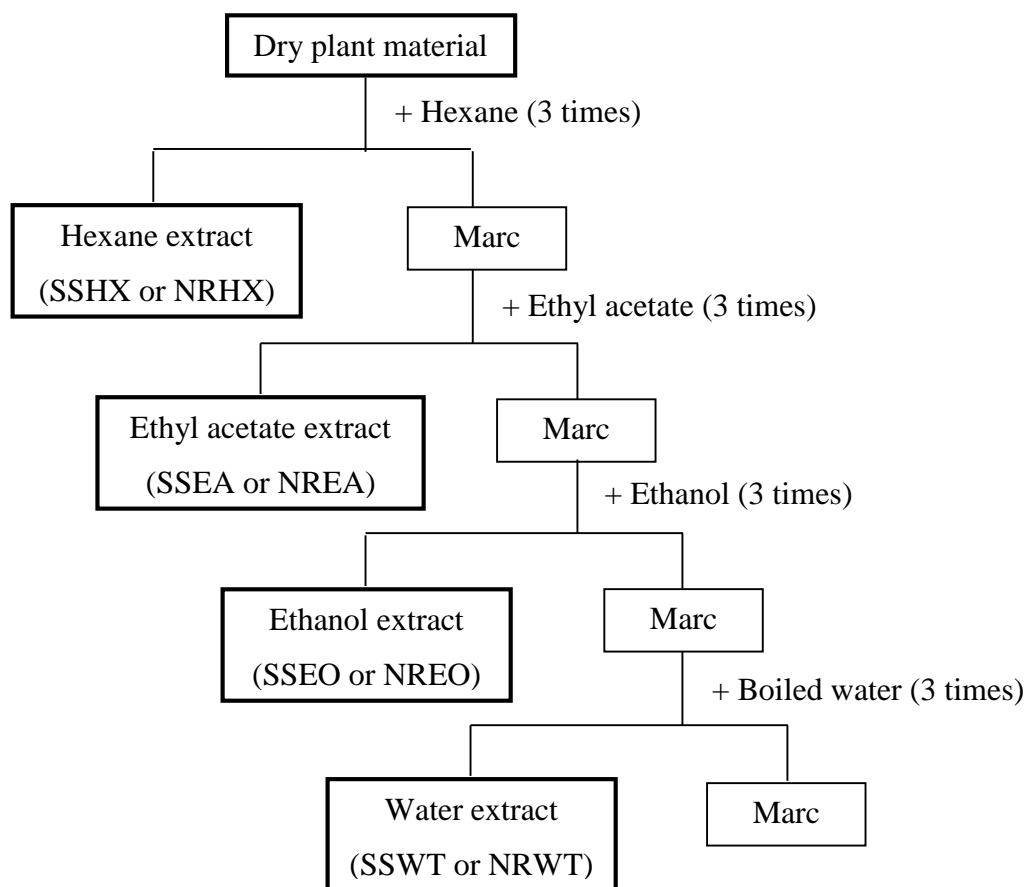
Scheme 3-1 The solvent extraction series of *S. stramonifolium* (SS) inflorescence and *N. racemosa* (NR) stem; HX = Hexane; EA = Ethyl acetate; EO = Ethanol; WT = Water

3.4 Phytochemical investigation

Briefly, the phytochemical investigation of plant extract were isolated base on the α-glucosidase inhibitory activity screening. The interested extracts of *S. stramonifolium* inflorescence and *N. racemosa* stem were separated by column chromatography such as quick column chromatography, classical column chromatography and gel filtration column chromatography. The sub-fractions from each separation were pooled and concentrated. The purity of separation was checked by thin layer chromatography (TLC) with three different solvent systems. Afterward, the isolated compounds were determined their chemical structure by using previous mention spectroscopy techniques, topic **3.2.4**.

3.4.1 Chromatographic techniques

3.4.1.1 Thin layer chromatography (TLC)

3.4.1.1.1 Normal phase TLC

Technique	:	Developing one way as upward direction
Absorbent	:	Silica gel 60 F_{254} pre-coated plate
Layer	:	0.2 mm.
Distance	:	5 to 7 cm.
Detection	:	1. Under UV- light of short wavelength (254 nm.) and long wavelength (365 nm.)
		2. Spraying with 50% sulphuric acid in ethanol and heat it at 100 ℃
		3. Spraying with anisaldehyde-sulphuric acid and heat it at 100 ℃

3.4.1.1.2 Reversed phase TLC

Technique	:	Developing one way as upward direction
Absorbent	:	Silica gel 60 RP-18 pre-coated plate
Layer	:	0.2 mm.
Distance	:	5 to 7 cm.
Detection	:	1. Under UV- light of short wavelength (254 nm.) and long wavelength (365 nm.)
		2. Spraying with anisaldehyde-sulphuric acid and heat it at 100 ℃

3.4.1.2 Quick column chromatography

Technique	:	Developing one way as downward direction with water bath pump
Absorbent	:	Silica gel 60 H (No. 9385) particle size 0.400-0.063 mm. (230-400 mesh ASTM)
Packing	:	Dry packing method
Loading	:	Dry loading method
Detection	:	The fractions were detected by normal phase

TLC as described in the previous topic 3.4.1.1.1

3.4.1.3 Classical column chromatography

Technique   :   Developing one way as downward direction

Absorbent   :   Silica gel 60 H (No. 9385) particle size 0.400-
0.063 mm. (230-400 mesh ASTM)

Packing   :   Wet packing method

Loading   :   Both dry and wet loading method

Detection   :   The fractions were detected by normal phase
TLC as described in the previous topic 3.4.1.1.1

3.4.1.4 Reversed phase column chromatography

Technique   :   Developing one way as downward direction

Absorbent   :   Silica gel RP-18 particle size 40-63 μm

Packing   :   Wet packing method

Loading   :   Wet loading method and air pump

Detection   :   The fractions were detected by reverse phase
TLC as described in the previous topic 3.4.1.1.2

3.4.1.5 Gel filtration column chromatography

Technique   :   Developing one way as downward direction

Absorbent   :   Sephadex® LH-20

Packing   :   Wet packing method

Loading   :   Wet loading method

Detection   :   The fractions were detected by TLC as described
in the previous topic 3.4.1.1

3.4.2 Isolation and purification of compounds from *S. stramonifolium* inflorescence extracts

3.4.2.1 *S. stramonifolium* inflorescence ethanol extract

The ethanol extract of *S. stramonifolium* inflorescence (SSEO) 7.34 g was isolated by using quick column with gradient solvents of hexane to ethyl

acetate and then to ethyl acetate: methanol (1:1). The given fractions were 45 fractions that were $SSEO_{A1}$ to $SSEO_{A45}$. The fraction $SSEO_{A12}$ was subjected to gel filtration column chromatography and eluted by methanol. The compound called **SS1** presented 1.0 mg. The Isolation and purification of compounds from SSEO extract were shown as **Scheme 3-2**.

```
                    ┌──────────────┐
                    │ SSEO extract │
                    └──────────────┘
                           │      ┌ ─ ─ ─ ┐
                           ├──────   I
                           │      └ ─ ─ ─ ┘
                    ┌──────────────┐
                    │  SSEO_{A12}  │
                    └──────────────┘
                           │      ┌ ─ ─ ─ ┐
                           ├──────   II
                           │      └ ─ ─ ─ ┘
                    ┌──────────────┐
                    │     SS1      │
                    └──────────────┘
```
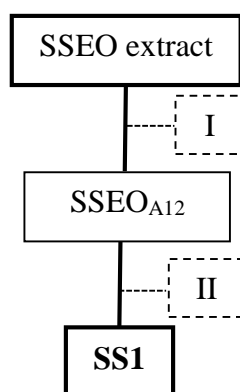
Scheme 3-2 The isolation and purification process of ethanol extract of *S. stramonifolium* inflorescence

I = Quick column chromatography [Hexane to EtOAc to EtOAc: MeOH (1:1)]

II = Gel filtration column chromatography [MeOH]

3.4.2.2 *S. stramonifolium* inflorescence hexane extract

The hexane extract of *S. stramonifolium* inflorescence (SSHX) 11.95 g was loaded to silica gel column and eluted with isocratic mode, Hexane: EtOAc (9:1). The combined fraction, $SSHX_{A32}$ to $SSHX_{A37,}$ was subjected to classical column and eluted with gradient mode, hexane to ethyl acetate to ethyl acetate: methanol (7:3). The pool fraction of $SSHX_{B18}$ to $SSHX_{B25}$ was loaded to another silica gel column with gradient mode, hexane to ethyl acetate and then to ethyl acetate: methanol (9:1). The given compound was loaded on normal phase TLC by using mixed-mobile phase of hexane: ethyl acetate: chloroform (6:2:2). TLC plates were scratched and then silica gel was washed with the mixing of hexane: ethyl acetate: chloroform (6:2:2). The compound 3.1 mg was named **SS2**.

Moreover, the combined yield of $SSHX_{B39}$ to $SSHX_{B45}$ was loaded to classical column and eluted with isocratic mode of hexane: ethyl acetate: chloroform (6:2:2). The collected fractions $SSHX_{D14}$ to $SSHX_{D34}$ were combined and loaded to the Sephadex® LH-20 column. This size exclusion chromatography was eluted with chloroform: methanol (2:8). The compound **SS1** (2.0 mg) was presented. It showed the same character as the previous **SS1**.The isolation and purification of compounds from SSHX extract were shown as **Scheme 3-3**.
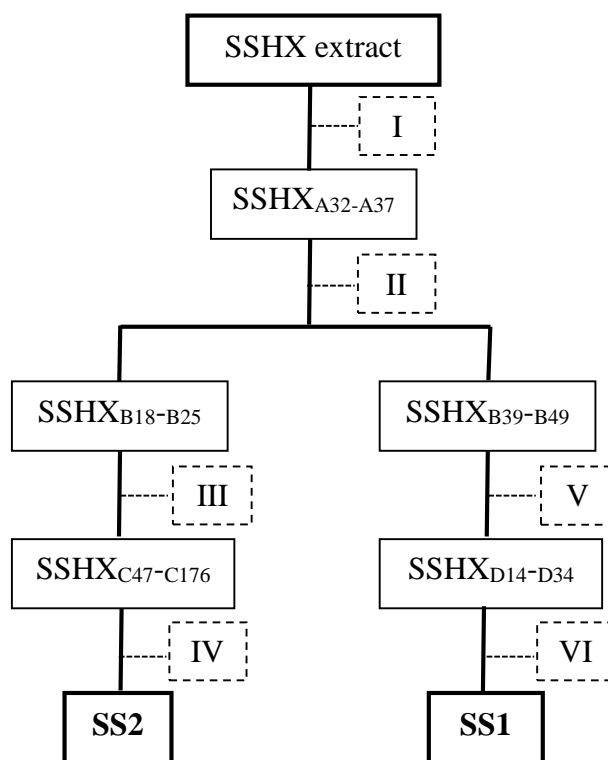
Scheme 3-3 The isolation and purification process of hexane extract of *S. stramonifolium* inflorescence

I = Classical column chromatography [Hexane: EtOAc (9:1)]

II = Classical column chromatography [Hexane to Hexane: EtOAc (7:3)]

III = Classical column chromatography [Hexane to EtOAc to EtOAc: MeOH (9:1)]

IV = Normal phase TLC [Hexane: EtOAc: $CHCl_3$ (6:2:2)]

V = Classical column chromatography [Hexane: EtOAc: $CHCl_3$ (6:2:2)]

VI = Gel filtration column chromatography [$CHCl_3$: MeOH (2:8)]

3.4.2.3 *S. stramonifolium* inflorescence ethyl acetate extract

The ethyl acetate extract of *S. stramonifolium* inflorescence (SSEA) 4.10 g was loaded to silica gel column. The mobile phase was used gradient mode that were chloroform to chloroform: methanol (1:1). The amorphous substance appeared in $SSEA_{A24}$ to $SSEA_{A32}$ fractions. They were pooled and washed by methanol. Next step, they were loaded on normal phase TLC by using mixed-mobile phase of hexane: ethyl acetate: chloroform (6:2:2). The interested band was detected under UV_{254} and scratched. The silica gel was washed by the mixing of hexane: ethyl acetate: chloroform (6:2:2). The compound **SS1** (6.0 mg) was exhibited. It showed the same character as the **SS1** which recieved from SSEO and SSHX extracts. The isolation and purification of compounds from SSEA extract were shown as **Scheme 3-4**.
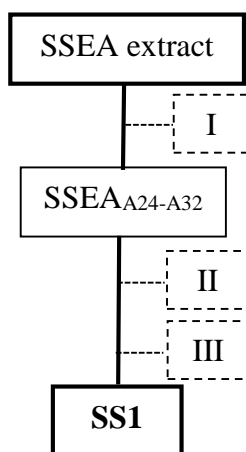
Scheme 3-4 The isolation and purification process of ethyl acetate extract of *S. stramonifolium* inflorescence

I   = Classical column chromatography [$CHCl_3$ to $CHCl_3$: MeOH (1:1)]

II   = Wash crystal [MeOH]

II   = Normal phase TLC [Hexane: EtOAc: $CHCl_3$ (6:2:2)]

3.4.2.4 *S. stramonifolium* inflorescence water extract

Firstly, the water extract of *S. stramonifolium* (SSWT) 144.10 g was separated with solvent partition method or liquid-liquid extraction. SSWT extract was dissolved by 90% of methanol in water. The extract solution was

partition with hexane. The two immiscible solvents were separated using separating funnel. The solution part of 90% of methanol in water (90% MeOH-SSWT) was evaporated to remove the methanol. The residue still had the remained water. Next step, chloroform was put into that residue. The two immiscible solvents were separated again with separating funnel. The solution of water solution was name Water-SSWT (x). Ethyl acetate was put in to Water-SSWT (x). Finally, the solution appeared two parts that were EtOAc-SSWT and Water-SSWT. After these solvent partition, four solution parts including Hexane-SSWT, CHCl₃-SSWT, EtOAc-SSWT and Water-SSWT were received as **Scheme 3-5**.

```
                        ┌─────────────────┐
                        │   SSWT extract  │
                        └─────────────────┘
                                 │ + 90% MeOH in Water
                                 │ + Hexane
                ┌────────────────┴────────────────┐
        ┌───────────────┐              ┌───────────────────┐
        │ Hexane-SSWT   │              │  90 % MeOH-SSWT   │
        └───────────────┘              └───────────────────┘
                                                 │ - MeOH (by evaporation)
                                                 │ + CHCl₃
                                ┌────────────────┴────────────────┐
                        ┌───────────────┐              ┌───────────────────┐
                        │ CHCl₃-SSWT    │              │  Water-SSWT (x)   │
                        └───────────────┘              └───────────────────┘
                                                                 │ + EtOAc
                                                ┌────────────────┴────────────────┐
                                        ┌───────────────┐              ┌───────────────┐
                                        │ EtOAc-SSWT    │              │  Water-SSWT   │
                                        └───────────────┘              └───────────────┘
```
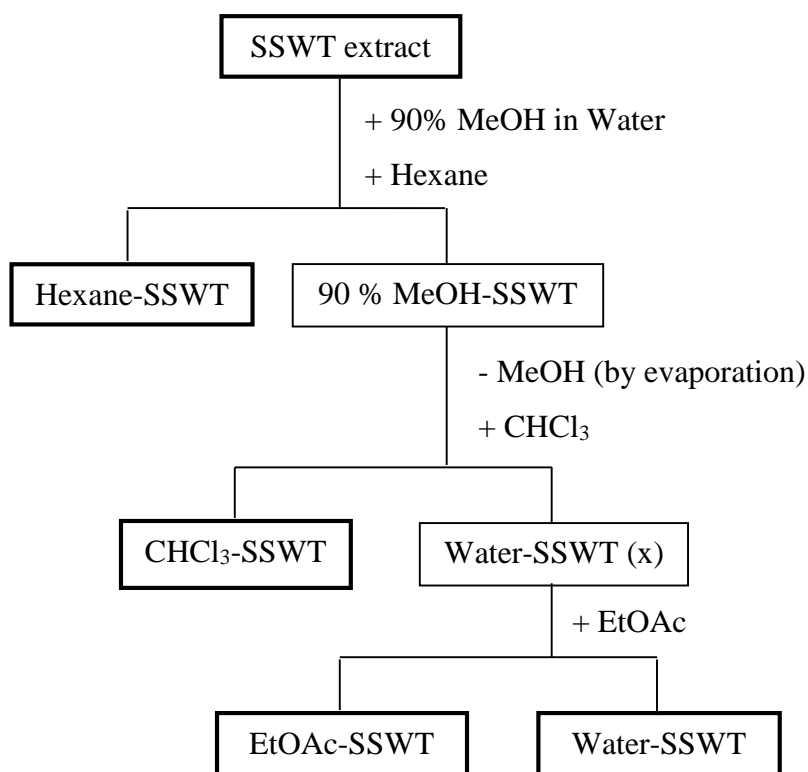
Scheme 3-5 The solvent partition of *S. stramonifolium* water extract

The EtOAc-SSWT extract from the previous liquid-liquid extraction was continued to separate. It was loaded to quick column using gradient solvents of hexane to chloroform to ethyl acetate and to ethyl acetate:

methanol (7:3). The combined fractions of EtOAC-SSWT$_{A10}$ and EtOAC-SSWT$_{A11}$ were isolated by Sephadex$^{®}$ LH-20 column with methanol as mobile phase. The compound named **SS3** presented 2.0 mg.

The other fractions that is EtOAC-SSWT$_{A15}$ were separated by gel filtration column using methanol mobile phase. The achieve yield of **SS4** was 2.0 mg. Furthermore, the two combined fractions that were EtOAC-SSWT$_{B36}$ to EtOAC-SSWT$_{B39}$ and EtOAC-SSWT$_{B48}$ to EtOAC-SSWT$_{B50}$ were continued to separate.

The combined fractions of EtOAC-SSWT$_{B36}$ to EtOAC-SSWT$_{B39}$ were loaded to gel filtration column and eluded by methanol. The combined yield of EtOAC-SSWT$_{C20}$ to EtOAC-SSWT$_{C35}$ was purified by normal phase with chloroform: methanol (9:1) as mobile phase. The interested band on TLC plates was detected under UV$_{254}$ and scratched. The silica gel powder was washed by the mixing of chloroform: methanol (9:1). The compound called **SS5** was presented 1.0 mg. For another separation, the combined fractions of EtOAC-SSWT$_{B48}$ to EtOAC-SSWT$_{B50}$ were loaded to reversed phase (RP-18) column using the isocratic mobile phase as methanol: water (1:1). The collected yield was **SS6** (1.6 mg). The Isolation and purification of compounds from EtOAc-SSWT extract were shown as **Scheme 3-6**.

```
                           ┌─────────────────────┐
                           │    EtOAc-SSWT        │
                           └─────────────────────┘
                                     ┊  ┌┈┈┈┐
                                     ┊┈┈┊ I ┊
                                        └┈┈┈┘
          ┌─────────────────────┐         ┌─────────────────────┐
          │ EtOAc-SSWT A10-A11  │         │   EtOAc-SSWT A15    │
          └─────────────────────┘         └─────────────────────┘
                   ┊  ┌┈┈┈┐                         ┊  ┌┈┈┈┐
                   ┊┈┈┊ II ┊                        ┊┈┈┊ III┊
                      └┈┈┈┘                            └┈┈┈┘
          ┌──────┐                                              ┌──────┐
          │ SS3  │  ┌──────────────────┐ ┌──────────────────┐   │ SS4  │
          └──────┘  │ EtOAc-SSWT B36-B39│ │EtOAc-SSWT B48-B50│   └──────┘
                    └──────────────────┘ └──────────────────┘
                          ┊  ┌┈┈┈┐              ┊  ┌┈┈┈┐
                          ┊┈┈┊ IV┊              ┊┈┈┊ VI┊
                             └┈┈┈┘                 └┈┈┈┘
                    ┌──────────────────┐      ┌──────┐
                    │EtOAc-SSWT C20-C35│      │ SS6  │
                    └──────────────────┘      └──────┘
                          ┊  ┌┈┈┈┐
                          ┊┈┈┊ V ┊
                             └┈┈┈┘
                        ┌──────┐
                        │ SS5  │
                        └──────┘
```
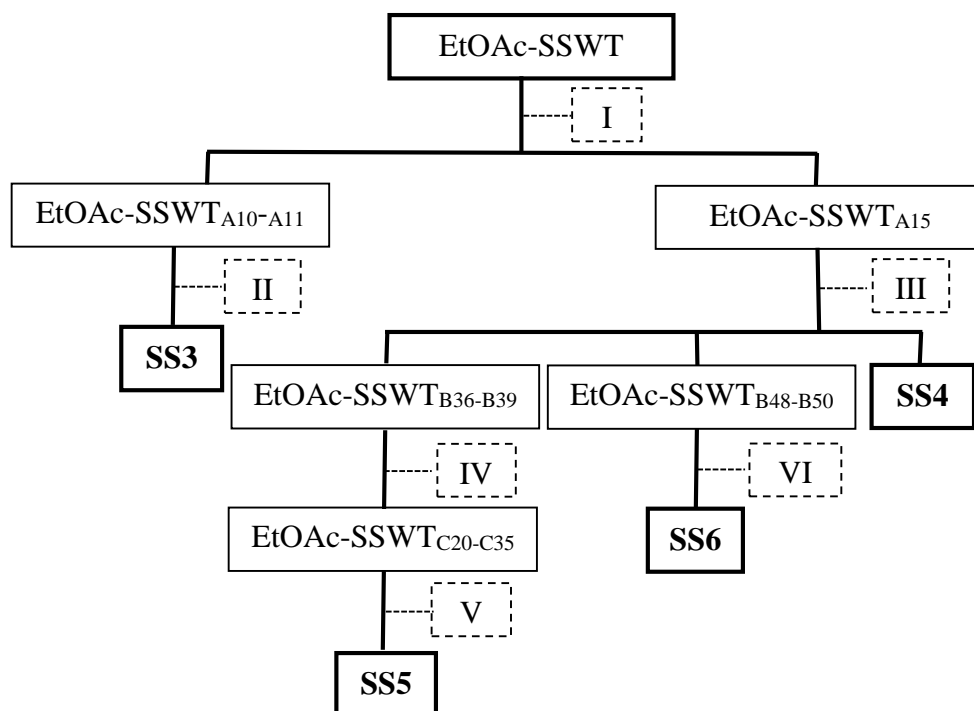
Scheme 3-6 The isolation and purification process of *S. stramonifolium* inflorescence water extract

I   = Quick column chromatography [Hexane to $CHCl_3$ to EtOAc to EtOAc: MeOH (7:3)]

II = Gel filtration column chromatography [MeOH]

III = Gel filtration column chromatography [MeOH]

IV = Gel filtration column chromatography [MeOH]

V   = Normal phase TLC [$CHCl_3$: MeOH (9:1)]

VI = Reversed phase column chromatography [MeOH: H_2O (1:1)]

3.4.3 Isolation and purification of compounds from *N. racemosa* stem ethanol extracts

The ethanol extract of *N. racemosa* (NREO) 25.01 g was isolated via quick column using gradient of hexane to ethanol to give 16 fractions that were $NREO_{A1}$ to $NREO_{A16}$. The fractions $NREO_{A7}$ and $NREO_{A8}$ were combined and loaded to the classical column by using the gradient of mobile phase as chloroform to chloroform: methanol (1:1) to achieve 12 fractions that were $NREO_{B1}$ to $NREO_{B12}$. The combined fractions of $NREO_{B4}$ to $NREO_{B5}$ were subjected to gel filtration column to collected 6 fractions, $NREO_{C1}$ to $NREO_{C6}$. $NREO_{C4}$ and $NREO_{C5}$ were

pooled and further separated by to the classical column by using the gradient mobile phase with increasing the solvent mixing from chloroform to ethyl acetate and then to ethyl acetate: methanol (9:1). The compound named **NR1** presented 3.9 mg.

The fractions NREO$_{B8}$ and NREO$_{B9}$ were combined and subjected to the classical column with the gradient mobile phase from dichloromethane to ethyl acetate and then to ethyl acetate: methanol (9:1). The given fractions were NREO$_{D1}$ and NREO$_{D15}$. The pooled fractions of NREO$_{D10}$ to NREO$_{D15}$ were washed by ethyl acetate to yield 1.9 mg of **NR2**.

The combined fractions of NREO$_{A13}$ and NREO$_{A14}$ were separated by the classical column with the gradient mobile phase as ethyl acetate to ethyl acetate: methanol (1:1). Sixteen fractions (NREO$_{E1}$ to NREO$_{E16}$) were collected. The fractions NREO$_{E6}$ and NREO$_{E7}$ were pooled and loaded to the classical column with the gradient mobile phase by using chloroform to chloroform: methanol (1:1) to achieve 1.4 mg of **NR3**.

The fractions NREO$_{A10}$ was chromatographed on classical column with gradient mobile phase from hexane: ethyl acetate (1:1) to ethyl acetate: methanol (9:1). Twenty-three fractions, NREO$_{F1}$ to NREO$_{F23}$, were presented. Fractions NREO$_{F8}$ to NREO$_{F11}$ were pooled and partitioned with 3 solvents including hexane, chloroform and methanol. The methanol part (MeOH-NREO$_{F8-F11}$) was subjected to the classical column with gradient mobile phase from chloroform to chloroform: methanol (9:1). The isolated compounds were **NR4** (1.8 mg) and **NR5** (9.9 mg). The isolation and purification of compounds from NREO extract were shown as **Scheme 3-7**.
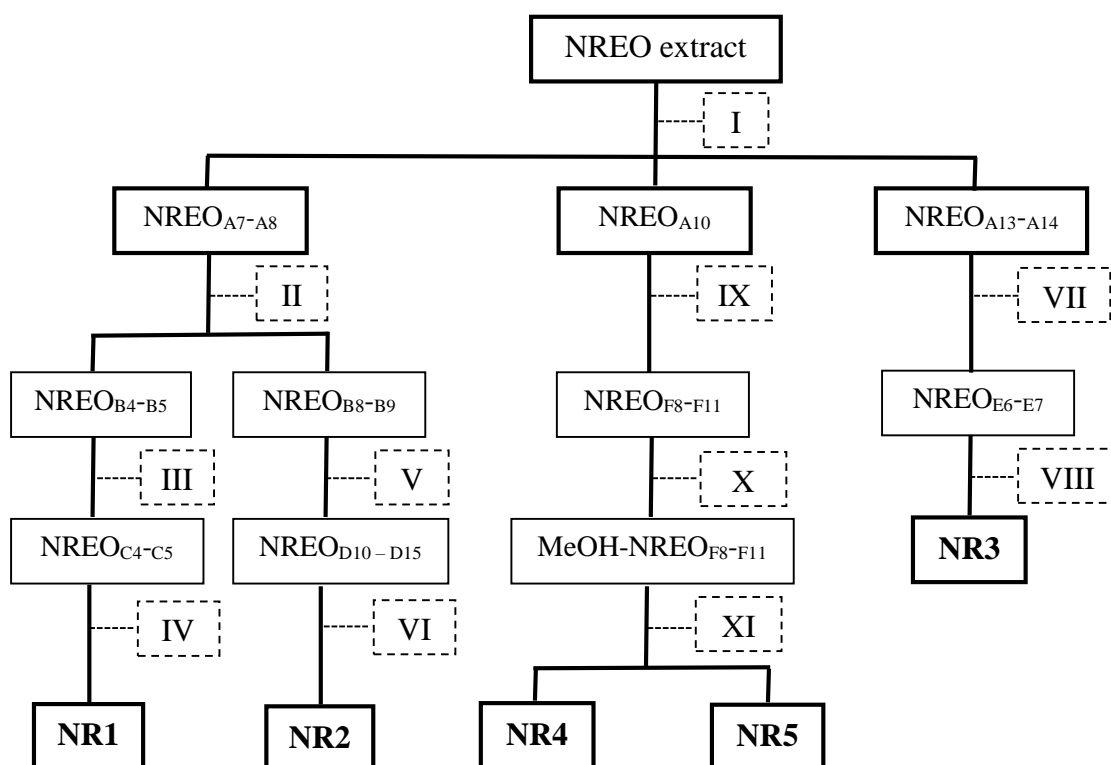
Scheme 3-7 The isolation and purification process of ethanol extract of *N. racemosa* stem

I   = Quick column chromatography [Hexane to EtOH]

II   = Classical column chromatography [$CHCl_3$ to $CHCl_3$: MeOH (1:1)]

III   = Gel filtration column chromatography [MeOH]

IV   = Classical column chromatography [$CHCl_3$ to EtOAc to EtOAc: MeOH (9:1)]

V   = Classical column chromatography [CH_2Cl_2 to EtOAc to EtOAc: MeOH (9:1)]

VI   = Wash by EtOAc

VII   = Classical column chromatography [EtOAc to EtOAc: MeOH (1:1)]

VIII   = Classical column chromatography [$CHCl_3$ to $CHCl_3$: MeOH (1:1)]

IX   = Classical column chromatography [Hexane: EtOAc (1:1) to EtOAc: MeOH (9:1)]

X   = Partition by Hexane, $CHCl_3$ and MeOH

XI   = Classical column chromatography [$CHCl_3$ to $CHCl_3$: MeOH (1:1)]

3.5 Biological determination

        The α-glucosidase inhibitory activity assay was performed following by Dej-adisai and Pitakbut (2015). The principle of α-glucosidase activity is the catalytic reaction of glucosidase enzyme. The enzyme catalyzes *p*-nitrophenol-α-D-glucopyranoside (*p*NPG), the translucent substrate, into *p*-nitrophenol (*p*NP) as following **Figure 3-1**. If sample has the inhibitory effect to enzyme activity, the enzyme reaction is stopped or slowly appear. The yellow yield of *p*NP was determined by colorimetric method using SPECTROstar Nano BMG Labtech microplate reader at 405 nm. The absorbed value varies directly as the *p*NP amount from the reaction.

para-nitrophenyl-α-D-glucopyranoside   α-glucopyranoside   *para*-nitrophenol
(yellow color)
absorb UV at 405 nm
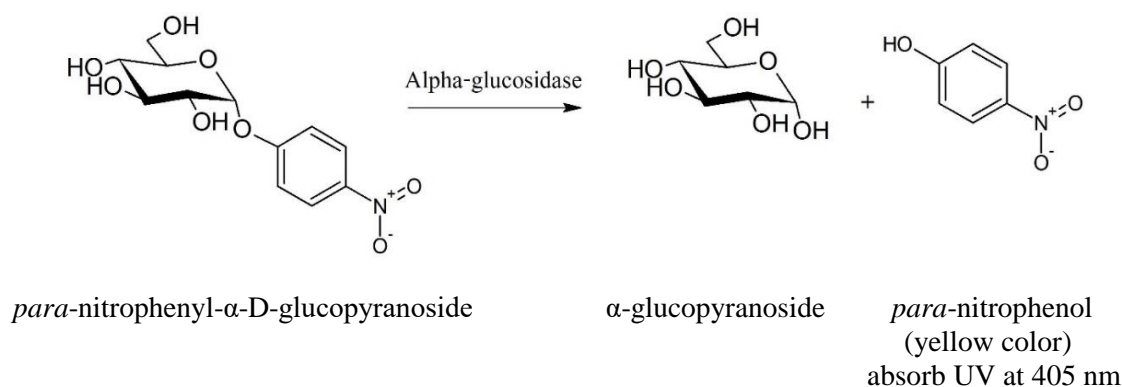
Figure 3-1 The reaction and determination of α-glucosidase activity (Dej-adisai and
         Pitakbut, 2015)

3.5.1 Solution preparation

3.5.1.1 Preparation of 0.01 M phosphate buffer (pH7)

        Firstly, the solution was prepared separately as 0.02 M $NaH_2PO_4.H_2O$ solution (call as solution A) and 0.02 M Na_2HPO_4 (call as solution B). The solution A prepared by dissolving $NaH_2PO_4.H_2O$ 0.312 g of with 100 ml of distilled water. The solution B prepared by dissolving Na_2HPO_4 0.284 g with 100 ml of distilled water. Afterward, the appropriate volumes of solution A and solution B were mixed until given the mixing solution (call as solution AB) that had pH 7. Finally, the solution AB was diluted by the equal volume

of distilled water to given the 0.01 M phosphate buffer (pH7) of stock solution.

The stock solution was kept in the refrigerator at 4 ºC. Before using, this solution was added bovine serum albumin (BSA) and sodium azide (NaN_3) as the concentration 0.2 mg/ml and 0.02 mg/ml, respectively.

3.5.1.2 Preparation of α-glucosidase enzyme solution (1 U/ml)

The α-glucosidase 1 unit from *Saccharomyces cerevisiae* (Type I, lyophilized powder, Sigma, EC 3.2.1.20) was dissolved in 1 ml of in used phosphate buffer solution.

3.5.1.3 Preparation of *para*-nitrophenyl-α-D-glucopyranoside

The *p*-nitrophenyl-α-D-glucopyranoside (*p*NPG), MW. = 301.25 g/mol., was used as the substrate of α-glucosidase activity reaction. The *p*NPG stock was prepared as 4 folds of the final concentration in the reaction.

For determination of α-glucosidase inhibitory activity, inhibitory concentration at 50 percentage (IC_{50}) and combination test, 4 mM *p*NPG was prepared by weighting 1.21 mg and then dissolved in 1 ml of in used phosphate buffer solution. For enzyme kinetic determination, 20 mM *p*NPG was prepared by weighting 6.025 mg and then dissolved in 1 ml of in used phosphate buffer solution. The concentrations of *p*NPG in this experiment were as 10, 5, 2.5 1.25 and 0.625 mM, respectively. They were prepared by series dilution from 20 mM *p*NPG.

3.5.1.4 Preparation of samples and standard drugs

The samples and standard drugs were diluted in 20% dimethylsulfoxide (DMSO) in distilled water. This prepared concentration was 4 folds of the final concentration in the reaction.

3.5.2 Determination of α-glucosidase inhibitory activity

In this experiment, the assay was tested in 96 wells plate and prepared solutions were described in the previous topic **3.5.1**. First step, 50 μl of 0.01 M

phosphate buffer with BSA and NaN$_3$ (PBS) added into well plate. Secondly, 50 µl of prepared samples or standard drugs was filled. Each tested sample or standard drug condition was repeated in 3 wells. Thirdly, 50 µl of α-glucosidase enzyme solution was added to wells. Moreover, the blank tested well which contained 100 µl of PBS and 50 µl of tested solution was also prepared. Afterward, the mixture solution in plate was incubated at 37°C for 2 minutes. Finally, 50 µl of *p*NPG was added in the wells. The *p*NP was performed and monitored at 405 nm every 1 minute for 20 minutes by microplate reader. The measured absorbance of tested wells was deleted with the measured absorbance of blank wells before using for the velocity calculation. The velocity was demined by relationship equation between the mention absorbance and time as following **Equation 1**.

Equation 1 $\text{Initial velocity (Vi)} = \dfrac{\Delta \text{absorbance at 405 nm}}{\Delta \text{Time}}$

The initial velocity (V_i) from initial reaction of each sample was determined and the percentage of inhibition was further calculated by **Equation 2** as showed below.

Equation 2 $\% \text{inhibition} = \dfrac{V_{i\,control} - V_{i\,sample}}{V_{i\,control}} \times 100$

3.5.3 Determination of the inhibitory concentration at 50 percentage (IC$_{50}$)

For this experiment, the samples were also determined the inhibitory concentration at 50 percentage (IC$_{50}$). The IC$_{50}$ value was received from the calibration plotted between percentages of inhibition and five concentrations of samples.

3.5.4 Enzyme kinetic determination

The selected extracts and compounds were determined the mode of inhibition by using the double reciprocal Linewerver-Burk plot manner. The Linewerver-Burk

plots was provided from **Equation 3**. The secondary plots conducted inhibition constant, Ki or Ki′. The Ki value was shown when the inhibitor binds to free enzyme of competitive inhibition. In the other way, Ki′ value was presented when the inhibitor binds to enzyme-substrate complex of uncompetitive inhibition. This experimental used the similar enzyme inhibition procedure as mention topic **3.5.2**. However, 5 concentrations of *p*NPG (2.5-0.15625 mM) and 3 concentrations of tested sample were evaluated for the inhibition manner.

Equation 3

$$\frac{1}{V} = \frac{K_m}{V_{max}}\left(\frac{1}{S}\right) + \frac{1}{V_{max}}$$

K_m = Michalis constant

V = velocity

V_{max} = maximum velocity

S = concentration of the substrate

3.5.5 Combination test

This experiment was generated by the computer software, CompuSyn®. However, the percent inhibition values of single sample and combined sample with acarbose 250 μg/ml gained from the laboratory experiment as previous topic **3.5.2**. This combination design was non-constant ratio. The combination index (CI) and the plots were automated by the CompuSyn®. The combined effect to α-glucosidase was analyzed from the plot of fraction affected (F_a) versus combination index (CI) and the normalized isobologram. Normally, the quantitative CI were defined to synergism as CI < 1, additive effect as CI = 1 and antagonism as CI > 1 (Chou, 2010). The expanded definition of the quantitative CI was presented in **Table 3-4**.

Table 3-4 The combination index (CI) description

Combination index range	Description (Chou, 2006)	Combination index range	Description (Chou, 2010)
< 0.1	Very strong synergism		
0.10 - 0.30	Strong synergism		
0.30 - 0.70	Synergism	<1	Synergism
0.70 - 0.85	Moderate synergism		
0.85 - 0.90	Slight synergism		
0.90 - 1.10	Nearly additive	1	Additive
1.10 - 1.20	Slight antagonism		
1.20 - 1.45	Moderate antagonism		
1.45 - 3.30	Antagonism	>1	Antagonism
3.30 - 10.00	Strong antagonism		
> 10.00	Very strong antagonism		

3.6 Molecular docking study

The docking experiment was operated by Mr. Thanet Pitabut, Ph.D. candidate at Department of Biochemical and Chemical Engineering, Technical University of Dormund, Dortmund, Germany. Before generated experiment, both target enzyme and compounds was prepared. The crystal structure of target protein, α-glucosidase (PDB ID: 3a4a) was obtained from RCB Protein Data Bank (http://www.rcsb.org). The chemical structure of isolated compounds from *S. stramonifolium* inflorescence and *N. racemosa* stem was downloaded from Pubchem (https://pubchem.ncbi.nlm.nih.gov).

Autodock Tool version 1.5.6 was used to prepare α-glucosidase and to identify the active site. The native glucose molecule was used as a guideline (Chetty and Soliman, 2015). The three-dimension grid of active site was presented center of x axis = 21.1, center of y axis = -7.4 and center of z axis = 24.2, respectively. The compounds of *S. stramonifolium* and *N. racemosa* were separated docking. The grid size of the isolated compounds from *S. stramonifolium* were set as 16 Å × 16 Å × 16 Å, while the grid size of the isolated compounds from *N. racemosa* were set as 17 Å × 17 Å × 17 Å. In this study, the two steps energy minimization of compounds used Avogadro Version 1.2.0,

while a geometric optimization used a general amber force field, GAFF (Hanwell *et al*., 2012). These parameters were set as a default except the exhaustiveness value which adjusted to 24. To validated docking experiment, the glucose molecule was re-docked into the identified active site. The accepted criterion of re-docking was since the root-mean-square deviation (RMSD) was less than 1 Å (Morris *et al*., 2009). For post-docking analysis, viewdock package of Chimera version 1.11.2 (Pettersen *et al*., 2004) was used to present the molecular interaction and evaluated the outcomes. Moreover, Autodock 4.2.6 was also used for evaluation of binding energy (Morris *et. al*., 2009; Dej-adisai *et. al*., 2021).

CHAPTER 4

RESULTS AND DISCUSSION

4.1 Screening on α-glucosidase inhibition of *S. stramonifolium* inflorescence and *N. racemosa* stem extracts

Initially, the dried *S. stramonifolium* inflorescence (481.61 grams) and *N. racemosa* stem (3.10 kilograms) were separately extracted by the series of solvent polarity. They were extracted by hexane (the lowest polarity solvent), ethyl acetate, ethanol, and boil water (the highest polarity solvent), respectively. All fractionated extracts of *S. stramonifolium* inflorescence and *N. racemosa* stem were tested on α-glucosidase inhibitory activity. The yield and the biological activity of *S. stramonifolium* inflorescence are shown in **Table 4-1**, while those of *N. racemosa* stem extracts are presented in **Table 4-2**.

Table 4-1 The percent yield and α-glucosidase inhibition of *S. stramonifolium* (SS) inflorescence extracts

No.	Extracted solvent	Code	Weight (g)	% Yield	% Inhibition at 2 mg/ml ± SD	IC_{50} (μg/ml)
1.	-	SS-Materials	487.61	-	-	-
2.	Hexane	SSHX	11.95	2.45	11.65 ± 9.44	3,134.85
3.	Ethyl acetate	SSEA	4.10	1.01	92.79 ± 1.07	215.92
4.	Ethanol	SSEO	7.34	1.51	96.63 ± 0.65	221.67
5.	Water	SSWT	144.10	29.55	69.34 ± 1.76	324.44
6.	Positive standard	Acarbose	-	-	76.44 ±3.06	241.40

Table 4-2 The percent yield and α-glucosidase inhibition of *N. racemosa* (NR) stem extracts

No.	Extracted solvent	Code	Weight (g)	% Yield	% Inhibition at 2 mg/ml ± SD	IC$_{50}$ (µg/ml)
1.	-	NR-Materials	3.10*	-	-	-
2.	Hexane	NRHX	3.89	0.13	28.93 ± 6.32	56.81**
3.	Ethyl acetate	NREA	5.27	0.17	92.44 ± 0.94	191.44
4.	Ethanol	NREO	39.24	1.27	98.82 ± 3.78	39.65
5.	Water	NRWT	147.40	4.75	46.21 ± 4.42	4.02***
6.	Positive standard	Acarbose	-		84.22 ± 1.23	245.95

* kg, ** g/ml, *** mg/ml

The high yields of both plant materials were water part. The α-glucosidase inhibition results of *S. stramonifolium* showed that the ethyl acetate extract (IC$_{50}$ = 215.92 µg/ml) and the ethanol extract (IC$_{50}$ = 221.67 µg/ml) exhibited the strong inhibitory activity over the standard drug, acarbose (IC$_{50}$ = 241.40 µg/ml). In the same way, the ethyl acetate and the ethanol extracts of *N. racemosa* showed the higher IC$_{50}$ values at 191.44 and 39.65 µg/ml, respectively, than IC$_{50}$ values of the acarbose at 245.95 µg/ml. These strong biological activities of the extracts were brought to further phytochemical investigation.

4.2 Structure determination of isolated compounds

Totally, eleven compounds were isolated, elucidated chemical structure through spectroscopic techniques such as Nuclear Magnetic Resonance (NMR), Mass Spctra (MS), Ultra-violet (UV) and Infra-red (IR), and compared with previous reports. Six compounds (**Figure 4-1**) were obtained from *S. stramonifolium* inflorescence and were determined as myricetin 3, 7, 4′, 5′-tetramethyl ether (SS1), combretol (SS2), kaempferol (SS3), kaempferol-7-O-β-glucopyranoside (SS4), 5-hydroxy-3, 7, 4′, 5′-tetramethoxyflavone-3′-*O*-glucopyranoside (SS5), mixture of isorhamnetin-3-*O*-

glucopyranoside (SS6-1) and kaempferol-3-*O*-glucopyranoside (SS6-2). Five compounds (**Figure 4-2**) were obtained from *Neuropeltis racemosa* stem and were identified as scopoletin (NR1), syringic acid (NR2), methyl 3-methyl-2-butenonoate (NR3), *trans-N*-feruloyltyramine (NR4) and *trans-N*-coumaroyltyramine (NR5).

Myricetin 3, 7, 4′, 5′-tetramethyl ether
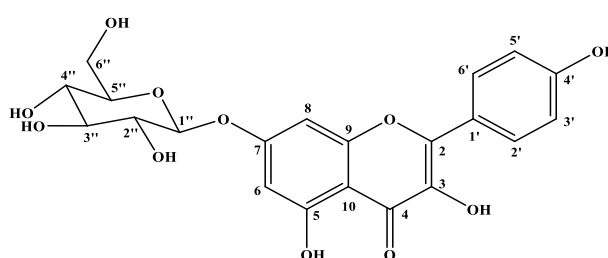
(SS1)

Combretol

(SS2)

Kaempferol

(SS3)

Kaempferol-7-*O*-β-glucopyranoside

(SS4)
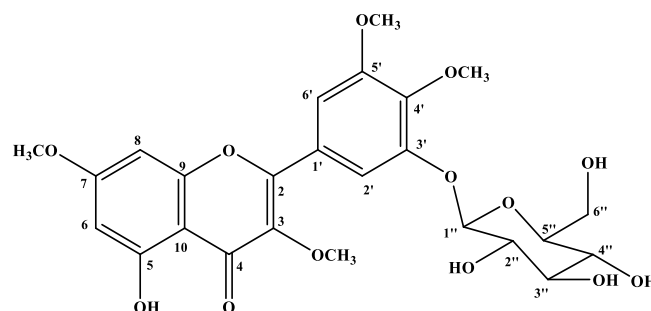
5-Hydroxy-3, 7, 4′, 5′-tetramethoxyflavone-3′-*O*-glucopyranoside

(SS5)

Figure 4-1 Isolated compounds from *S. stramonifolium* inflorescence

Isorhamnetin-3-*O*-glucopyranoside
(SS6-1)

Kaempferol-3-*O*-glucopyranoside
(SS6-2)
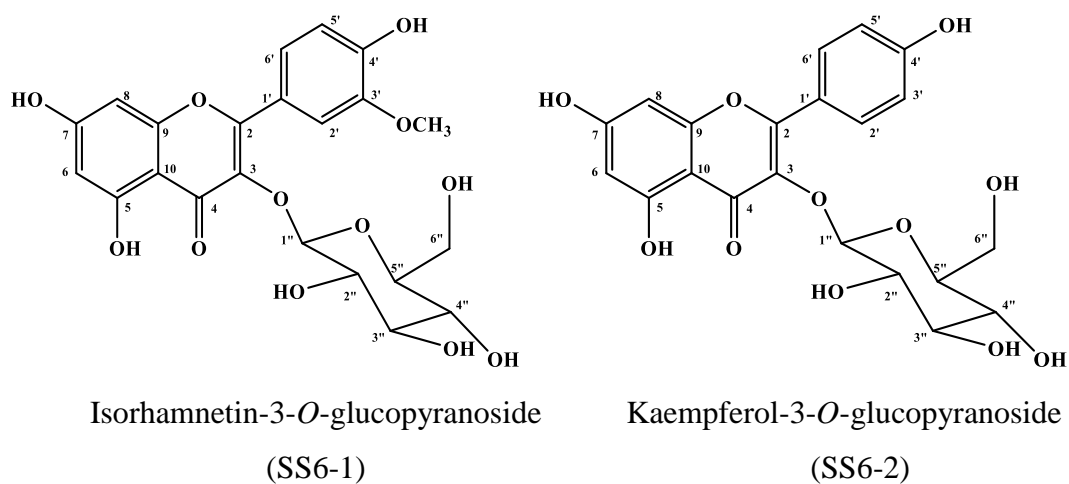
Figure 4-1 Isolated compounds from *S. stramonifolium* inflorescence (**continued**)

Scopoletin
(NR1)

Syringic acid
(NR2)

Methyl 3-methyl-2-butenonoate
(NR3)

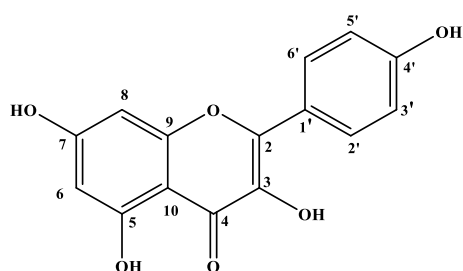*trans-N*-Feruloyltyramine
(NR4)

trans-N-Coumaroyltyramine
(NR5)

Figure 4-2 Isolated compounds from *N. racemosa* stem
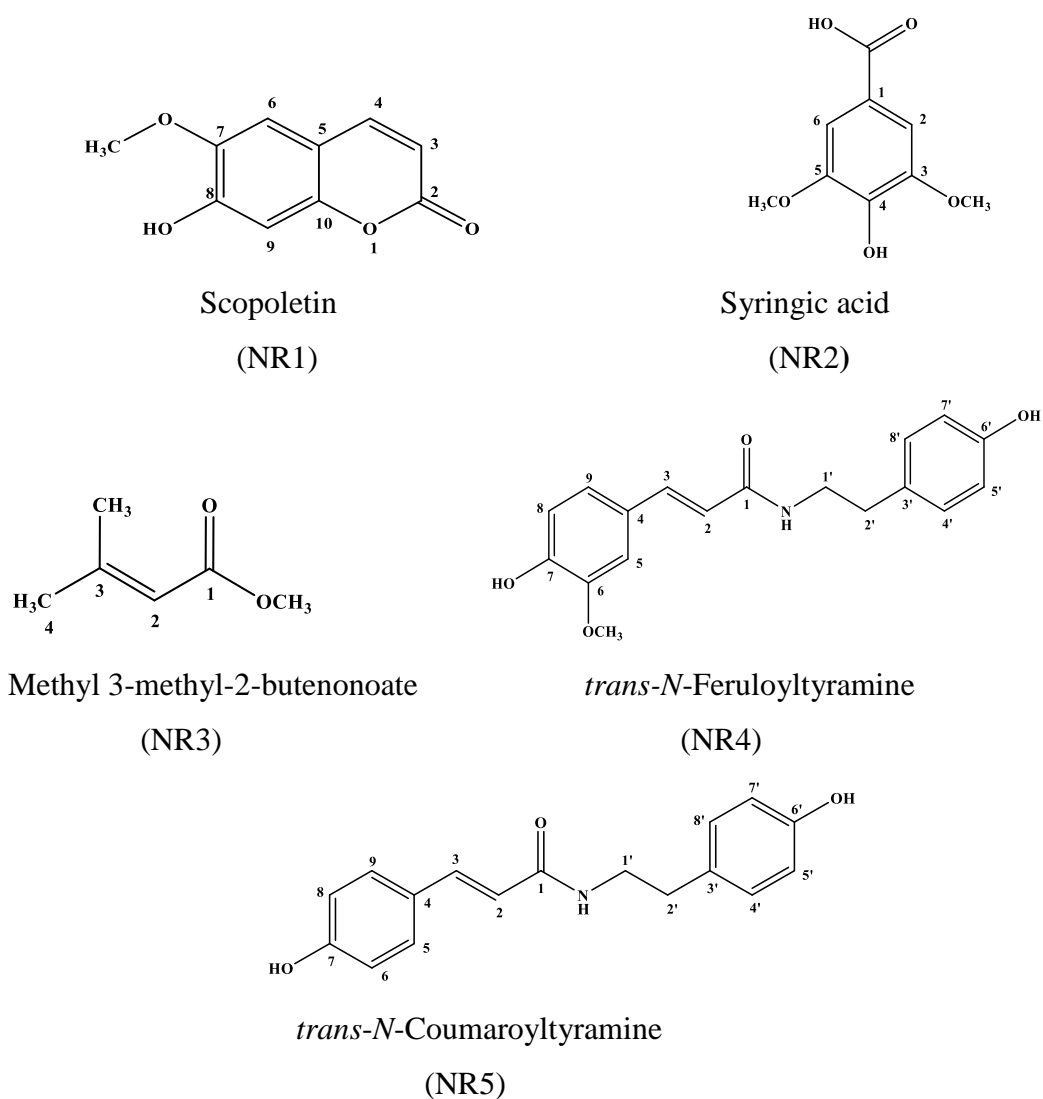
4.2.1 The isolated compounds from *S. stamonifolium* inflorescence

4.2.1.1 Structure determination of SS1

Molecular formula   : $C_{19}H_{18}O_8$

ESI Mass $(M-H)^-$: 373.0929

        SS1 (9 mg) was obtained as a yellow amorphous solid and dissolved in chloroform. The UV spectrum in chloroform (**Appendix 1**) showed λ_{max} at 270 and 330 nm. IR spectrum (**Appendix 2**) demonstrated absorption band at 3436 cm^{-1} (-OH), 2963 cm^{-1} (-CH$_3$), 1651 cm^{-1} (C=O), 1594-1455 cm^{-1} (C=C), 1260-1160 cm^{-1}(-OCH$_3$), 1104-1027 cm^{-1} (-C-O) and 803 (=C-H).

        The ^{1}H-NMR spectrum of SS1 (500 MHz in CDCl$_3$, **Appendix 3**) exhibited four doublet and six singlet proton signals. Two doublet signals at δ_H 6.34 (1H, d, J = 2.19 Hz) and 6.42 (1H, d, J = 2.19 Hz) were assigned as H-6 and H-8, respectively. Other two doublet signals at δ_H 7.34 (1H, d, J = 2.00 Hz) and 7.33 (1H, d, J = 2.00 Hz) were determined as the *meta*-protons of ring B due to J-value. Four of six singlet proton signals, δ_H 3.859, 3.860, 3.92 and 3.98, belong to four methoxy groups due to chemical shifts and 3H integration ratio of each signal. Other singlet proton signals (δ_H 5.90 and 12.55) were distinguished as two phenolic hydroxyl groups based on their chemical shifts. The phenolic hydroxyl group at δ_H 12.55 (OH-5) was shifted downfield which was the effect of hydrogen bonding with the carbonyl group. ^{1}H NMR data of SS1 in CDCl$_3$ were compared with previous report (Demetzoc *et al*., 2001) as **Table 4-3**.

        The ^{13}C-NMR spectrum of SS1 (125 MHz in CDCl$_3$, **Appendix 4**) showed nineteen carbon signals (**Table 4-4**) that were determined as eight oxygenated aromatic carbon signals, four tertiary aromatic carbon signals, four methoxy carbon signals, two quaternary carbon signals and one carbonyl signal. The chemical shifts of eight oxygenated aromatic carbon signals showed at δ_C 137.74, 139.50, 149.17, 152.03, 155.33, 156.74, 161.98 and 165.57. Two of four tertiary aromatic carbon signals at δ_C 92.17 and 97.95 were assigned as C-8 and C-6, respectively. The remaining tertiary aromatic carbon signals at δ_C 104.99 and 108.55 were determined as C-2′ and C-6′. The signals at δ_C 105.00 and 125.95 were indicated as the two quaternary carbons at C-10 and C-1′, respectively. The four methoxy carbon signals were also presented at δ_C 55.83, 56.07, 60.33 and 61.11. Moreover, the carbonyl signal was found at δ_C 178.83.

When these ^{13}C-NMR data was compared with the previous report of myricetin 3, 7, 4′, 5′-tetramethyl ether in CDCl$_3$ (Datta *et al*., 2000) as **Table 4-4**.

The HMBC experiment was also used to confirm the correlation signals of SS1. H-6 and H-8 exhibited correlation with carbon of ring A. H-6′ showed correlation with the resonance at δ_C 155.33 (C-2) that were presented the binding between ring B and ring C. Moreover, four methoxy groups were correlated with four oxygenated aromatic carbons. HMBC data of SS1 were showed in **Table 4-5** and **Figure 4-3**. The structure of SS1 (**Figure 4-1**) was determined as myricetin 3, 7, 4′, 5′-tetramethyl ether. The HR-ESIMS data of SS1 showed [M-H]$^-$ peak at *m/z* 373.0929 (**Appendix 5**) which agreed with myricetin 3, 7, 4′, 5′-tetramethyl ether molecular weight.

Table 4-3 The comparison of ^{1}H-NMR spectral data between SS1 and myricetin 3, 7, 4′, 5′-tetramethyl ether

Position	δ_H (ppm)	
	SS1 in CDCl$_3$ (^{1}H: 500 MHz)	**myricetin 3, 7, 4′, 5′-tetramethyl ether in CDCl$_3$** (^{1}H: 300 MHz) (Demetzoc *et al*., 2001)
6	6.34 (d, 2.19)	6.33 (d)
8	6.42 (d, 2.19)	6.42 (d)
2′	7.34 (d, 2.00)	7.33 (d)
6′	7.33 (d, 2.00)	7.31 (d)
OCH$_3$-3	3.860 (s)	3.98 (s)
OCH$_3$-7	3.859 (s)	3.85 (s)
OCH$_3$-4′	3.98 (s)	3.86 (s)
OCH$_3$-5′	3.92 (s)	3.92 (s)
OH-5	12.55 (s)	12.54 (s)
OH-3′	5.90 (brs)	5.93 (brs)

Table 4-4 The comparison of ^{13}C-NMR spectral data between SS1 and myricetin 3, 7, 4′, 5′-tetramethyl ether

Position	δ$_C$ (ppm)	
	SS1 in CDCl₃ **(^{13}C: 125 MHz)**	**myricetin 3, 7, 4′, 5′-tetramethyl ether in CDCl₃ (^{13}C: 125 MHz)** (Datta *et al*., 2000)
2	155.33	155.3
3	139.50	139.7
4	178.83	178.8
5	161.98	162.0
6	97.95	98.0
7	165.57	165.6
8	92.17	92.2
9	156.74	156.8
10	105.00	106.1
1′	125.95	126.0
2′	108.55	108.6
3′	149.17	149.2
4′	137.74	137.8
5′	152.03	152.0
6′	104.99	105.1
OCH₃-3	60.33	60.3
OCH₃-7	55.83	56.1
OCH₃-4′	61.11	61.1
OCH₃-5′	56.07	55.8

Table 4-5 The ^{1}H- and ^{13}C-NMR spectral data of SS1

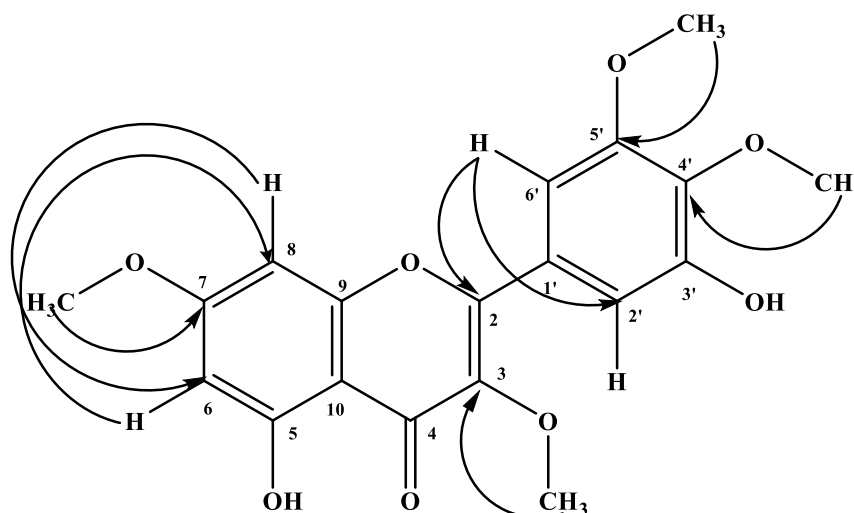| Position	SS1 in CDCl₃ (^{1}H: 500 MHz; ^{13}C: 125 MHz)		
	δ_C (ppm)	δ_H (ppm), Multiplicity, J (Hz)	HMBC
2	155.33	-	H-6′
3	139.50	-	OCH₃-3
4	178.83	-	-
5	161.98	-	H-6
6	97.95	6.34 (d, 2.19)	H-8
7	165.57	-	H-6, H-8, OCH₃-7
8	92.17	6.42 (d, 2.19)	H-6
9	156.74	-	H-8
10	105.00	-	H-6
1′	125.95	-	-
2′	108.55	7.34 (d, 2.00)	H-6′
3′	149.17	-	H-6′
4′	137.74	-	H-6′, OCH₃-4′
5′	152.03	-	H-2′, OCH₃-5′
6′	104.99	7.33 (d, 2.00)	-
OCH₃-3	60.33	3.860 (s)	-
OCH₃-7	55.83	3.859 (s)	-
OCH₃-4′	61.11	3.98 (s)	-
OCH₃-5′	56.07	3.92 (s)	-
OH-5	-	12.55 (s)	-
OH-3′	-	5.90 (brs)	-

Figure 4-3 The main HMBC correlation of SS1

4.2.1.2 Structure determination of SS2

Molecular formula   : $C_{20}H_{20}O_8$

ESI Mass (M-H)$^-$: 387.1086

        SS2 (3.1 mg) was obtained as a yellow amorphous solid and dissolved in chloroform. The UV spectrum in chloroform (**Appendix 6**) showed λ_{max} at 268 and 347 nm. IR spectrum (**Appendix 7**) demonstrated absorption band at 3502 cm^{-1} (-OH), 2922-2850 cm^{-1} (-CH$_3$), 1657 cm^{-1} (C=O), 1601-1353 cm^{-1} (C=C), 1247-1126 cm^{-1} (-OCH$_3$), 1048-1017 cm^{-1} (-C-O) and 812-768 (=C-H).

        The ^{1}H-NMR spectrum of SS2 (500 MHz in CDCl$_3$, as showed in **Table 4-6** and **Appendix 8**) exhibited the quite similar pattern with ^{1}H-NMR of SS1. SS2 spectrum showed two doublet and seven singlet proton signals. Two doublet signals at δ_H 6.35 (1H, d, $J = 2.19$ Hz) and 6.45 (1H, d, $J = 2.44$ Hz) were determined as H-6 and H-8, respectively. Two singlet signals with three protons integration ratio at δ_H 3.854 and 3.860 were consequently assigned as OCH$_3$-3 and OCH$_3$-7. Singlet signal with one proton integration ratio at δ_H 12.57 belongs to OH-5. Ring A protons (H-6 and H-8), hydroxyl proton (OH-5) and methoxy protons (OCH$_3$-3 and OCH$_3$-7) had similar signals which found from ^{1}H-NMR of SS1. Moreover, three singlet signals at δ_H 7.34, 3.926 and 3.927 were indicated as signals of substitued aromatic ring (ring B). The singlet signal with two protons integration ratio at δ_H 7.34 was assigned as two protons

(H-2′ and H-6′) and the singlet signals with six protons integration ratio at δ_H 3.926 were assumed as two methoxy protons (OCH$_3$-3′ and OCH$_3$-5′). The remaining singlet signals with three protons integration at δ_H 3.927 was indicated as methoxy protons of OCH$_3$-4′.

The ^{13}C-NMR spectrum of SS2 (125 MHz in CDCl$_3$, **Appendix 9**) showed twenty carbon signals (**Table 4-6**) that were determined as eight oxygenated aromatic carbon signals, four methoxy carbon signals, three tertiary aromatic carbon signals, two quaternary carbon signals and one carbonyl signal. The carbon signals of ring A and ring C of SS2 were similar to the carbon signals of SS1. The differences between SS2 and SS1 were carbon signals of ring B. The carbon signals of SS2-ring B showed δ_C 105.90 (C-2′ and C-6′), 125.45 (C-1′), 140.50 (C-4′) and 153.10 (C-3′ and C-5′) due to three methoxy substitution on C-3′, C-4′ and C-5′. These methoxy carbons showed two signals at δ_C 56.31 and 61.02. The NMR signals of SS2 were confirmed the correlation by HMBC and were compared with previous report of 5-hydroxy-3, 3′, 4′, 5′, 7-pentamethoxyflavone in CDCl$_3$ (Dachriyanus *et al*., 2004) as shown in **Table 4-6** and **Figure 4-4**, respectively. The HR-ESIMS data of SS2 showed [M-H]$^-$ peak at *m/z* 387.1086 (**Appendix 10**) which agreed with 5-hydroxy-3, 3′, 4′, 5′, 7-pentamethoxyflavone molecular weight. So, SS2 (**Figure 4-1**) was indicated as 5-hydroxy-3, 3′, 4′, 5′, 7-pentamethoxyflavone or combretol.

Table 4-6 The comparison of ^{1}H- and ^{13}C-NMR spectral data between SS2 and 5-hydroxy-3, 3′, 4′, 5′, 7-pentamethoxyflavone

Position	SS2 in CDCl₃ (^{1}H: 500 MHz; ^{13}C: 125 MHz)			5-hydroxy-3, 3′, 4′, 5′, 7-pentamethoxyflavone in CDCl₃ (^{1}H: 500 MHz; ^{13}C: 125 MHz) (Dachriyanus *et al.*, 2004)	
	δ_C (ppm)	δ_H (ppm), Multiplicity, J (Hz)	HMBC	δ_C (ppm)	δ_H (ppm), Multiplicity, J (Hz)
2	155.61	-	H-2′, H-6′	155.53	-
3	139.39	-	H-2′, H-6′, OCH₃-3′	139.34	-
4	178.76	-	-	178.70	-
5	162.03	-	-	161.96	-
6	97.92	6.35 (d, 2.19)	H-8, OH-5	97.87	6.34 (d, 2.2)
7	165.50	-	H-6, H-8, OCH₃-7	165.51	-
8	92.26	6.45 (d, 2.44)	-	92.18	6.43 (d, 2.2)
9	156.70	-	H-6, H-8	156.65	-
10	106.06	-	H-6, H-8, OH-5	106.00	-
1′	125.45	-	H2′, H-6′	125.40	-
2′	105.90	7.34 (s)	H-6′	106.00	7.35 (s)
3′	153.10	-	H-2′, H-6′, OCH₃-3′, OCH₃-4′	153.06	-
4′	140.50	-	OCH₃-4′	140.54	-
5′	153.10	-	H-2′, H-6′, OCH₃-4′, OCH₃-5′	153.06	-

Table 4-6 The comparison of ^{1}H- and ^{13}C-NMR spectral data between SS2 and 5-hydroxy-3, 3′, 4′, 5′, 7-pentamethoxyflavone **(continued)**

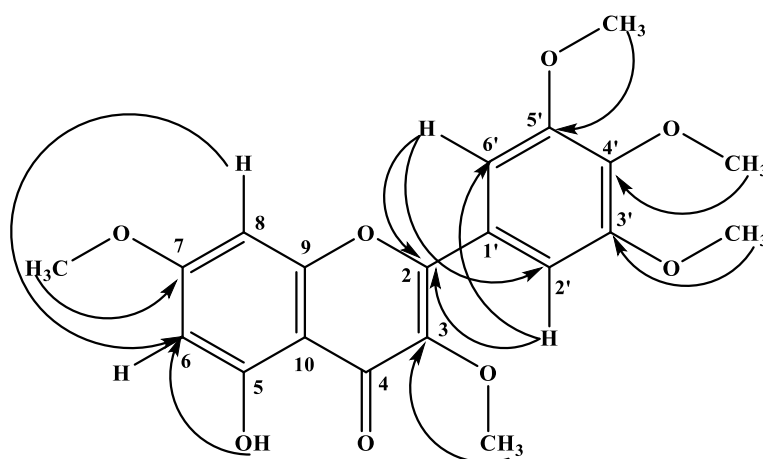| Position	SS2 in CDCl₃ (^{1}H: 500 MHz; ^{13}C; 125 MHz)			5-hydroxy-3, 3′, 4′, 5′, 7-pentamethoxyflavone in CDCl₃ (^{1}H: 500 MHz; ^{13}C: 125 MHz) (Dachriyanus *et al*., 2004)	
	δ_C (ppm)	δ_H (ppm), Multiplicity, J (Hz)	HMBC	δ_C (ppm)	δ_H (ppm), Multiplicity, J (Hz)
6′	105.90	7.34 (s)	H-2′	106.00	7.35 (s)
OCH₃-3	60.36	3.854 (s)	-	60.27	3.861 (s)
OCH₃-7	55.85	3.860 (s)	-	55.79	3.864 (s)
OCH₃-3′	56.31	3.926 (s)	-	56.28	3.932 (s)
OCH₃-4′	61.02	3.927 (s)	-	60.95	3.935 (s)
OCH₃-5′	56.31	3.926 (s)	-	56.28	3.932 (s)
OH-5	-	12.57 (s)	OH-5	-	12.56 (s)

Figure 4-4 The main HMBC correlation of SS2

4.2.1.3 Structure determination of SS3

Molecular formula   : $C_{15}H_{10}O_6$

ESI Mass (M-H)[-]   : 285.0407

        SS3 (2 mg) was obtained as a yellow amorphous solid and dissolved in methanol. The UV spectrum in methanol (**Appendix 11**) showed λ_{max} at 211, 265 and 366 nm.

        The ^{1}H-NMR spectrum of SS3 (500 MHz in CD₃OD, **Appendix 12**) presented four proton signals with δ_H 6.20 (1H, d, J = 2.0 Hz), 6.42 (1H, d, J = 2.0 Hz), 6.93 (2H, d, J = 8.5 Hz) and 8.11 (2H, d, J = 10.0 Hz). The protons at δ_H 6.20 and 6.42 ppm were determined as the meta-coupled of aromatic proton which agreed with H-6 and H-8, respectively. Other two doublet signals with two protons integration ratio, at δ_H 6.93 and 8.11 ppm, were assigned as four aromatic protons. The NMR data of SS3 and previous kaempferol (Aisyah *et al*., 2017) were compared in **Table 4-7**. Moreover, HR-ESIMS data of SS3 which showed [M-H][-] peak at *m/z* 285.0407 (**Appendix 13**) confirmed the structure of SS3 (**Figure 4-1**) as kaempferol.

Table 4-7 The comparison of ^{1}H-NMR spectral data between SS3 and kaempferol

Position	SS3 in CD₃OD (500 MHz)	Kaempferol in CD₃OD (500 MHz) (Aisyah *et al*., 2017)
	δ_H (ppm), Multiplicity, J (Hz)	δ_H (ppm), Multiplicity, J (Hz)
6	6.20 (d, 2.0)	6.28 (d, 2.0)
8	6.42(d, 2.0)	6.52 (d, 2.0)
2′	8.11 (d, 10.0)	8.04 (dd, 2.8, 11.5)
3′	6.93 (d, 8.5)	6.95 (dd, 2.7, 9.8)
5′	6.93 (d, 8.5)	6.95 (dd, 2.7, 9.8)
6′	8.11 (d, 10.0)	8.04 (dd, 2.8, 11.5)

4.2.1.4 Structure determination of SS4

Molecular formula : $C_{21}H_{20}O_{11}$

ESI Mass (M-H)⁻ : 447.0933

    SS4 (2 mg) was obtained as a yellow amorphous solid and dissolved in methanol. The UV spectrum in methanol (**Appendix 14**) showed λ_{max} at 209, 254 and 363 nm.

    The ^{1}H-NMR spectrum of SS4 (500 MHz in DMSO-d_6, as showed in **Table 4-8** and **Appendix 15**) presented the doublet signals at δ_H 6.42 (1H, d, J = 1.5 Hz) and 6.80 (1H, d, J = 2 Hz) were indicated to H-6 and H-8, respectively. The singlet signal at δ_H 12.53 was determined as the phenolic hydroxyl proton of position 5 (OH-5). Two doublet signals at δ_H 6.94 (2H, d, J = 9 Hz) and 8.09 (2H, d, J = 7.5 Hz) were assigned as four aromatic protons (H-2′, H-3′, H-5′and H-6′) of ring B. The proton chemical shifts of ring A and ring B were indicated that SS4 structure had typical kaempferol aglycone when compared with SS3 (**Table 4-9**). Additionally, the doublet signal with one proton integration ratio at δ_H 5.07 (J = 7.5 Hz) was determined as the anomeric proton of glucosyl unit. The J value of anomeric proton suggested the β configuration. The NOESY correlation of δ_H 5.07 (H-1″) to δ_H 6.42 (H-6) and 6.80 (H-8) were used to identify the linkage between sugar moiety and aglycone at C-7 (**Table 4-8**, **Figure 4-5** and **Appendix 16**).

    The ^{13}C-NMR spectrum of SS4 (125 MHz in DMSO-d_6, as showed in **Table 4-8** and **Appendix 17**) showed nineteen carbon signals. The six oxygenated aromatic carbons displayed at δ_C 136.72 (C-3), 147.96 (C-2), 156.20 (C-9), 159.84 (C-7), 160.82 (C-4′) and 163.13(C-5). Two of tertiary aromatic carbon signals which found at δ_C 99.20 and 100.33 were assigned as C-8 and C-6, respectively. Other two tertiary aromatic carbon signals (δ_C 115.94 and 130.08) were indicated to four carbons (C3′/C5′ and C2′/C6′) of ring B. The two quaternary aromatic carbons at δ_C 105.16 and 122.05 were assigned as C-10 and C-1′. The carbonyl signal was found at δ_C 176.09 (C-4). These signal belong to flavonol aglycone unit. The signals of anomeric carbon presented at δ_C 94.81 (C-1″), while the signals at δ_C 61.07 (C-6″), 70.02 (C-4″), 73.59 (C-2″), 76.90 (C-3″), and 77.64 (C-5″) were the five oxygenated carbon signals of sugar unit. The proton and carbon chemical shift values of SS4 were in accordance with flavonol glycoside that previously reported of kaempferol 7-*O*-β-glycopyranoside

(Pereira *et al*., 2012) as showed in **Table 4-10**. The HR-ESIMS data of SS4 was found [M-H]⁻ peak at *m/z* 447.0933 (**Appendix 18**) which agreed that the structure of SS4 (**Figure 4-1**) as kaempferol-7-*O*-β-glycopyranoside.

Table 4-8 The NMR spectral data of SS4

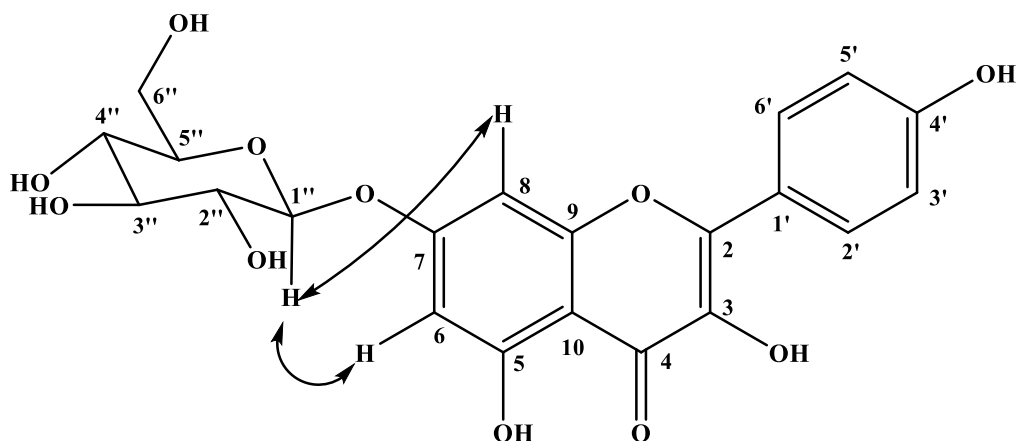| Position	SS4 in DMSO-d_6 (^{1}H: 500 MHz; ^{13}C: 125 MHz)		
	δ_C (ppm)	δ_H (ppm), Multiplicity, *J* (Hz)	NOESY
2	147.96	-	-
3	136.72	-	-
4	176.09	-	-
5	163.13	-	-
6	100.33	6.42 (d, 1.5)	-
7	159.84	-	-
8	99.20	6.80 (d, 2.0)	-
9	156.20	-	-
10	105.16	-	-
1′	122.05	-	-
2′	130.08	8.09 (d, 7.5)	-
3′	115.94	6.94 (d, 9.0)	-
4′	160.82	-	-
5′	115.94	6.94 (d, 9.0)	-
6′	130.08	8.09 (d, 7.5)	-
1″	94.81	5.07 (d, 7.5)	H-6, H-8
2″	73.59	3.14 -3.73 (m)	-
3″	76.90	3.14 -3.73 (m)	-
4″	70.02	3.14 -3.73 (m)	-
5″	77.64	3.14 -3.73 (m)	-
6″	61.07	3.14 -3.73 (m)	-
5-OH	-	12.53 (brs)	-

Figure 4-5 NOESY correlations of SS4

Table 4-9 The comparison of ¹H-NMR spectral data between SS3 and SS4

Position	δ_H (ppm), Multiplicity, *J* (Hz)	
	SS3 in CD₃OD (¹H: 500 MHz; ¹³C: 125 MHz)	**SS4 in DMSO-*d₆*** (¹H: 500 MHz; ¹³C: 125 MHz)
6	6.20 (d, 2.0)	6.42 (d, 1.5)
8	6.42 (d, 2.0)	6.80 (d, 2.0)
2′	8.11 (d, 10.0)	8.09 (d, 7.5)
3′	6.93 (d, 8.5)	6.94 (d, 9.0)
5′	6.93 (d, 8.5)	6.94 (d, 9.0)
6′	8.11 (d, 10.0)	8.09 (d, 7.5)
1″	-	5.07 (d, 7.5)
2″	-	3.14 -3.73 (m)
3″	-	3.14 -3.73 (m)
4″	-	3.14 -3.73 (m)
5″	-	3.14 -3.73 (m)
6″	-	3.14 -3.73 (m)
5-OH	-	12.53 (brs)

Table 4-10 The comparison of ^{1}H- and ^{13}C-NMR spectral data between SS4 and kaempferol-7-O-β-glucopyranoside

Position	SS4 in DMSO-d_6 (^{1}H: 500 MHz; ^{13}C: 125 MHz)		Kaempferol 7-O-β-glucopyranoside in DMSO-d_6 (^{1}H: 500 MHz; ^{13}C: 125 MHz) (Pereira *et al*., 2012)	
	δ_C (ppm)	δ_H (ppm), Multiplicity, J (Hz)	δ_C (ppm)	δ_H (ppm), Multiplicity, J (Hz)
2	147.96	-	147.5	-
3	136.72	-	136.1	-
4	176.09	-	176.1	-
5	163.13	-	160.4	-
6	100.33	6.42 (d, 1.5)	103.0	6.44 (d, 1.7)
7	159.84	-	157.9	-
8	99.20	6.80 (d, 2.0)	98.0	6. 81 (d, 1.7)
9	156.20	-	155.8	-
10	105.16	-	104.7	-
1′	122.05	-	121.5	-
2′	130.08	8.09 (d, 7.5)	130.5	7.96 (d, 8.8)
3′	115.94	6.94 (d, 9.0)	116.2	6.80
4′	160.82	-	159.4	-
5′	115.94	6.94 (d, 9.0)	116.2	6.80
6′	130.08	8.09 (d, 7.5)	130.5	7.96 (d, 8.8)
1″	94.81	5.07 (d, 7.5)	96.9	5.50 (d, 7.6)
2″	73.59	3.14 -3.73 (m)	73.1	3.36
3″	76.90	3.14 -3.73 (m)	76.4	3.30
4″	70.02	3.14 -3.73 (m)	69.6	3.65
5″	77.64	3.14 -3.73 (m)	77.2	3.32
6″	61.07	3.14 -3.73 (m)	60.6	3.37
5-OH	-	12.53 (brs)	-	12.85 (s)

4.2.1.5 Structure determination of SS5

Molecular formula   : $C_{25}H_{28}O_{13}$

ESI Mass (M-H)$^{-}$: 535.1457

        SS5 (1 mg) was obtained as a yellow amorphous solid and dissolved in methanol. The UV spectrum in methanol (**Appendix 19**) showed λ_{max} at 212, 268 and 337 nm.

        The ^{1}H-NMR spectrum of SS5 (500 MHz in DMSO-d_6, as showed in **Table 4-11** and **Appendix 20**) showed two doublet signals at δ_H 6.41 (1H, d, J = 2.0 Hz) and 6.85 (1H, d, J = 2.5 Hz) were indicated as H-6 and H-8, respectively. The singlet signal at δ_H 12.55 (1H, s) belongs to the phenolic hydroxyl proton, OH-5. The two doublet signals at δ_H 7.46 (1H, d, J = 2.0 Hz) and 7.52 (1H, d, J = 2.0 Hz) were determined as the *meta*-proton of ring B, while the doublet signal δ_H 4.96 (1H, d, J = 7.5 Hz) was indicated as anomeric proton of sugar substitution. Other doublet signals (at δ_H 5.36 (1H, d, J = 5.0 Hz), 5.13 (1H, d, J = 5.0 Hz) and 5.05 (1H, d, J = 5.0 Hz)) and triplet signal (at δ_H 4.68 (1H, t, J = 6, 5.0 Hz)) were suggested as hydroxyl proton of sugar unit. The signals at δ_H 3.18 (m), 3.33(m), 3.38 (m) and 3.52 (m) belong to glucosyl hydrogen atoms. Besides, four singlet signals at δ_H 3.84, 3.87, 3.88 and 3.884 were determined as fours methoxy groups presence on the structure.

        The ^{13}C-NMR spectrum of SS5 (125 MHz in DMSO-d_6, as showed in **Table 4-11** and **Appendix 21**) demonstrated twenty-five carbon signals. Eight oxygenated carbons appeared at δ_C 139.30 (C-3), 141.25 (C-4′), 151.49 (C-3′), 153.28 (C-5′), 155.47 (C-2), 156.50 (C-9), 161.34 (C-5) and 165.80 (C-7). Two tertiary aromatic carbons of ring A were observed at δ_C 98.39 (C-6) and 93.17(C-8), while two tertiary aromatic carbons of ring B were found at δ_C 107.23 (C-6′) and 110.23 (C-2′). The carbonyl carbon displayed at δ_C 178.71 (C-4). Two quaternary aromatic carbons showed at δ_C 105.81 (C-10) and 125.32 (C-1′). Four methoxy carbons present at δ_C 56.59 (OCH$_3$-5′), 56.61 (OCH$_3$-7), 60.52 (OCH$_3$-3) and 61.03 (OCH$_3$-4′). These carbon signals belong to aglycone part of SS5 which were similar to those reported for SS1 as comparable **Table 4-12**. Interestingly, C-3′ chemical shift of SS5 located a bit downfield than C-3′chemical shift of SS1. The signal at δ_C 101.92 was indicated as the anomeric carbon (C-1″), while residue five carbon signals (δ_C 73.76, 70.27, 77.22,

77.89 and 61.34) were assigned as oxygenated carbons of sugar moiety. So, the structure of SS5 were suggested as flavonoid mono-glycoside.

The HMBC correlation data (**Table 4-11**, **Figure 4-6** and **Appendix 22**) of SS5 indicated that the 3,7-dimethoxyflavone skeleton and the 4′,5′-dimethoxy substituted ring B was preserved as compared with SS1 (**Table 4-12**). The aromatic proton at δ_H 7.52 (H-2′) showed three bond correlation with carbons at δ_C 155.47 (C-2) and 107.23 (C-6′), while it exhibited two bond correlation with carbon at δ_C 151.49 (C-3′). The anomeric proton at δ_H 4.96 (H-1″) presented three bond correlation with carbons at δ_C 151.49 (C-3′). In addition, NOESY correlation (**Table 4-11** and **Figure 4-7**) displayed space correlation between the aromatic proton at δ_H 7.52 (H-2′) and the anomeric proton at δ_H 4.96 (H-1″). These correlations supported the sugar substitution at carbon position C-3′. The *J* value of the anomeric proton indicated the β configuration. Due to review of the literature on previous reported flavonoid glycosides have not been full matched with SS5 NMR data. Besides the SS5 NMR data were compared with SS1 NMR data to confirm the 3, 7-dimethoxyflavone skeleton (**Table 4-12**), the data were also compared with the biotransformation compound, 3′-*O*-β-D-(4″-*O*-methylglucopyranosylo)-5, 7, 4′, 5′-tetramethoxyflavone (Łużny *et al*., 2021), to displayed the presence of sugar substitution at carbon position C-3′ (**Table 4-13**). So, the structure of SS5 (**Figure 4-1**) was determined as 5-hydroxy-3, 7, 4′, 5′-tetramethoxyflavone-3′-*O*-β-glucopyranoside. The HR-ESIMS data of SS5 was found [M-H]⁻ peak at *m/z* 535.1457 (**Appendix 24**) which agreed that the structure of SS5 as 5-hydroxy-3, 7, 4′, 5′-tetramethoxyflavone-3′-*O*-β-glucopyranoside. The glucopyranoside substitution at this position of the aglycone has not been reported before.
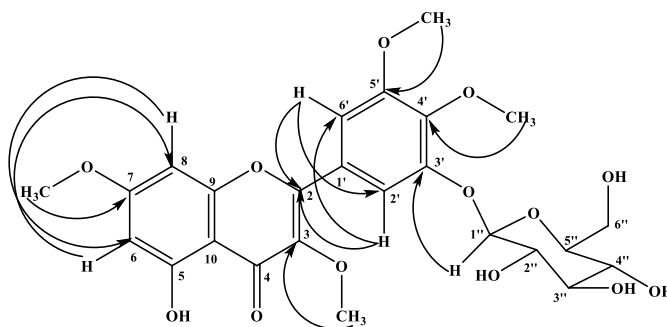

Figure 4-6 The main HBMC correlations of SS5

Table 4-11 The NMR spectral data of SS5

Position	SS5 in DMSO-d_6 (^{1}H: 500 MHz; ^{13}C: 125 MHz)			
	δ$_C$ (ppm)	δ$_H$ (ppm), Multiplicity, J (Hz)	HMBC	NOESY
2	155.47	-	H-6′, H-2′	-
3	139.30	-	OCH$_3$-3	-
4	178.71	-	-	-
5	161.34	-	OH-5	-
6	98.39	6.41 (d, 2.0)	H-8, OH-5	-
7	165.80	-	H-6, H-8, OCH$_3$-7	-
8	93.17	6.85 (d, 2.5)	H-6	-
9	156.50	-	H-8	-
10	105.81	-	H-6, H-8, OH-5	-
1′	125.32		H-2′, H-6′	-
2′	110.23	7.52 (d, 2.0)	H-6′	H-1″
3′	151.49	-	H-2′, H-1″	-
4′	141.25	-	H-6′, H-2′, OCH$_3$-4′	-
5′	153.28	-	H-6′, OCH$_3$-5′	-
6′	107.23	7.46 (d, 2.0)	H-2′	-
1″	101.92	4.96 (d, 7.5)	-	H-2′
2″	77.22	3.18-3.74 (m)	-	-
3″	73.76	3.18-3.74 (m)	-	-
4″	70.27	3.18-3.74 (m)	-	-
5″	77.89	3.18-3.74 (m)	-	-
6″	61.34	3.18-3.74 (m)	-	-
OCH$_3$-3	60.52	3.87 (s)	-	-
OCH$_3$-7	56.61	3.88 (s)	-	-
OCH$_3$-4′	61.03	3.84 (s)	-	-
OCH$_3$-5′	56.59	3.884 (s)	-	-
OH-5	-	12.55 (s)	-	-
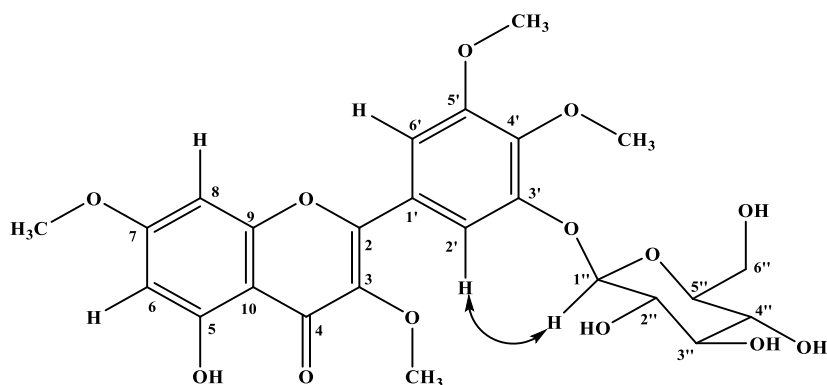
Figure 4-7 NOESY correlations of SS5

Table 4-12 The comparison of ^{1}H-, ^{13}C- and HMBC NMR spectral data between SS5
and SS1

Position	SS1 in CDCl₃ (^{1}H: 500 MHz; ^{13}C: 125 MHz)			SS5 in DMSO-d_6 (^{1}H: 500 MHz; ^{13}C: 125 MHz)		
	δ$_C$ (ppm)	δ$_H$ (ppm), Multiplicity, J (Hz)	HMBC	δ$_C$ (ppm)	δ$_H$ (ppm), Multiplicity, J (Hz)	HMBC
2	155.33	-	H-6′	155.47	-	H-6′, H-2′
3	139.50	-	OCH₃-3	139.30	-	OCH₃-3
4	178.83	-	-	178.71	-	
5	161.98	-	H-6	161.34	-	OH-5
6	97.95	6.34 (d, 2.19)	H-8	98.39	6.41 (d, 2.00)	H-8, OH-5
7	165.57	-	H-6, H-8, OCH₃-7	165.80	-	H-6, H-8, OCH₃-7
8	92.17	6.42 (d, 2.19)	H-6	93.17	6.85 (d, 2.50)	H-6
9	156.74	-	H-8	156.50	-	H-8

Table 4-12 The comparison of ^{1}H-, ^{13}C- and HMBC NMR spectral data between SS1 and SS5 **(continued)**

Position	SS1 in CDCl$_3$ (^{1}H: 500 MHz; ^{13}C: 125 MHz)			SS5 in DMSO-d_6 (^{1}H: 500 MHz; ^{13}C: 125 MHz)		
	δ_C (ppm)	δ_H (ppm), Multiplicity, J (Hz)	HMBC	δ_C (ppm)	δH (ppm), Multiplicity, J (Hz)	HMBC
10	105.00	-	H-6	105.81	-	H-6, H-8, OH-5
1′	125.95	-	-	125.32		H-2′, H-6′
2′	108.55	7.34 (d, 2.00)	H-6′	110.23	7.52 (d, 2.00)	H-6′
3′	149.17	-	H-6′	151.49	-	H-2′, H-1″
4′	137.74	-	H-6′, OCH$_3$-4′	141.25	-	H-6′, H-2′, OCH$_3$-4′
5′	152.03	-	H-2′, OCH$_3$-5′	153.28	-	H-6′, OCH$_3$-5′
6′	104.99	7.33 (d, 2.00)	-	107.23	7.46 (d, 2.0)	H-2′
1″	-	-	-	101.92	4.96 (d, 7.5)	
2″	-	-	-	77.22	3.18-3.74 (m)	
3″	-	-	-	73.76	3.18-3.74 (m)	
4″	-	-	-	70.27	3.18-3.74 (m)	
5″	-	-	-	77.89	3.18-3.74 (m)	
6″	-	-	-	61.34	3.18-3.74 (m)	
OCH$_3$-3	60.33	3.860 (s)	-	60.52	3.87 (s)	-
OCH$_3$-7	55.83	3.859 (s)	-	56.61	3.88 (s)	-

Table 4-12 The comparison of ^{1}H-, ^{13}C- and HMBC NMR spectral data between SS1 and SS5 **(continued)**

Position	SS1 in CDCl₃ ([1]H: 500 MHz; [13]C: 125 MHz)			SS5 in DMSO-d_6 ([1]H: 500 MHz; [13]C: 125 MHz)		
	δ_C (ppm)	δ_H (ppm), Multiplicity, J (Hz)	HMBC	δ_C (ppm)	δH (ppm), Multiplicity, J (Hz)	HMBC
OCH₃-4′	61.11	3.98 (s)	-	61.03	3.84 (s)	-
OCH₃-5′	56.07	3.92 (s)	-	56.59	3.884 (s)	-
OH-5	-	12.55 (s)	-	-	12.55 (s)	-
OH-3′	-	5.90 (brs)	-	-	-	-

Table 4-13 The comparison of ^{1}H- and ^{13}C-NMR spectral data between SS5 and 3′-*O*-β-D-(4″-*O*-methylglucopyranosylo)-5, 7, 4′, 5′-tetramethoxyflavone

Position	SS5 in DMSO-d_6 ([1]H: 500 MHz; [13]C: 125 MHz)		3′-*O*-β-D-(4″-*O*-methylglucopyranosylo)-5, 7, 4′, 5′-tetramethoxyflavone in DMSO-d_6 ([1]H: 600 MHz; [13]C: 151 MHz) (Łużny *et al*., 2021)	
	δ_C (ppm)	δ_H (ppm), Multiplicity; J (Hz)	δ_C (ppm)	δ_H (ppm), Multiplicity; J (Hz)
2	155.47	-	159.17	-
3	139.30	-	108.04	6.84 (s)
4	178.71	-	175.78	-
5	161.34	-	160.23	-
6	98.39	6.41 (d, 2.0)	96.26	6.51 (d, 2.3)
7	165.80	-	166.64	-
8	93.17	6.85 (d, 2.5)	93.52	6.91 (d, 2.3)
9	156.5	-	159.26	-
10	105.81	-	108.29	-
1′	125.32	-	126.03	-

Table 4-13 The comparison of ^{1}H- and ^{13}C-NMR spectral data between SS5 and 3′-
O-β-D-(4″-O-methylglucopyranosylo)-5, 7, 4′, 5′-tetramethoxyflavone
(continued)

Position	SS5 in DMSO-d_6 ([1]H: 500 MHz; [13]C: 125 MHz)		3′-O-β-D-(4″-O-methylglucopyranosylo)-5, 7, 4′, 5′-tetramethoxyflavone in DMSO-d_6 ([1]H: 600 MHz; [13]C: 151 MHz) (Łużny *et al.*, 2021)	
	δ_C (ppm)	δ_H (ppm), Multiplicity; *J* (Hz)	δ_C (ppm)	δ_H (ppm), Multiplicity; *J* (Hz)
2′	110.23	7.52 (d, 2.0)	107.33	7.48 (d, 2.0)
3′	151.49	-	151.26	
4′	141.25	-	140.93	-
5′	153.28	-	153.35	-
6′	107.23	7.46 (d, 2.0)	104.37	7.33 (d, 2.0)
1″	101.92	4.96 (d, 7.5)	100.88	5.03 (d, 7.9)
2″	77.22	3.18-3.74 (m)	73.58	3.30-3.34 (m)
3″	73.76	3.18-3.74 (m)	76.49	3.45 (dd, 9.0, 5.6)
4″	70.27	3.18-3.74 (m)	79.40	3.00 (t, 9.3)
5″	77.89	3.18-3.74 (m)	75.90	3.48-3.56 (m)
6″	61.34	3.18-3.74 (m)	60.56	3.48-3.56 (m), 3.69 (dd, 10.3, 5.1)
OCH$_3$-3	60.52	3.87 (s)	-	-
OCH$_3$-5	-	-	56.08	3.83 (s)
OCH$_3$-7	56.61	3.88 (s)	55.84	3.90 (s)
OCH$_3$-4′	61.03	3.84 (s)	60.51	3.79 (s)
OCH$_3$-5′	56.59	3.884 (s)	55.97	3.90 (s)
OCH$_3$-4″	-	-	59.71	3.47 (s)
OH-5	-	12.55 (s)	-	-

4.2.1.6 Structure determination of SS6 (Mixture)

        SS6 (1.6 mg) was obtained as a yellow amorphous solid and dissolved in methanol. The UV spectrum in methanol (**Appendix 25**) showed λ_{max} at 210, 256 and 352 nm. Analysis of purification of SS6 using high performance liquid chromatography (HPLC) with hypersil ODS column (250×4.0 mm, 5 μm particle size) and diode array detector (260, 292, 370 nm) showed two peaks (**Appendix 26**). The HPLC chromatogram of SS6 indicated that the compound was mixture. The NMR data (**Appendix 27 and Appendix 28**) of mixture compound (SS6-1 and SS6-2) were determined as two flavonoid glycosides.

SS6-1

Molecular formula SS6-1: $C_{22}H_{22}O_{12}$

ESI Mass (M-H)⁻   : 477.1042

        The ^{1}H-NMR spectrum of SS6-1 (500 MHz in DMSO-d_6, as **Table 4-14**) showed two doublet signals at δ_H 6.18 (1H, m) and 6.40 (1H, m) were determined as H-6 and H-8, respectively. Singlet signal at δ_H 12.60 belongs to OH-5. These protons consisted of 5, 7-dihydroxy-substituted ring A of the flavonoid pattern. Two doublet signals at δ_H 6.91 ($J = 8.5$ Hz) and 7.95 ($J = 2.1$ Hz) and a doublet of doublet at δ_H 7.48 ($J = 8.5, 2.1$ Hz) were assigned as H-2′, H-5′ and H-6′ of ring B, respectively. Additionally, the singlet signal at δ_H 3.84 was determined as the present of methoxy group of ring B, OCH$_3$-3′. The doublet signal with one proton integration ratio at δ_H 5.58 ($J = 7$ Hz) was attributed to the anomeric proton of glucosyl moiety that substituted at position 3 of ring C. Other signals (at δ_H 3.03-3.23 (m)) belong to glucosyl hydrogen atoms. ^{1}H NMR data of SS6-1 in DMSO-d_6 were compared with previous report (Lee *et al*., 2005) as showed in **Table 4-15**.

        The ^{13}C-NMR spectrum of SS6-1 (125 MHz in DMSO-d_6) showed twenty-two carbon signals (**Table 4-14**) that were determined as the characteristic of flavonoid glycoside. The flavonol aglycone displayed the chemical shift of seven oxygenated aromatic carbons, five tertiary aromatic carbons, two quaternary aromatic carbons, one carbonyl carbon and one methoxy carbon. The chemical shifts of seven oxygenated aromatic carbons showed at δ_C 133.57, 147.34, 149.86, 156.52, 156.95, 161.65 and 165.80. The carbon signals at δ_C 99.48 and 94.31 were assigned as tertiary

aromatic carbon of ring A, while the signals at δ_C 113.91, 115.66 and 122.44 were indicated as tertiary aromatic carbon of ring B. The two quaternary aromatic carbons displayed at δ_C 104.07 and 121.56. The carbonyl signal was found at δ_C 177.75 and the methoxy carbon signal was showed at δ_C 56.11. Additionally, the presence of one glucose unit through signal of one anomeric carbon at δ_C 101.38 and five oxygenated carbons at δ_C 61.29, 70.34, 74.69, 76.88, 77.96 and 101.38. The NMR signals of SS6-1 were confirmed the correlation by HMBC and COSY (**Table 4-14**, **Figure 4-8** and **Figure 4-9**, **Appendix 29** and **Appendix 30**). The ^{1}H and ^{13}C spectra of SS6-1 were compared to chemical shifts from previous report of 3′-*O*-methylquercetin 3-*O*-glucoside in DMSO-*d₆* (Lee *et al*., 2005) as showed in **Table 4-13**. The negative HR-ESIMS data of SS6-1 which showed [M-H]⁻ peak at *m/z* 477.1042 (**Appendix 31**) supporting the molecular formula [($C_{22}H_{22}O_{12}$)-H]⁻. The quasi-molecular ion fragments which were found the mass peak at *m/z* at 314.0441, 299.0200 and 285.0412 were proposed fragmentation as showed in **Figure 4-10** (**Appendix 32**). So, SS6-1 (**Figure 4-1**) was indicated as 3′-*O*-methylquercetin 3-*O*-glucoside or isorhamnetin 3-*O*-glucoside.

Table 4-14 The NMR spectral data of SS6-1

Position	SS6-1 in DMSO-*d₆* (^{1}H: 500 MHz; ^{13}C: 125 MHz)			
	δ_C (ppm)	δ_H (ppm), Multiplicity; *J* (Hz)	HMBC	COSY
2	156.52	-	H-2′, H-6′	-
3	133.57	-	H-6′	-
4	177.75	-	-	-
5	161.65	-	H-5, H-6, 5-OH	-
6	99.48	6.18 (m)	H-8, 5-OH	H-8
7	165.80	-	H-8	-
8	94.31	6.40 (m)	H-6	H-6
9	156.95	-	H-8	-
10	104.07	-	H-8, H-6, 5-OH	-

Table 4-14 The NMR spectral data of SS6-1 **(continued)**

Position	SS6-1 in DMSO-d_6 (^{1}H: 500 MHz; ^{13}C: 125 MHz)			
	δ_C (ppm)	δ_H (ppm), Multiplicity; J (Hz)	HMBC	COSY
1′	121.56	-	H-2′	-
2′	113.91	7.95 (d, 2.10)	H-6′	H-6′
3′	147.34	-	H-2′, H-5′, 3′-OCH$_3$	-
4′	149.86	-	H-2′, H-5′, H-6′	-
5′	115.66	6.91 (d, 8.50)	-	H-6′
6′	122.44	7.48 (dd, 8.50, 2.10)	H-2′	H-2′, H-5′
1″	101.38	5.58 (d, 7.00)	-	H-2″
2″	76.88	3.22 (m)	-	H-1″
3″	74.69	3.23 (m)	-	-
4″	70.34	3.09 (m)	-	-
5″	77.96	3.11 (m)	-	-
6″	61.29	3.29 (m)	-	-
3′-OCH$_3$	56.11	3.84 (3H, s)	-	-
5-OH	-	12.60 (1H, s)	-	-
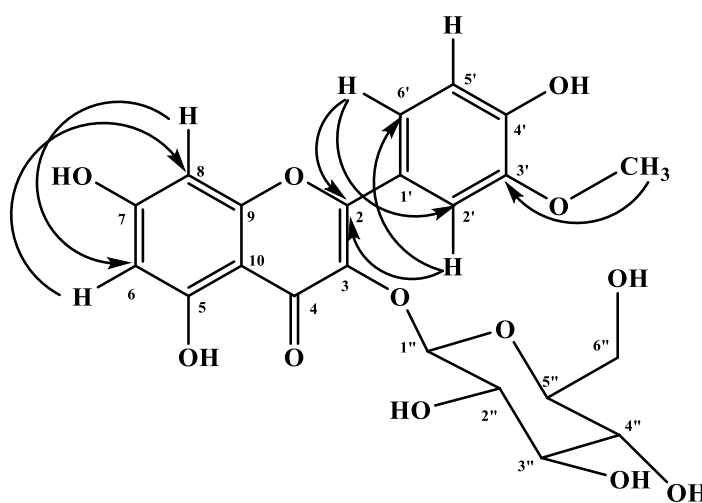
Figure 4-8 The main HMBC correlations of SS6-1
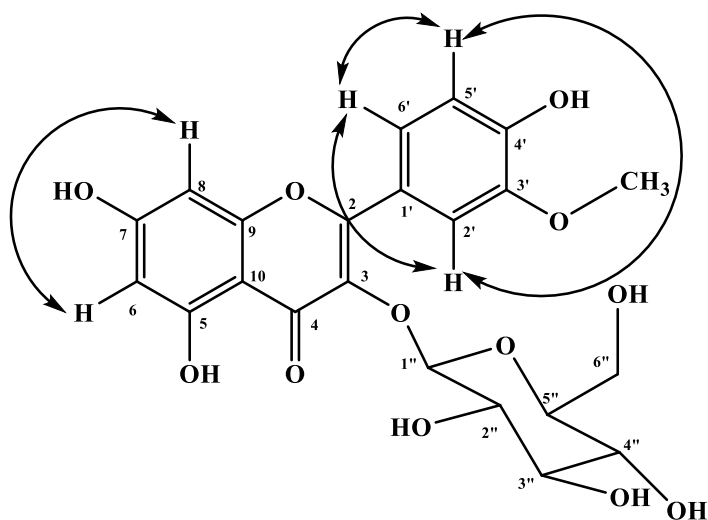
Figure 4-9 COSY correlations of SS6-1

Table 4-15 The comparison of ^{1}H- and ^{13}C-NMR spectral data between SS6-1 and 3′-
O-methylquercetin 3-O-β-D-glucopyranoside

| Position | SS6-1 in DMSO-d_6 | | 3′-O-Methylquercetin 3-O-β-D-glucopyranoside in DMSO-d_6 | |
| | (^{1}H: 500 MHz; ^{13}C: 125 MHz) | | (^{1}H: 400 MHz; ^{13}C: 100 MHz) (Lee *et al*., 2005) | |
	δc (ppm)	δн (ppm), Multiplicity, *J* (Hz)	δc (ppm)	δн (ppm), Multiplicity, *J* (Hz)
2	156.52	-	156.4	-
3	133.57	-	133.0	-
4	177.75	-	177.4	-
5	161.65	-	161.2	-
6	99.48	6.18 (m)	98.7	6.20 (d, 2.00)
7	165.80	-	164.3	-
8	94.31	6.40 (m)	93.7	6.44 (d, 2.00)
9	156.95	-	156.3	-
10	104.07	-	104.0	-
1′	121.56	-	121.1	-

Table 4-15 The comparison of ^{1}H- and ^{13}C-NMR spectral data between SS6-1 and 3′-
O-methylquercetin 3-O-β-D-glucopyranoside **(continued)**

Position	SS6-1 in DMSO-d_6 (^{1}H: 500 MHz; ^{13}C: 125 MHz)		3′-O-Methylquercetin 3-O-β-D-glucopyranoside in DMSO-d_6 (^{1}H: 400 MHz; ^{13}C: 100 MHz) (Lee *et al*., 2005)	
	δ_C (ppm)	δ_H (ppm), Multiplicity, J (Hz)	δ_C (ppm)	δ_H (ppm), Multiplicity, J (Hz)
2′	113.91	7.95 (d, 2.10)	113.4	7.94 (d, 2.00)
3′	147.34	-	146.9	-
4′	149.86	-	149.4	-
5′	115.66	6.91 (d, 8.50)	115.2	6.91 (d, 8.40)
6′	122.44	7.48 (dd, 8.50, 2.10)	122.0	7.49 (dd, 8.40, 2.00)
1″	101.38	5.58 (d, 7.00)	100.8	5.57 (d, 7.40)
2″	76.88	3.03-3.23 (m)	74.3	Not report
3″	74.69	3.03-3.23 (m)	77.5	Not report
4″	70.34	3.03-3.23 (m)	69.8	Not report
5″	77.96	3.03-3.23 (m)	76.4	Not report
6″	61.29	3.03-3.23 (m)	60.6	Not report
3′-OCH$_3$	56.11	3.84 (s)	55.7	3.83 (s)
5-OH	-	12.60 (s)	-	12.61 (s)

$[M-H]^- = 477$

$[M-H-C_6H_{11}O_5]^- = 314$

$[M-H-C_6H_{10}O_6]^- = 299$

$[M-H-CH_2O-C_6H_{10}O_5]^- = 285$
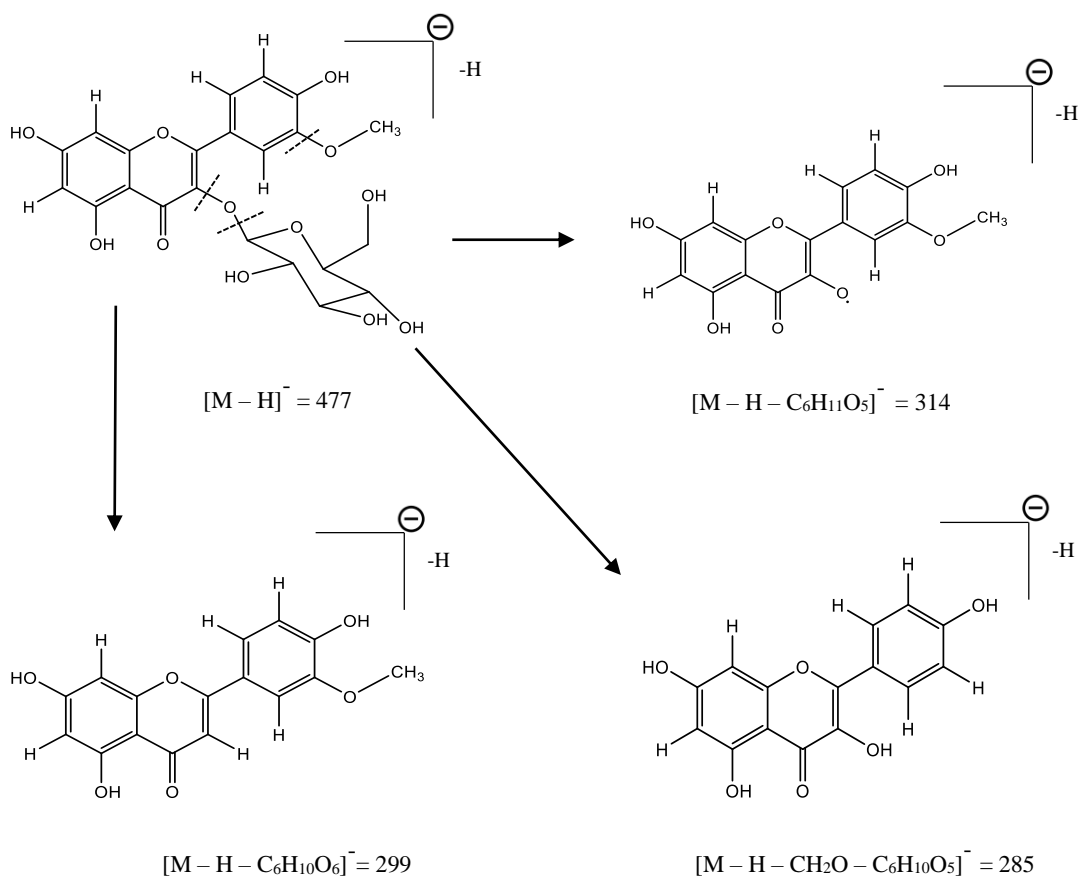
Figure 4-10 The proposed fragmentation of SS6-1

SS6-2

Molecular formula SS6-2: $C_{21}H_{20}O_{11}$

ESI Mass (M-H)⁻ : 447.0938

        The ^{1}H NMR spectrum of SS6-2 (500 MHz in DMSO-d_6) was quite similar pattern to ^{1}H-NMR of SS4-1 (as **Table 4-16**). Two doublet signals at δ_H 6.18 (1H, m) and 6.40 (1H, m) were determined as H-6 and H-8, respectively. The singlet signal at δ_H 12.60 also belongs to OH-5 of SS6-2. These indicated that SS6-2 also had 5,7-dihydroxy-substituted ring A of the flavonoid structure. The doublet signal with two protons integration ratio (at δ_H 6.88) and doublet of doublet signal with two protons integration ratio (at δ_H 8.04) were assigned as four aromatic protons of ring B. Moreover, the doublet signal with one proton integration ratio at δ_H 5.45 ($J = 7.5$ Hz)

was indicated as the anomeric proton of glucosyl unit. The signals (at δ_H 3.03-3.23 m)) belong to glucosyl hydrogen atoms.

The ^{13}C NMR spectrum of SS6-2 (125 MHz in DMSO-d_6) consisted of nineteen carbon signals. These carbon signals also showed the characteristic of flavonoid glycoside similar with SS6-1 (**Table 4-16**). The six oxygenated aromatic carbons displayed at δ_C 133.33, 156.50, 156.95, 160.42, 161.65 and 165.80. The carbon signals at δ_C 99.48 and 94.31 were indicated as tertiary aromatic carbon of ring A, while the signals at δ_C 115.57 and 131.32 were assigned as tertiary aromatic carbon of symmetric ring B. The two quaternary aromatic carbons were found at δ_C 104.07 and 121.38, while the carbonyl signal presented at δ_C 177.69. These carbon signals (six oxygenated aromatic carbon signals, six tertiary aromatic carbon signals, two quaternary aromatic carbon signals and one carbonyl carbon signal) indicated to the presence of flavonol aglycone unit. Moreover, the anomeric carbon signals at δ_C 101.27 and five oxygenated carbons signals at δ_C 61.03, 70.26, 74.80, 76.71 and 77.90 were found. The structure was predicted as flavonol glycoside. The NMR signals of SS6-2 were confirmed the correlation by HMBC and COSY (**Table 4-17** and **Figure 4-11** to **4-12**). The ^1H and ^{13}C spectra of SS6-2 were compared to chemical shifts from previous report of kaempferol-3-O-glycoside in DMSO-d_6 (Moura *et al*., 2019) as showed in **Table 4-18**. The HR-ESIMS data of SS6 was found [M-H]$^-$ peak at *m/z* 447.0938 (**Appendix 31**) which indicated that the structure of SS6-2 (**Figure 4-1**) as kaempferol-3-O-glycoside or astragalin.

Table 4-16 The comparison of ^1H- and ^{13}C-NMR spectral data between SS6-1 and SS6-2

Position	SS6-1 in DMSO-d_6 (^1H: 500 MHz; ^{13}C: 125 MHz)		SS6-2 in DMSO-d_6 (^1H: 500 MHz; ^{13}C: 125 MHz)	
	δ_C (ppm)	δ_H (ppm), Multiplicity, *J* (Hz)	δ_C (ppm)	δ_H (ppm), Multiplicity, *J* (Hz)
1′	121.56	-	121.38	-
2′	113.91	7.95 (d, 2.10)	131.32	8.04 (dd, 8.50, 2.10)
3′	147.34	-	115.57	6.88 (d, 8.50)

Table 4-16 The comparison of ¹H- and ¹³C-NMR spectral data between SS6-1 and SS6-2 (continued)

Position	SS6-1 in DMSO-d_6 (¹H : 500 MHz; ¹³C: 125 MHz)		SS6-2 in DMSO-d_6 (¹H: 500 MHz; ¹³C: 125 MHz)	
	δ_C (ppm)	δ_H (ppm), Multiplicity, *J* (Hz)	δ_C (ppm)	δ_H (ppm), Multiplicity, *J* (Hz)
4′	149.86	-	160.42	-
5′	115.66	6.91 (d, 8.50)	115.57	6.88 (d, 8.50)
6′	122.44	7.48 (dd, 8.50, 2.10)	131.32	8.04 (dd, 8.50, 2.10)
3′-OCH₃	5.11	3.84 (s)	-	-

Table 4-17 The NMR spectral data of SS6-2

Position	SS6-2 in DMSO-d_6 (¹H: 500 MHz; ¹³C: 125 MHz)			
	δ_C (ppm)	δ_H (ppm), Multiplicity, *J* (Hz)	HMBC	COSY
2	156.50	-	H-2′, H6′	-
3	133.33	-	-	-
4	177.69	-	-	-
5	161.65	-	5-OH, H-6	-
6	99.48	6.18 (m)	5-OH, H-8	H-8
7	165.80	-	H-8	-
8	94.31	6.40 (m)	H-6	H-6
9	156.95	-	H-8	-
10	104.07	-	5-OH, H-8, H-6	-
1′	121.38	-	H-3′, H-5′	-
2′	131.32	8.04 (dd, 8.50, 2.10)	H-6′	H-3′, H-5′
3′	115.57	6.88 (d, 8.50)		H-2′, H6′
4′	160.42	-	H-2′, H6′, H-3′, H-5′	-
5′	115.57	6.88 (d, 8.50)		H-2′, H6′
6′	131.32	8.04 (dd, 8.50, 2.10)	H-2′	H-3′, H-5′
1″	101.27	5.45 (d, 7.50)	-	-

Table 4-17 The NMR spectral data of SS6-2 **(continued)**

Position	SS6-2 in DMSO-d_6 (^{1}H: 500 MHz; ^{13}C: 125 MHz)			
	δc (ppm)	δн (ppm), Multiplicity, *J* (Hz)	HMBC	COSY
2″	76.71	3.03-3.23 (m)	-	-
3″	74.80	3.03-3.23 (m)	-	-
4″	70.26	3.03-3.23 (m)	-	-
5″	77.90	3.03-3.23 (m)	-	-
6″	61.03	3.03-3.23 (m)	-	-
5-OH	-	12.60 (s)	C-5, C-6, C10	-
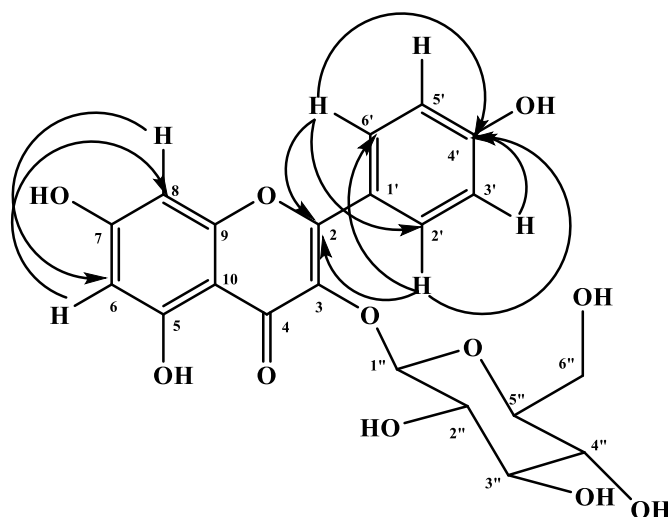
Figure 4-11 The main HMBC correlations of SS6-2
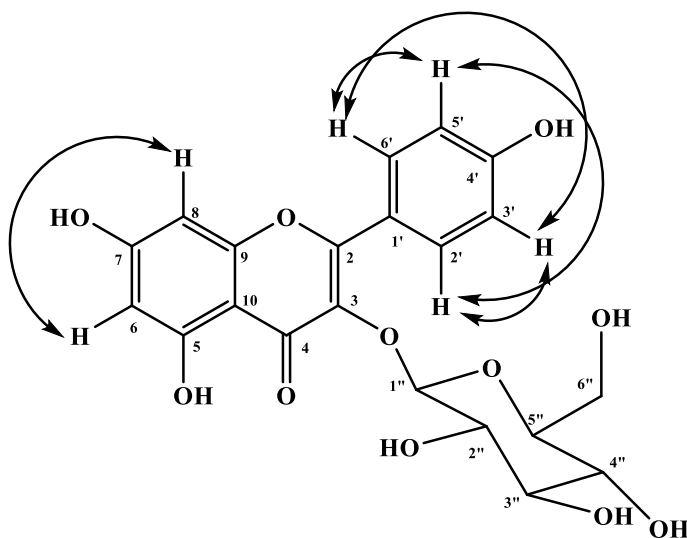
Figure 4-12 COSY correlations of SS6-2

Table 4-18 The comparison of ^{1}H- and ^{13}C-NMR spectral data between SS6-2 and
kaempferol-3-*O*-glycoside

Position	SS6-2 in DMSO-d_6 ([1]H: 500 MHz; [13]C: 125 MHz)		Kaempferol 3-*O*-glycoside in DMSO-d_6 ([1]H: 400 MHz; [13]C: 100 MHz) (Moura *et al.*, 2019)	
	δ_C (ppm)	δ_H (ppm), Multiplicity, *J* (Hz)	δ_C (ppm)	δ_H (ppm), Multiplicity, *J* (Hz)
2	156.50	-	156.5	-
3	133.33	-	133.3	-
4	177.69	-	177.5	-
5	161.65	-	161.2	-
6	99.48	6.18 (m)	98.7	6.22 (d, 2 Hz)
7	165.80	-	164.2	-
8	94.31	6.40 (m)	93.7	6.44 (d, 2 Hz)
9	156.95	-	156.2	-
10	104.07	-	104.0	-
1′	121.38	-	120.9	-

Table 4-18 The comparison of ^{1}H- and ^{13}C-NMR spectral data between SS6-2 and
kaempferol-3-*O*-glycoside **(continued)**

Position	SS6-2 in DMSO-d_6 (^{1}H: 500 MHz; ^{13}C: 125 MHz)		Kaempferol 3-*O*-glycoside in DMSO-d_6 (^{1}H: 400 MHz; ^{13}C: 100 MHz) (Moura *et al.*, 2019)	
	δ_C (ppm)	δ_H (ppm), Multiplicity, *J* (Hz)	δ_C (ppm)	δ_H (ppm), Multiplicity, *J* (Hz)
2′	131.32	8.04 (dd, 8.5, 2.1)	130.9	8.04 (d, 8.8 Hz)
3′	115.57	6.88 (d, 8.5)	115.2	6.89 (d, 8.8 Hz)
4′	160.42	-	160.0	-
5′	115.57	6.88 (d, 8.5 Hz)	115.2	6.89 (d, 8.8 Hz)
6′	131.32	8.04 (dd, 8.5, 2.1)	130.9	8.04 (d, 8.8 Hz)
1″	101.27	5.45 (d, 7.5)	100.8	5.47 (d, 7.3 Hz)
2″	76.71	3.03-3.23 (m)	74.3	3.18 (m)
3″	74.80	3.03-3.23 (m)	77.5	3.08 (m)
4″	70.26	3.03-3.23 (m)	69.9	3.08 (m)
5″	77.90	3.03-3.23 (m)	76.4	3.21 (m)
6″	61.03	3.03-3.23 (m)	60.9	3.32 (m) and 3.57 (m)
5-OH	-	12.60 (s)	-	12.65 (s)

4.2.2 The isolated compounds from *N. racemosa* stem

4.2.2.1 Structure determination of NR1

Molecular formula : $C_{10}H_8O_4$

NR1 (3.9 mg) was obtained as a yellow pale needles and dissolved in chloroform. The UV spectrum in chloroform (**Appendix 33**) showed λ_{max} at 341 nm. The IR spectrum (**Appendix 34**) demonstrated maximum absorption band at 3460 cm^{-1} (-OH), 1651 cm^{-1} (C=O), 1218 cm^{-1} (C-C), 772 cm^{-1} (C=CH) and 669 cm^{-1} (C=CH).

The ^{1}H-NMR spectrum of NR1 (500 MHz in CDCl$_3$, **Appendix 35**) exhibited six proton signals with δ_H 3.94 (s), 6.17 (s), 6.25 (d, *J* = 9.5 Hz), 6.63 (s), 6.90

(s), 7.58 (d, J = 9.5 Hz). The two doublet signals with one proton integration ratio and J = 9.5 Hz of coupling constant at δ_H 6.25 and 7.58 were determined as olefinic protons of H-3 and H-4, respectively. Two singlet signals with one proton integration ratio at δ_H δ 6.63 and 6.90 belong to aromatic protons of H-6 and H-9, consequently. The singlet signal with one proton integration ratio at δ_H 6.17 (OH-8) was assigned as the signal of hydroxyl group. Moreover, singlet signals with three protons integration ratio at δ_H 3.94 (OCH$_3$-7) were determined as signals of methoxyl proton.

The ^{13}C-NMR spectrum of NR1 (125 MHz in CDCl$_3$, **Appendix 36**) showed ten carbon signals that were assigned as three oxygenated aromatic carbon signals, two tertiary aromatic carbon signals, two olefinic methine signals, one quaternary carbon signals, one carbonyl signal and one methoxyl signal. The chemical shifts of three oxygenated aromatic carbon signals showed at δ_C 143.96 (C-7),149.64 (C-8) and 150.23 (C-10). Two tertiary aromatic carbon signals were presented at δ_C 103.18 (C-9) and 107.44 (C-6), while two olefinic methine signals were found at δ_C 113.42 (C-3) and 143.29 (C-4). The signal at δ_C 111.48 (C-5) was indicated as quaternary carbon. In addition, the carbon signals at δ_C 56.39 (OCH$_3$-7) and 161.43 (C-2) were assigned as one methoxy signal and cabonyl signal, respectively.

NMR spectral data of NR1 were showed in **Table 4-19**. The HMBC were used to confirm the correlations of proton to carbon on NR1 structure (**Figure 4-13**, **Appendix 37**). The NOESY experiment exhibited the correlation between the methoxy proton of C-7 (OCH$_3$-7) and the proton of C-6 (H-6) which showed as **Table 4-19**, **Figure 4-14** and **Appendix 38**. Therefore, NR1 (**Figure 4-2**) was indicated as 7-hydroxy-6-methoxy-2H-benzopyran-2-one or scopoletin. The NMR data of NR1 were compared with previous report (Siddiqui *et al*., 2007) as shown in **Table 4-19**.

Table 4-19 The comparison of ^{1}H- and ^{13}C-NMR spectral data between NR1 and scopoletin

Position	NR1 in CDCl₃ ([1]H: 500 MHz; [13]C: 125 MHz)				Scopoletin in CDCl₃ ([1]H: 400 MHz; [13]C: 100 MHz) (Siddiqui *et al.*, 2007)		
	δ_C (ppm)	δ_H (ppm), *J* (Hz)	HMBC	NOESY	δ_C (ppm)	δ_H (ppm), *J* (Hz)	HMBC
2	161.43	-	H-3, H-4	-	160.5	-	H-3
3	113.42	6.25 (d; 9.5)	-	-	112.5	6.26 (d; 9.4)	H-4
4	143.29	7.58 (d; 9.5)	H-6	-	142.0	7.58 (d; 9.4)	H-3
5	111.48	-	H-3, H-9	-	110.5	-	H-4, H-6
6	107.44	6.63 (s)	H-4	OCH₃-7	107.5	6.89 (s)	
7	143.96	-	H-9, OCH₃-7, OH-8	-	143.0	-	H-6, OCH₃-7
8	149.64	-	H-6, OH-8	-	149.5	-	H-9
9	103.18	6.90 (s)	OH-8	-	102.0	6.82 (s)	
10	150.23	-	H-4, H-6	-	150.0	-	H-9
OCH₃-7	56.39	3.94 (s)	-	H-6	55.2	3.93 (s)	
OH-8	-	6.17 (s)	-	-	-	-	

Figure 4-13 The main HMBC correlations of NR1
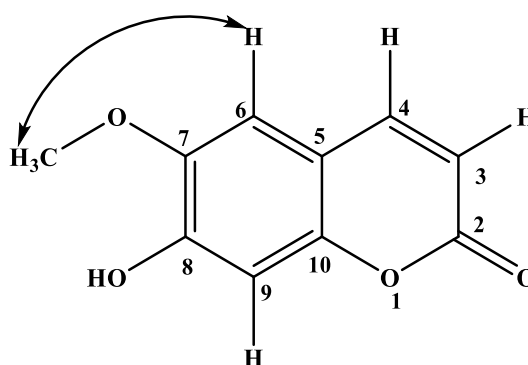
Figure 4-14 NOESY correlations of NR1

4.2.2.2 Structure determination of NR2

Molecular formula   : $C_9H_{10}O_5$

NR2 (1.9 mg) was obtained as an orange amorphous solid and dissolved in methanol. The UV spectrum in methanol (**Appendix 39**) showed λ_{max} at 289 nm. The IR spectrum (**Appendix 40**) demonstrated bands at 3434 cm^{-1} (-OH), 1640 cm^{-1} (C=O), 1426 cm^{-1} (C-O).

The ^{1}H-NMR spectrum of NR2 (500 MHz in DMSO-d_6, **Appendix 41**) exhibited three singlet proton signals with δ_H 3.78 (s), 7.19 (s), 9.07 (brs). First, the singlet signal with six protons integration ratio at δ_H δ 3.78 was assigned as two methoxyl proton signals of OCH$_3$-3 and OCH$_3$-5. Second, the singlet signal with two protons integration ratio at δ_H 7.19 was determined as aromatic protons of H-2 and H-6. The last broad singlet signal with one proton integration ratio at δ_H 9.07 ppm belongs

to the carboxylic proton, COOH-1. From ^{1}H-NMR data, it indicated that the NR2 structure was the polysubstitued benzene. ^{1}H-NMR and ^{13}C-NMR data of NR2 in DMSO-d_6 (**Appendix 41** and **Appendix 42**) corresponding to previous report of syringic acid (Phadungkit and Luanratana, 2006) as showed in **Table 4-20**. The HR-ESIMS data of NR2 was found [M-H][-] peak at *m/z* 197.0456 (**Appendix 43**) which indicated that the structure of NR2 (**Figure 4-2**) as 4-hydroxy-3,5-dimethoxybenzoic acid or syringic acid.

Table 4-20 The comparison of ^{1}H-NMR spectral data between NR2 and syringic acid

Position	NR2 in DMSO-d_6 ([1]H: 500 MHz; [13]C: 125 MHz)		Syringic acid in DMSO-d_6 ([1]H: 500 MHz; [13]C: 125 MHz) (Phadungkit and Luanratana, 2006)	
	δ_C (ppm)	δ_H (ppm), Multiplicity, *J* (Hz)	δ_C (ppm)	δ_H (ppm), Multiplicity, *J* (Hz)
1	139.96	-	141.67	-
2	147.50	7.19 (s)	148.79	7.33 (s)
3	107.03	-	108.24	-
4	121.67	-	121.87	-
6	147.50	7.19 (s)	148.79	7.33 (s)
5	107.03	-	108.24	-
COOH-1	167.53	9.07 (br)	169.93	-
OCH$_3$-3	56.11	3.78 (s)	56.73	3.82 (s)
OCH$_3$-5	56.11	3.78 (s)	56.73	3.82 (s)

4.2.2.3 Structure determination of NR3

Molecular formula   : $C_6H_{10}O_2$

NR3 (1.4 mg) was obtained as a brown amorphous solid and dissolved in chlorofrom. The UV spectrum in chlorofrom (**Appendix 44**) showed λ_{max} at 290 nm. The IR spectrum (**Appendix 45**) demonstrated bands at 2922 cm^{-1} (-CH$_3$), 1698-1595 cm^{-1} (C=C), 1457 cm^{-1} (-CH$_3$), 1260-1220 cm^{-1} (-OCH$_3$), 1110 cm^{-1} (-C-O), 874-800 cm^{-1} (=C-H).

The ^{1}H-NMR spectrum of NR3 (500 MHz in CDCl$_3$, **Appendix 46**) showed three singlet proton signals with δ_H 1.20 (s), 3.80 (s), 5.80 (s). The first singlet signal with six protons integration ratio at δ_H 1.20 belongs to two methyl proton signals which were methyl of C-4 and methyl substitution on C-3 (CH$_3$-3). The second singlet signal with three protons integration ratio at δ_H 3.80 was determined as methoxy proton signal which substituted at C-1 (OCH$_3$-1). The third singlet signal with one proton integration ratio at δ 5.80 ppm was identified as olefinic proton of C-2. ^{1}H-NMR data of NR3 in CDCl$_3$ were compared with previous report (Hagens *et al*., 1970) as **Table 4-21**.

The ^{13}C-NMR spectrum of NR3 (125 MHz in CDCl$_3$, **Appendix 47**) showed six carbon signals (**Table 4-21**) that were determined as one quaternary carbon signal (C-3), one olefinic methine signal (C-2), one cabonyl signal (C-1), one methoxyl signal (OCH$_3$-1) and two methyl signals (C-4 and CH$_3$-3). The analysis of HMBC data (**Table 4-21**, **Figure 4-15** and **Appendix 48**) confirmed the structure of NR3 (**Figure 4-2**) as methyl 3-methyl-2-butenonoate.

Table 4-21 The comparison of NMR spectral data between NR3 and methyl 3-methyl-2-butenonoate

Position	NR3 in CDCl$_3$ (^{1}H: 500 MHz; ^{13}C: 125 MHz)			Methyl 3-methyl-2-butenonoate in CCl$_4$ (Hagens *et al*., 1970)
	δ_C (ppm)	δ_H (ppm), Multiplicity	HMBC	δ_H (ppm), Multiplicity, *J* (Hz)
1	186.84	-	H-2	-
2	107.42	5.80 (s)	-	5.70 (septet; 1.5)
3	157.30	-	H-2, OCH$_3$-1	-
4	29.69	1.20 (s)	CH$_3$-3	2.15 (d; 1.5)
OCH$_3$-1	56.48	3.80 (s)	-	3.60 (s)
CH$_3$-3	29.35	1.20 (s)	H-4	1.86 (d; 1.5)
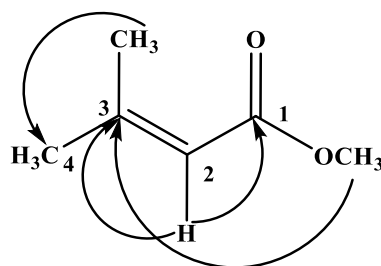
Figure 4-15 The main HMBC correlations of NR3

4.2.2.4 Structure determination of NR4

Molecular formula   : $C_{18}H_{19}NO_4$

NR4 (1.8 mg) was obtained as a white amorphous solid and dissolved in methanol. The UV spectrum in methanol (**Appendix 49**) showed λ_{max} at 318 nm. The IR spectrum (**Appendix 50**) demonstrated bands at 3434 cm^{-1} (-OH), 1652 cm^{-1} (-C=O), 1542 cm^{-1} (-NH) and 978 cm^{-1} (-CH=CH).

The ^{1}H-NMR spectrum of NR4 (500 MHz in CD$_3$OD, **Appendix 51**) were found one methoxy proton signals as singlet at δ_H 3.87. The two trans protons (H-2 and H-3) that conjugated to the carbonyl group were determined from the set of two doublets at δ_H 6.39 and 7.42 (both J = 15.62 Hz), respectively. In addition, the two doublet of doublet signals at δ_H 3.45 and 2.75 (both J = 7.08 and 7.56 Hz) were assigned as methylene protons (H-1′ and H-2′) that conjugated to secondary amine and aromatic parts, respectively. Other five proton signals at δ_H 6.72, 6.78, 7.01, 7.05 and 7.11 were indicated as protons of two aromatic rings. One of these rings is para substituented aromatic due to the same pattern of proton signals that are δ_H 6.72 (2H, dd; 9.27, 2.40) and 7.05 (2H, dd; 9.27, 2.40). ^{1}H-NMR data of NR4 in CD$_3$OD were compared with previous report (Jiang *et al*., 2017) as **Table 4-22**.

The ^{13}C-NMR spectrum of NR4 (125 MHz in CD$_3$OD, **Appendix 52**) showed sixteen carbon signals that were indicated as eighteen carbons. The carbon chemical shift at δ_C 169.19 was assigned as the carbonyl carbon (C-1) while the carbon at δ_C 56.42 was indicated as the methoxy cabon (OCH$_3$-6). Two methylene carbon signals of C-1′ and C-2′ showed at δ_C 42.53 and 35.81, respectively. Two olefinic methine carbon signal were presented at δ_C, 118.79 (C-2) and 142.01 (C-3), while two quaternary aromatic carbon signals were found at δ_C 128.31 (C-4), 131.22 (C-3′). Three

oxygenated aromatic carbons were observed at δ_C 149.32 (C-6), 149.88 (C-7), 156.94 (C-6′). The signals at δ_C 111.63 (C-5), 116.42 (C-8), 123.22 (C-9) were assigned as tertiary aromatic carbons of polysubstituted aromatic ring, while signals at δ_C 130.72 (C-4′ and C-8′) and 116.28 (C-5′ and C -7′) were indicated as tertiary aromatic carbons of para substituted aromatic ring.

Based on NMR data of NR4 was corresponding with the HR-ESIMS data that showed [M+Na]$^+$ peak at *m/z* 336.1206 (**Appendix 53**) and the previous report from Jiang and his colleagues (2017) (**Table 4-22**). The analysis of these data confirmed the structure of NR4 (**Figure 4-2**) as trans-*N*-feruloyltyramine.

Table 4-22 The comparison of ^{1}H- and ^{13}C-NMR spectral data between NR4 and *trans-N*-feruloyltyramine in CD$_3$OD

Position	NR4 in CD₃OD (^{1}H: 500 MHz; ^{13}C: 125 MHz)		*trans-N*-feruloyltyramine in CD₃OD (^{1}H: 500 MHz; ^{13}C: 125 MHz) (Jiang *et al*., 2017)	
	δ_C (ppm)	δ_H (ppm), Multiplicity, *J* (Hz)	δ_C (ppm)	δ_H (ppm), Multiplicity, *J* (Hz)
1	169.19	-	169.20	-
2	118.79	6.39 (d, 15.62)	118.78	6.40 (d,15.65)
3	142.01	7.42 (d, 15.62)	142.02	7.43 (d, 15.65)
4	128.31	-	128.29	-
5	111.63	7.11 (d, 1.95)	111.61	7.11 (d, 1.85)
6	149.32	-	149.33	-
7	149.88	-	149.91	-
8	116.42	6.78 (d, 8.06)	116.50	6.80 (d, 8.15)
9	123.22	7.01 (dd, 1.95, 8.29)	123.22	7.02 (dd, 8.20, 1.90)
1′	42.53	3.45 (dd, 7.08, 7.56)	42.53	3.47 (t, 7.15)

Table 4-22 The comparison of ^{1}H- and ^{13}C-NMR spectral data between NR4 and *trans-N*-feruloyltyramine in CD$_3$OD **(continued)**

Position	NR4 in DMSO-d_6 (^{1}H: 500 MHz; ^{13}C: 125 MHz)		*trans*-*N*-feruloyltyramine in CD$_3$OD (^{1}H: 500 MHz; ^{13}C: 125 MHz) (Jiang *et al*., 2017)	
	δ_C (ppm)	δ_H (ppm), Multiplicity, J (Hz)	δ_C (ppm)	δ_H (ppm), Multiplicity, J (Hz)
2′	35.81	2.75 (dd, 7.08, 7.56)	35.81	2.76 (t, 7.25)
3′	131.33	-	131.33	-
4′	130.72	7.05 (dd, 2.40, 9.27)	130.73	7.05 (m)
5′	116.28	6.72 (dd, 2.40, 9.27)	116.28	6.72 (m)
6′	156.94	-	156.94	-
7′	116.28	6.72 (dd, 2.40, 9.27)	116.28	6.72 (m)
8′	130.72	7.05 (dd, 2.40, 9.27)	130.73	7.05 (m)
OCH$_3$-6	56.42	3.87 (s)	56.42	3.88 (s)

4.2.2.5 Structure determination of NR5

Molecular formula   : C$_{17}$H$_{17}$NO$_3$

NR5 (9.9 mg) was obtained as a white amorphous solid and dissolved in methanol. The UV spectrum in methanol (**Appendix 54**) showed λ_{max} at 295 nm. The IR spectrum (**Appendix 55**) demonstrated maximum absorption band at 3434 cm^{-1} (-OH), 1637 cm^{-1}(-C=O), 1541 cm^{-1} (-NH) and 980 (-CH=CH-).

The ^{1}H-NMR spectrum of NR5 (500 MHz in CD$_3$OD, **Appendix 56** and **Table 4-23**) was quite similar pattern to ^{1}H-NMR of NR4. The doublet signals at δ_H

6.38 and 7.44 were indicated as two trans protons of position 2 (H-2) and 3 (H-3), respectively. The doublet of doublet signals at δ_H 3.45 and 2.75 were assigned as two methylene protons of position 1′ (H-1′) and 2′ (H-2′), consequently. Moreover, four proton signals, δ_H 6.70 (2H, dt; 8.5, 2.00), 6.78 (2H, dt; 8.5, 2.00), 7.05 (2H, dt; 8.5, 2.00) and 7.38 (2H, dt; 8.5, 2.00), were also assigned as protons on two para substituted aromatic rings. ^{1}H-NMR data of NR5 was compared with previously reported data of *trans-N*-coumaroyltyramine in CD$_3$OD (**Table 4-23**).

The ^{13}C-NMR of NR5 (125 MHz in CD$_3$OD, **Appendix 57**) showed thirteen carbon signals that were indicated as seventeen carbons. The comparison of ^{13}C-NMR data between NR5 and NR 4 was found the similar signals of one carbonyl carbon (at δ_C 169.25 (C-1)), two methylene signals (at δ_C 35.82 (C-2′) and 42.53 (C-1′)), two olefinic methine carbon signals (at δ_C 118.49 (C-2) and 141.76 (C-3)) and two quaternary carbon signals (at δ_C 127.77 (C-4) and 131.34 (C-3′)). Two oxygenated aromatic carbons were observed at δ_C 156.92 (C-6′) and 160.50 (C-7). The four signals (at δ_C 130.3 (C-5 and C-9), 116.72 (C-5′ and C -7′), 116.28 (C-6 and C-8) and 130.72 (C-4′ and C-8′)) were assigned as eight tertiary aromatic carbons of two para substituented rings. The difference in ^{13}C-NMR data between NR4 and NR5 were indicated the difference amount of oxygenated aromatic carbons, tertiary aromatic carbons and methoxy substitution. The structure of NR5 (**Figure 4-2**) was determined as *trans-N*-coumaroyltyramine. ^{13}C-NMR data of NR5 in CD$_3$OD were compared with previous report as showed in **Table 4-23** (Jiang *et al*., 2017). The HR-ESIMS data of NR5 showed [M+Na]$^+$ peak at *m/z* 306.1101 (**Appendix 58**) which agreed with *trans-N*-coumaroyltyramine mass.

Table 4-23 The comparison of ^{1}H- and ^{13}C-NMR spectral data between NR5 and *trans-N*-coumaroyltyramine in CD$_3$OD

Position	NR5 in CD₃OD (^{1}H: 500 MHz; ^{13}C: 125 MHz)		*trans-N*- coumaroyltyramine in CD₃OD (^{1}H: 500 MHz; ^{13}C: 125 MHz) (Jiang *et al*., 2017)	
	δc (ppm)	δH (ppm)	δc (ppm)	δH (ppm)
1	169.25	-	169.2	-
2	118.49	6.38 (d, 15.86)	118.4	7.44 (d; 15.5)
3	141.76	7.44 (d, 15.86)	141.8	6.38 (d; 15.5)
4	127.77	-	127.7	-
5	130.53	7.38 (dt, 2.00, 8.50)	130.5	7.41 (d; 8.4)
6	116.28	6.78 (dt, 2.00, 8.50)	116.2	6.80 (d; 8.4)
7	160.50	-	160.5	-
8	116.28	6.78 (dt, 2.00, 8.50)	116.2	6.80 (d; 8.4)
9	130.53	7.38 (dt, 2.00, 8.50)	130.5	7.41 (d; 8.4)
1′	42.53	3.45 (2H, dd, 7.07, 7.57)	42.5	3.46 (t; 7.5)
2′	35.82	2.75 (2H, dd, 7.08, 7.56)	35.8	2.75 (t; 7.5)
3′	131.34	-	131.3	-
4′	130.72	7.05 (dt, 2.00, 8.50)	130.7	7.06 (d; 8.6)
5′	116.72	6.70 (dt, 2.00, 8.50)	116.7	6.73 (d; 8.6)
6′	156.92	-	156.9	-
7′	116.72	6.70 (dt, 2.00, 8.50)	116.7	6.73 (d; 8.6)
8′	130.72	7.05 (dt, 2.00, 8.50)	130.7	7.06 (d; 8.6)

4.3 The biological activity on α-glucosidase inhibitory test

4.3.1 Mode of action of the extracts

The five selected extracts that showed the IC_{50} of α-glucosidase inhibition below 500 µg/ml were determined on mode of action (MoA). Three selected extracts from *S. stramonifolium* inflorescence were SSEA (IC_{50} = 215.92 µg/ml), SSEO (IC_{50} = 221.67 µg/ml) and SSWT (IC_{50} = 324.44 µg/ml), while two selected extracts from *N. racemosa* stem were NREA (IC_{50} = 191.44 µg/ml) and NREO (IC_{50} = 39.65 µg/ml). The standard acarbose showed IC_{50} = 241.40-245.95 µg/ml (**Table 4-1** and **Table 4-2**). The samples were evaluated their MoA by the double reciprocal Lineweaver-Burk plot and were determined the inhibition constants (Ki) by secondary plot.

From Lineweaver–Burk plots of SSWT (**Figure 4-16**) and NREA (**Figure 4-18**), the values of both y-intercept and x-intercept were increased following with the increasing of the extract concentration, while their slopes of the plots were similar. This phenomenon indicated that SSWT and NREA were the uncompetitive inhibitors. The uncompetitive manner is the inhibitor binding to the enzyme-substrates (ES) complex that effect to maximal velocity (V_m) of the system. Moreover, the inhibitor binding also effects to Michaelis constant (K_m) because it changes substrate and enzyme affinity. The values of both V_m and K_m are decrease, when an uncompetitive inhibitor concentrations of the system increase (Copeland, 2005). The second plot of SSWT (**Figure 4-17**) and NREA (**Figure 4-19**) were presented the Ki′ values, inhibitor constant when inhibitor bound with ES, as 199.27 and 88.01 µg/ml, respectively.

Lineweaver–Burk plots of SSEA (**Figure 4-20**), SSEO (**Figure 4-21**) and NREO (**Figure 4-22**) presented the relation of the increasing of extract concentration which effected to both intercept and slope. These plot manners indicated that SSEA, SSEO and NREO were mixed type inhibitors. The mixed-type inhibition was defined as the situation that two inhibitor molecules bind to different sites on the enzyme (Copeland, 2005).

Lineweaver–Burk plots of acarbose standard (**Figure 4-23**) exhibited the intercept value was constant but the slope and x-intercept values changed with

different acarbose concentations. This situation of acarbose implied to competitive inhibition manner. For competitive model, the inhibitor (I) competes with substrate to bind exclusively to enzyme (E) for enzyme-inhibitor (EI) forming. The high concentration of inhibitor reduces ES complex forming, so the EI complex forming effects to K_m value for substrate of the enzyme. However, the EI complex forming does not alter V_m value of the system (Copeland, 2005; Waldrop, 2020). The secondary plot of acarbose (**Figure 4-24**) showed the Ki value, the inhibition constant when inhibitor bound with E, as 125.57 μg/ml. The summary inhibition kinetic information of the selected extracts and acarbose were presented in **Table 4-24**.
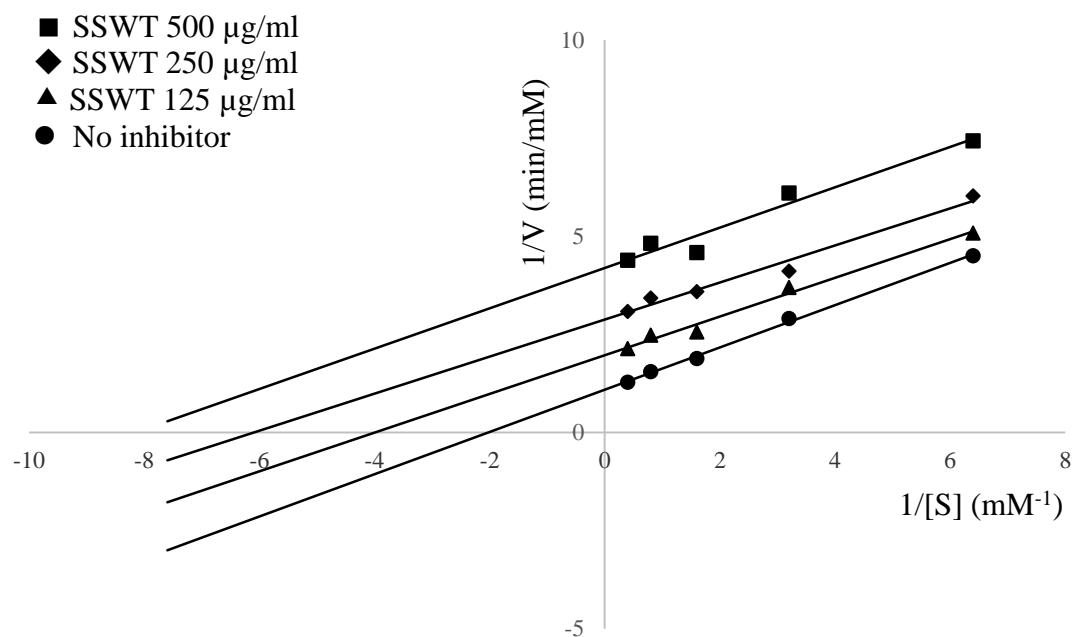
Figure 4-16 Lineweaver-Burk plot of *S. stamonifolium* water (SSWT) extract

(V = velocity; [S] = substrate concentration)
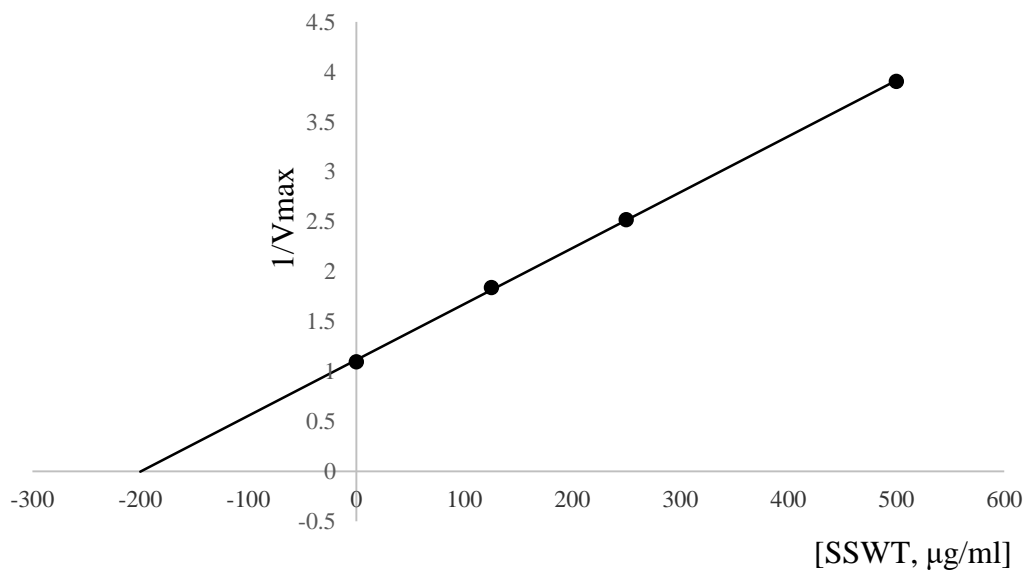
Figure 4-17 The secondary plot of SSWT

(V$_{max}$ = maximum velocity)
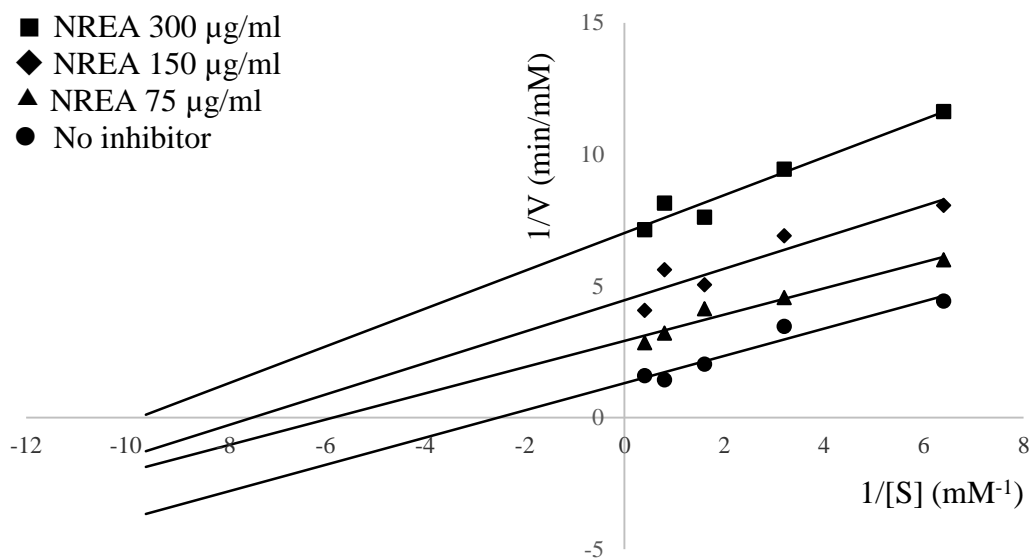
Figure 4-18 Lineweaver-Burk plot of *N. racemosa* ethyl acetate (NREA) extract

(V = velocity; [S] = substrate concentration)
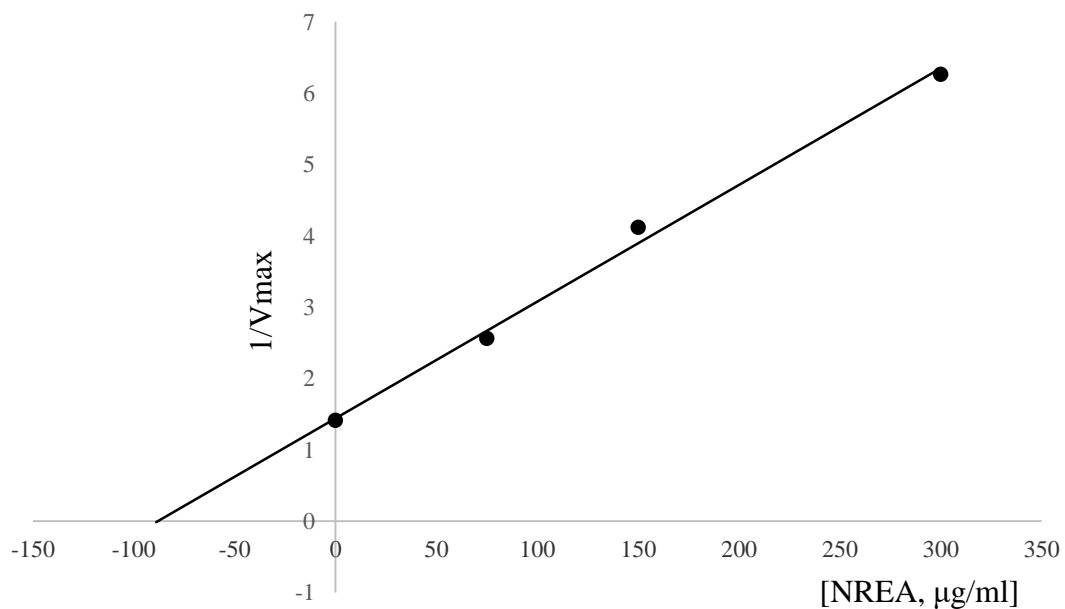
Figure 4-19 The secondary plot of NREA

(V_{max} = maximum velocity)
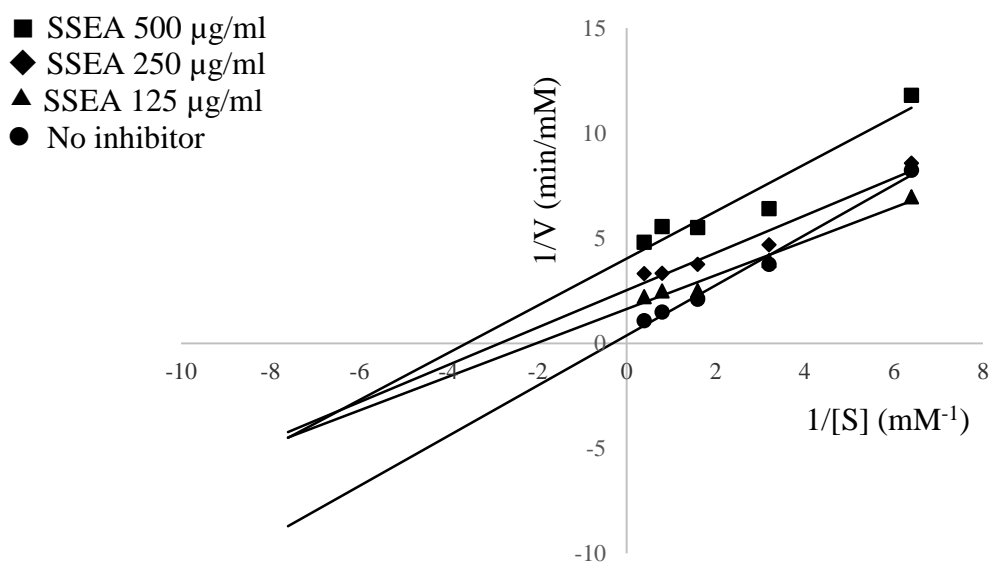
Figure 4-20 Lineweaver-Burk plot of *S. stamonifolium* ethyl acetate (SSEA) extract

(V = velocity; [S] = substrate concentration)
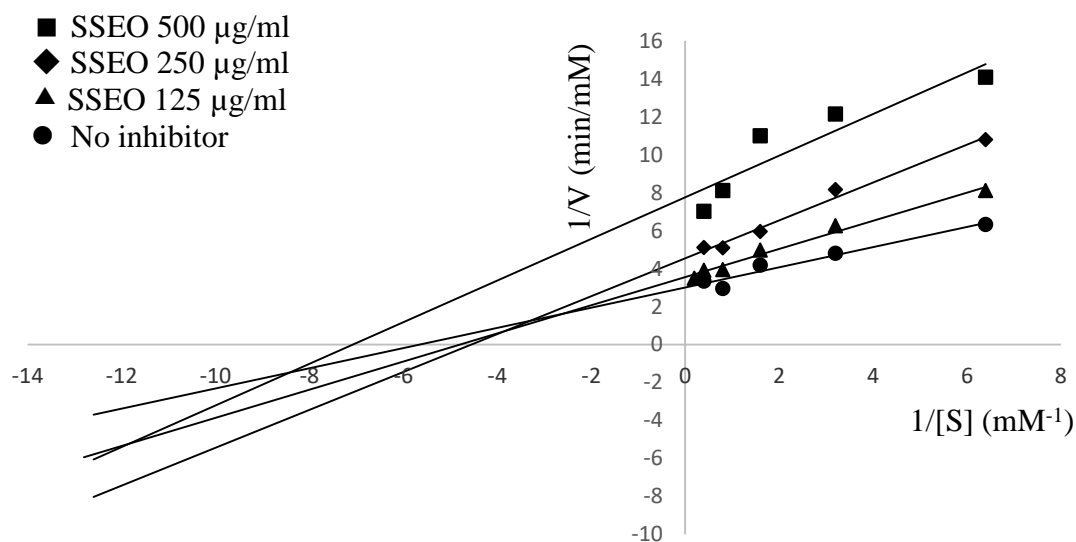
Figure 4-21 Lineweaver-Burk plot of *S. stamonifolium* ethanol (SSEO) extract

(V = velocity; [S] = substrate concentration)
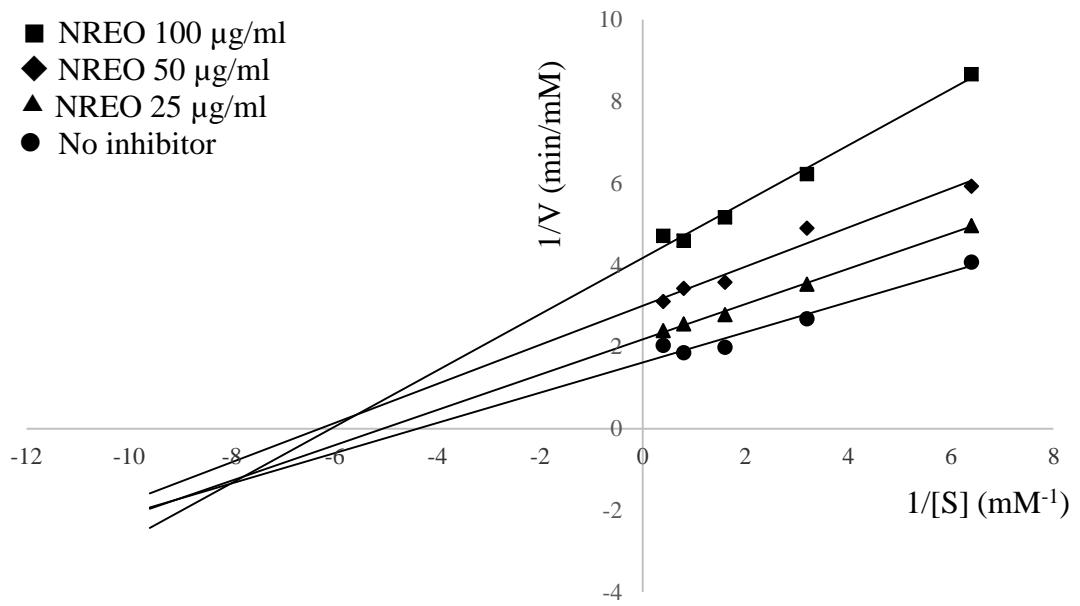
Figure 4-22 Lineweaver-Burk plot of *N. racemosa* ethanol (NREO) extract

(V = velocity; [S] = substrate concentration)
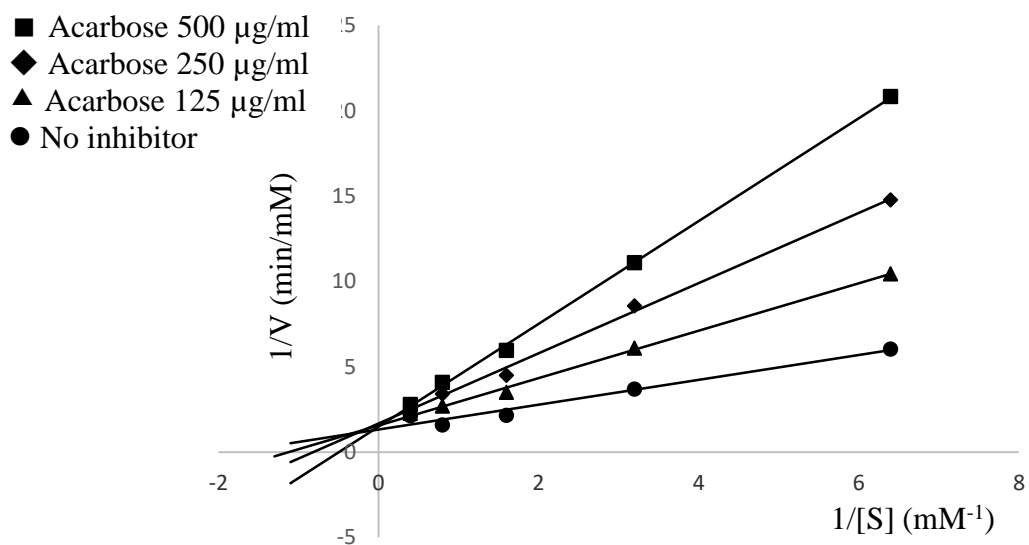
Figure 4-23 Lineweaver-Burk plot of acarbose

(V = velocity; [S] = substrate concentration)
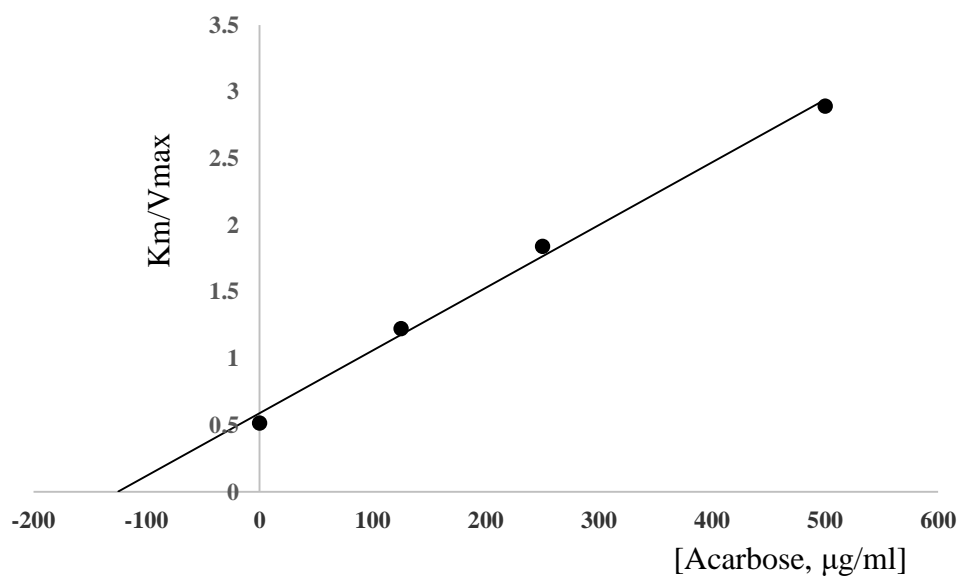
Figure 4-24 The secondary plot of acarbose

(K_m = Michaelis constant; V_{max} = maximum velocity)

Table 4-24 Kinetic inhibition mode of *S. stamonifolium* inflorescence and *N. racemosa* stem fractions to α-glucosidase enzyme

Source of extract	Extracted solvent	Code name	Kinetic inhibition mode	Ki[a] or Ki′[b] (μg/ml)
S. stamonifolium	Ethyl acetate	SSEA	Mixed inhibition	-
	Ethanol	SSEO	Mixed inhibition	-
	Water	SSWT	Uncompetitive inhibition	199.27 [b]
N. racemosa	Ethyl acetate	NREA	Uncompetitive inhibition	88.01 [b]
	Ethanol	NREO	Mixed inhibition	-
Acarbose (Standard)			Competitive inhibition	125.57[a]

[a] Inhibition constant when the inhibitor bound with free enzyme

[b] Inhibition constant when the inhibitor bound with enzyme-substrate complex

4.3.2 Combination test of the extracts

There have some evidences suggested that the combination of different bioactive compounds might support the inhibitory effect over than those of individual compound did (Wang *et al*., 2010; Jin *et al*., 2021). Moreover, some studies revealed beneficial of the combination of acarbose standard with natural extract and compounds (Akkarachiyasit *et al*., 2010; Adisakwattana *et al*., 2011; Sun *et al*., 2017). The current study was designed to investigate the combined effects of acarbose and the natural products. Since, the isolated compounds were less amount, there insufficient for further study of the combination effect with standard drug, acarbose. *S. stramonifolium* the crude extracts were selected for this study instead of isolated compounds. According to the selected extract isolation, four extracts of *S. stramonifolium* and two extracts of *N. racemosa* were also chosen for the combination study. The five different concentrations of each extract covered their IC$_{50}$ were combined with the standard acarbose at 250 μg/ml. The combination of acarbose and extract was non-constant ratio. The plots of fraction affected (F$_a$) versus combination index (CI) and the

normalized isobolograms of combined between acarbose and extract were used for investigation the combined effect on α-glucosidase.

The combination between acarbose 250 μg/ml and hexane extracts of *S. stramonifolium* (SSHX) were shown the inhibition and CI as showed in **Table 4-25**. The combined doses inhibited the α-glucosidase in range 47.08 - 53.68 % inhibition, while the CI values showed over 0.90. According to **Table 3-4**, the combination of acarbose and SSHX at 1000 and 2000 μg/ml were appointed as nearly additive effect (0.9-1.10), while the combination of acarbose and SSHX at 250, 500 and 4000 μg/ml had slight to moderate antagonism effect (1.10-1.45). The F_a-CI plot (**Figure 4-25**) showed the F_a value of the combination nearly 0.5. This figured out that the combinations were about 50 % inhibition. The normalized isobologram of combined acarbose 250 μg/ml and SSHX were observed as **Figure 4-26**. The actual combination points of acarbose and SSHX at 1000, 2000 and 4000 μg/ml were presented the ratio of median effect dose between acarbose and combined drug (A) over 0.8, while were showed the ratio of median effect dose between SSHX and combined drug (B) below 0.4. This imply that the inhibition may result from the standard acarbose more than SSHX.

Table 4-25 The α-glucosidase inhibition and combination index (CI) of acarbose and SSHX

Name	SSHX (μg/ml)						
	Concentration (μg/ml)		250	500	1000	2000	4000
		% inhibition	0.15	4.13	9.76	13.03	38.44
Acarbose (Standard)	62.5	25.94	Not determined				
	125	40.85					
	250	46.79	47.08 (1.24)*	46.07 (1.33)*	52.68 (0.98)*	53.68 (1.01)*	53.09 (1.21)*
	500	65.12	Not determined				
	1000	74.36					

* Combination index (CI) of acarbose 250 μg/ml combined with SSHX
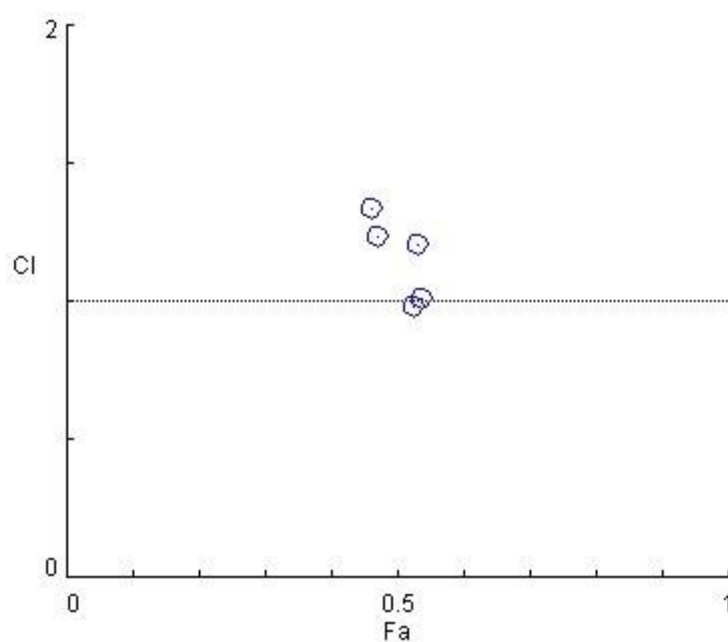
Figure 4-25 Fraction affected (F_a) versus combination index (CI) plot of acarbose
250 µg/ml and SSHX
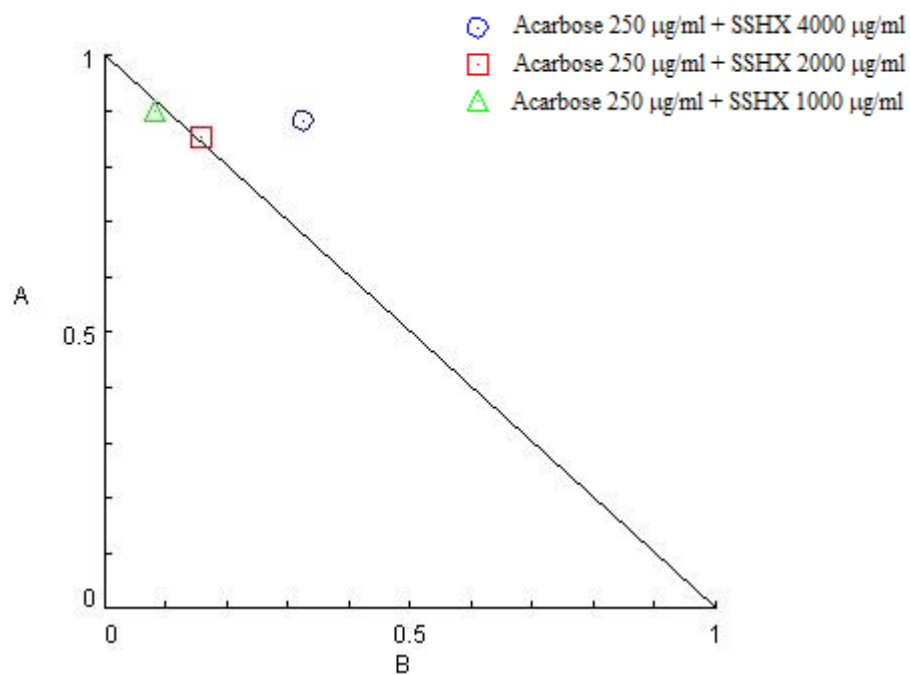
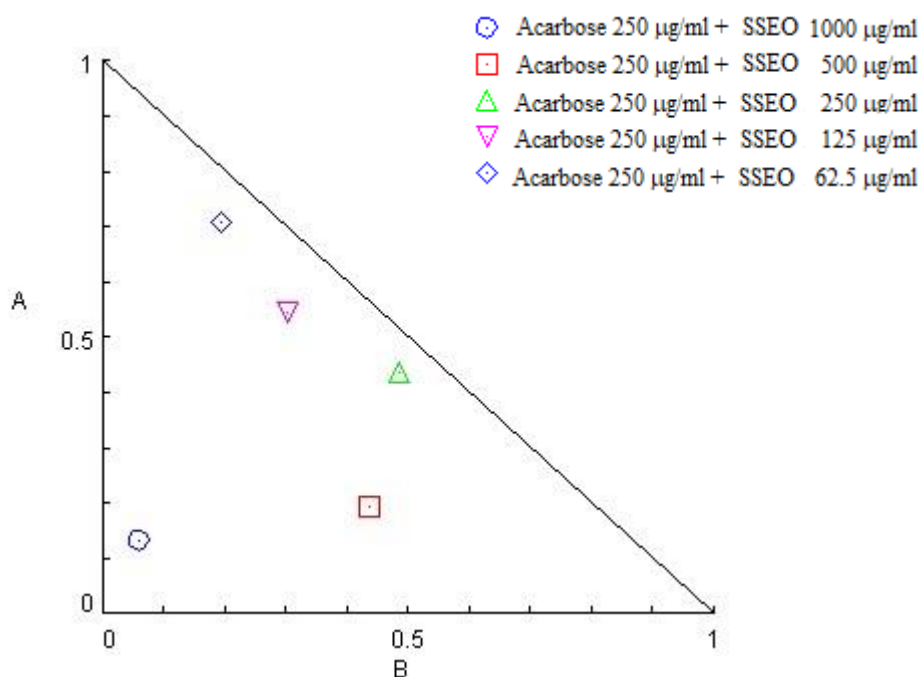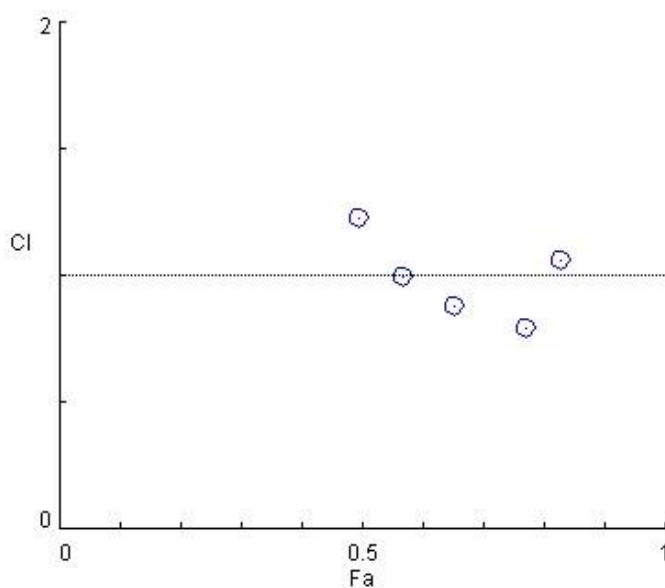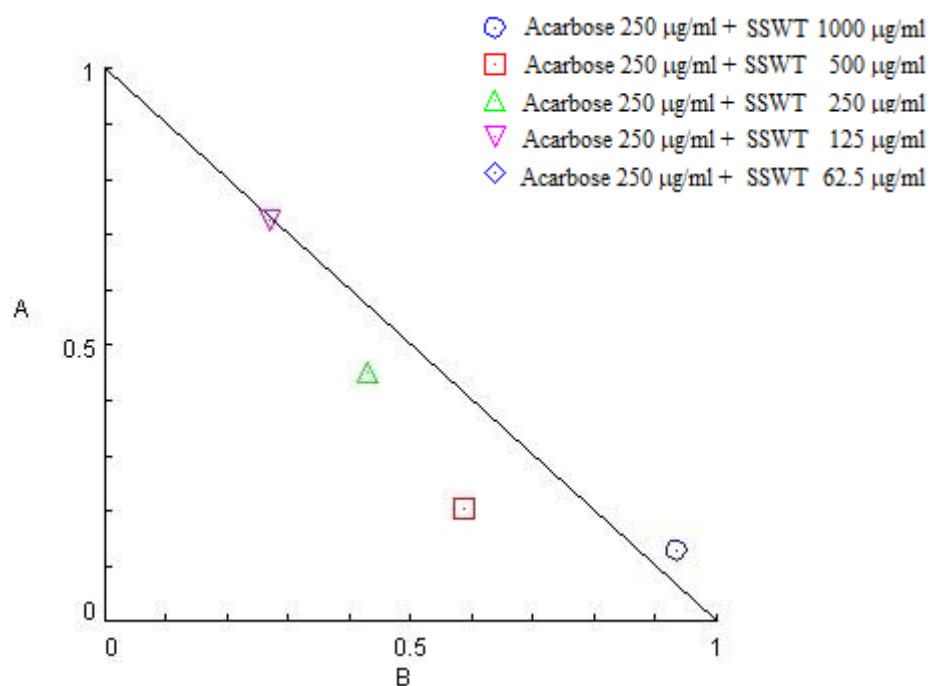**Figure 4-26** Isobolograms of acarbose 250 µg/ml and SSHX combination

(A = The ratio of median effect dose between acarbose and combined
drug; B = the ratio of median effect dose between SSHX and combined
drug)

The combination between acarbose 250 µg/ml and ethyl acetate extracts of *S. stramonifolium* (SSEA) were presented the inhibition and CI as showed in **Table 4-26**. The combined doses exhibited the increasing inhibition compared to the single drug. The CI values of acarbose and SSEA at 125, 250, 500 and 1000 µg/ml were indicated as moderate synergism effect (CI 0.7-0.85), while the CI value of acarbose and SSEA at 62.5 µg/ml was appointed as nearly additive effect (0.90-1.10). The F_a-CI plot (**Figure 4-27**) presented the F_a value of the combination above 0.5. The normalized isobologram of combined acarbose 250 µg/ml and SSEA were observed as **Figure 4-28**. The increasing dose of SSEA resulted to the actual combination points changing. When SSEA doses increased, the ratio values of median effect dose between SSEA and combined drug (B) were increased. This was implied that the increasing concentrations of SSEA resulted to the increasing ability of the acarbose to the α-glucosidase inhibition.

Table 4-26 The α-glucosidase inhibition and combination index (CI) of acarbose and SSEA

Name	SSEA (µg/ml)					
	Concentration (µg/ml)		62.5	125	250	500	1000
		% inhibition	20.51	48.47	53.75	68.15	81.54
Acarbose (Standard)	62.5	25.94	Not determined				
	125	40.85					
	250	46.79	54.09 (1.09)*	63.68 (0.83)*	70.01 (0.83)*	79.09 (0.77)*	86.10 (0.80)*
	500	65.12	Not determined				
	1000	74.36					

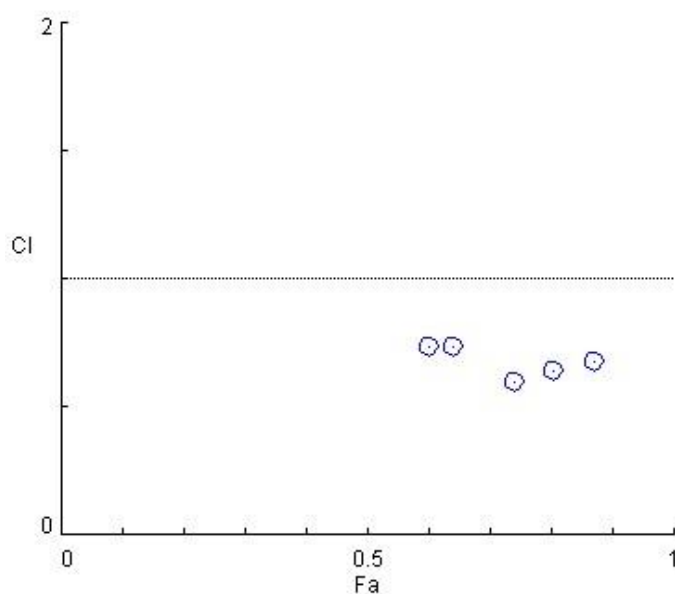* Combination index (CI) of acarbose 250 µg/ml combined with SSEA
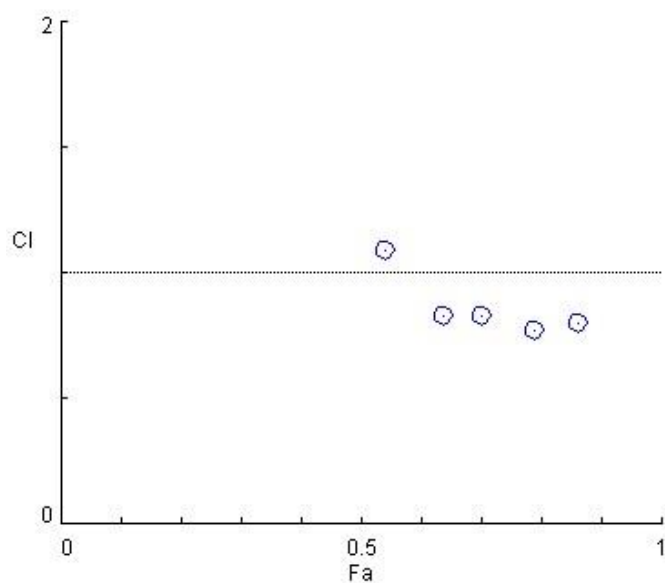
**Figure 4-27** Fraction affected (F_a) versus combination index (CI) plot of acarbose 250 μg/ml and SSEA
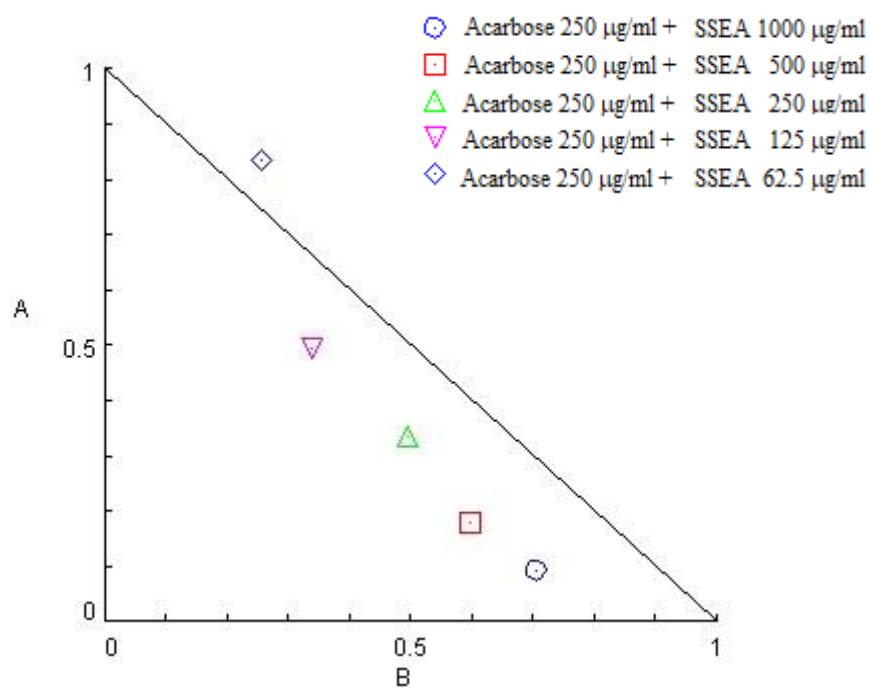
Figure 4-28 Isobolograms of acarbose 250 μg/ml and SSEA combination

(A = The ratio of median effect dose between acarbose and combined drug; B = the ratio of median effect dose between SSEA and combined drug)

The result of combination between acarbose 250 μg/ml and ethanol extract of *S. stramonifolium* (SSEO) were summarized in **Table 4-27**. All combined inhibitions were better than single drug inhibition. The CI values of the combined drugs showed lower than 1 indicated the synergistic effect of the combination. The interested fraction was the combination of acarbose 250 μg/ml and SSEO 1000 μg/ml. It was the strong synergism effect (CI = 0.19; 82.46% > 46.79%), according to synergistic description level (**Table 3-4**). The CI-F_a plot (**Figure 4-29**) showed the F_a value of the combination above 0.5. The isobolograms of combined acarbose 250 μg/ml and SSEO were presented as **Figure 4-30**. The plots of median effect ratio of acarbose 250 μg/ml and SSEO were range from 62.5 to 250 μg/ml which showed the direct changing from increasing of SSEO concentrations. On the other hand, the median effect ratio plots of acarbose and SSEO 500 and 1000 μg/ml were decreased. This was implied that the exhibited inhibition of combined acarbose with SSEO 500 and 1000 μg/ml were resulted from synergism effect. This indicated that high concentrations of SSEO could support the enzyme inhibition of acarbose.

Table 4-27 The α-glucosidase inhibition and combination index (CI) of acarbose and SSEO

Name	SSEO (μg/ml)						
	Concentration (μg/ml)		62.5	125	250	500	1000
		% inhibition	29.03	39.69	48.31	66.99	76.59
Acarbose (Standard)	62.5	25.94	Not determined				
	125	40.85					
	250	46.79	57.15 (0.90)*	61.94 (0.85)*	65.75 (0.92)*	77.89 (0.63)*	82.46 (0.19)*
	500	65.12	Not determined				
	1000	74.36					

* Combination index (CI) of acarbose 250 μg/ml combined with SSEO
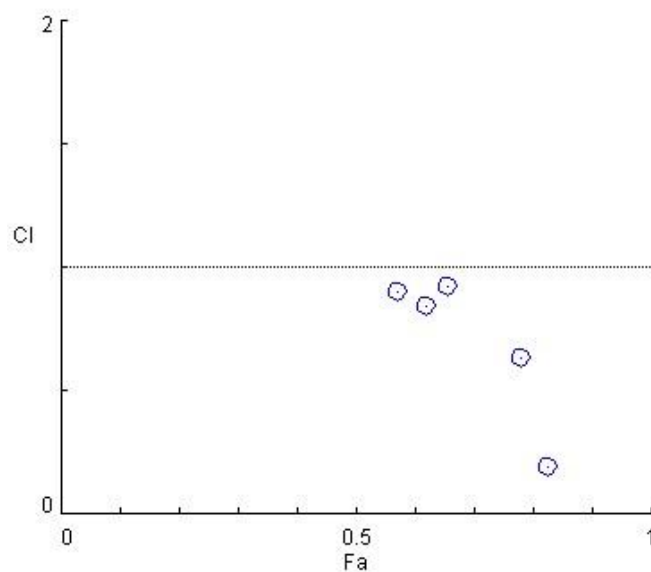
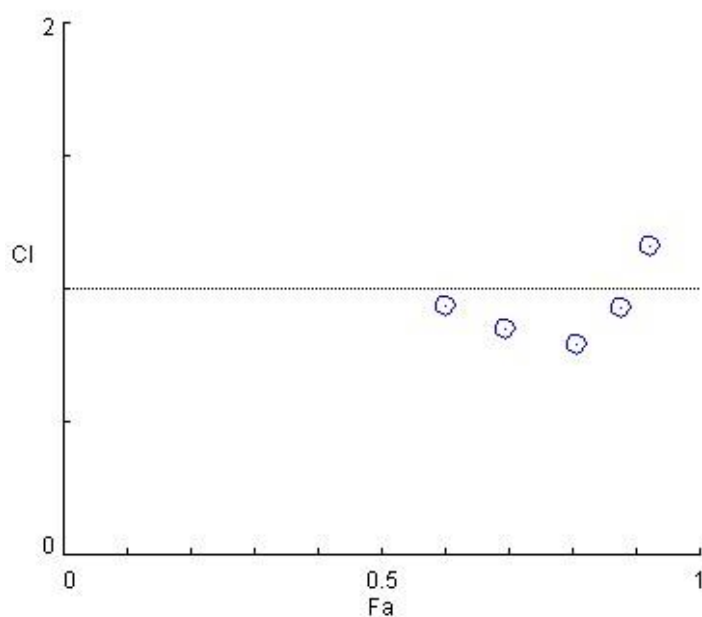**Figure 4-29** Fraction affected (F$_a$) versus combination index (CI) plot of acarbose
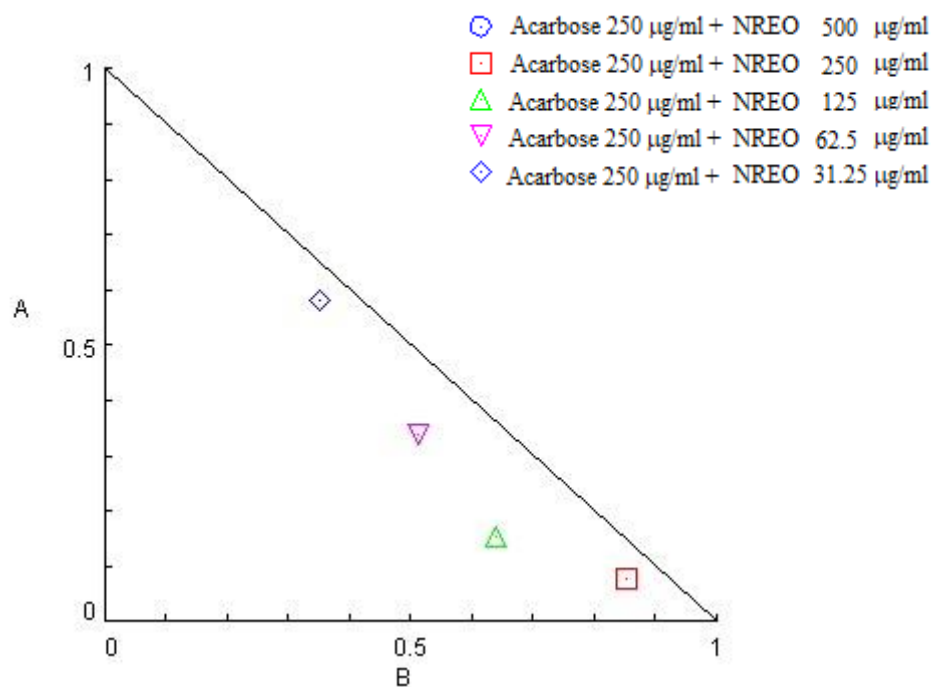250 μg/ml and SSEO

Figure 4-30 Isobolograms of acarbose 250 μg/ml and SSEO combination
(A = The ratio of median effect dose between acarbose and combined
drug; B = the ratio of median effect dose between SSEO and combined
drug)

The combination between acarbose 250 μg/ml and water extract of *S. stramonifolium* (SSWT) were summarized in **Table 4-28**. The inhibition of combined drug showed higher than single drug inhibition. The CI values of SSWT 250 μg/ml and 500 μg/ml were 0.88 and 0.79, respectively. From CI values, they were consequently categorized as slight synergism and moderate synergism. The CI values of SSWT 125 μg/ml and 1000 μg/ml were in the range of 0.90-1.10 which were indicated as nearly additive. Besides of this, the CI value of SSWT 62.5 μg/ml was 1.23 which were appointed as moderate antagonism. The CI-F_a plot (**Figure 4-31**) showed four F_a values above 0.5, while have only one F_a value below 0.5. The isobolograms of combined acarbose 250 μg/ml and SSWT were observed as **Figure 4-32**. The plots of median effect ratio were increased due to the increasing dose of SSWT. However, isobolograms showed that at only two concentrations of SSWT, 250 and 500 μg/ml, showed synergistic effect. This was implied that the concentration of SSWT which suitable supported the α-glucosidase inhibition of the acarbose were in the range of 250 - 500 μg/ml.

Table 4-28 The α-glucosidase inhibition and combination index (CI) of acarbose and SSWT

Name	SSWT (μg/ml)						
	Concentration (μg/ml)		62.5	125	250	500	1000
		% inhibition	3.31	22.18	39.97	60.53	76.70
Acarbose (Standard)	62.5	25.94	Not determined				
	125	40.85					
	250	46.79	49.46 (1.23)*	56.68 (1.00)*	65.19 (0.88)*	77.25 (0.79)*	82.96 (1.06)*
	500	65.12	Not determined				
	1000	74.36					

* Combination index (CI) of acarbose 250 μg/ml combined with SSWT

109

Figure 4-31 Fraction affected (F_a) versus combination index (CI) plot of acarbose 250 µg/ml and SSWT

Figure 4-32 Isobolograms of SSWT and acarbose combination

(A = The ratio of median effect dose between acarbose and combined drug; B = the ratio of median effect dose between SSWT and combined drug)

The combination between acarbose 250 µg/ml and ethyl acetate extract of *N. racemosa* (NREA) were presented the inhibition and CI as showed in **Table 4-29**. All combined inhibitions were better than single drug inhibition with CI values lower than 0.8. From the CI categorized (**Table 3-4**), the combination of NREA 125, 250 and 500 µg/ml were categorized into synergism (0.30-0.70), while the combination of NREA 31.25 and 62.5 µg/ml were classified as moderate synergism (0.70-0.85). The CI-F_a plot (**Figure 4-33**) presented the F_a value of the combination above 0.5. The isobolograms of combined acarbose 250 µg/ml and NREA (**Figure 4-34**) were observed that the increasing dose of NREA exhibited to increase the median effect ratio plots. This was implied that the higher concentration of NREA supported the α-glucosidase inhibition of the acarbose more than the lower concentration of NREA.

Table 4-29 The α-glucosidase inhibition and combination index (CI) of acarbose and NREA

Name	NREA (µg/ml)						
	Concentration (µg/ml)		31.25	62.5	125	250	500
		% inhibition	19.15	31.40	48.81	66.57	80.18
Acarbose (Standard)	62.5	23.84	Not determined				
	125	40.01					
	250	47.10	60.18 (0.74)*	64.14 (0.74)*	74.19 (0.60)*	80.58 (0.64)*	87.24 (0.68)*
	500	64.96	Not determined				
	1000	73.18					

* Combination index (CI) of acarbose 250 µg/ml combined with NREA

Figure 4-33 Fraction affected (F$_a$) versus combination index (CI) plot of acarbose

250 µg/ml and NREA
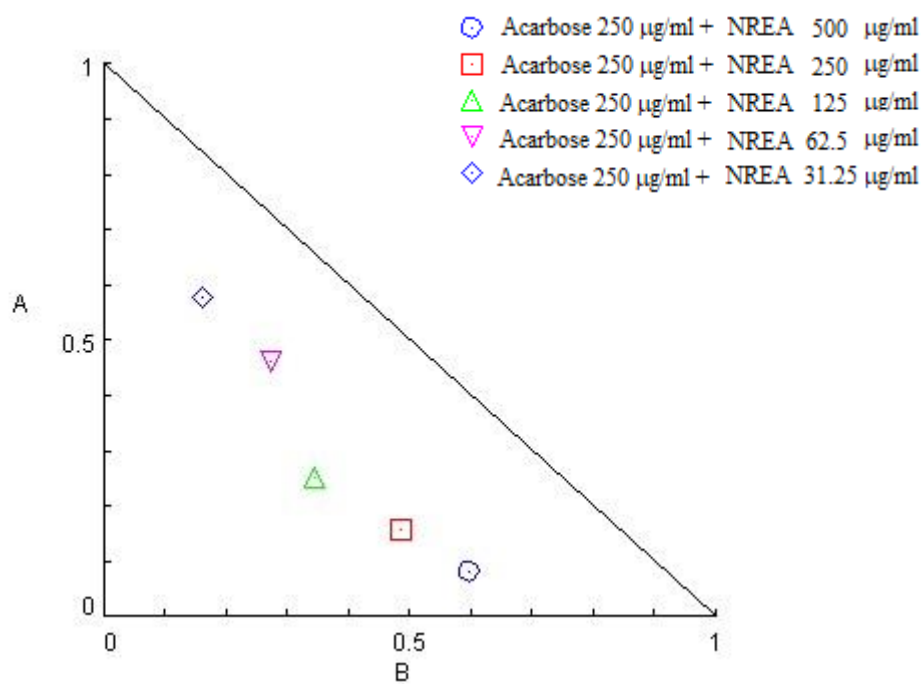
Figure 4-34 Isobolograms of NREA and acarbose combination

(A = The ratio of median effect dose between acarbose and combined

drug; B = the ratio of median effect dose between NREA and combined

drug)

The result of combination between acarbose 250 μg/ml and ethanol extract of *N. racemosa* (NREO) were summarized in **Table 4-30**. All combined inhibitions were better than single drug inhibition. From the CI categorized (**Table 3-4**), the CI value of NREO 125 μg/ml (CI = 0.79) and 62.5 μg/ml (CI = 0. 85) were appointed to moderate synergism (CI = 0.70-0.85); the CI values of NREO 250 μg/ml (CI = 0.93) and 31.25 μg/ml (CI = 0.94) were categorized into nearly additive (CI = 0.90-1.10); and the CI value of NREO 500 μg/ml (CI = 1.16) were indicated as slight anatagonism. The CI-F_a plot (**Figure 4-35**) showed the F_a value of the combination above 0.5. The isobolograms of combined acarbose 250 μg/ml and NREO (**Figure 4-36**) were observed that the varying dose of NREO exhibited to the median effect ratio. This result was implied that the increasing inhibitions resulted from increasing NREO concentrations because the acarbose concentration was fixed.

Table 4-30 The α-glucosidase inhibition and combination index (CI) of acarbose and NREO

Name	NREO (μg/ml)						
	Concentration (μg/ml)		31.25	62.5	125	250	500
		% inhibition	33.47	51.25	70.35	83.64	90.78
Acarbose (Standard)	62.5	23.84	Not determined				
	125	40.01					
	250	47.10	60.00 (0.94)*	69.50 (0.85)*	80.71 (0.79)*	87.63 (0.93)*	92.40 (1.16)*
	500	64.96	Not determined				
	1000	73.18					

* Combination index (CI) of acarbose 250 μg/ml combined with NREO

Figure 4-35 Fraction affected (F_a) versus combination index (CI) plot of acarbose
250 µg/ml and NREO

Figure 4-36 Isobolograms of NREO and acarbose combination
(A = The ratio of median effect dose between acarbose and combined
drug; B = the ratio of median effect dose between NREO and combined
drug)

4.3.3 α- Glucosidase inhibitory activity and mode of action of the isolated compounds

Whole of the isolated compounds from *S. stramonifolium* inflorescence and *N. racemosa* stem were investigated their α- glucosidase inhibitory activity as shown in **Table 4-31** to **4-32**. Since, the chemical compounds were isolated with small amount. So, they were insufficient amount for further determined the IC_{50} values. However, the isolated compounds were observed their binding mode of action on α-glucosidase enzyme by the double reciprocal Lineweaver-Burk plot and were evaluated the inhibition constant (Ki) by secondary plot.

The α- glucosidase inhibitory activities of six compounds from *S. stramonifolium* inflorescence were presented into two concentration categories, at 400 and 200 µg/ml, as shown in **Table 4-31**. The isolated compounds from *S. stramonifolium* (SS1-SS6) were flavonoids or flavonoid-glycoside. Their α-glucosidase inhibitory activities were less than acarbose standard as shown in **Table 4-31**. To investigate the IC_{50} of flavonoid compounds, kaempferol and astragalin standards were purchased and tested. However, flavonoid compounds had limited solubility then they were tested under restricted conditions (Tungjai *et al.*, 2008). The tested condition had not exceeded 5% DMSO as co-solvent. The IC_{50} values of kaempferol and astragalin standards were predicted from the tested exponential equations as 585.63 µg/ml and 40.07 mg/ml, respectively, as shown **Table 4-32**. The Lineweaver-Burk plot of kaempferol (**Figure 4-37**) and astragalin (**Figure 4-38**) displayed mixed-type inhibition. The standard acarbose exhibited Lineweaver-Burk plot manner as competitive inhibition (**Figure 4-39**) and showed secondary plot with Ki values as 110.48 µM (**Figure 4-40**). As mention in topic **4.3.1**, the competitive inhibition is the manner that the inhibitor scramble for enzyme-inhibitor (EI) complex forming. The mixed-type inhibition is the inhibitory manner that two inhibitors can bind to different parts of the enzyme. In addition, the non-competitive inhibition exhibits binding to both free enzyme (E) and enzyme-substrate (ES) complex with equivalent or un-equivalent affinity (Copeland, 2005). Two previous reports were determined the inhibitory activity of kaempferol on α-glucosidase in different manners, mixed-type inhibitor and non-competitive inhibitor (Peng *et al.*, 2016; Şöhretoğlu *et*

al., 2018). Moreover, the literature reported that astragalin was a non-competitive inhibitor to α-glucosidase (Jin *et al*., 2021).

Table 4-31 Inhibitory activity of the isolated compounds from *S. stamonifolium* inflorescence on α-glucosidase

Compounds		% Inhibition ± SD	
Code	Name	at 400 µg/ml	at 200 µg/ml
SS1	3, 4′, 5′, 7-tetramethyl ether of myricetin	12.78±4.89	-
SS2	Combretol	8.51±3.79	-
SS3	Kaempferol	13.01±2.69	-
SS4	Kaempferol-7-*O*-β glucopyranoside	7.68±0.33	-
SS5	5-hydroxy-3, 7, 4′, 5′-tetramethoxyflavone-3′-*O*-glucopyranoside	-	0.84±0.21
SS6	Mixture of Isorhamnetin-3-*O*-glucopyranoside and Astragalin (Kaempferol-3-*O* –glucopyranoside)	1.99±5.42	-
	Acarbose (Positive control)	60.78±3.61	45.27±4.45

Table 4-32 α-Glucosidase inhibitory activity of the selected compounds

Compounds	IC$_{50}$ (µg/ml)	Inhibition type	Ki [a] (µM)
Kaempferol	585.63	Mixed	-
Astragalin	40,066.98	Mixed	-
Acarbose (Positive control)	191.12	Competitive	110.48

[a] Inhibition constant
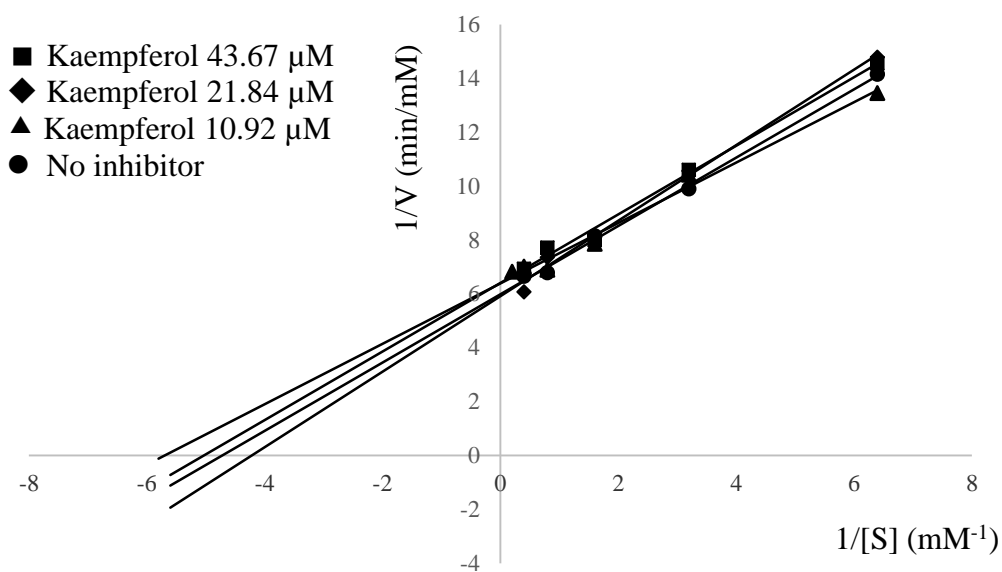
Figure 4-37 Lineweaver-Burk plot of kaempferol

(V = velocity; [S] = substrate concentration)
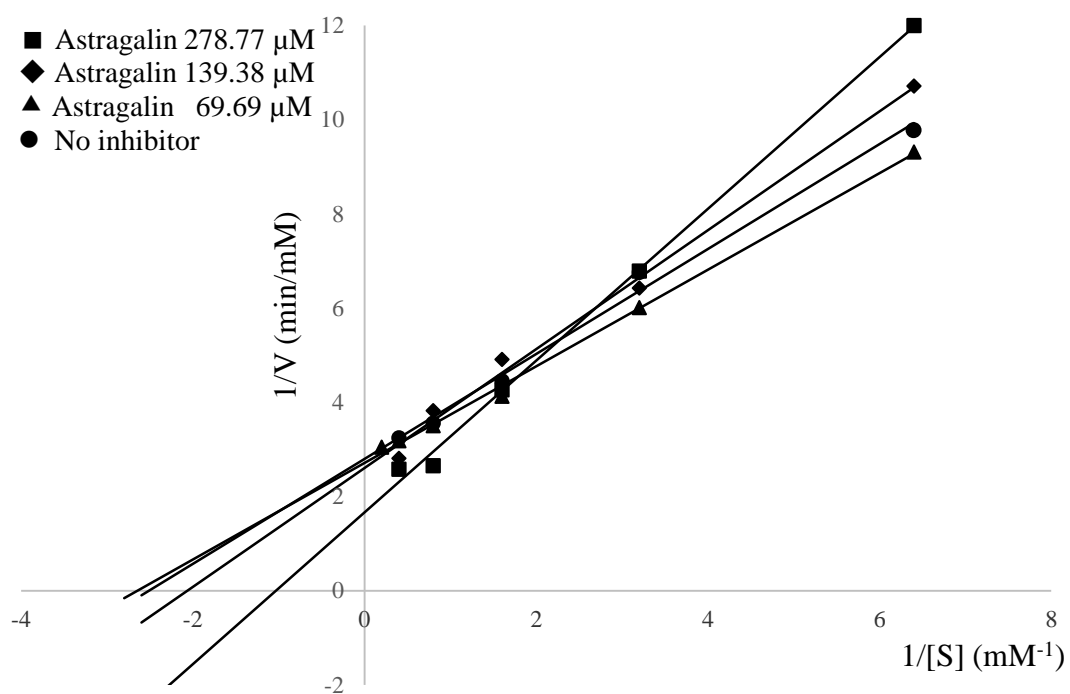
Figure 4-38 Lineweaver-Burk plot of astragalin

(V = velocity; [S] = substrate concentration)
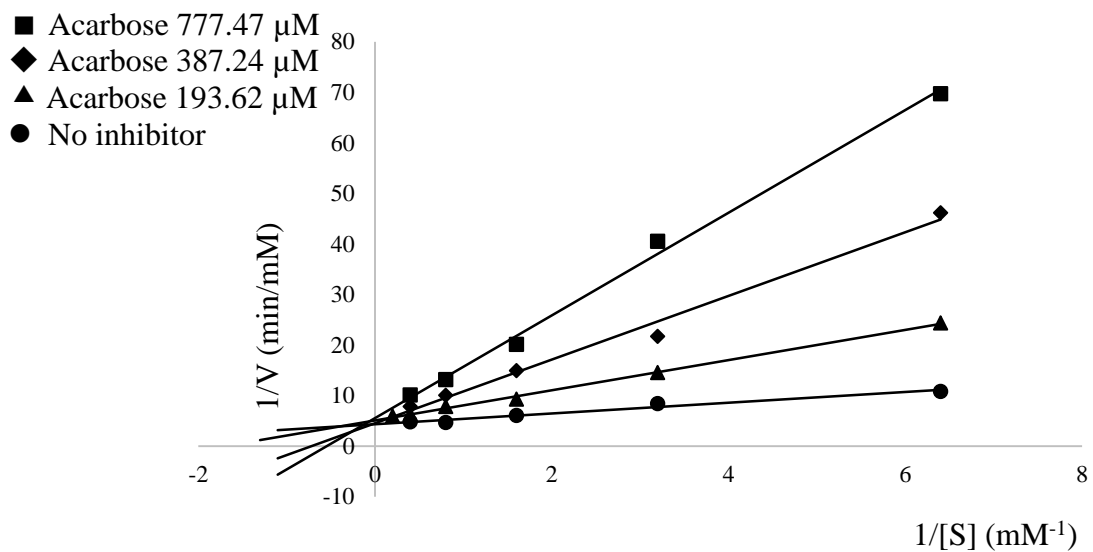
Figure 4-39 Lineweaver-Burk plot of acarbose

(V = velocity; [S] = substrate concentration)
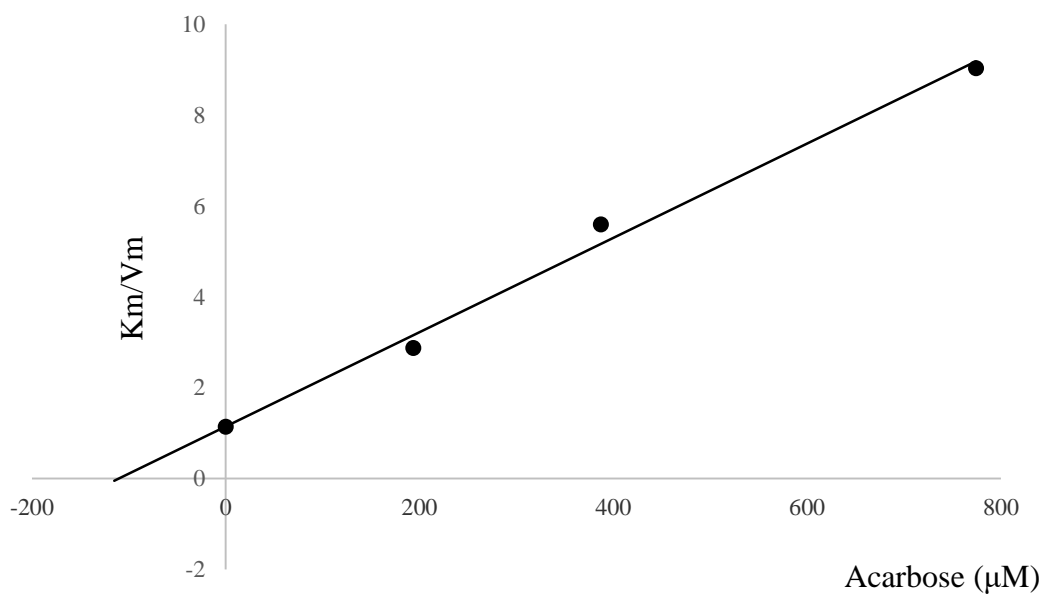
Figure 4-40 The secondary plot of acarbose

(K_m = Michaelis constant; V_{max} = maximum velocity)

To determined α-glucosidase inhibition of isolated compounds from *N. racemosa* stem, the IC_{50} values were presented inhibitory ability of the compounds as showed in **Table 4-33**. Three isolated compounds that were NR1 (IC_{50} = 110.97 μg/ml), NR4 (IC_{50} = 29.87 μg/ml) and NR5 (IC_{50} = 0.92 μg/ml) showed stronger α-glucosidase inhibition than the acarbose standard (IC_{50} = 272.72 μg/ml). For further explore the inhibition types of these compound, the double-reciprocal plots were displayed. The Lineweaver-Burk plot of NR1 (**Figure 4-41**) exhibited mixed-type inhibition, while the plots of NR4 (**Figure 4-42**) and NR5 (**Figure 4-44**) displayed the uncompetitive inhibition. The secondary plot with Ki′ values of NR4 (**Figure 4-43**) and NR5 (**Figure 4-45**) were indicated as 51.81 and 1.99 μM, respectively. The positive control, acarbose, showed the double reciprocal plot as the typical of competitive inhibition (**Figure 4-46**) and the Ki values from the secondary plot as 264.46 μM (**Figure 4-47**). However, the previous study indicated that NR1 was competitive inhibitor (Wu *et al.*, 2009). Some literature reports suggested that NR4 and NR5 were uncompetitive inhibitor, while some study claimed that they were non-competitive inhibitor (Liu *et al.*, 2011; Song *et al.*, 2016; Panidthananon *et al.*, 2018). The different kinetic analysis of the enzymatic inhibition may result from different condition of the assays. Promyos and his colleagues (2017) also suggested that many assay factors such as enzyme concentration, substrate concentration, buffer concentration, reaction temperature, wavelength of absorbance, sensitivity of spectrophotometer, reaction time and solvent may be caused of different binding detection.

Table 4-33 α-Glucosidase inhibitory activity of isolated compounds from *N. racemosa* stem

Compounds		IC$_{50}$	Inhibition	Ki^b or Ki′^{c}
Code	Name	(µg/ml)	type	(µM)
NR1	Scopoletin	110.97	Mixed	-
NR2	Syringic acid	> 500	N.T.^{a}	-
NR3	Methyl 3-methyl-2-butenonate	> 500	N.T.^{a}	-
NR4	*trans-N*-feruloyltyramine	29.87	Uncompetitive	51.81^c
NR5	*trans-N*-coumaroyltyramine	0.92	Uncompetitive	1.99^c
	Acarbose (Positive control)	272.72	Competitive	264.46^b

^{a} Not tested
^{b} Inhibition constant when inhibitor bound with free enzyme
^{c} Inhibition constant when inhibitor bound with enzyme-substrate complex
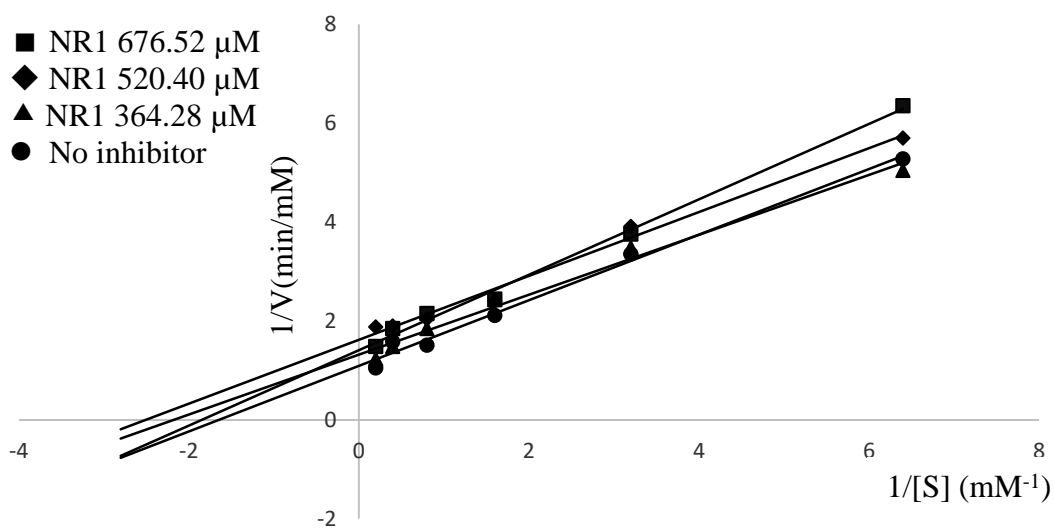
Figure 4-41 Lineweaver-Burk plot of NR1

(V = velocity; [S] = substrate concentration)
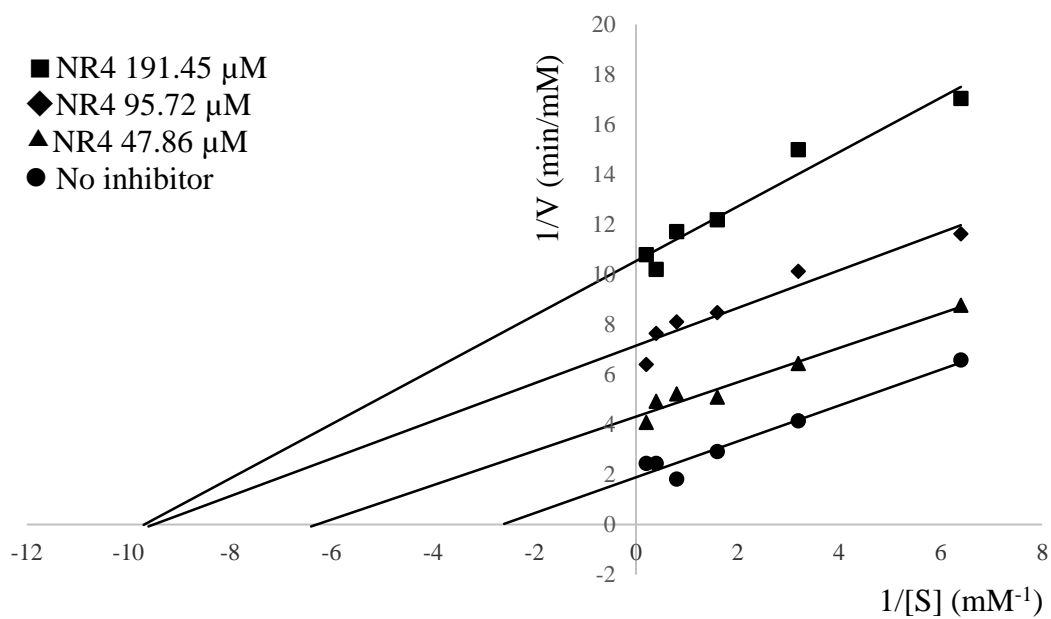
Figure 4-42 Lineweaver-Burk plot of NR4

(V = velocity; [S] = substrate concentration)
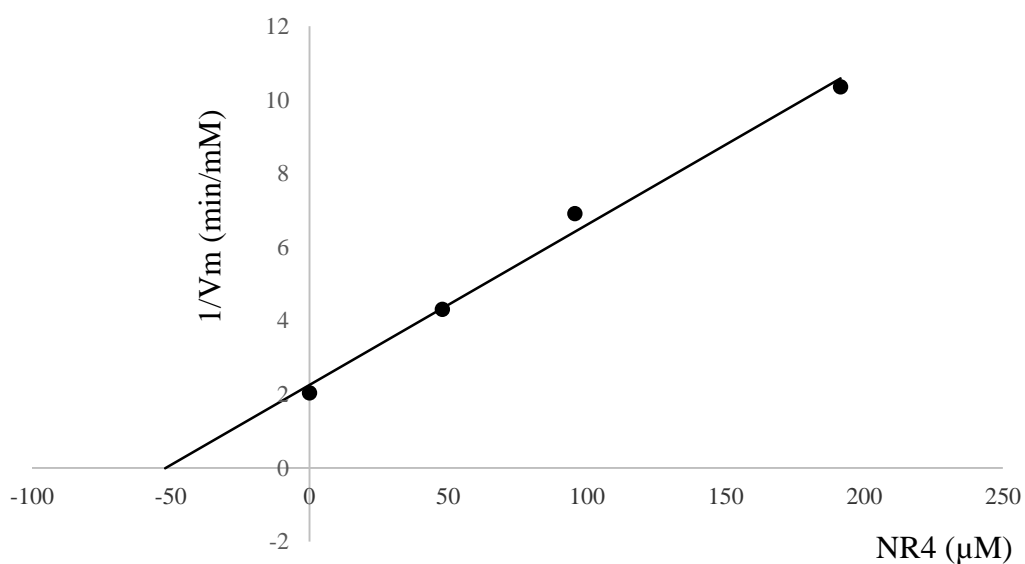
Figure 4-43 The secondary plot of NR4

(V_{max} = maximum velocity)
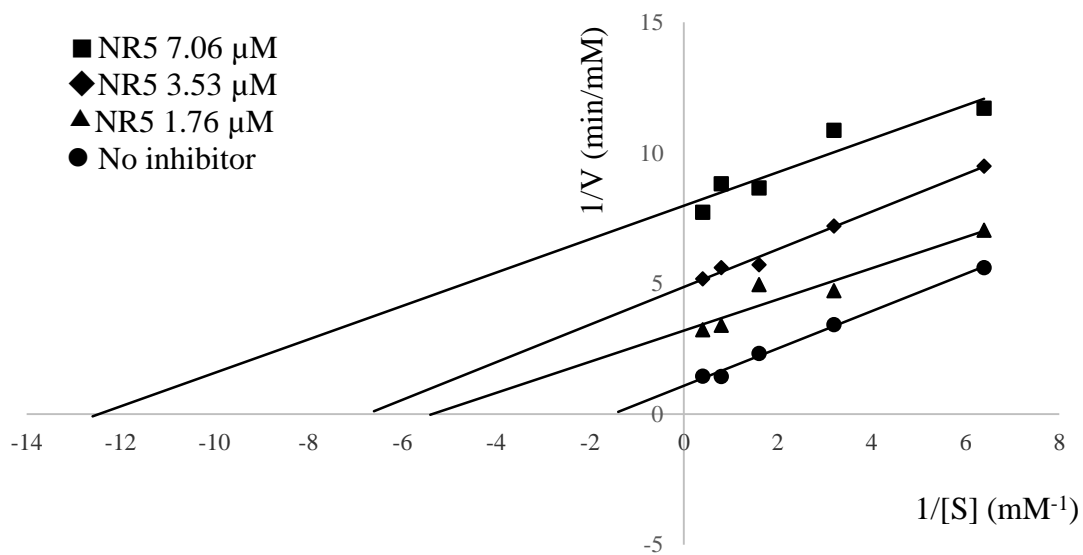
Figure 4-44 Lineweaver-Burk plot of NR5

(V = velocity; [S] = substrate concentration)
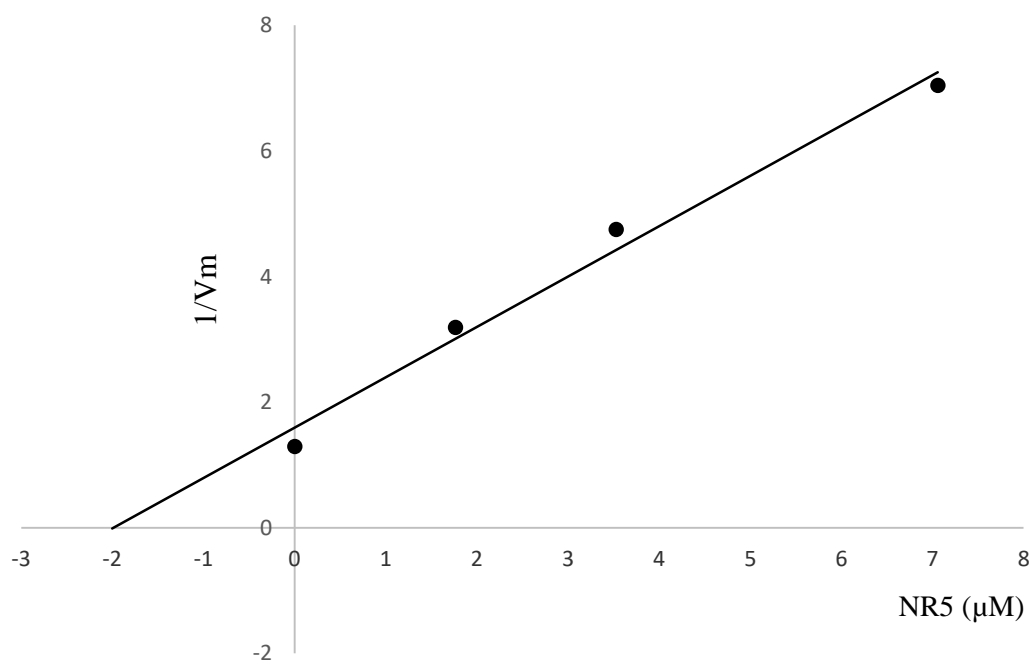
Figure 4-45 The secondary plot of NR5

(V_{max} = maximum velocity)
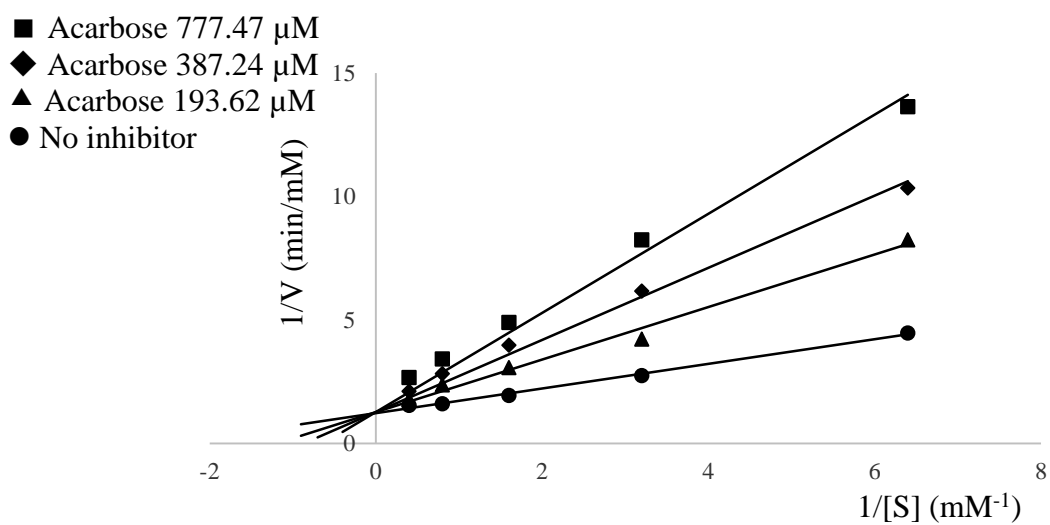
Figure 4-46 Lineweaver-Burk plot of acarbose

(V = velocity; [S] = substrate concentration)
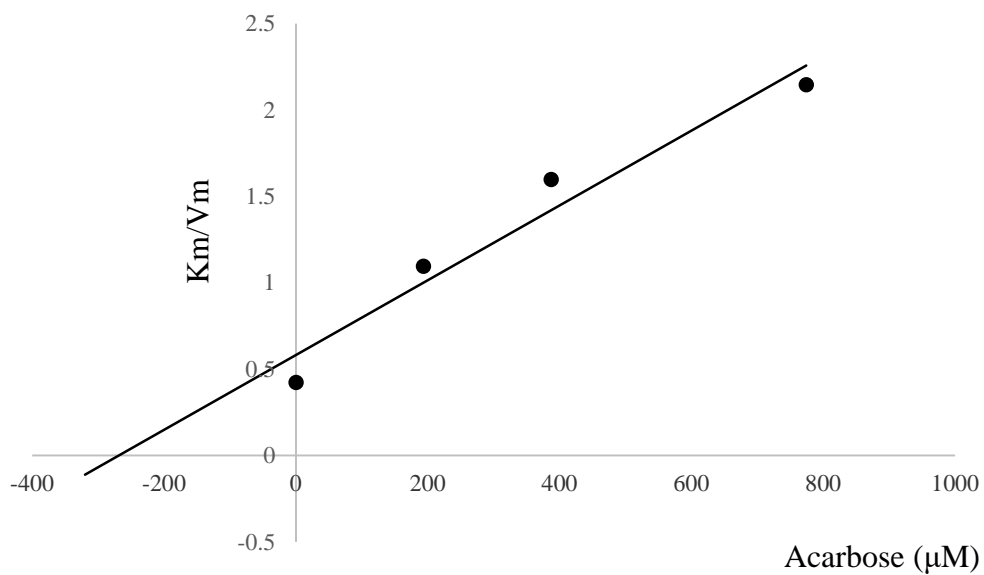
Figure 4-47 The secondary plot of acarbose

(K_m = Michaelis constant; V_{max} = maximum velocity)

4.3.4 Combination test of the selected compounds

        In addition, the study was conducted to evaluate the combination effect of acarbose with pure compounds, kaempferol and kaempferol-3-*O*-glucopyranoside (astragalin), on inhibition of α-glucosidase. Due to the limited solubility of the compounds, five different concentrations diluted from maximum solubility of each compounds were combined with the standard acarbose at 250 μg/ml. The dose-effect curves of non-constant ratio and the plots of fraction affected (F_a) versus combination index (CI) between acarbose and compounds were used for investigate the combined effect on α-glucosidase.

        The α-glucosidase inhibition of combination between acarbose 250 μg/ml and and CI values were showed in **Table 4-34**. All combined inhibitions were better than single kaempferol inhibition but less than the inhibition of acarbose at 250 μg/ml. The CI values showed over 1.21. Refer to the CI categorized in **Table 3-4**, the CI values of kaempferol's combination at 0.391-3.125 μg/ml were classified into moderate antagonism (CI = 1.20-1.45), while the combination of the compound at 6.250 μg/ml showed antagonism effect (CI = 1.45-3.30). The Fa-CI plot (**Figure 4-48**) showed the F_a value of the combination of nearly 0.5. However, the results figured out that the tested kaempferol decreased the inhibition of the standard acarbose.

Table 4-34 The α-glucosidase inhibition and combination index (CI) of acarbose and kaempferol

Name	Kaempferol (μg/ml)						
	Concentration (μg/ml)		0.391	0.781	1.563	3.125	6.250
		% inhibition	4.49	6.30	15.18	15.98	21.47
	62.5	29.16	Not determined				
Acarbose	125	41.23					
(Standard)	250	59.29	49.38 (1.36)*	49.56 (1.35)*	51.56 (1.21)*	48.63 (1.42)*	42.88 (1.93)*
	500	67.66	Not determined				
	1000	75.90					

* Combination index (CI) of acarbose 250 μg/ml combined with kaempferol
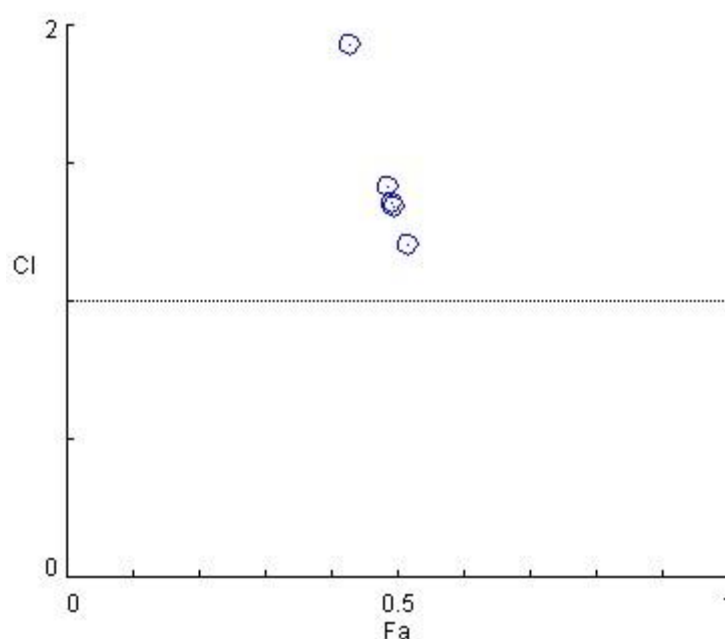
Figure 4-48 Fraction affected (F_a) versus combination index (CI) plot of acarbose
250 µg/ml and kaempferol

The result of α-glucosidase inhibition of combination between acarbose
250 µg/ml and standard astragalin (one composition of the mixture compound SS6) and
CI values were shown in **Table 4-35**. The α-glucosidase was inhibited with the
combined doses in the range of 39.97 - 48.44 % inhibition. All combined inhibitions
were better than single astragalin inhibition, however they were less than the inhibition
of acarbose at 250 µg/ml. Interestingly, when the astragalin concentration of
combination increased, the percentage of inhibition decreased. This differed from the
single astragalin inhibition. The percentage of inhibition increased when the
concentration of the single astragalin increased. The results implied that astragalin may
overshadow the binding effect of acarbose to α-glucosidase. The CI values of the
combination showed above 1.00. According to **Table 3-4**, the combination of astragalin
at 7.813 µg/ml exhibited moderate antagonism effect (CI = 1.20-1.45), while the
combination of the compound at 15.625-125 µg/ml were classified into antagonism (CI
= 1.45-3.30). The Fa-CI plot (**Figure 4-49**) showed only two points of CI below 2 that
these F_a values were nearly 0.5.

Table 4-35 The α-glucosidase inhibition and combination index (CI) of acarbose and astragalin

Name	Astragalin (µg/ml)						
	Concentration (µg/ml)		7.813	15.625	31.25	62.50	125
		% inhibition	1.72	6.92	13.54	13.91	17.27
Acarbose (Standard)	62.5	31.26	Not determined				
	125	45.57					
	250	58.26	48.44 (1.40)*	47.21 (1.56)*	43.21 (2.19)*	42.78 (2.35)*	39.97 (3.13)*
	500	63.25	Not determined				
	1000	64.11					

* Combination index (CI) of acarbose 250 µg/ml combine with astragalin
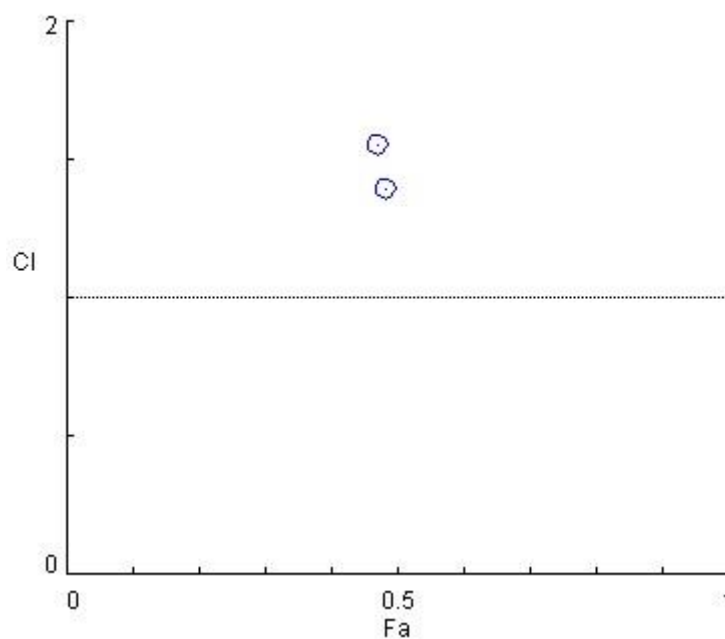
Figure 4-49 Fraction affected (F_a) versus combination index (CI) plot of acarbose 250 µg/ml and astragalin

4.4 Computer molecular docking of compounds

Due to the limitation solubility of some isolated compound and to obtain more information about the α-glucosidase inhibition of the isolated compounds, the computer docking experiment was used as a tool to provide the molecular understanding of the interaction between isolated compounds and enzyme. The isolated flavonoid compounds from *S. stamonifolium* inflorescence and the isolated aromatic compounds from *N. racemosa* stem were separated docking. Two docking programs, Autodock4 and Autodock Vina, were used to evaluate binding energies. Because of, each applied docking program used a different calculation approach (Boittier *et al*., 2020).

4.4.1 The docking of the isolated flavonoid compounds from *S. stamonifolium* inflorescence

The seven compounds from *S. stramonifolium* inflorescence were divided into three sub-groups that are myricetin derivatives (SS1, SS2 and SS5), kaempferol derivatives (SS3, SS4 and SS6-2) and others (SS6-1). The grid box for these compounds were set a size as 16 Å × 16 Å × 16 Å. To validate the protocol, the RMSD between the native and the redocked glucose was 0.936 Å (**Appendix 59**). The docking results (**Figure 4-50**) showed that all isolated flavonoid molecules laid on the same site. They were blocking the substrate from entering the active site. Furthermore, the molecular interactions (as hydrogen bond, Pi-cation, Pi-anion, Pi-Pi and unfavorable interaction) between isolated flavonoid sub-groups and amino acid residues in the active site of α-glucosidase were presented in **Figure 4-51** to **4-53**. Noticeably, at least five amino acid residues such as TYR158, GLU277, ARG315, ASP352, ARG442 were highly conserved in molecular interaction of seven flavonoids, as shown in **Table 4-36**. GLU277 and ASP352 were defined as the catalytic domain of α-glucosidase. TYR158 and ARG315 were indicated as the non-catalytic domain, while ARG442 was reported as stabilizer domain of the enzyme (Yamamoto *et al.*, 2010; Phoopha *et al.*, 2020). Besides this, some residues were distinctively conserved in a specific sub-group. TYR72 was only conserved among the kaempferol derivatives (SS4 and SS6-2), while PHE178, HIS280 and TYR316 were conserved among myricetin derivatives (SS1, SS2 and SS5).

127
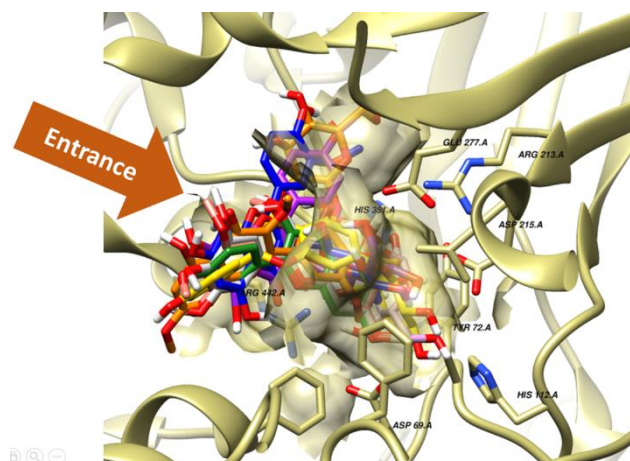
Figure 4-50 3D Diagram of all isolated flavonoid molecules from *S. stamonifolium* docked at the entrance of the active site of α-glucosidase
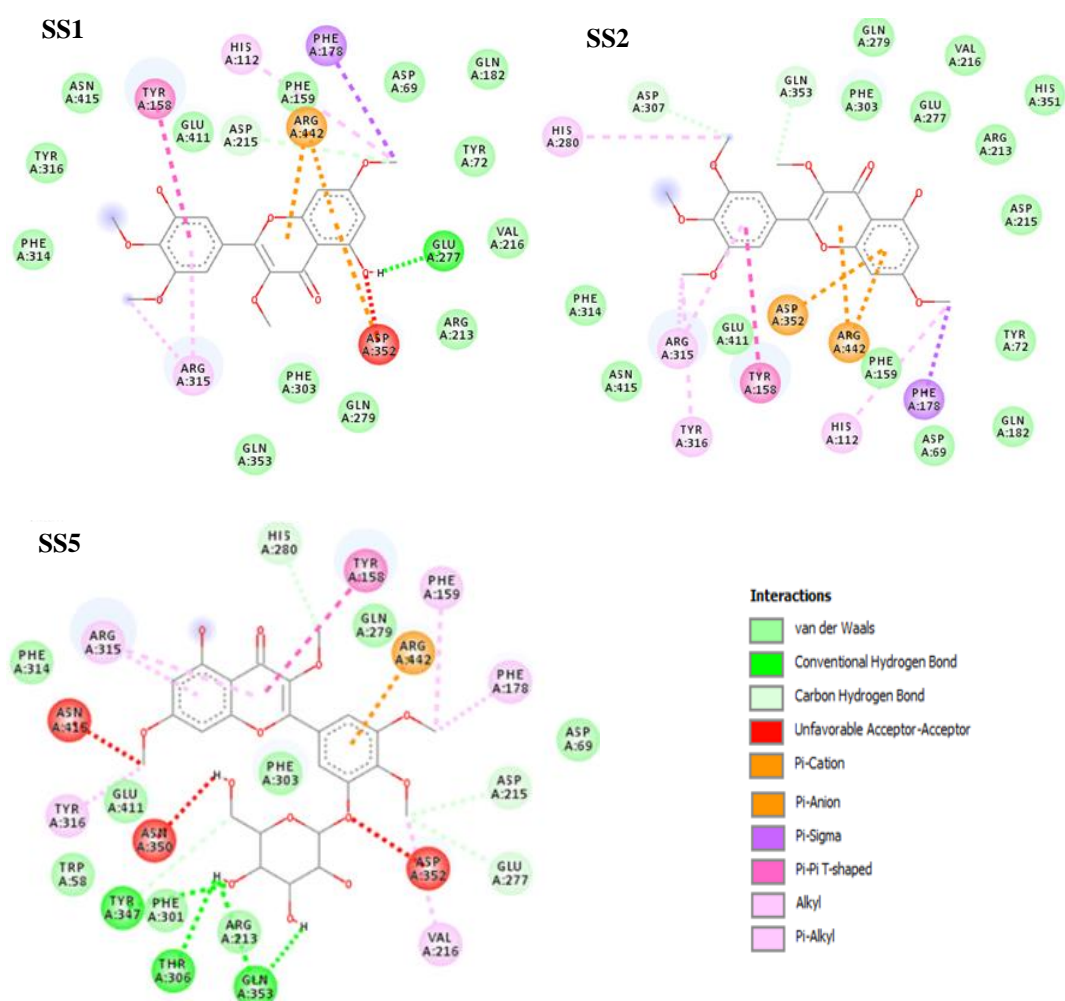
Figure 4-51 Diagrams of molecular interactions of myricetin derivatives (SS1, SS2 and SS5).

128
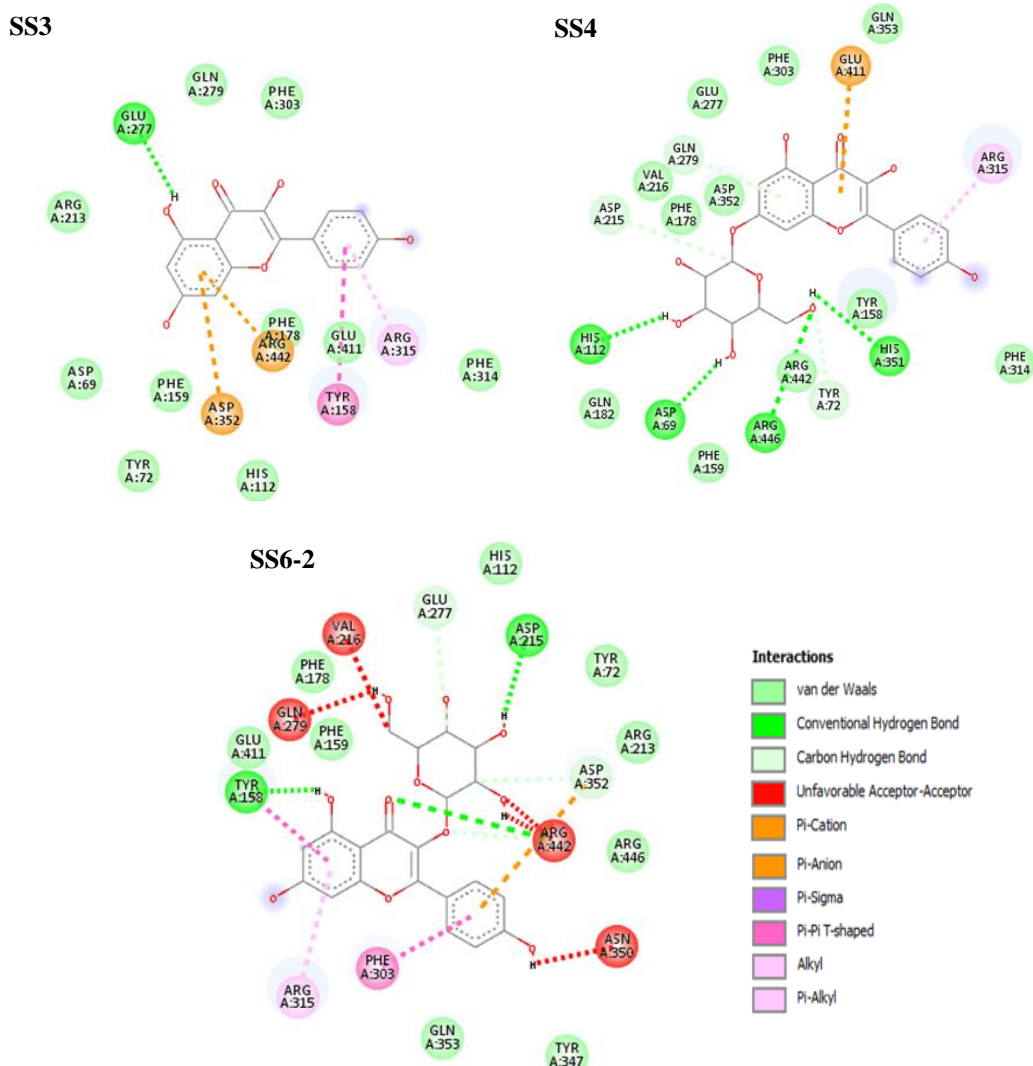
Figure 4-52 Diagrams of molecular interactions of kaempferol derivatives (SS3, SS4 and SS6-2).
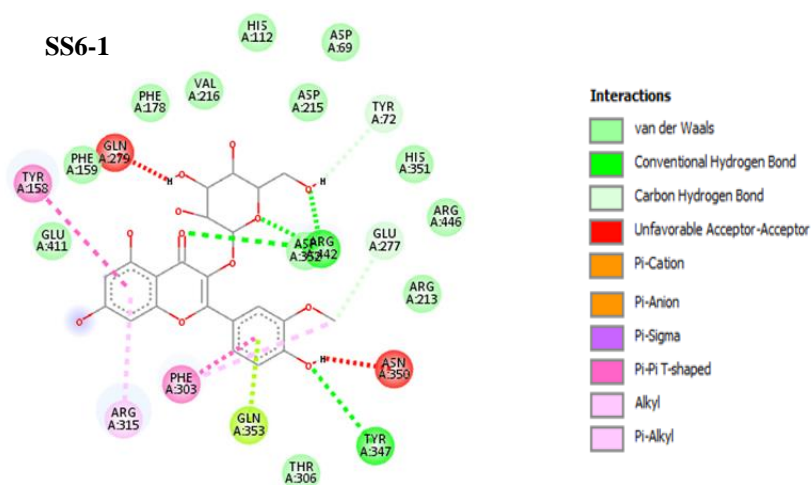
Figure 4-53 Diagrams of molecular interactions of SS6-1.

Table 4-36 Molecular interactions between the isolated compounds and amino acid
residues from α-glucosidase

No	Residues	Myricetin derivatives			Kaemferol derivatives			Other	Consensus
		SS1	SS2	SS5	SS3	SS4	SS6-2	SS6-1	
1	ASP69	-	-	-	-	✓	-	-	1
2	**TYR72**	-	-	-	-	✓	✓	-	2
3	HIS112	✓	✓	-	-	✓	-	-	3
4	**TYR158**	✓	✓	✓	✓	-	✓	✓	6
5	PHE159	-	-	✓	-	-	-	-	1
6	**PHE178**	✓	✓	✓	-	-	-	-	3
7	ASP215	✓	-	✓	-	✓	-	✓	4
8	VAL216	-	-	✓	-	-	-	✓	2
9	**GLU277**	✓	-	✓	✓	-	✓	✓	5
10	GLN279	-	-	-	-	-	✓	✓	2
11	**HIS280**	-	✓	✓	-	-	-	-	2
12	PHE303	-	-	-	-	-	✓	✓	2
13	THR306	-	-	✓	-	-	-	-	1
14	ASP307	-	✓	-	-	-	-	-	1
15	**ARG315**	✓	✓	✓	✓	✓	✓	✓	7
16	**TYR316**	-	✓	✓	-	-	-	-	2
17	TYR347	-	-	✓	-	-	✓	-	2
18	ASN350	-	-	✓	-	-	✓	✓	3
19	HIS351	-	-	-	-	✓	-	-	1
20	**ASP352**	✓	✓	✓	✓	-	✓	✓	6
21	GLN353	-	-	✓	-	-	✓	-	2
22	GLU411	-	-	-	-	✓	-	-	1
23	ASN415	-	-	✓	-	-	-	-	1
24	**ARG442**	✓	✓	✓	✓	-	✓	✓	6
25	ARG446	-	-	-	-	✓	-	-	1

Table 4-36 Molecular interactions between the isolated compounds and amino acid
residues from α-glucosidase (**continued**).

No	Residues	Compounds							Consensus
		Myricetin derivatives			Kaemferol derivatives			Other	
		SS1	SS2	SS5	SS3	SS4	SS6-2	SS6-1	
	Total	8	9	16	5	8	11	10	

Gray highlight indicated the conserved residues in all sub-groups, while bold indicated
the conserved residues in a particular sub-group.

The rescored binding energy from Autodock4.2.6 evaluated more
energetic parameter than Autodock Vina. The docking results as **Table 4-37** showed a
contradiction in the obtained binding energies from two program. The contradictory
result of two program may occur from different calculations (such as scoring function
and searching algorithm) of each applied docking program (Boittier *et al*., 2020).
Therefore, the comparison of docking result and the experimental data was essential as
Table 4-38. The % inhibition of isolated myricetin derivatives (SS1 and SS2) at 400
μg/ml to α-glucosidase agreed with molecular docking results from Autodock Vina. It
disagreed with the result of binding energy from Autodock4.2.6. Unfortunately, a
glycosylated compound (SS5) isolation got less yield. The experimental of SS5 was
tested only % inhibition at 200 μg/ml to the enzyme. However, both of docking
programs agreed together that a glycosylated compound exhibited the looser binding
because it showed higher affinity energy than non-glycosylated compound (SS2). The
structure-activity relationships (SARs) on the flavonoid structure was mentioned from
the previous reports that the glycosylation at C-3 position of ring C decrease the
inhibitory activity to α-glucosidase (Proença *et al.*, 2017; Şöhretoğlu *et. al*., 2018;
Şöhretoğlu *et al*., 2020). Interestingly, the numerous higher energy levels fom Van der
Waals (vdW) and hydrogen bonding (Hbond) of SS5 as 51.35 Kcal/mol (showed in
Table 4-37) contributed to higher estimate binding energy which resulted to less
potency of enzyme inhibition.

The % inhibition of isolated kaempferol derivatives (SS3 and SS4) at
400 μg/ml to α-glucosidase agreed with molecular docking results from both

Autodock4.2.6 and Autodock Vina as **Table 4-37**. Due to SS6 is the mixture compound, the docking results were valuable information for explanation of compound interactions to the enzyme. SS4 and SS6-2 are glycosylated compounds which have the similar aglycone part with SS3. Both of them are different each other from glycosylated position. Similar trend with SS5, SS6-2 which have the glycosylation at C-3 position demonstrated a greater of vdW and Hbond energies than SS3. In contrast, SS4 which have the glycosylation at C-7 position exhibited a smaller of vdW and Hbond energies than SS3. Moreover, SS6-1 which have the glycosylation at C-3 position of ring C and methoxy substitution at C-3′ position of ring B showed a smaller vdW and Hbond energies than SS6-2. The previous studies of flavonoids SAR reported that O-glycosylation at C-3 and C-7 and O-methylation at C-3′ of flavonoid structure decreased the α-glucosidase inhibitory activity (Xiao *et. al*., 2015; Şöhretoğlu *et al*., 2020; Proença *et al*., 2021). Finally, desolvation and torsion-free energies were slightly higher from the glycosylated compounds (SS4, SS5, SS6-1 and SS6-2). These mean that substitutions on flavonoid structure affected their α-glucosidase interactions.

Table 4-37 Obtained binding energy of the isolated flavonoid compounds from Autodock 4.2.6 compared to Autodock Vina

Compound	Autodock 4.2.6								Autodock Vina
	vdW+Hbond (1)	Elec. Energy (2)	Desol. Energy (3)	Total Intermol. Interact. Energy (4; 1+2+3)	Total Internal Energy (5)	Tors. Free Energy (6)	Unbound's Energy (7)	Estimate Free Energy of Binding (Kcal/mol) (4+5+6-7)	Affinity (Kcal/mol)
Myricetin derivatives									
SS1	-7.49	0.06	5.53	-1.90	-2.05	2.09	0.00	-1.86	-6.6
SS2	-10.43	0.47	5.51	-4.46	-1.16	2.09	0.00	-3.53	-6.0
SS5	51.35	0.86	9.30	61.50	-1.60	3.88	0.00	63.78	0.0
Kaempferol derivatives									
SS3	-7.99	0.26	4.22	-3.50	-1.01	1.49	0.00	-3.02	-5.9
SS4	-9.62	-0.10	7.91	-1.80	-2.77	3.28	0.00	-1.29	-4.6
SS6-2	47.06	0.29	7.62	54.97	-2.78	3.28	0.00	55.47	-4.2
Other									
SS6-1	-12.98	0.23	8.34	-4.41	-2.07	3.58	0.00	-2.90	-6.3

vdW+Hbonding = Van der Waals + Hydrogen bonding, Elec. Energy = Electrostatic energy, Desol. Energy = Desolvation energy,

Total Intermol. Interact. Energy = Total Intermolecule Interaction energy, Tors. Free energy = Torsion free energy

Table 4-38 Molecular docking energy and inhibitory activity of the isolated flavonoid compounds to α-glucosidase

Compounds	Molecular docking		% Inhibition ± SD at 400 µg/ml
	Autodock 4.2.6 Energy of binding (Kcal/mol)	**Autodock Vina** Affinity (Kcal/mol)	
Myricetin derivatives			
SS1	-1.86	-6.6	12.78±4.89
SS2	-3.53	-6.0	8.51±3.79
SS5	63.78	0.0	0.84±0.21*
Kaempferol derivatives			
SS3	-3.02	-5.9	13.01±2.69
SS4	-1.29	-4.6	7.68±0.33
SS6-2	55.47	-4.2	1.99±5.42
SS6-1 (other)	-2.90	-6.3	

*% Inhibition ± SD at 200 µg/ml

4.4.2 The docking of the isolated aromatic compounds from *N. racemosa* stem

The four isolated aromatic compounds from *N. racemosa* that are NR1, NR2, NR4 and NR5 were investigated the protein-ligand binding through *in silico* docking study. The grid box for these compounds used a size of 17 Å × 17 Å × 17 Å. The RMSD between the native and the redocked glucose was 0.969 Å (**Appendix 60**). The docking results (**Figure 4-54**) showed that these compounds laid on the entrance area of active site, while the glucose molecular was in the pocket. The present study agreed with the previous reports which suggested that these compounds bond to the α-glucosidase (Song *et al.*, 2016; Mahomoodally *et al.*, 2018; Mahnashi *et al.*, 2022).

The docking result showed that NR1 bound at the entrance area of enzyme active site (**Figure 4-54B**, yellow structure) and had the interaction with Glucose 601 at pocket site (**Table 4-39**). The distances between NR1 and glucose601 was 3.41 Å. This manner was consistent with the competitive inhibition that prevented the substrate entrance to the enzyme active site. However, the docking experiment focused only around interested area. The compound might bind to the enzyme more

than one site because the kinetic prediction of NR1, as mention above, was the mixed-type manner (Copeland, 2005). Moreover, the molecular docking presented that NR2 binding may prohibit the substrate entering the active site or prevented product leaving (**Figure 4-54B**, pink structure). NR2 showed the interaction with TYR158, the amino acid of non-catalytic domain, at distance 2.05 Å and with glucose601 at distance 1.36, 3.14 and 4.21 Å (**Table 4-39**).
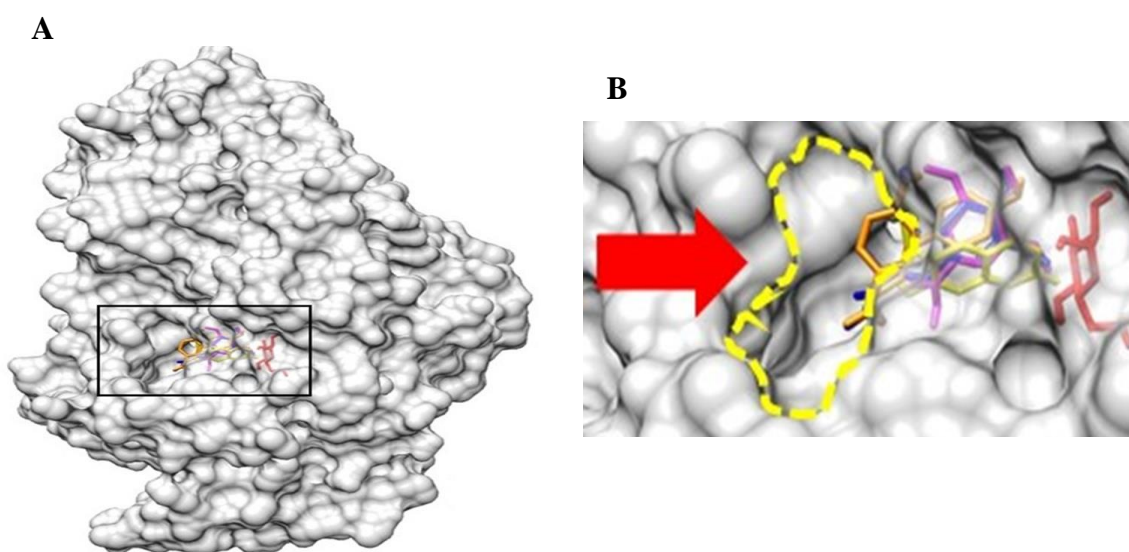
Figure 4-54 Molecular docking between the α-glucosidase and the isolated compounds of *N. racemosa*

    A) The position of the best interaction between the α-glucosidase and the isolated compounds from *N. racemosa*

    B) The expanded picture at the active site of α-glucosidase. The dashed circle in yellow color was the entrance gate to the active site. The red arrow was used to emphasis the entrance gate. Red structure was glucose. Yellow structure was NR1. Pink structure was NR2. Blue structure was NR4. Orange structure was NR5.

Table 4-39 Binding interaction of the isolated aromatic compounds from *N. racemosa* and α-glucosidase (AG)

Complex-ligand	Number (s) of interaction	Interaction sites	Distances (Å)
NR1-AG	1	Glucose601	3.41
NR2-AG	4	TYR158	2.05
		Glucose601	1.36
			3.14
			4.21
NR4-AG	4	ARG315	4.60
		ASN415	4.18
		Glucose601	3.21
			4.33
NR5-AG	4	ARG315	4.64
		ASN415	4.28
		Glucose601	2.88
			4.14

NR4 and NR5 were the two tyramine-derived amides which docking result presented in **Figure 4-54** as blue and orange structure, respectively. They aligned at the exit part of α-glucosidase which would prohibit the release of the product from the enzyme. These finding agreed with the suggested mechanism of the uncompetitive inhibitor manner which would rather prevent the product releasing than blocked the substrate from entering the active site (Song *et al*., 2016). Both NR4 and NR5 presented the interaction with ARG315, ASN415 and Glucose601. Their distances were also showed as **Table 4-39**. Moreover, structural activity relationship (SAR) of NR4 and NR5 were suggested that the hydroxyl group of A ring and α-β unsaturated carbonyl group played an important role in the interaction between these compounds and α-glucosidase (Song *et al*., 2016). The previous reports exhibited that methoxyl substitution at position C-6 of ring A significantly effected to reduce the inhibitory activity to α-glucosidase (Liu *et al*., 2011; Panidthananon *et al.*, 2018). To describe the effect of methoxyl substitution, the molecular docking evaluated the best poses of NR4 and NR5 as **Figure 4-55A**. The results indicated that the methoxyl substitution at C-6 could rotate ring A around 60 degree (**Figure 4-55B**) and turned α-β unsaturated carbonyl group approximately 160 degree (**Figure 4-55C**). Even though the

geometrical structures of both compounds were different, but these were less impact to the distance between these compounds and the enzyme residues (**Table 4-39**). These evidences have been used for explain why NR4 showed the less potency than NR5.
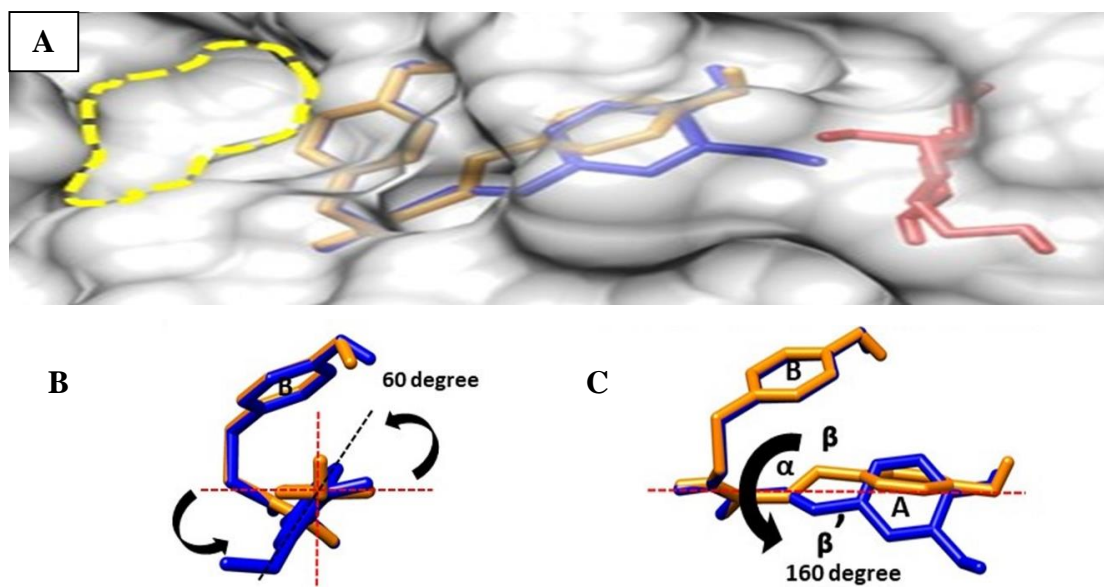
Figure 4-55 The molecular docking of α-glucosidase with NR4 and NR5

> A) The comparison between the docked conformations of NR4 (blue structure) and NR5 (orange structure) at the entrance gate of α-glucosidase active site.
>
> B) The docked conformation alteration of ring A.
>
> C) The docked conformation alteration of α-β unsaturated carbonyl group. The red dashed lines indicated the X and Y-axis, while the black arrows indicated the changing of the position in the chemical structure.

The rescored binding energy from Autodock4.2.6 accorded with Autodock Vina. NR2 which exhibited the least *in vitro* inhibitory activity showed the highest binding energy from *in silico* study (**Table 4-40**). From the experimental study, NR4 had less potent inhibitory activity than NR5. NR4 should be have the binding predicted score over than NR5. In contrast, the molecular predicted results from both docking programs were showing that NR4 had lower binding energy than NR5 (**Table 4-40**). Hence, each binding energy values had reconsidered as showed in **Table 4-41**.

The desolvation and torsion free energies of NR4 were 2.60 and 2.39 Kcal/mol, respectively, which higher than the values of NR5 (**Table 4-41**). These two parameters were less favorable for enzyme inhibition. Therefore, they might be used to explain why NR4 showed a lower activity than NR5.

Table 4-40 Molecular docking energy and inhibitory activity of the isolated aromatic compounds from *N. racemosa* to α-glucosidase

Compounds	Molecular docking		IC$_{50}$ (μM)
	Autodock 4.2.6 Energy of binding (Kcal/mol)	**Autodock Vina** Affinity (Kcal/mol)	
NR1	-4.62	-6.3	577.46
NR2	-1.07	-5.7	> 2,523.09
NR4	-5.42	-7.5	95.34
NR5	-5.15	-7.0	3.25

Table 4-41 Binding energy of the isolated aromatic compounds from *N. racemosa*

Compound	Autodock 4.2.6								Autodock Vina
	vdW+Hbond (1)	Elec. Energy (2)	Desol. Energy (3)	Total Intermol. Interact. Energy (4; 1+2+3)	Total Internal Energy (5)	Tors. Free Energy (6)	Unbound's Energy (7)	Estimate Free Energy of Binding (Kcal/mol) (4+5+6-7)	Affinity (Kcal/mol)
NR1	-6.34	0.01	1.80	-4.53	-0.69	0.60	0	-4.62	-6.3
NR2	-6.67	1.70	3.00	-1.98	-0.58	1.49	0	-1.07	-5.7
NR4	-9.27	0.30	2.60	-6.36	-1.45	2.39	0	-5.42	-7.5
NR5	-8.22	0.29	2.05	-5.88	-1.36	2.09	0	-5.15	-7.0

vdW+Hbonding = Van der Waals + Hydrogen bonding, Elec. Energy = Electrostatic energy, Desol. Energy = Desolvation energy,

Total Intermol. Interact. Energy = Total Intermolecule Interaction energy, Tors. Free energy = Torsion free energy

CHAPTER 5

CONCLUSION

This work has done on the phytochemical investigation of two selected plants from order Solanales which were *Solanum stramonifolium* and *Neuropeltis racemosa*. Based on preliminary α-glucosidase inhibitory screening, the methanol extracts of *S. stramonifolium* inflorescence and *N. racemosa* stem exhibited higher inhibitory activity than acarbose standard. Four solvents (lowest to highest polarity) were sequential used for plant material extraction. All extractions were tested the power of enzyme inhibition. The highest powerful on α-glucosidase inhibition of both material extracts was the ethanol extract, while the second was the ethyl acetate extract. By the bioactive guided fractionation, the ethanol and the ethyl acetate extracts of *S. stramonifolium* and the ethanol extract of *N. racemosa* were selected to further chemical investigation. The isolated compounds from the top two powerful extracts of *S. stramonifolium* were less amount and they have not been reported on the chemical compounds from *S. stramonifolium* inflorescence before.

The biological activities on α-glucosidase inhibition of the extracts were evaluated as the percent of inhibition, the half-maximal inhibitory concentration (IC_{50}), the mode of action and the combination test with one concentration of standard acarbose at 250 µg/ml. The SSEA and NREO extracts exhibited the highest inhibitory activity among *S. stramonifolium* and *N. racemosa* extracts, respectively. The SSEA, SSEO and NREO extracts showed mixed-type inhibition, while the SSWT and NREA extracts presented uncompetitive inhibition. The combination index (CI) between the selected extracts and acarbose standard implied that SSEA, SSEO, SSWT, NREA and NREO extracts supported the ability of acarbose to α-glucosidase inhibition.

From the bioassay guided fractionation, ten compounds and one mixture compound were isolated. Briefly, the extracts were separated by classical column chromatographic techniques and the purified compounds were analyzed by spectroscopic techniques such as UV-Vis, FTIR, HRMS, and NMR (^{1}H-NMR, ^{13}C-NMR, HMQC, HMBC, NOESY). The obtained compounds from *S. stramonifolium*

were flavonoid derivatives as 3, 4′, 5′, 7-tetramethyl ether of myricetin (SS1), combretol (SS2), kaempferol (SS3), kaempferol-7-O-β-glucopyranoside (SS4), 5-hydroxy-3, 7, 4′, 5′-tetramethoxyflavone-3′-O-glucopyranoside (SS5), and the mixture (SS6) of isorhamnetin-3-O-glucopyranoside (SS6-1) and kaempferol-3-O-glucopyranoside (SS6-2). As literature survey, the flavonoid glycoside, SS5 has not been reported. SS5, NMR data of flavonoid skeleton was compared with SS1, while the sugar substitution at C-3′ was compared with the previous reported data of 3′-O-β-D-(4″-O-methylglucopyranosylo)-5, 7, 4′, 5′-tetramethoxyflavone. Furthermore, the isolated compounds from *N. racemosa* were scopoletin (NR1), syringic acid (NR2), methyl 3-methyl-2-butenonoate (NR3), *trans-N*-feruloyltyramine (NR4) and *trans-N*-coumaroyltyramine (NR5).

SS1-SS6 were low-yield isolated. Their yields were only enough for the percent of α-glucosidase inhibition test. All of them showed less activity than the standard acarbose. So, the purchased kaempferol and astragalin standard were used as the representatives to the mechanism of action analysis. Both of them exhibited mixed-type inhibition, while the acarbose showed competitive inhibition. The CI values indicated that kaempferol and astragalin decreased acarbose's activity when they were combined with standard acarbose.

NR1-NR5 were also estimated their potential of α-glucosidase inhibition. The IC_{50} of NR1 (110.97 μg/ml), NR4 (29.87 μg/ml) and NR5 (0.92 μg/ml) exhibited stronger than acarbose (272.72 μg/ml), while NR2 and NR3 showed the lower activity with IC_{50} >500 μg/ml. So, NR1, NR4 and NR5 were chosen for mode of action analysis. NR1 performed the mixed-type inhibition, while two tyramine-derived amides (NR4 and NR5) presented uncompetitive inhibition.

The docking study was used to provide the better understanding about the interaction between compounds and targeted protein. Seven flavonoid structures including SS1, SS2, SS3, SS4, SS5, SS6-1 and SS6-2 from *S. stramonifolium* and four aromatic compounds as NR1, NR2, NR4 and NR5 from *N. racemosa* were graphically computed by molecular study. The docking study demonstrated that these compounds may inhibit the reaction by blocking substrate entering to the active site or prevention of the product releasing. Beside of the total energy, each binding energy values such as Van der Wals, hydrogen bonding, desolvation and torsion free energies should be

analyzed. These were useful for explaination of the docking results when compared with the laboratory data.

Based on the results, these findings justify the values of Thai vegetable, *S. stramonifolium*, and traditional Thai medicinal plant, *N. racemosa*. They can be the resourses of lead antidiabetic compounds. This is the first report of *S. stramonifolium* inflorescence and *N. racemosa* stem on the phytochemical investigation, *in vitro* α-glucosidase inhibitory activity, the combination effect with acarbose standard and the mode of action to α-glucosidase inhibition. Moreover, *in silico* study provided the useful information for the obtained compounds. Additional studies such as *in vivo* study should be investigated to verify the potential of isolated compounds.

REFERENCES

กองการประกอบโรคศิลปะ. (2541). *ตำราแพทย์แผนโบราณทั่วไป สาขาเภสัชกรรม* (น. 62). สำนักงานปลัดกระทรวงสาธารณสุข.

เต็ม สมิตินันทน์. (2557). *ชื่อพรรณไม้แห่งประเทศไทย ฉบับแก้ไขเพิ่มเติม* (น. 520). โรงพิมพ์ สำนักงานพระพุทธศาสนาแห่งชาติ. กรุงเทพฯ.

วุฒิ วุฒิธรรมเวช. (2540). *ร่วมอนุรักษ์มรดกไทย สารานุกรมสมุนไพร รวมหลักเภสัชกรรมไทย* (น. 370). สำนักพิมพ์โอเดียนสโตร์. กรุงเทพฯ.

Abd El-Mohsen M. M., Rabed M. A., Abou-Setta L., El-Rashedy A. A. and Hussein A. A. (2014). Marrubiin: a potent α-glucosidase inhibitor from *Marrubium alysson*. *International Journal of Applied Research in Natural Products*. *7*(1), 21-27.

Abuelizz H. A., Iwana N. A. N. I., Ahmad R., Anouar E., Marzouk M., Al-Salahi R. (2019). Synthesis, biological activity and molecular docking of new tricyclic series as α-glucosidase inhibitors. *BMC Chemistry*. *13*(52), 1-14.

Adisakwattana S., Yibchok-Anun S., Charoenlertkul P., Wongsasiripat N. (2011). Cyanidin-3-rutinoside alleviates postprandial hyperglycemia and its synergism with acarbose by inhibition of intestinal α-glucosidase. *Journal of Clinical Biochemistry and Nutrition*. *49*(1), 36-41.

Ahmed D., Kumar V., Sharma M. and Verma A. (2014). Target guided isolation, *in-vitro* antidiabetic, antioxidant activity and molecular docking studies of some flavonoids from *Albizzia lebbeck* Benth. bark. *BMC Complementary and Alternative Medicine*. *14*(155), 1-12.

Aisyah L. S., Yun Y. F., Herlina T., Julaeha E., Zainuddin A., Nurfarida I., hidayat A. T., Supratman U., Shiono Y. (2017). Flavonoid compounds from the leaves of *Kalanchoe prolifera* and their cytotoxic activity against P-388 murine leukemia cells. *Natural Product Sciences*. *23*(2), 139-145.

Akkarachiyasit S., Charoenlertkul P., Yibchok-anun S., Adisakwattana S. (2010). Inhibitory activities of cyanidin and its glycosides and synergistic effect with acarbose against intestinal α-glucosidase and pancreatic α-amylase. *International Journal of Molecular Science*. *11*(9), 3387-3396.

Alssema M., Ruijgrok C., Blaak E. E., Egli L., Dussort P., Vinoy S., Dekker J. M., Robertson M. D. (2021). Effects of alpha-glucosidase-inhibiting drugs on acute postprandial glucose and insulin responses: a systematic review and meta-analysis. *Nutrition and Diabetes. 11*, 11.

American Diabetes Association [ADA]. (2022a). Classification and diagnosis of diabetes mellitus: standards of medical care in diabetes-2022. *Diabetes Care. 45*(suppl 1), S17-38.

American Diabetes Association [ADA]. (2022b). Classification and diagnosis of diabetes mellitus: standards of medical care in diabetes-2022. *Diabetes Care. 45*(suppl 1), S125-143.

Arulselvan P., Ghofar H. A. A., Karthivashan G., Halim M. F. A., Ghafar M. S. A., Fakurazi S. (2014). Antidiabetic therapetics from natural source: a systematic review. *Biomedicine & Preventive Nutrition. 4*: 607-617.

Azem S. S., Uddin R., Wadood A. (2012). Structure and dynamics of alpha-glucosidase through molecular dynamics simulation studies. *Journal of Molecular Liquids. 174*, 58-62.

Balasundaram B., Harrison S., Bracewell D. G. (2009). Advances in product release strategies and impact on bioprocess design. *Trends in Biotechnology. 27*(8), 477- 485.

Bendz G., Santesson J. (1973). *Chemistry in Botanical Classification* (pp. 235-240). Nobel Foundation. Stockholm, Sweden.

Bharatham K., Bharatham N., Park K. H., Lee K. W. (2008). Binding mode analyses and pharmacophore model development for sulfonamide chalcone derivatives, a new class of α -glucosidase inhibitors. *Journal of Molecular Graphics and Modelling. 26*, 1202-1212.

Boittier E. D., Tang Y. Y., Buckley M. E., Schuurs Z. P., Richard D. J., Gandhi N. S. (2020). Assessing molecular docking tools to guide targeted drug discovery of CD38 inhibitors. *International Journal of Molecular Sciences. 21*(15), 5183.

Chanmee W., Chicharoenpong C., Petsom A. (2013). Lipase inhibitor from fruits of *Solanum stramonifolium* Jacq. *Food and Nutrition Sciences. 4*, 554-558.

Chetty S., Soliman M. E. S. (2015). Possible allosteric binding site on Gyrase B, a key target for novel anti-TB drugs: Homology modelling and binding site

identification using molecular dynamics simulation and binding free energy calculations. *Medicinal Chemistry Research. 24*, 2055–2074.

Chiba S. (1997). Molecular mechanism in α-glucosidase and glucoamylase. *Bioscience, Biotechnology, and Biochemistry. 61*(8), 1233-1239.

Chou T. C. (2006). Theoretical basis, experimental design, and computerized simulation of synergism and antagonism in drug combination studies. *Pharmacological Reviews. 58*(3), 621-681.

Chou T. C. (2010). Drug combination studies and their synergy quantification using the Chou-Talalay method. *Cancer Research. 70*(2), 440-446.

Copeland R.A. (2005). *Evaluation of Enzyme Inhibitors in Drug Discovery, A Guide for Medicinal Chemists and Pharmacologists: Reversible Modes of Inhibitor Interactions with Enzymes* (pp. 48–81). John Wiley & Sons. New Jersey, United States.

Dachriyanus, F. R., Sargent M. V., Skelton B. W. and White A.H. (2004). 5-Hydroxy-3-3',4',5',7-pentamethoxyflavone. *Acta Crystallographica. E60*(1), o86-o88.

Dammak I., Neves M., Souilem S., Isoda H., Sayadi S., Nakajima M. (2015). Material balance of olive components in virgin olive oil extraction processing. *Food Science and Technology Research. 21*(2), 193-205.

Datta B. K., Datta S. K., Rashid M. A., Nash R. J., Sarker S. D. (2000). A sesquiterpene acid and flavonoids from *Polygonum viscosum. Phytochemistry. 54*(2), 201-205.

Dej-adisai S., Pitakbut T. (2015). Determination of α-glucosidase inhibitory activity from selected Fabaceae plants. *Pakisatan Journals of Pharmaceutical Sciences. 28*(5), 1679-1683.

Dej-adisai S., Rais I.R., Wattanapiromsakul C., Pitakbut T. (2021). Alpha-glucosidase inhibitory assay-screened isolation and molecular docking model from *Bauhinia Pulla* active compounds. *Molecules. 26*(19), 5970.

Demetzoc C., Angelopoulou D., Kolocouris A., Daliani I., Mavromoustakos T. (2001). Structure elucidation, conformational analysis and thermal effects on membrane bilayers of an antimicrobial myricetin ether derivative. *Journal of Heterocyclic Chemistry. 38*(3), 703-710.

Derosa G., Maffioli P. (2012). α-Glucosidase inhibitors and their use in clinical practice. *Archives of Medical Science. 8*(5), 899-906.

Dhital S., Lin A.H-M., Hamaker B.R., Gidley M.J., Muniandy A. (2013). Mammalian mucosal α-glucosidase coordinate with α-amylase in initial strach hydrolysis stage to have a role in starch digestion beyond glucogenesis. *PlosOne. 8*(4), e62546.

Dinicolantonio J. J., Bhutani J., O'Keefe1 J. H. (2015). Acarbose: safe and effective for lowering postprandial hyperglycaemia and improving cardiovascular outcomes. *Open Heart. 2*(1), e000327.

Dirir A. M., Daou M., Yousef A. F., Yousef L. F. (2022). A review of alpha-glucosidase inhibitors from plants as potential candidates for the treatment of type-2 diabetes. *Phytochemistry Reviews. 21*(4), 1049-1079.

Escandón-Rivera S., González-Andrade M., Bye R., Linares E., Navarrete A., Mata R. (2012). α-Glucosidase inhibitors from *Brickellia cavanillesii*. *Journal of Natural Products. 75*, 968-974.

Estevez Y., Castillo D., Pisango MT., Arevalo J., Rojas R., Alban J., Deharo E., Bourdy G., Sauvain M. (2007). Evaluation of the leishmanicidal activity of plants used by Peruvian Chayahuita ethnic group. *Journal of Ethnopharmacology. 114*, 254-259.

Ferreira L. G., Santos R. N., Oliva G., Andricopulo A. D. (2015). Molecular docking and structure-based drug design strategies. *Molecules. 20*(7), 13384-13421.

Fisman E. Z., Tenenbaum A. (2021). The dual glucose-dependent insulinotropic polypeptide (GIP) and glucagon-like peptide-1 (GLP-1) receptor agonist tirzepatide: a novel cardiometabolic therapeutic prospect. *Cardiovascular Diabetology. 20*(225), 1-25.

Hagens G., Wasacz J. P., Joullie M., Yates P. (1970). Photolysis of 2,2,5,5,-tetramethyldihydro-3-furanone. *The Journal of Organic Chemistry. 35*(11), 3682-3685.

Hanwell M. D., Curtis D. E., Lonie D. C., Vandermeersch T., Zurek E., Hutchison G. R. (2012). Avogadro: An advanced semantic chemical editor, visualization, and analysis platform. *Journal of Cheminformatics. 4*, 1-17.

Haraguchi M., Gorniak S. L., Ikeda K., Minami Y., Kato A., Watson A. A., Nash R. J., Molyneux R. J., Asno N. (2003). Alkaloidal components in the poisonous plant, *Ipomoea carnea* (Convolvulaceae). *Journal of Agricultural and Food Chemistry*. *51*, 4995-5000.

Hyun T. K., Eom S. H., Kim J. (2014). Molecular docking studies for discovery of plant-derived α-glucosidase. *Plant Omics Journal. 7*(3), 166-170.

International Diabetes Federation (IDF). (2021). IDF Diabetes Atlas Tenth Edition 2021. Retrieved December 25, 2021, from https://diabetesatlas.org/atlas/tenth-edition

Jiang M., Zhang W., Yang X., Xiu F., Xu H., Ying X., Stien D. (2017). An isoindole alkaloid from *Portulaca oleracea* L. *Natural Product Research. 32*(20), 1-6.

Jie-Hong L., Jie-Tao P., Yong-Qin Y. (2016). Two novel resin glycoside isolated from *Ipomoea cairica* with α-glucosidase inhibitory activity. *Chinese Journal of Natural Medicines. 14*(3), 227-231.

Jin D., He J., Zhang K., LuoX., Zhang T. (2021). α-Glucosidase inhibition action of major flavonoids identified from *Hypericum Attenuatum* Choisy and their synergistic effects. *Chemistry & Biodiversity. 18*(10), e2100244.

Jocković N., Fischer W., Brandsch M., Brandt W., Dräger B. (2013). Inhibition of human intestinal α-glucosidase by calystegines. *Journal of Agricultural and Food Chemistry. 61*(23), 5550-5557.

Kato A., Zhang Z., Wang H., Jia Y., Yu C., Kinami K., Hirokami Y., Tsuji Y., Adachi I., Nash RJ., Fleet GWJ., Koseki J., Nakagome I., Hirono S. (2015). Design and synthesis of labystegines, hybrid iminosugars from lab and calystegine, as inhibitors of intestinal α-glucosidases: binding conformation and interaction for ntSI. *The Journal of Organic Chemistry. 80*(9), 4501-4515.

Kimura A., Lee J., Lee I., Lee H., Park H., Chiba S., Kim D. (2004). Two potent competitive inhibitors discriminating α-glucosidase family I from family II. *Carbohydrate Research. 339*, 1035-1040.

Krentz A. J., Bailey C.J. (2005) Oral antidiabetic agents: current role in type 2 diabetes mwllitus. *Drugs. 65*(3), 385-411.

Lee Y. S., Lee S., Lee H. S., Kim B., Ohuchi K., Shin K. H. (2005). Inhibitory effects of isorhamnetin-3-*O*-b-D-glucoside from *Salicornia herbacea* on rat lens aldose

reductase and sorbitol accumulation in streptozotocin-induced diabetic rat tissues. *Biological and Pharmaceutical Bulletin. 28*(5), 916-918.

Liu J., Kong Y., Miao J., Mei X., Wu S., Yan Y., Cao X. (2020). Spectroscopy and molecular docking analysis reveal structural specificity of flavonoids in the inhibition of α-glucosidase activity. *International Journal of Biological Macromolecules. 152*, 981-989.

Liu X., Luo J., Kong L. (2011). Phenylethyl cinnamides as potential alpha-glucosidase inhibitors from the roots of *Solanum melongena. Natural Product Communications. 6*(6), 851-853.

Łużny M., Tronina T., Kozłowska E., Kostrzewa-Susłow E., Janeczko T. (2021). Biotransformation of 5,7-methoxyflavones by selected entomopathogenic filamentous fungi. *Journal of Agricultural and Food Chemistry. 69*(13), 3879-3886.

Mahnashi M. H., Alqahtani Y. S., Alyami B. A., Alqarni A. O., Alqahl S. A., Ullah F., Sadiq A., Zeb A., Ghufran M., Kuraev A., Nawaz A., Ayaz M. (2022). HPLC-DAD phenolics analysis, α-glucosidase, α-amylase inhibitory, molecular docking and nutritional profiles of *Persicaria hydropiper* L. *BMC Complementary Medicine and Therapies. 22*(26).

Mahomoodally M. F., Vlaisavljevic S., Berezni S., Abdallah H. H., Zengin G., Atanasov A. G., Mollica A., Lobine D., Aktumsek A. (2018). Abdurrahman A. *Lotus aegaeus* (Gris.) Boiss and *Iberis sempervirens* L.: chemical fingerprints, antioxidant potential, and inhibition activities and docking on key enzymes linked to global health problems. *Industrial Crop & Products. 120*(15), 271-278.

Meneses M. J., Silva B. M., Sousa M., Sa R., Oliveira P. F., Alves M. G. (2015). Antidiabetic drugs: mechanisms of action and potential outcomes on cellular metabolism. *Current Pharmaceutical Design. 21*, 3606-3620.

Meng X., Zang H., Mezei M., Cui M. (2011). Molecular docking: a powerful approach for structure-based drug discovery. *Current Computer-Aided Drug Design. 7*(2), 146-157.

Mollor D. E. (2001). New drug targets for type 2 diabetes and the metabolic syndrome. *Nature. 414*, 821-827.

Morris G. M., Huey R., Lindstrom W., Sanner M. F., Belew R. K., Goodsell D. S., Olson A.J. (2009). AutoDock4 and AutoDockTools4: Automated docking with selective receptor flexibility. *Journal of Computational Chemistry. 30*(16), 2785–2791.

Moura C. A., Oliveira-Júnior R. G., Oliveira A. P., Silva A. L. N., Silva J. M. S., Santos R. F., Santos M. C. M., Alves C. S. C., Dutra L. M., Costa E. V., Almeida J. R. G. S. (2019). Chemical constituents from the leaves of *Morus nigra* L. (Moraceae) collected in Casa Nova, Bahia, Brazil. *Revista Virtual de Quimica. 11*(2), 394-400.

Naimi M., Vlavcheski F., Shamshoum H., Tsiani E. (2017). Rosemary extract as a potential anti-hyperglycemic agent: current and future perspectives. *Nutrients. 9*, 968.

Neamsuvan O. (2016a). Note for a description of *Solanum stramonifolium* Jacq. Faculty of Traditional Thai Medicine, Prince of Songkla University, Songkhla, Thailand.

Neamsuvan O. (2016b). Note for a description of *Neuropeltis racemosa* Wall. Faculty of Traditional Thai Medicine, Prince of Songkla University, Songkhla, Thailand.

Pan J., Yu B., Yin Y., Li J., Wang L., Guo L., Shen Z. (2015). Four new pentasaccharide resin glycosides from *Ipomoea cairica* with strong α-glucosidase inhibitory activity. *Molecules. 20*(4), 6601-6610.

Panidthananon W., Chaowasku T., Sritularak B., Likhitwitayawuid K. (2018). A new benzophenone C-glucoside and other constituents of *Pseuduvaria fragrans* and their α-glucosidase inhibitory activity. *Molecules. 23*(7), 1600.

Parmar C. (2018). Coconilla (*Solanum stramonifolium*). Retrieved May 4, 2022, from http://www.fruitipedia.com/2018/12/coconilla_solanum-stramonifolium

Peng X., Zhang G., Liao Y., Gong D. (2016). Inhibitory kinetics and mechanism of kaempferol on α-glucosidase. *Food Chemistry. 190*, 207–215.

Pereira C., Júnior C. B. B., Kuster R. M., Simas N. K., Sakuragui C. M., Porzel A., Wessjohann L. (2012). Flavonoids and a neolignan glucoside from *Guarea macrophylla* (Meliaceae). *Quimica Nova. 35*(6), 1123-1126.

Pettersen E. F., Goddard T. D., Huang C. C., Couch G. S., Greenblatt D. M., Meng E. C., Ferrin T. E. (2004). UCSF Chimera-a visualization system for exploratory research and analysis. *Journal of Computational Chemistry. 25*(13), 1605-1612.

Phadungkit M., Luanratana O. (2006). Anti-*Salmonella* activity of constituents of *Ardisia elliptica* Thunb. *Natural Product Research. 20*(7), 693-696.

Phoopha S., Wattanapiromsakul C., Pitakbut T., Dej-adisai S. (2020). Chemical constituents of *Litsea elliptica* and their alpha-glucosidase inhibition with molecular docking. *Pharmacognosy Magazine. 16*(70), 327-334.

Proença C., Freitas M., Ribeiro D., Oliveira E. F. T., Sousa J. L. C., Tomé S. M., Ramos M. J., Silva A. M. S., Fernandes P. A., Fernandes E. (2017). α-Glucosidase inhibition by flavonoids: an *in vitro* and *in silico* structure–activity relationship study. *Journal of Enzyme Inhibition and Medicinal Chemistry. 32*(1), 1216-1228.

Proença C., Ribeiro D., Freitas M., Fernandes E. (2021). Flavonoids as potential agents in the management of type 2 diabetes through the modulation of α-amylase and α-glucosidase activity: a review. *Critical Reviews in Food Science and Nutrition*. *62*(2). 3137-3207.

Promyos N., Temviriyanukul P., Suttisansanee U. (2017). Evaluation of α-glucosidase inhibitory assay using different sub-classes of flavonoids. *Current Applied Science and Technology. 17*(2), 172-180.

Sadat-Ebrahimi S. E., Rahmani A., Mohammadi-Khanaposhtani M., Jafari N., Mojtabavi S., Faramarzi M. A., Emadi M., Yahya-Meymandi A., Larijani B., Biglar M., Mahdavi M. (2020). New phthalimide-benzamide-1,2,3-triazole hybrids; design, synthesis, α-glucosidase inhibition assay, and docking study. *Medicinal Chemistry Research. 29*, 868-876.

Saeedi P., Petersohn I., Salpea P., Malanda B., Karuranga S., Unwin N., Colagiuri S., Guariguata L., Motala A. A., Ogurtsova K., Shaw J. E., Bright D., Williams R., On behalf of the IDF Diabetes Atlas Committee. (2019). Global and regional diabetes prevalence estimates for 2019 and projections for 2030 and 2045: results from the International Diabetes Federation Diabetes Atlas, 9th edition. *Diabetes Ressearch and Clinical Practice*. *157*, 107843.

Santisuk T., Larsen K. (2010). *Flora of Thailand volume 10 part 3 Anacardiaceae & Convolvulaceae* (pp. 440-450). Prachachod Co. Ltd. Bangkok, Thailand.

Sarnthima R., Khannuang S. (2012). Antibacterial activities of *Solanum stramonifolium* seed extract. *Internation Journal of Agriculture & Biology. 14*(1), 111-115.

Serina J. J. C. (2010). Enzymatic inhibitiory activity of hydroxycinnamates (HCs) *In silico* studies [Master dissertation]. Universidade da Madeira.

Siddiqui B. S., Sattar F. A., Ahmad F., Begum S. (2007). Isolation and structural elucidation of chemical constituents from the fruits of *Morinda citrifolia* Linn. *Archives Pharmacal Research. 30*(8), 919-923.

Sim L. (2010). Structural and inhibition studies of human intestinal glucosidases [Doctor dissertation]. University of Toronto.

Sim L., Quezada-Calvillo R., Sterchi E. E., Nichols B. L., Rose D. R. (2008). Human intestinal maltase–glucoamylase: crystal structure of the N-terminal catalytic subunit and basis of inhibition and substrate specificity. *Journal of Molecular. 375*(3), 782-792.

Şöhretoğlua D., Sarib S. (2020). Flavonoids as alpha-glucosidase inhibitors: mechanistic approaches merged with enzyme kinetics and molecular modelling. *Phytochemistry Reviews. 19*, 1081-1092.

Şöhretoğlua D., Sarib S., Barutc B., Özelc A. (2018). Discovery of potent α-glucosidase inhibitor flavonols: Insights into mechanism of action through inhibition kinetics and docking simulations. *Bioorganic Chemistry. 79*, 257–264.

Song Y. H., Kim D. W., Curtis-Long M. J., Park C., Son M., Kim J. Y., Yuk H. J., Lee K. W., Park K. H. (2016). Cinnamic acid amides from *Tribulus terrestris* displaying uncompetitive α-glucosidase inhibition. *European Journal Medicinal Chemi*stry. *114*, 201-208.

Stumvoll M., Goldstein B., Haeften T.W. (2005). Type 2 diabetes: principles of pathogenesis and therapy. *The Lancet. 365*, 1333-1346.

Subroto E., Jeanette G., Meiyanasari Y., Luwinsky I., Baraddiaz S. (2020). Review on the analysis methods of starch, amylose, amylopectinin food and agricultural products.

Sun W., Sang Y., Zhang B., Yu X., Xu Q., Xiu Z., Dong Y. (2017). Synergistic effects of acarbose and an *Oroxylum indicum* seed extract in streptozotocin and high-

fat-diet induced prediabetic mice. *Biomedicine & Pharmacotherapy. 87*, 160-170.

Takahashi K., Yoshioka Y., Kato E., Katsuki S., Iida O., Hosokawa K., Kawabata J. (2010). Methyl caffeate as an α-glucosidase inhibitor from *Solanum torvum* fruits and activity of related compounds. *Bioscience, Biotecnology, and Biochemistry. 74*(4), 741-745.

Tiwari A. K., Rao J. M. (2002). Diabetes mellitus and multiple therapeutic approaches of phytochemicals: present status and future prospects. *Current Science. 83*(1), 30-38.

Tropilab ®Inc. (2016). *Solanum stramonifolium*-Coconilla. Retrieved June 2, 2016, from http://www.tropilab.com/solanum-stram.html.

Tungjai M., Poompimon W., Loetchutinat C., Kothan S., Dechsupa N., Mankhetkorn S. (2008). Spectrophotometric characterization of behavior and the predominant species of flavonoids in physiological buffer: determination of solubility, lipophilicity and anticancer efficacy. *The Open Drug Delivery Journal. 2*, 10-19.

Waldrop G. L. (2020). *Encyclopedia of Biological Chemistry: Kinetics of enzyme inhibition* (Vol.3, pp. 14-20). Elsevier Inc. Los Angeles, United States.

Wang H., Dub Y., Song H. (2010). α-Glucosidase and a-amylase inhibitory activities of guava leaves. *Food Chemistry. 123*(1), 6-13.

Wu Q., Yang X., Zou L., Fu D. (2009). Bioactivity guided isolation of alpha-glucosidase inhibitor from whole herbs of *Crossostephium chinense. Zhongguo Zhong Yao Za Zhi. 34*(17), 2206-2211.

Xiao J. B., Högger P. (2015). Dietary polyphenols and type 2 diabetes: current insights and future perspectives. *Current Medicinal Chemistry. 22*(1), 23–38.

Yamamoto K., Miyake H., Kusunoki M., Osaki S. (2010). Crystal structures of isomaltase from *Saccharomyces cerevisiae* and in complex with its competitive inhibitor maltose. *FEBS Journal. 277*(20), 4205-4214.

Yin Z., Zhang W., Feng F., Zhang Y., Kang W. (2014). α-Glucosidase inhibitors isolated from medicinal plants. *Food Science and Human Wellness. 3*, 136-174.

Zechel D. L., Withers S. G. (2000). Glycosidase mechanisms: anatomy of a finely tuned catalyst. *Accounts of Chemical Ressearch. 33*(1), 11-18.

Zhang L., Tu Z., Yuan T., Wang H., Xie X., Fu Z. (2016). Antioxidants and α-glucosidase inhibitors from *Ipomoea batatas* leaves identified by bioassay-guided approach and structure-activity relationships. *Food Chemistry. 208*, 61-67.

Zhi-yun Z., An-ming L., D'Arcy W.G. (1994). *Flora of China volume 17 Verbenaceae through Solanaceae* (Vol.17, pp. 300-332). Science Press. Beijing, China.

APPENDIX
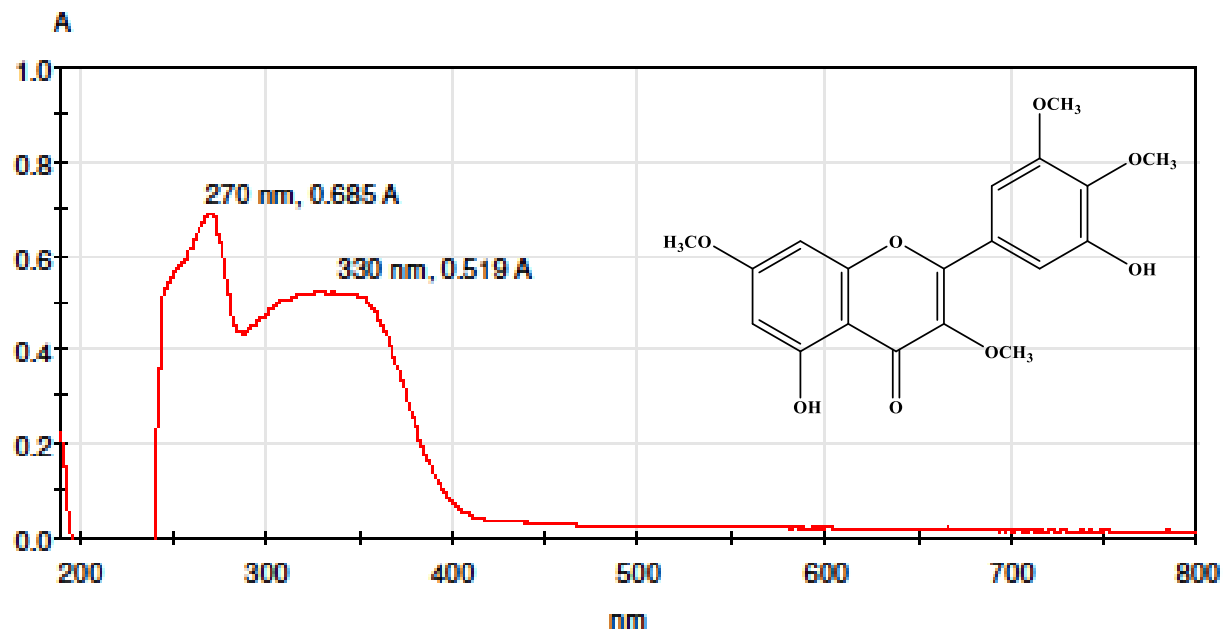
Appendix 1 UV-Visible spectrum of SS1 in chloroform
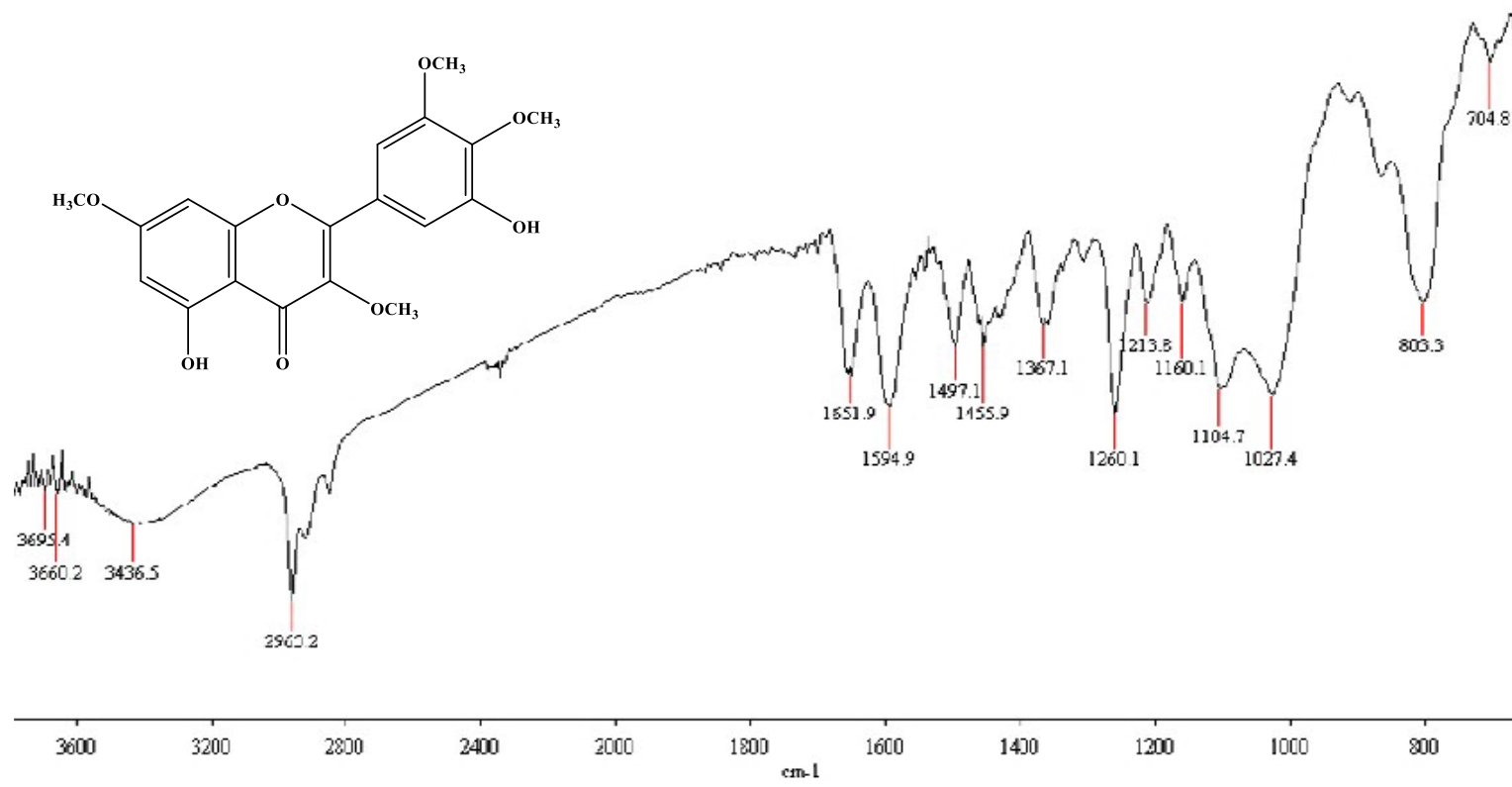
Appendix 2 IR spectrum of SS1 in chloroform
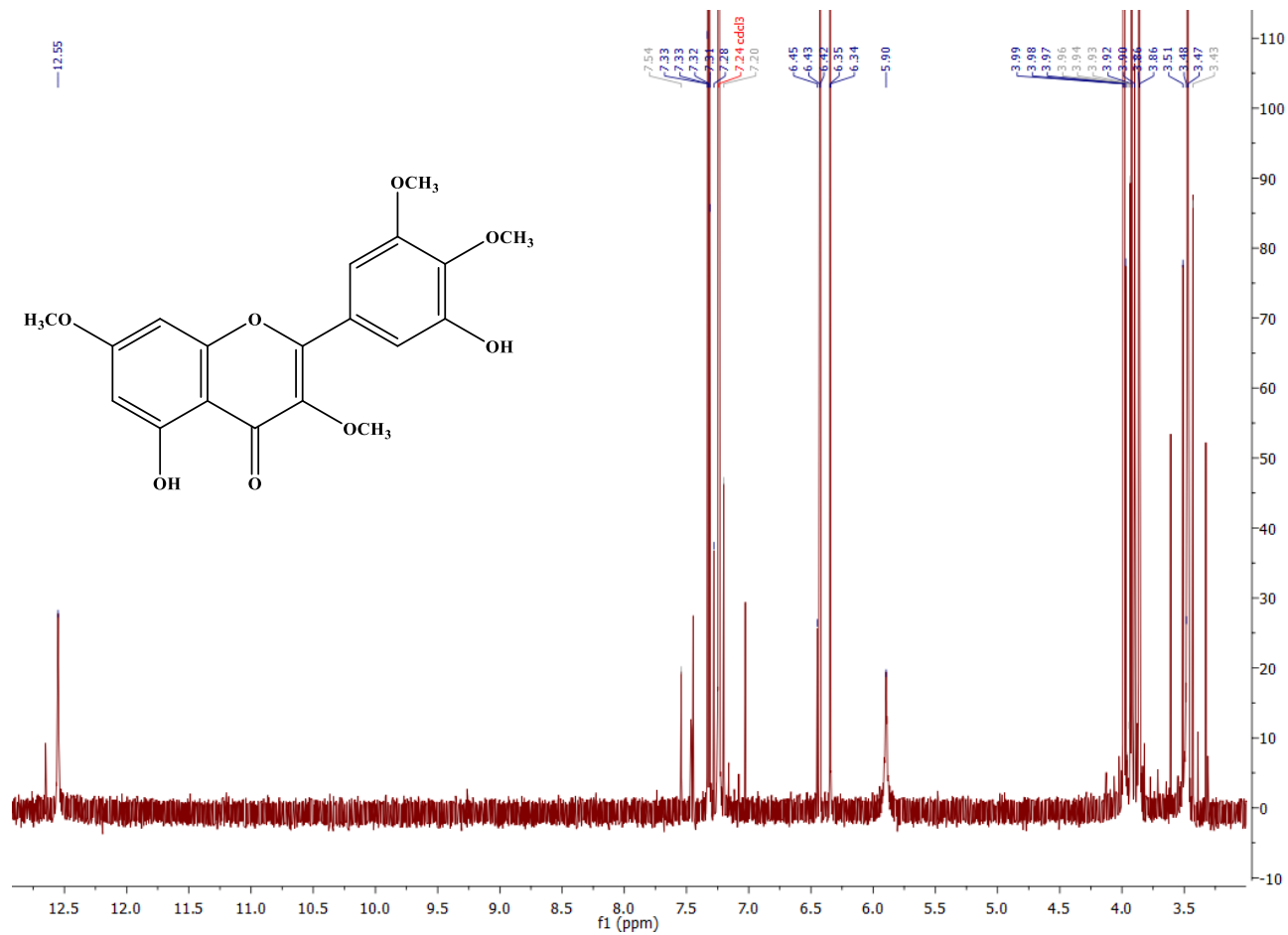
Appendix 3 ^{1}H NMR of SS1 (500 MHz in CDCl$_3$)
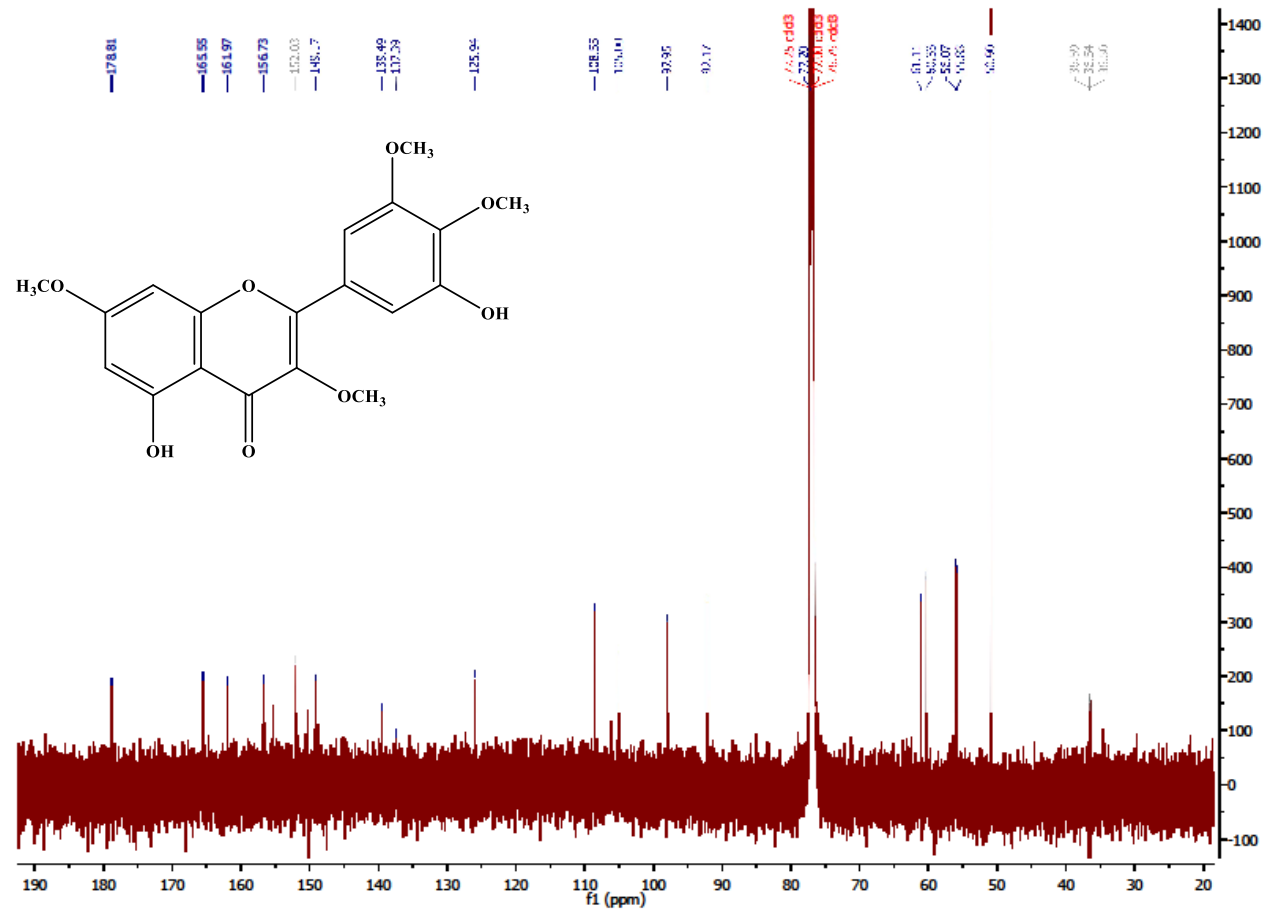
Appendix 4 ^{13}C NMR of SS1 (125 MHz in CDCl$_3$)
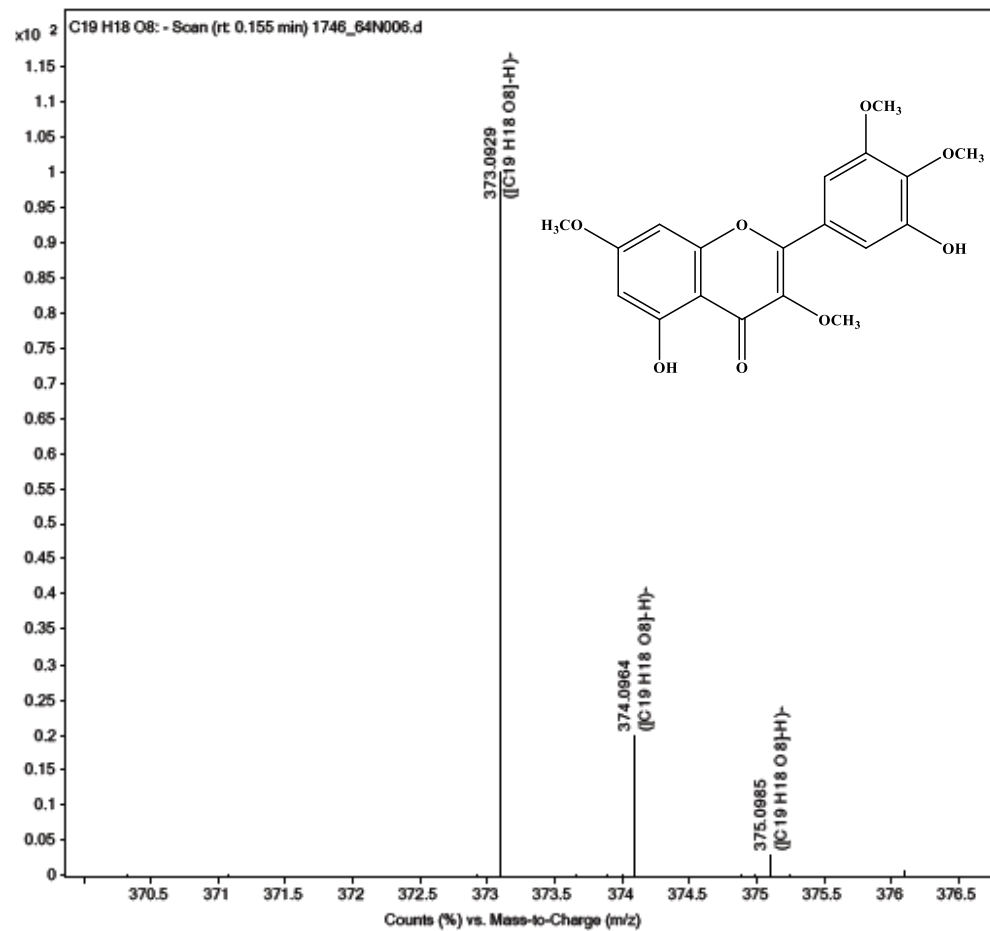
Appendix 5 HRESI-Mass spectrum of SS1
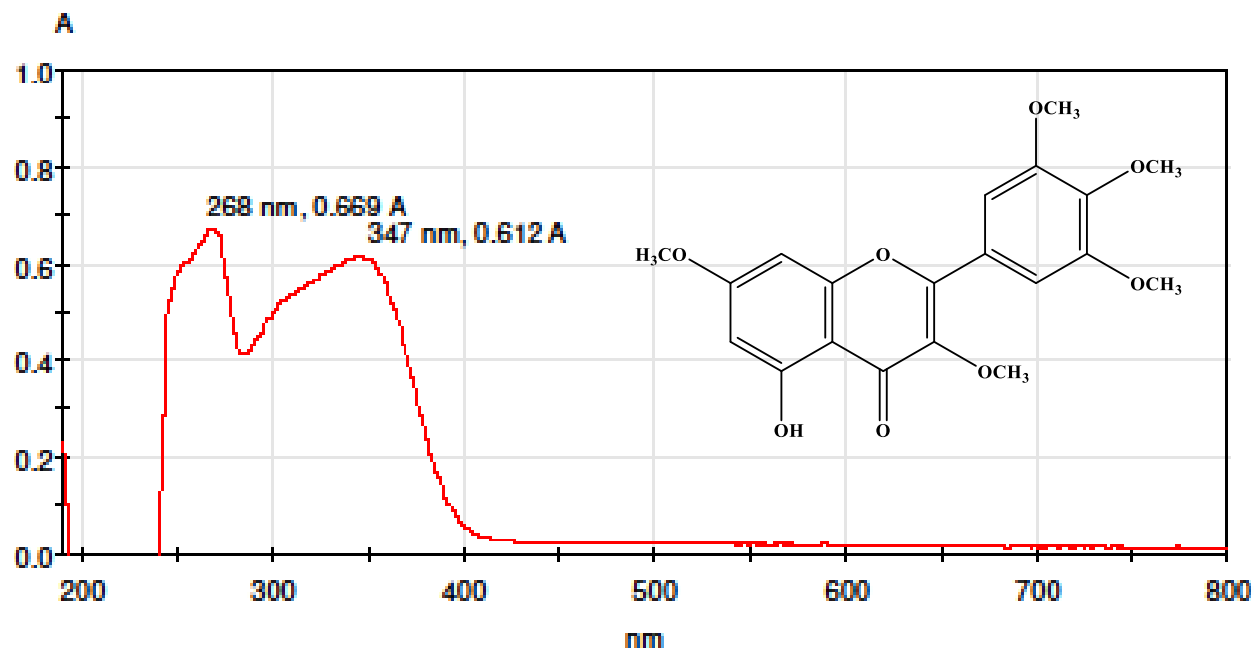
Appendix 6 UV-Visible spectrum of SS2 in chloroform
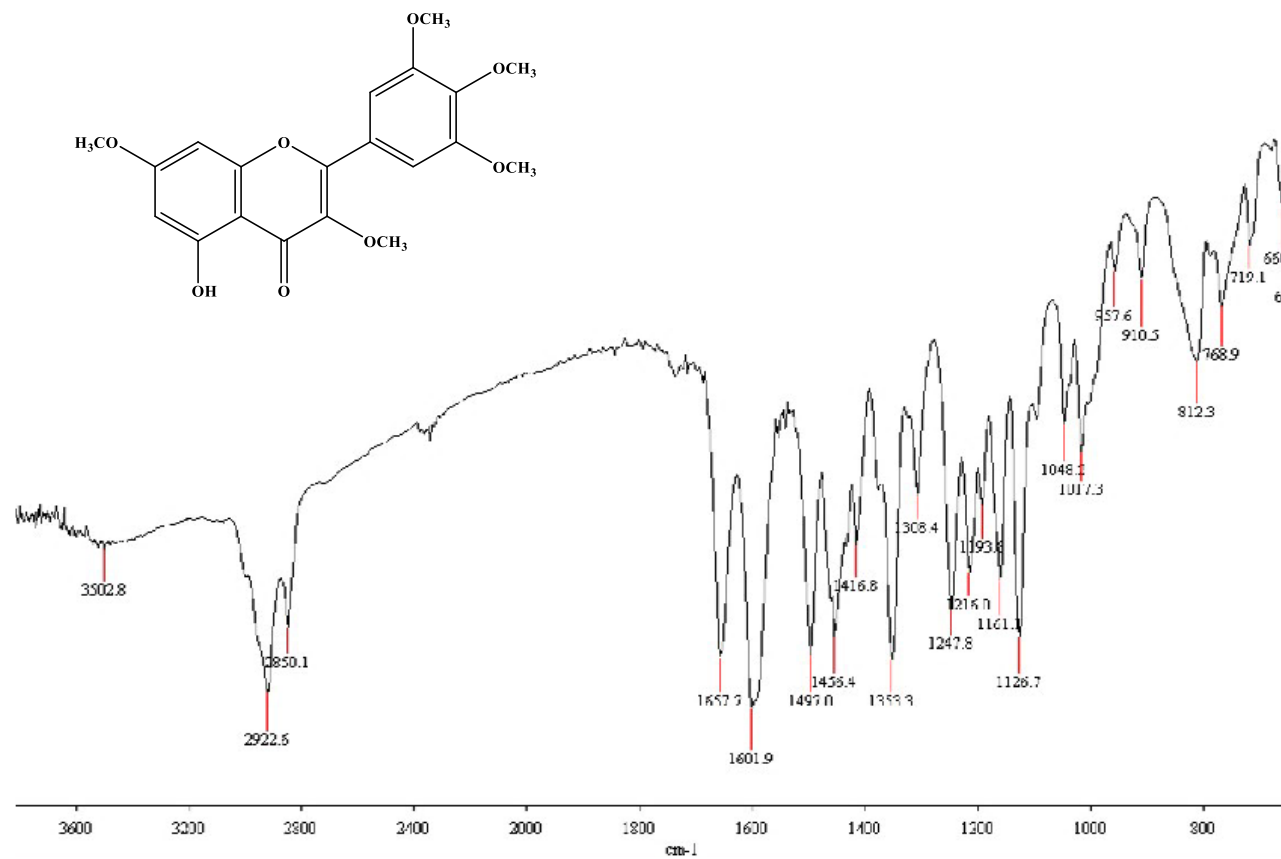
Appendix 7 IR spectrum of SS2 in chloroform
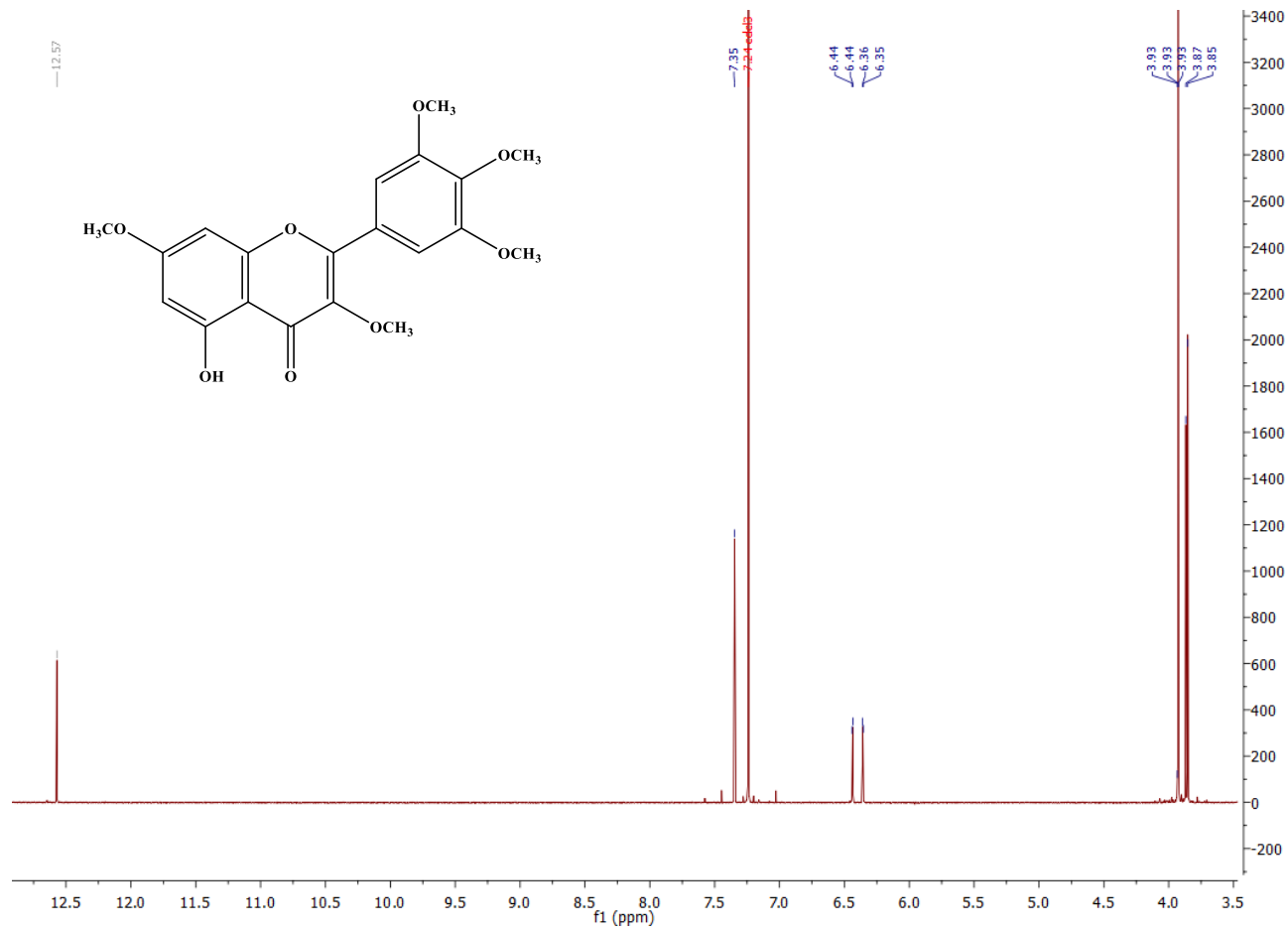
Appendix 8 ^{1}H NMR of SS2 (500 MHz in CDCl$_3$)
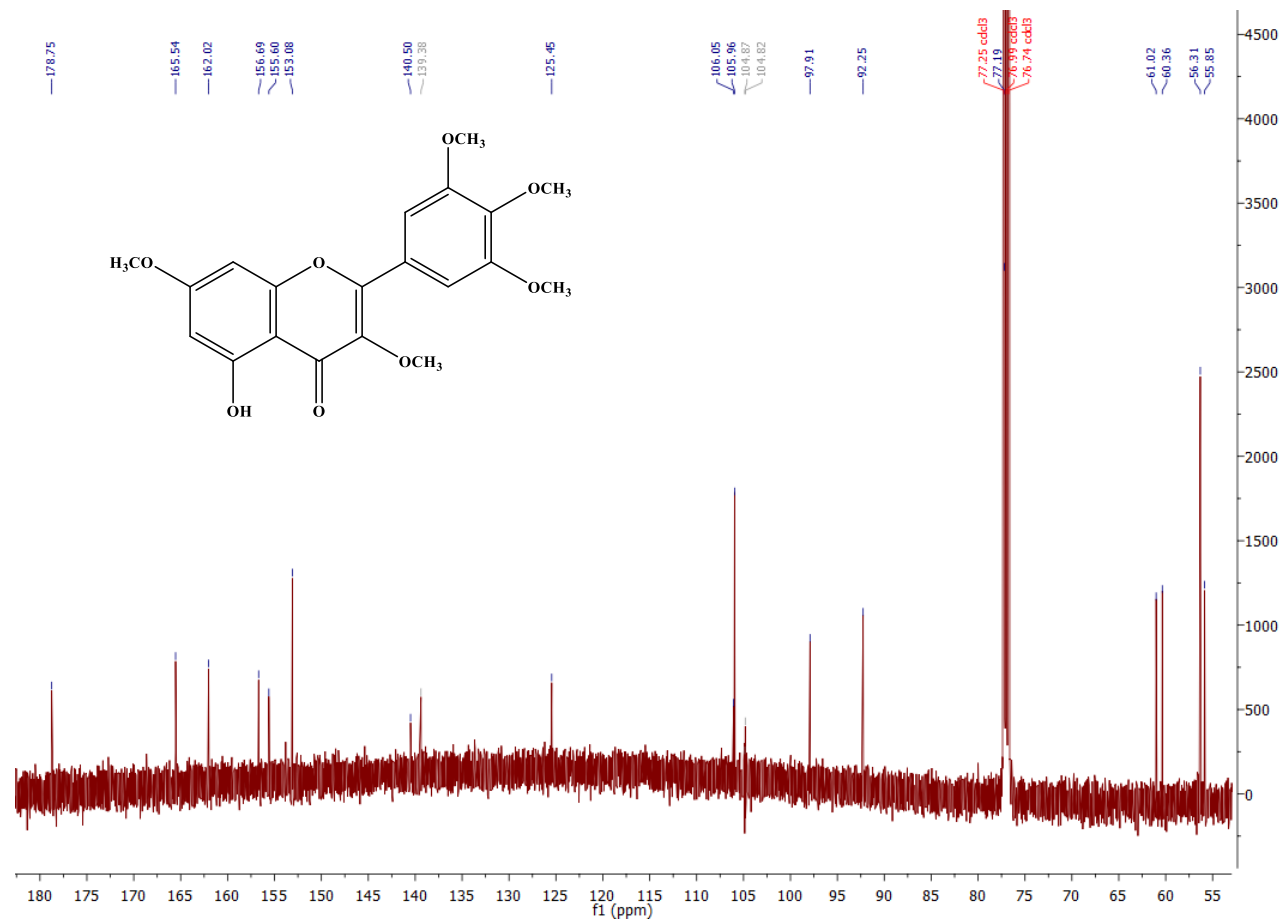
Appendix 9 ^{13}C NMR of SS2 (125 MHz in CDCl$_3$)
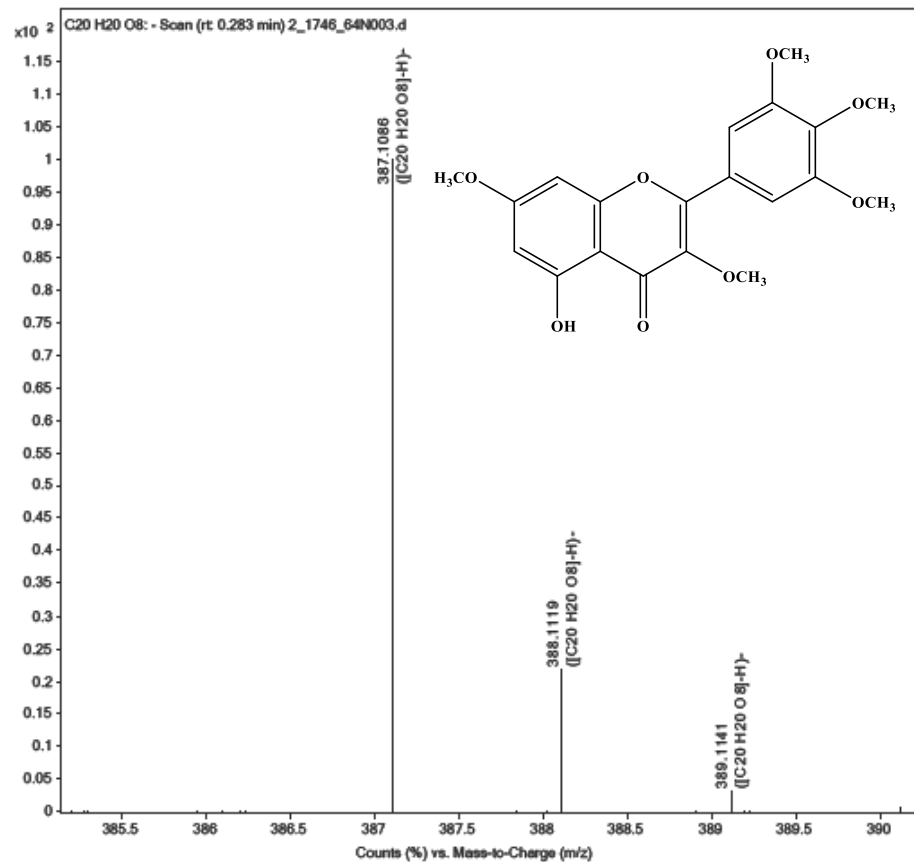
Appendix 10 HRESI-Mass spectrum of SS2
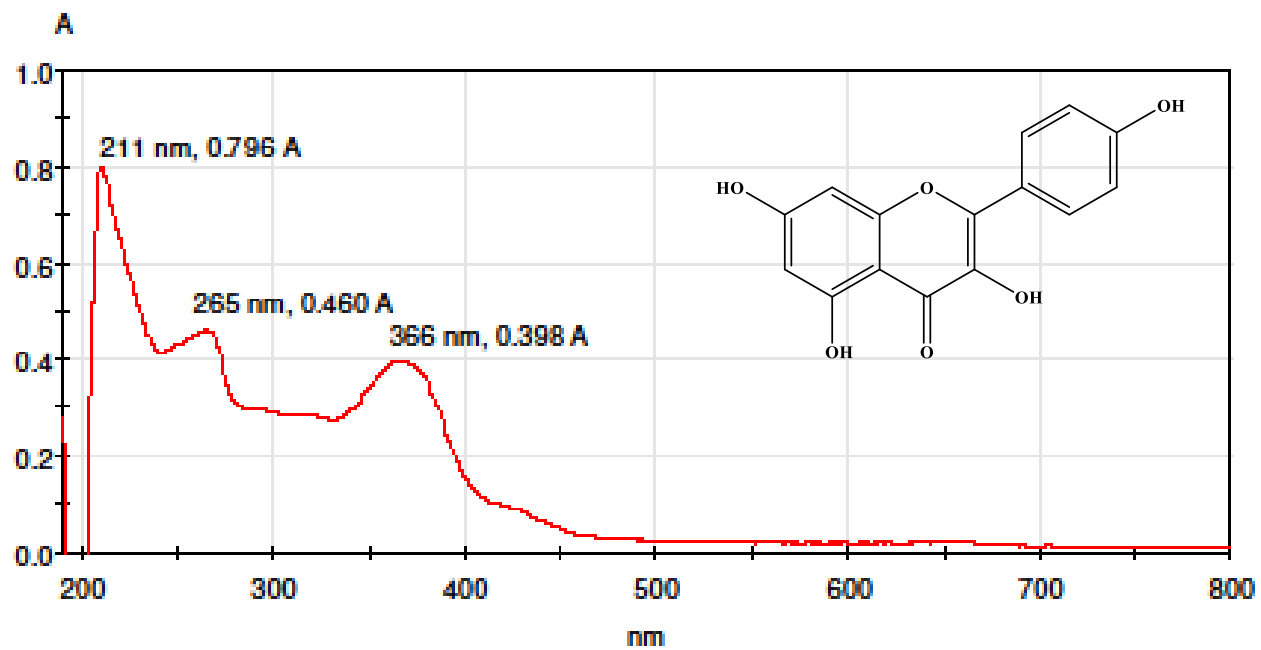
Appendix 11 UV-Visible spectrum of SS3 in methanol
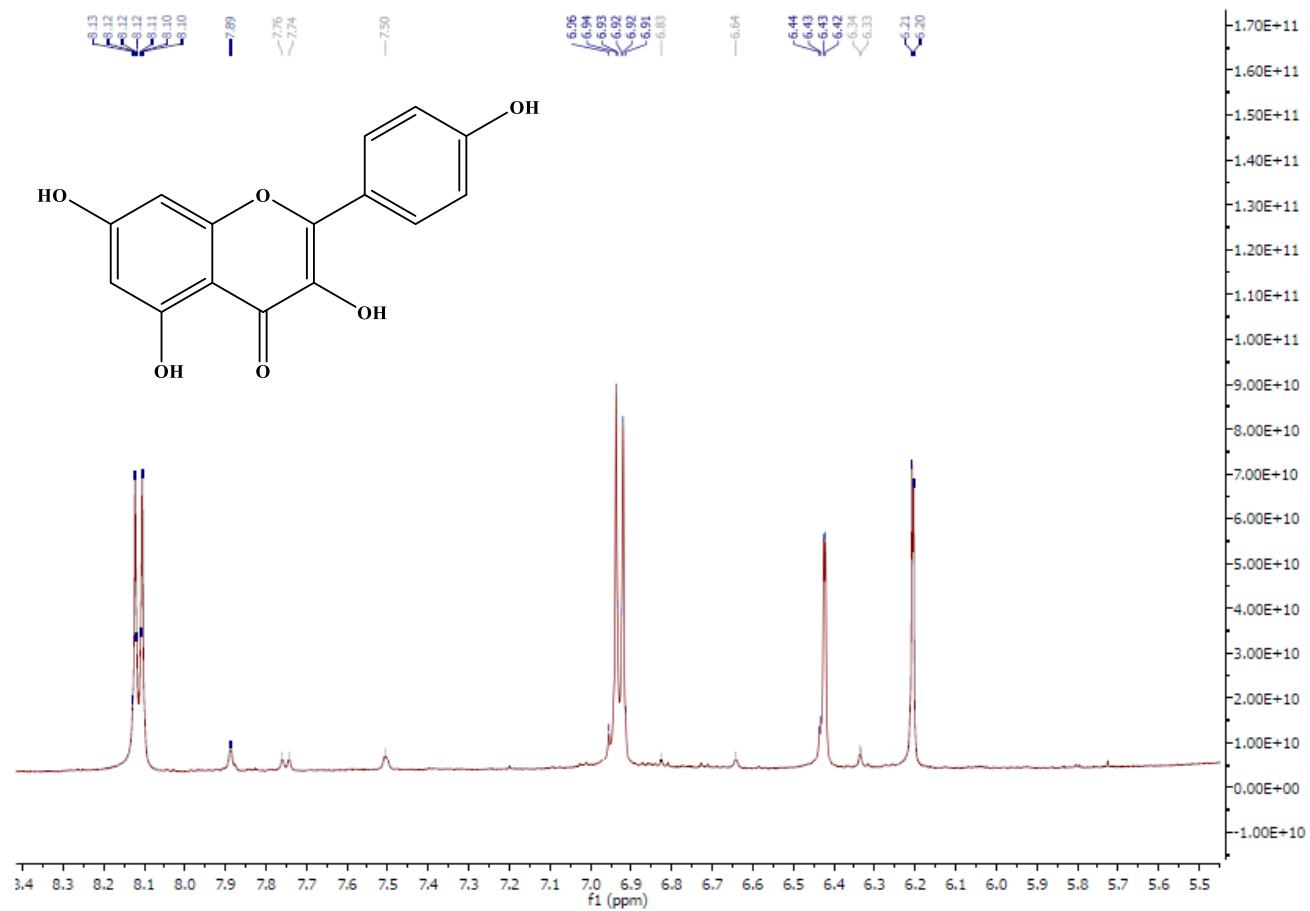
Appendix 12 ^{1}H NMR of SS3 (500 MHz in CD$_3$OD$_3$)
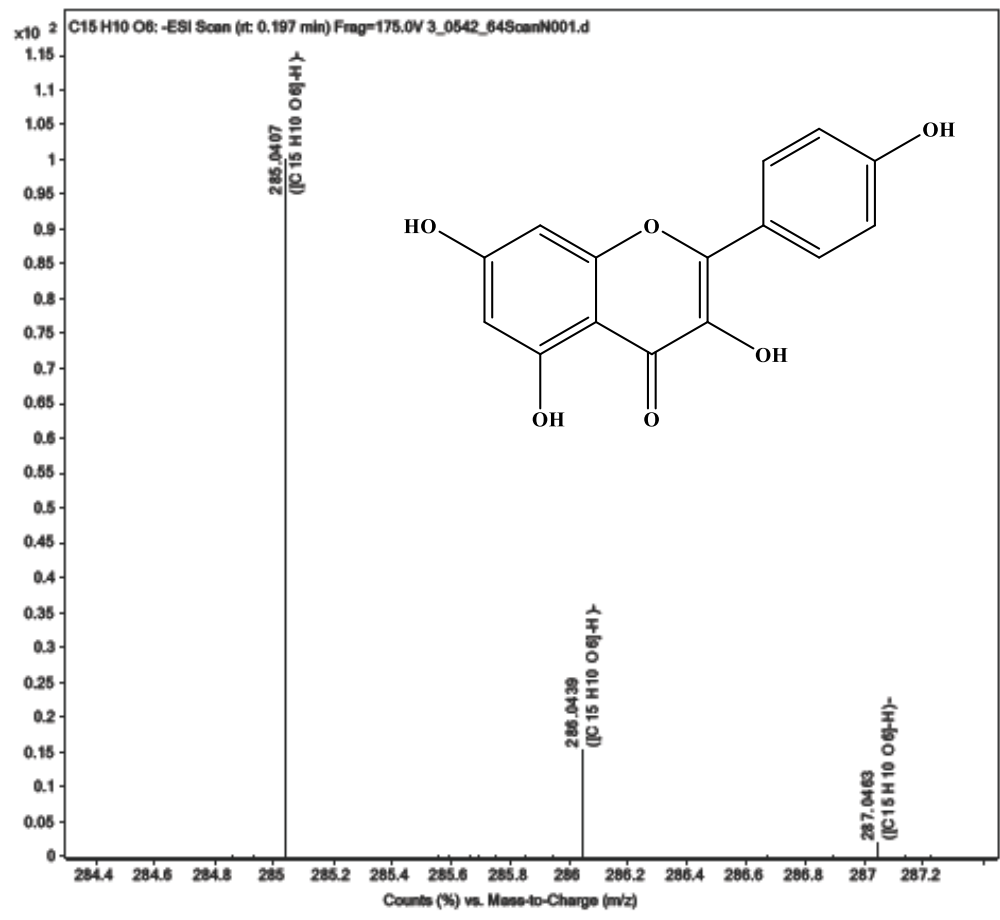
Appendix 13 HRESI-Mass spectrum of SS3
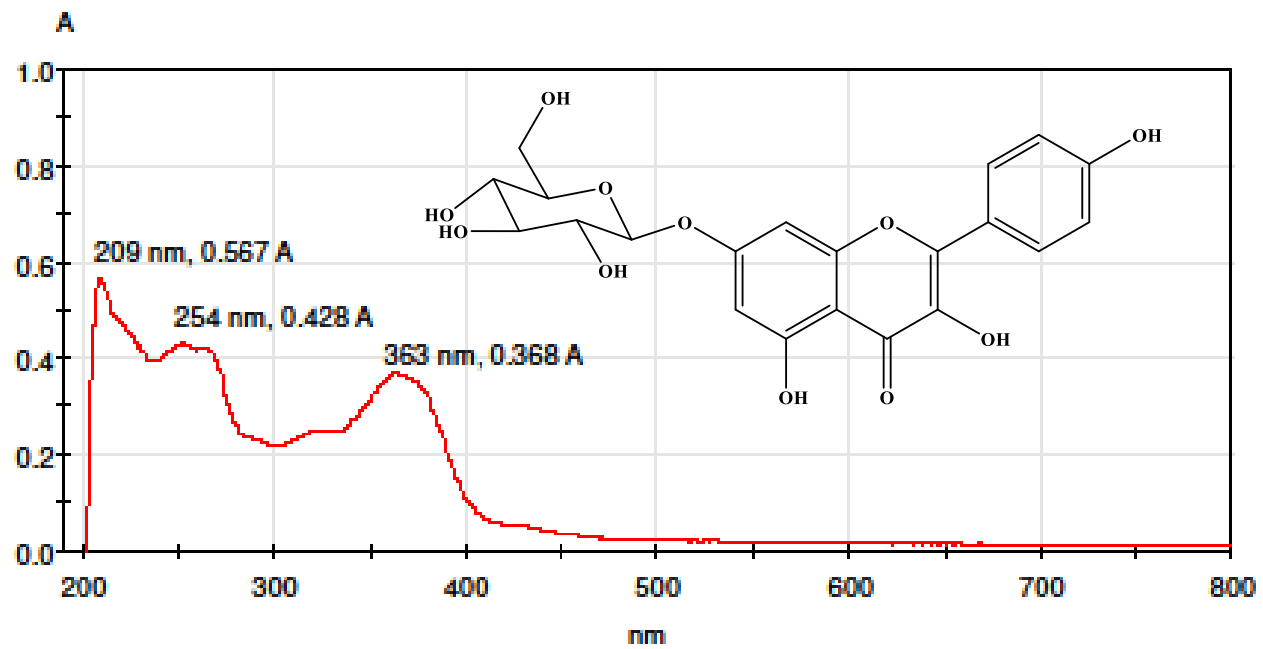
Appendix 14 UV-Visible spectrum of SS4 in methanol
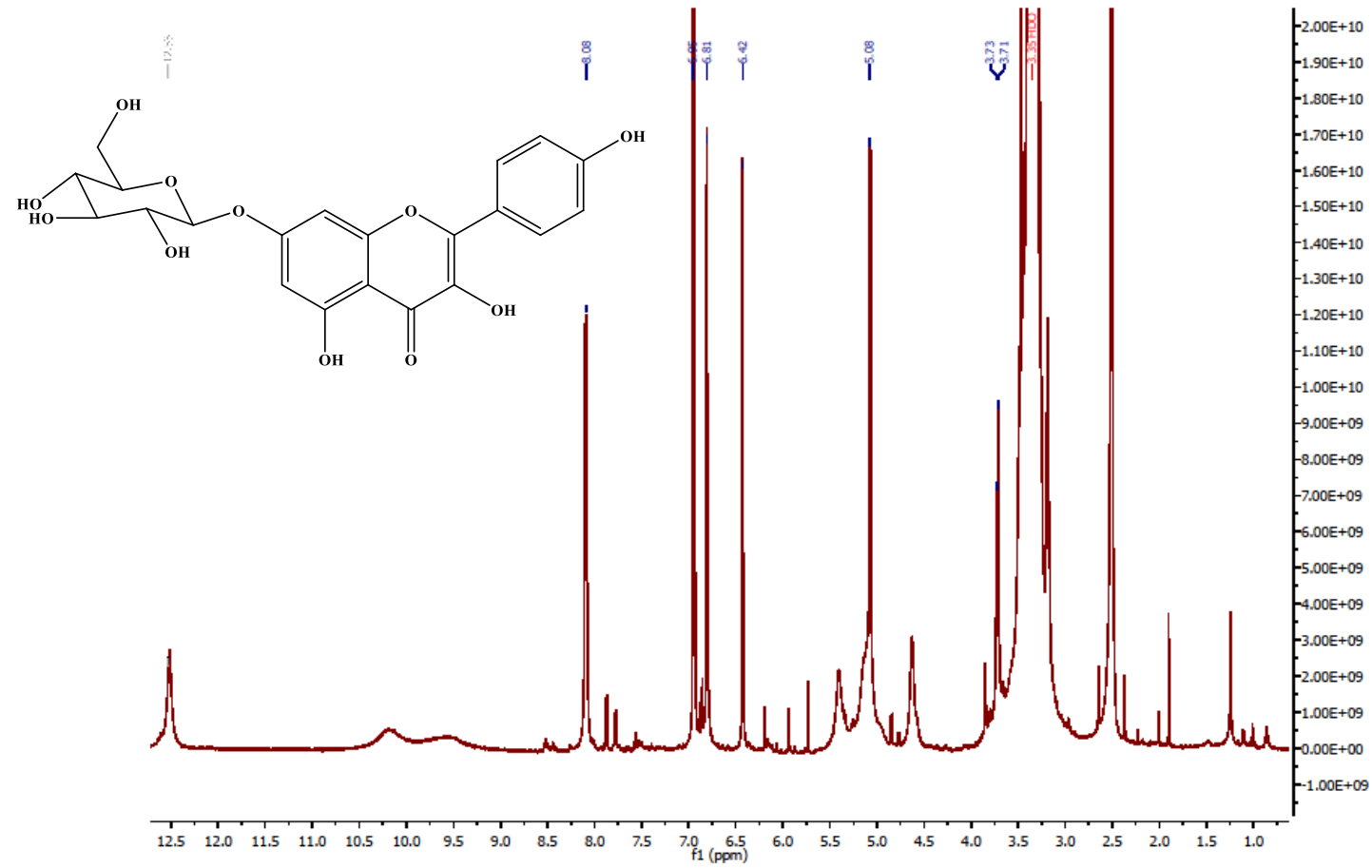
Appendix 15 ^{1}H NMR of SS4 (500 MHz in DMSO-d_6)
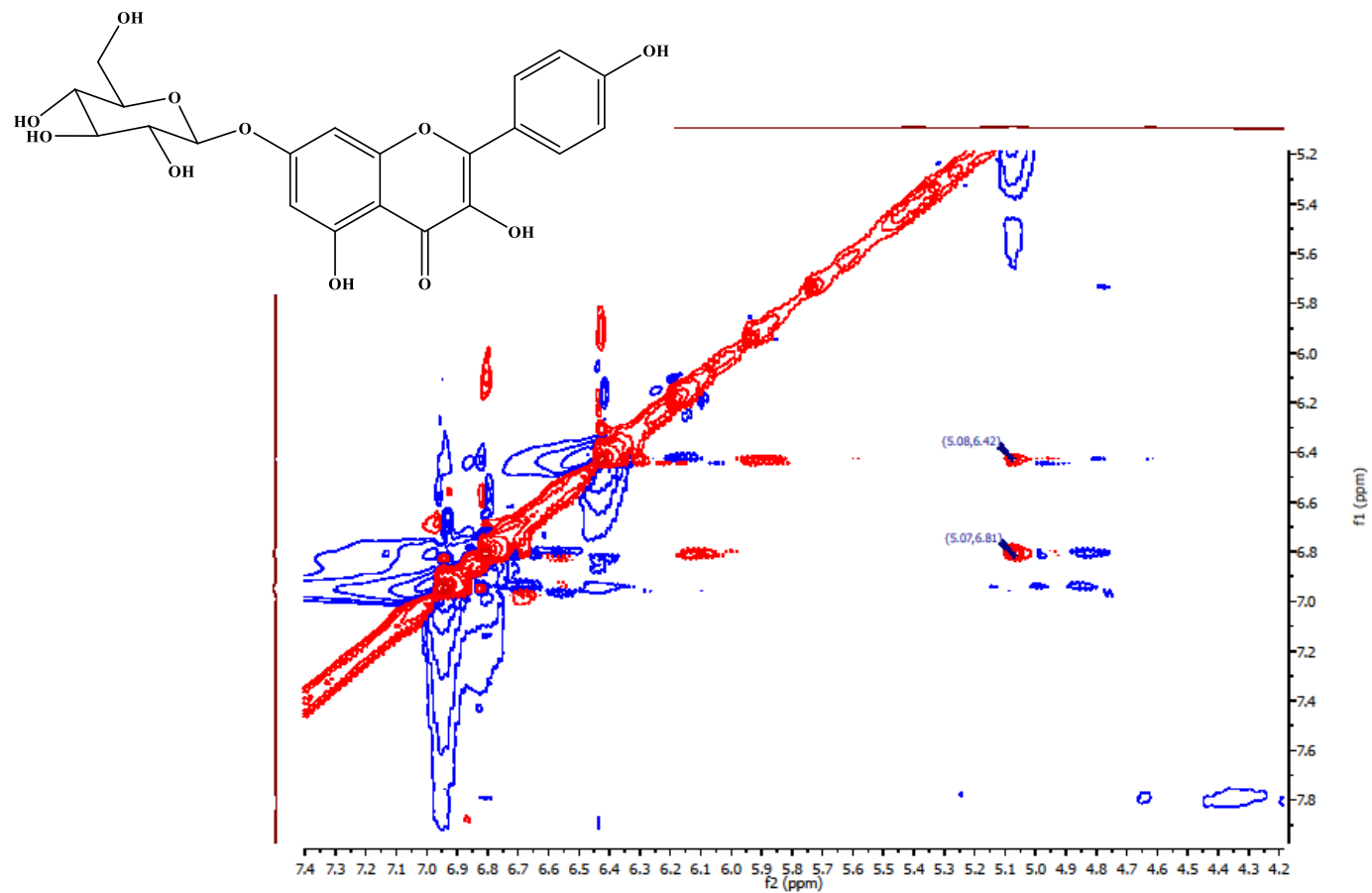
Appendix 16 NOESY of SS4 (500 MHz in DMSO-*d₆*)
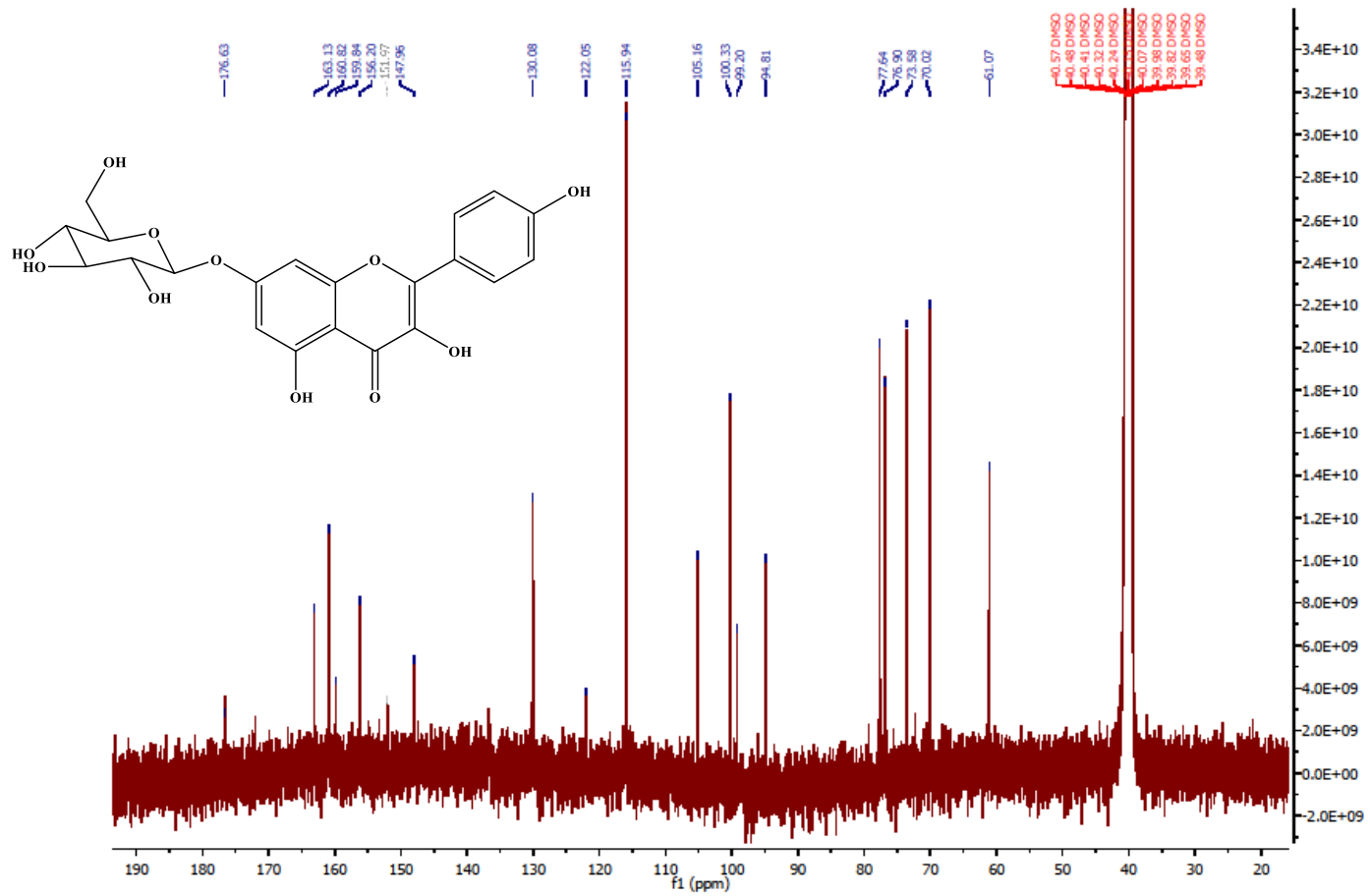
Appendix 17 ^{13}C NMR of SS4 (500 MHz in DMSO-d_6)
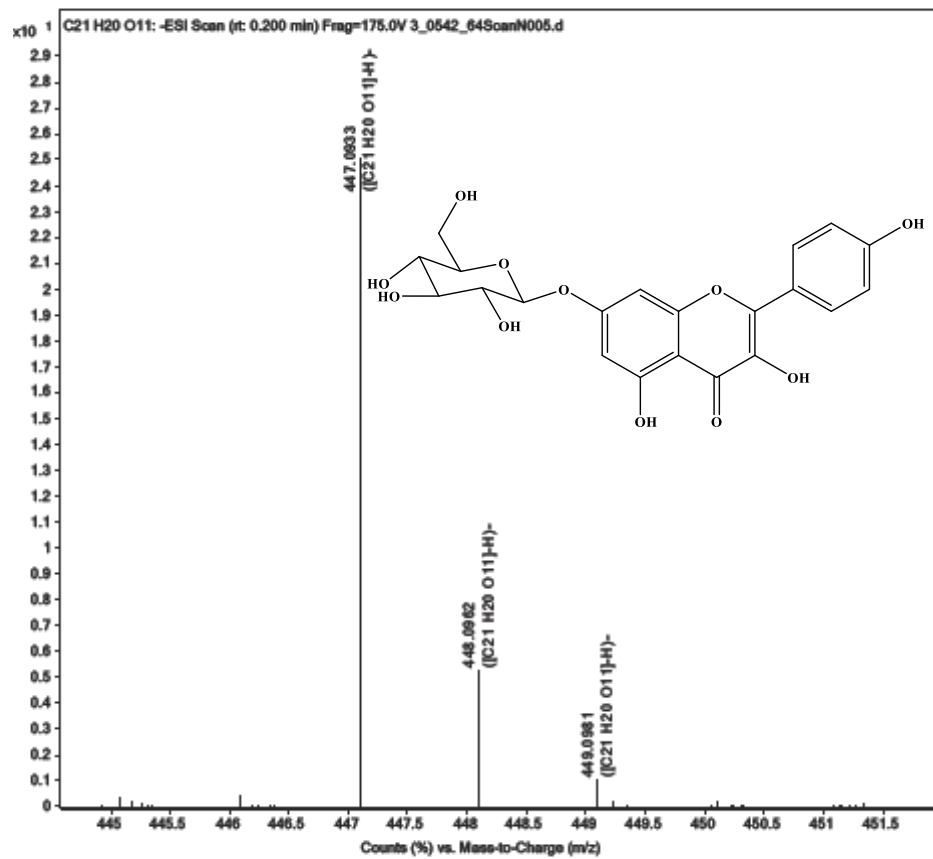
Appendix 18 HRESI-Mass spectrum of SS4
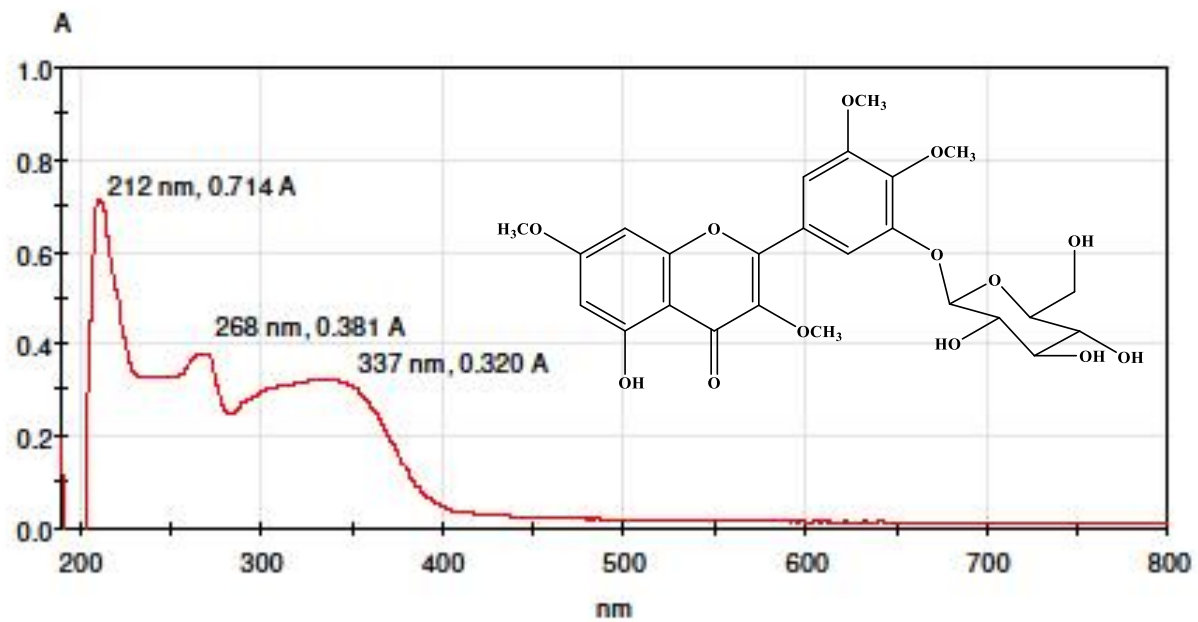
Appendix 19 UV-Visible spectrum of SS5 in methanol
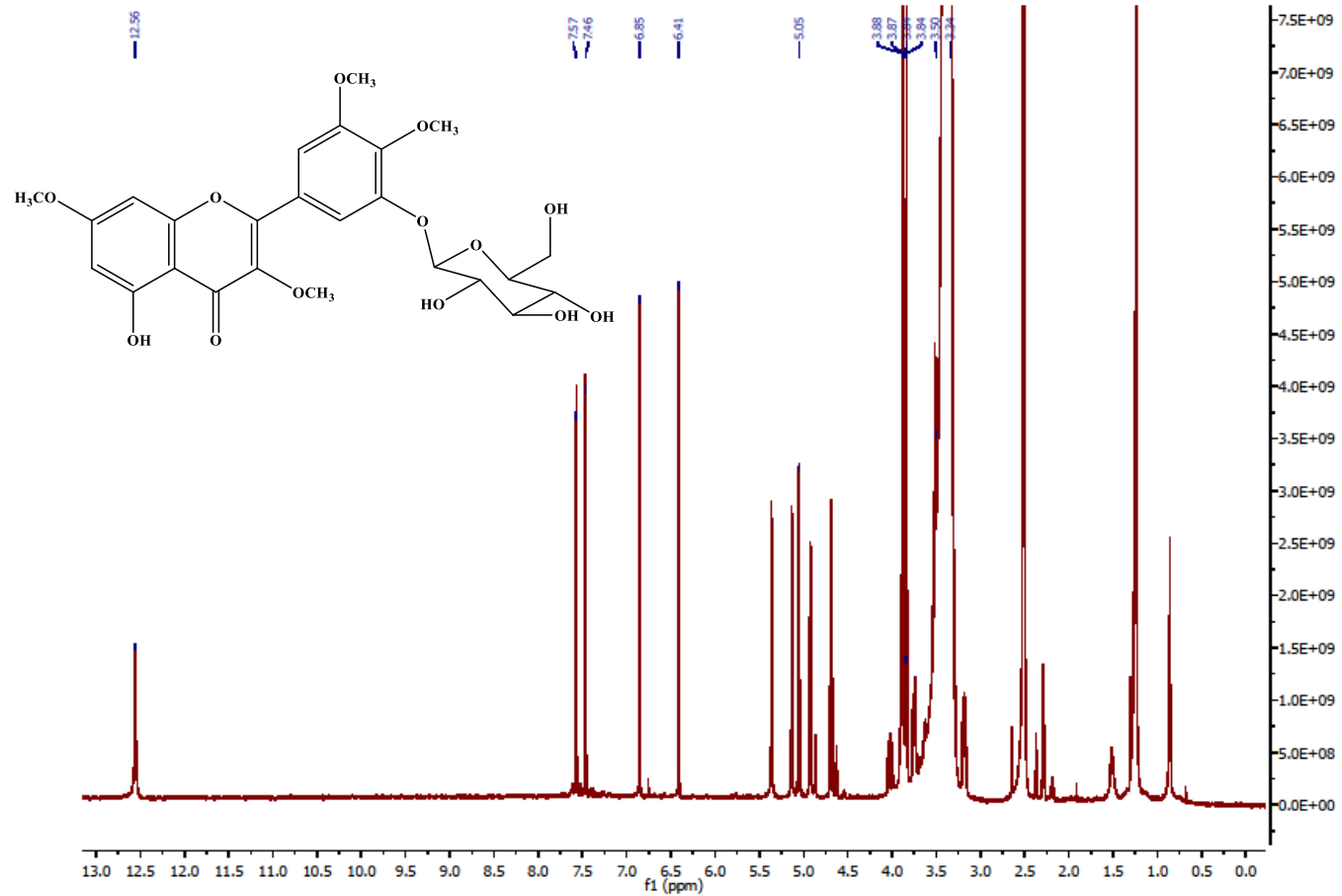
Appendix 20 ^{1}H NMR of SS5 (500 MHz in DMSO-d_6)
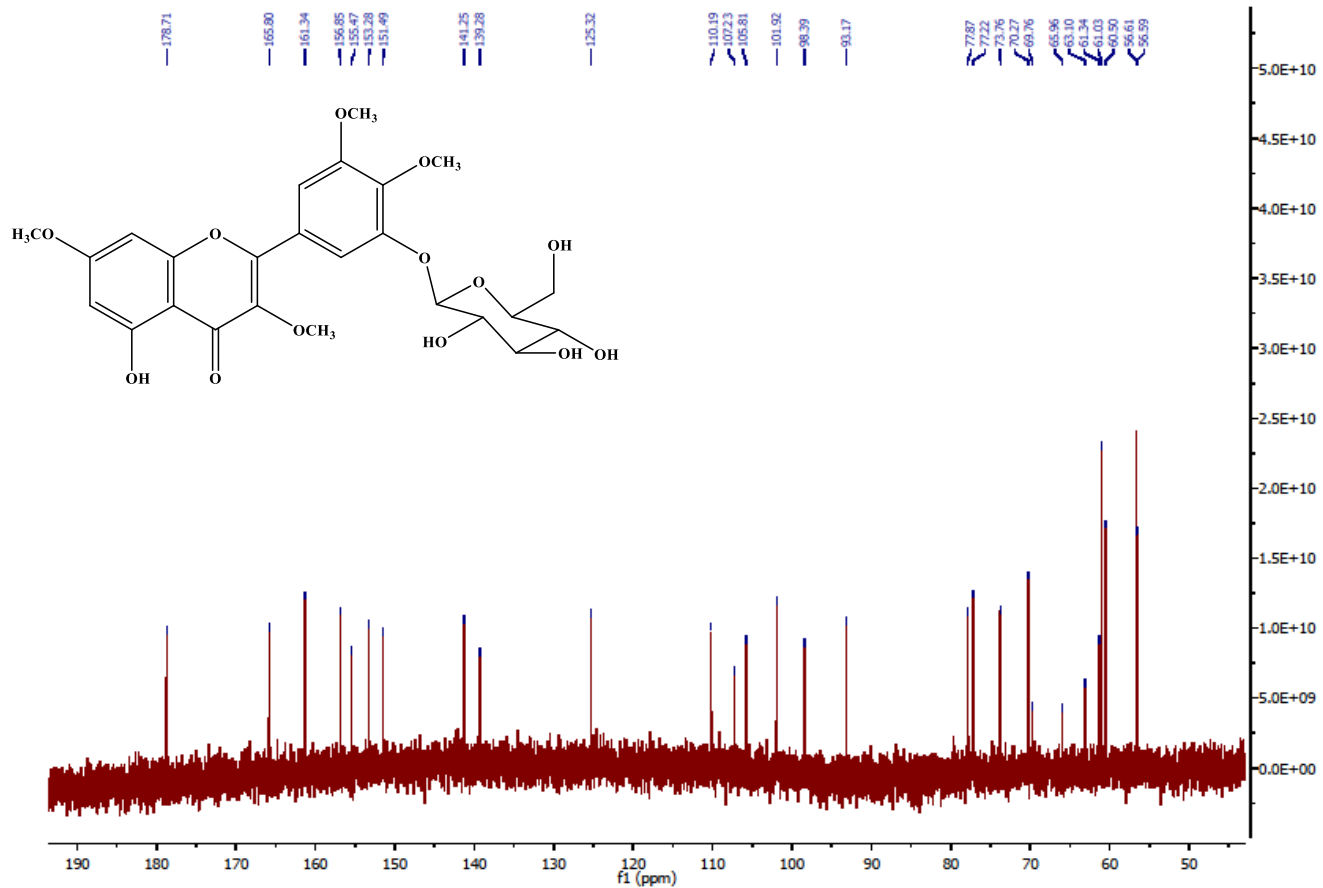
Appendix 21 ^{13}C NMR of SS5 (125 MHz in DMSO-d_6)
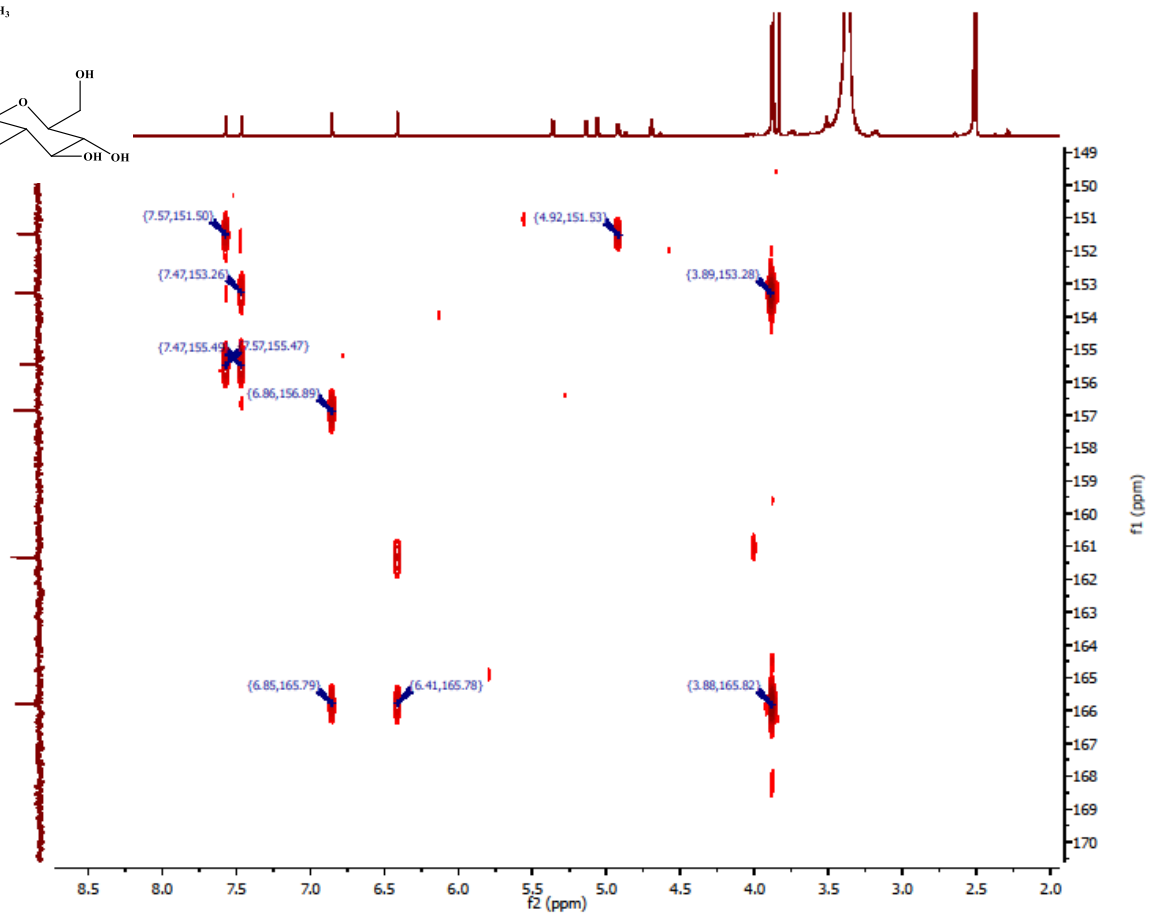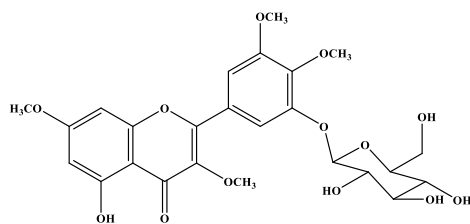
Appendix 22 HMBC of SS5 (500 MHz in DMSO-*d₆*)
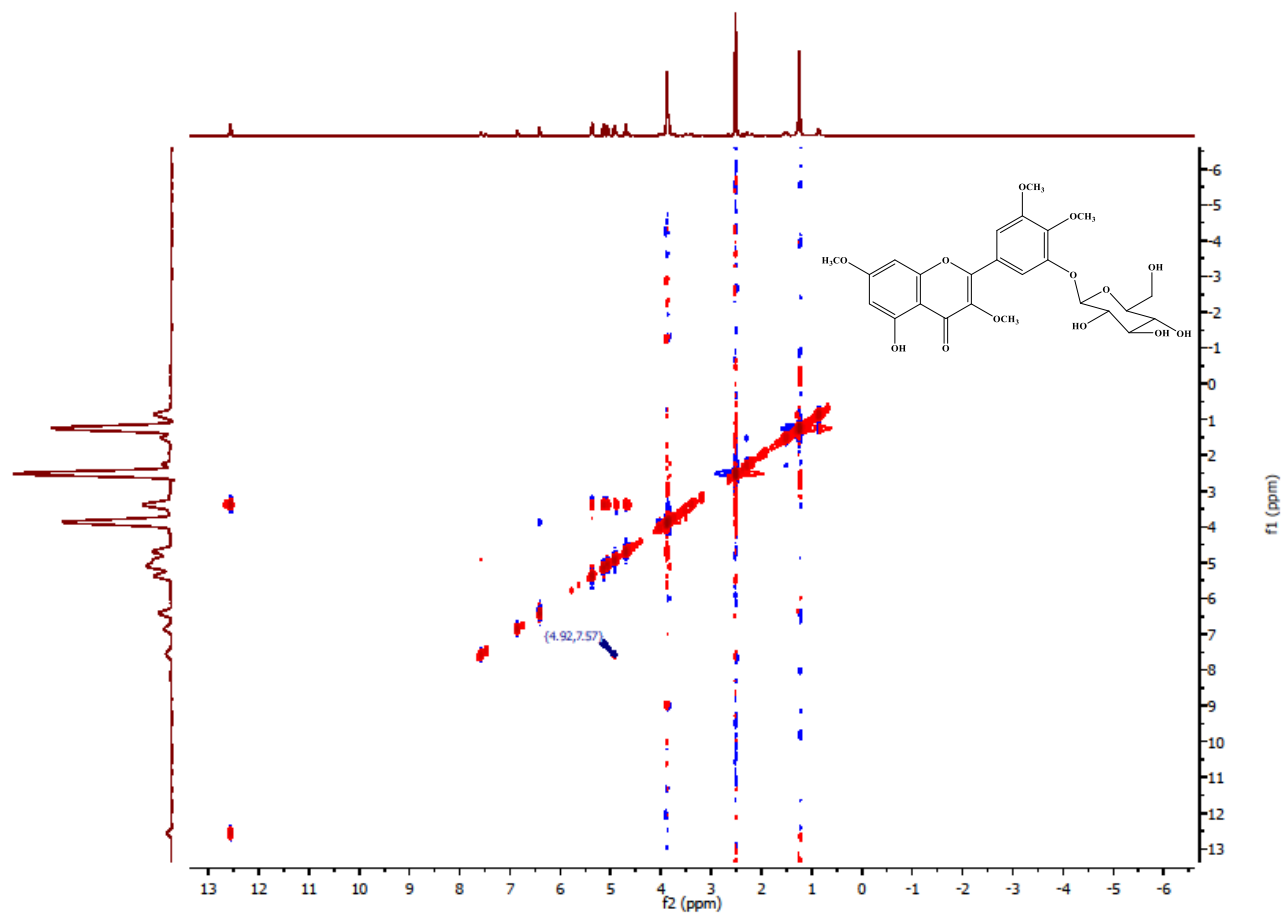
Appendix 23 NOESY of SS5 (500 MHz in DMSO-*d₆*)
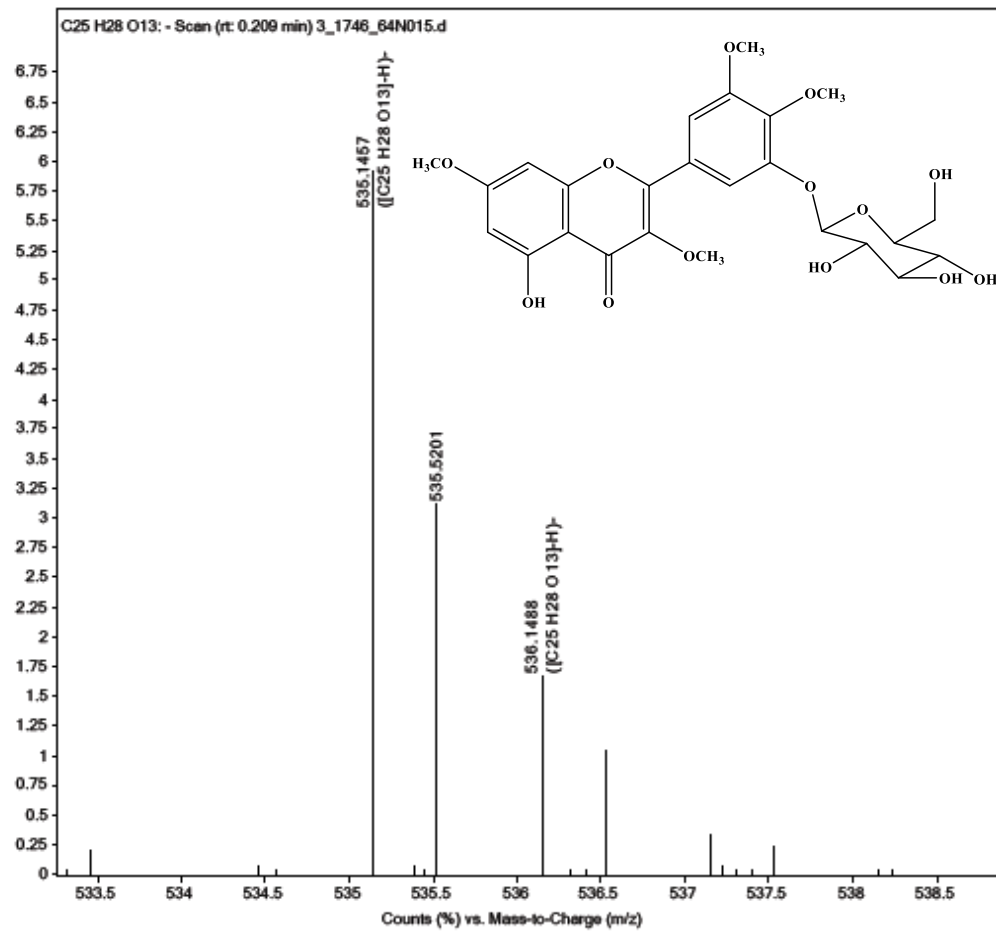
Appendix 24 HRESI-Mass spectrum of SS5
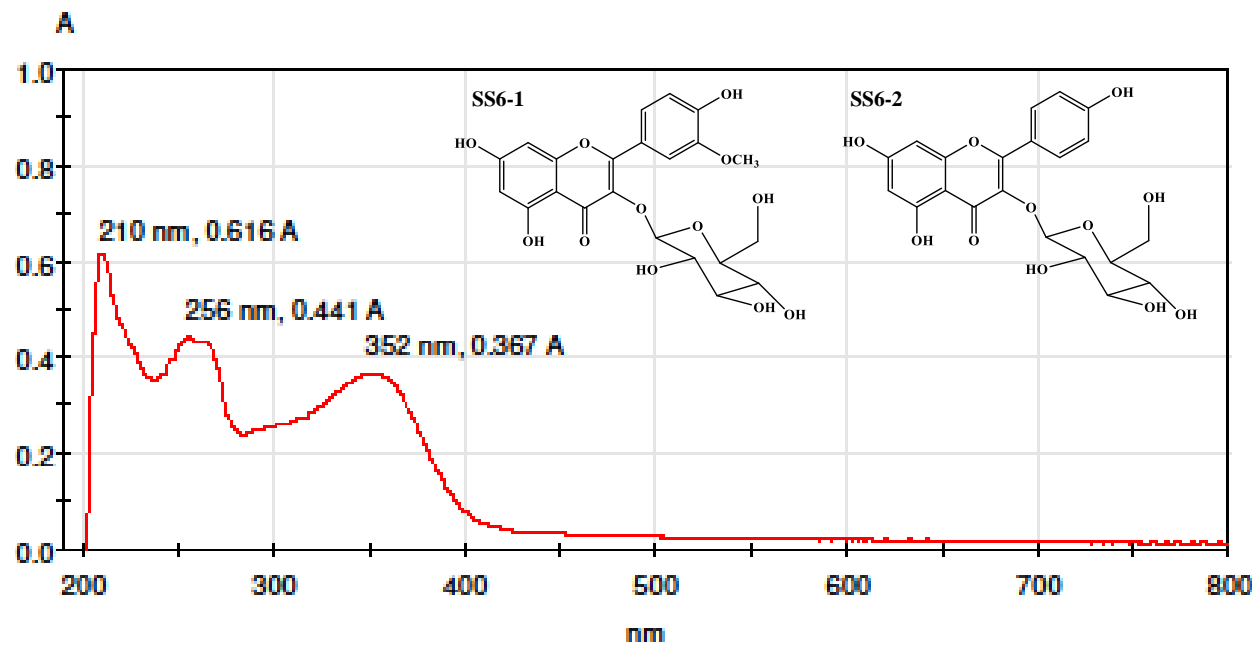
Appendix 25 UV-Visible spectrum of SS6 in methanol
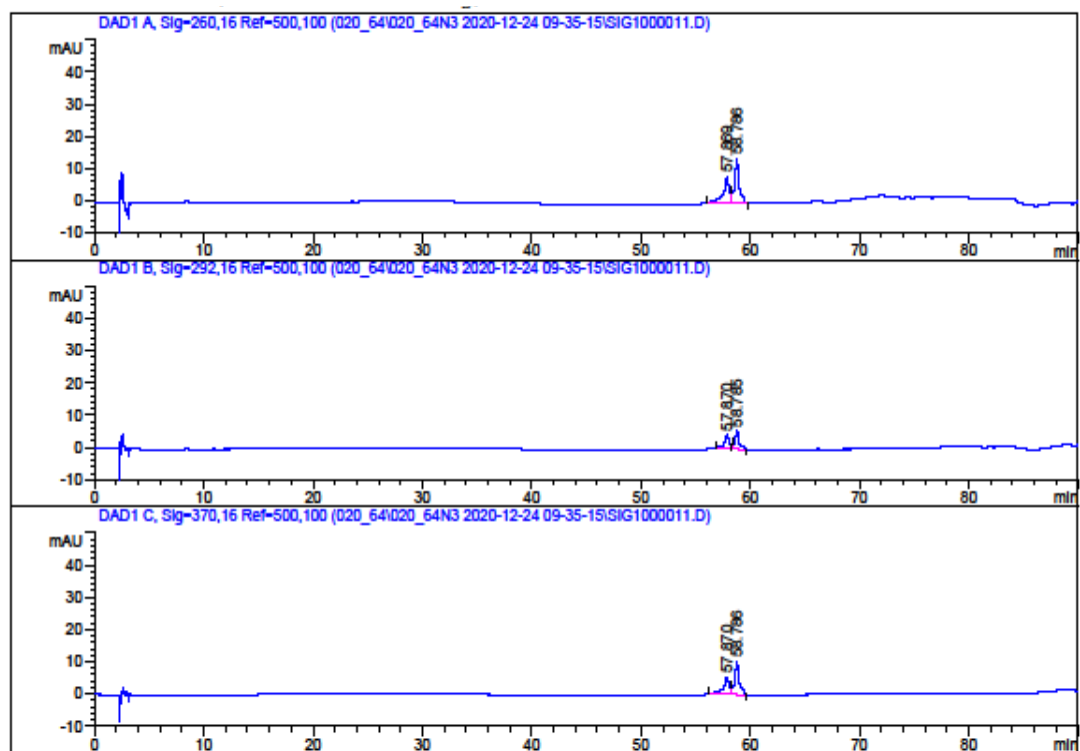
Appendix 26 HPLC chromatogram of SS6
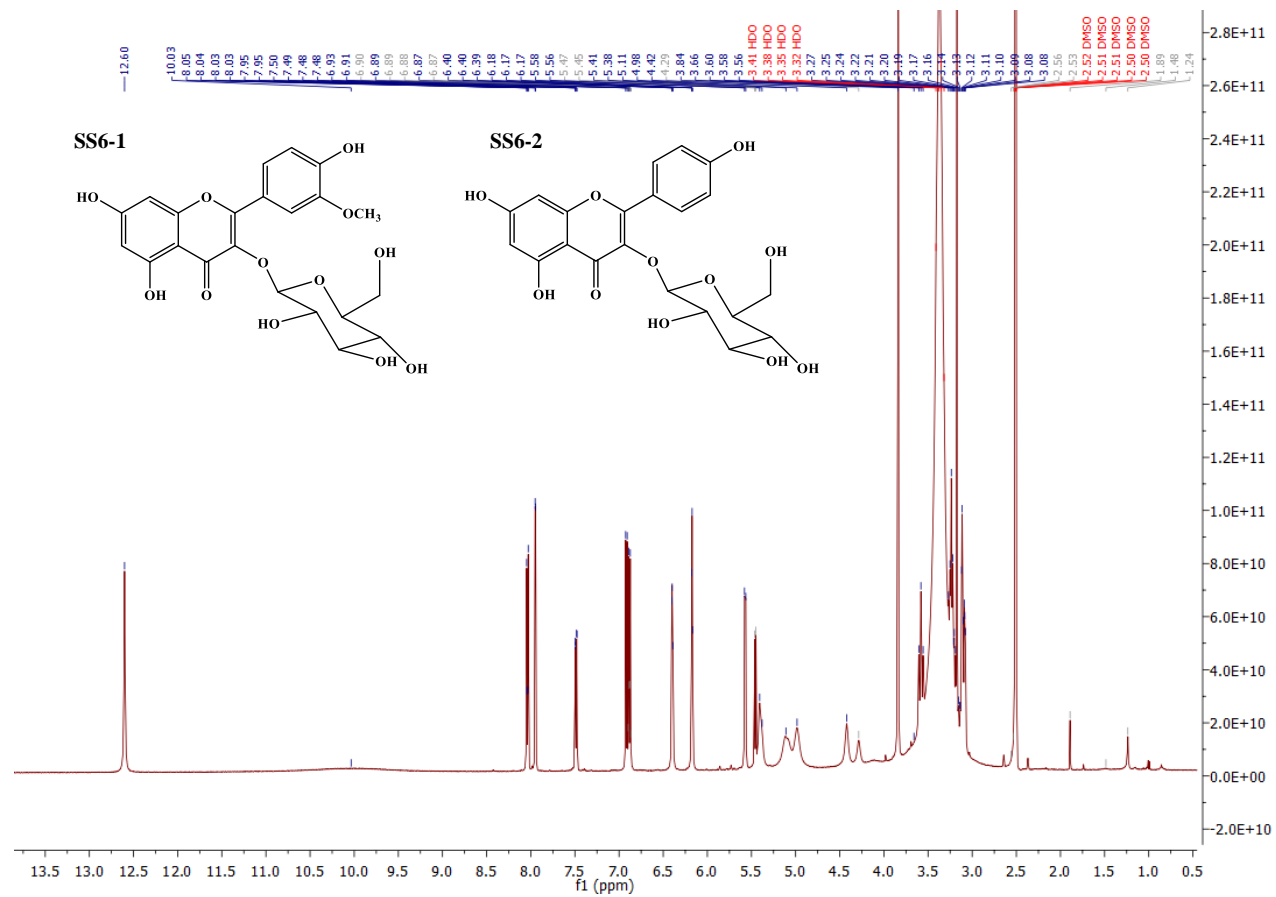
Appendix 27 ^{1}H NMR of SS6 (500 MHz in DMSO-d_6)
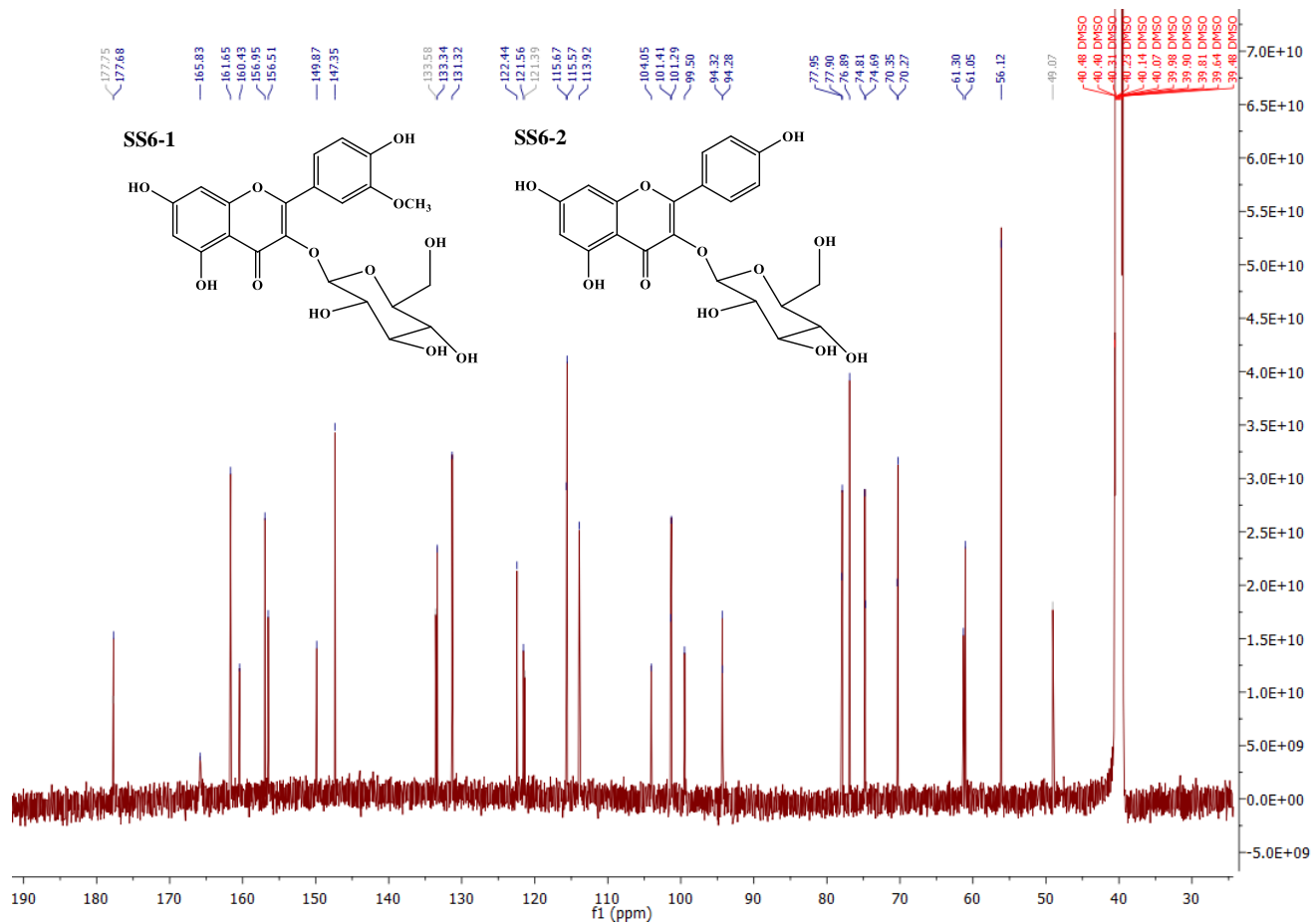
Appendix 28 ^{13}C NMR of SS6 (125 MHz in DMSO-d_6)
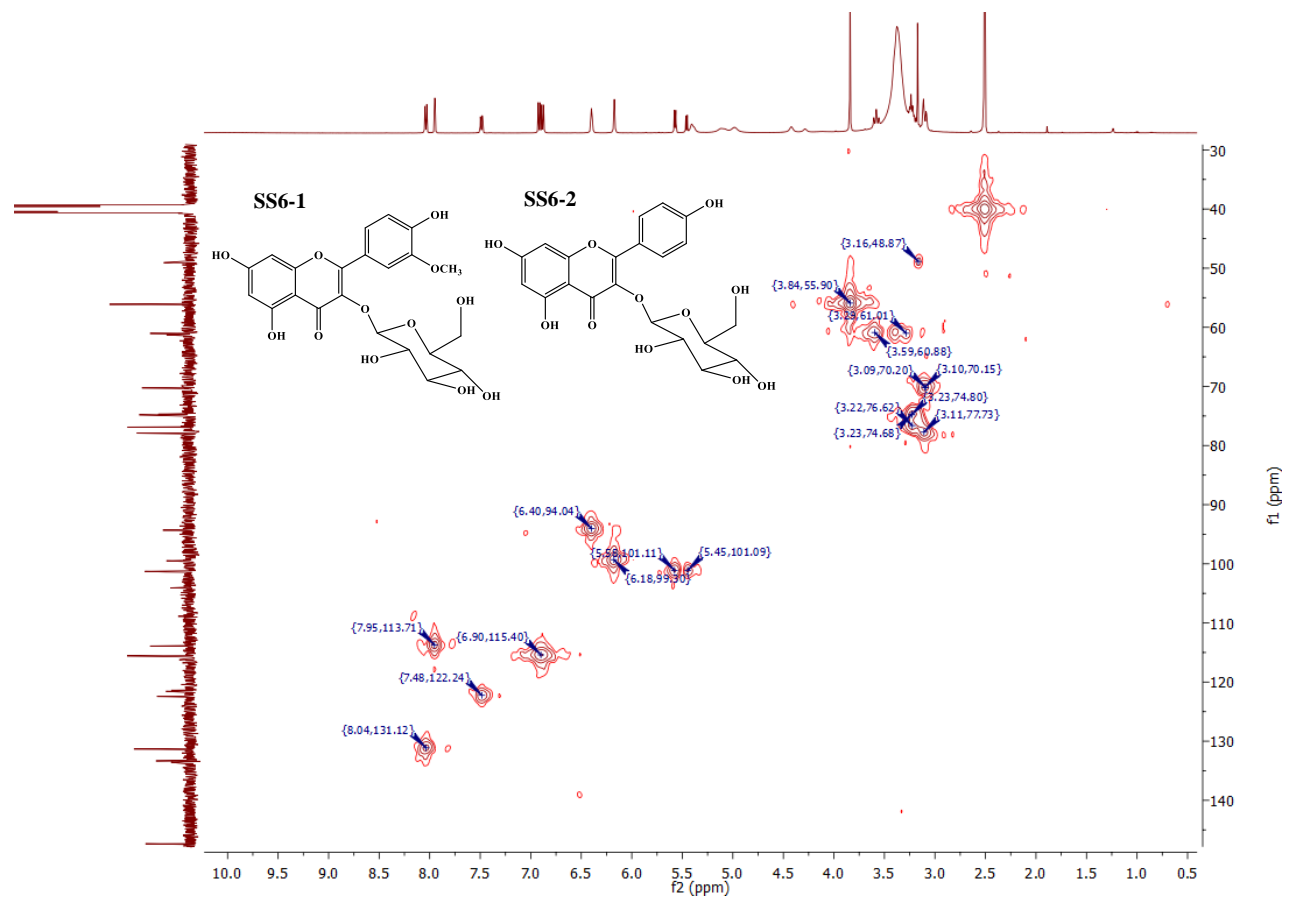
Appendix 29 HMBC of SS6 (125 MHz in DMSO-*d₆*)
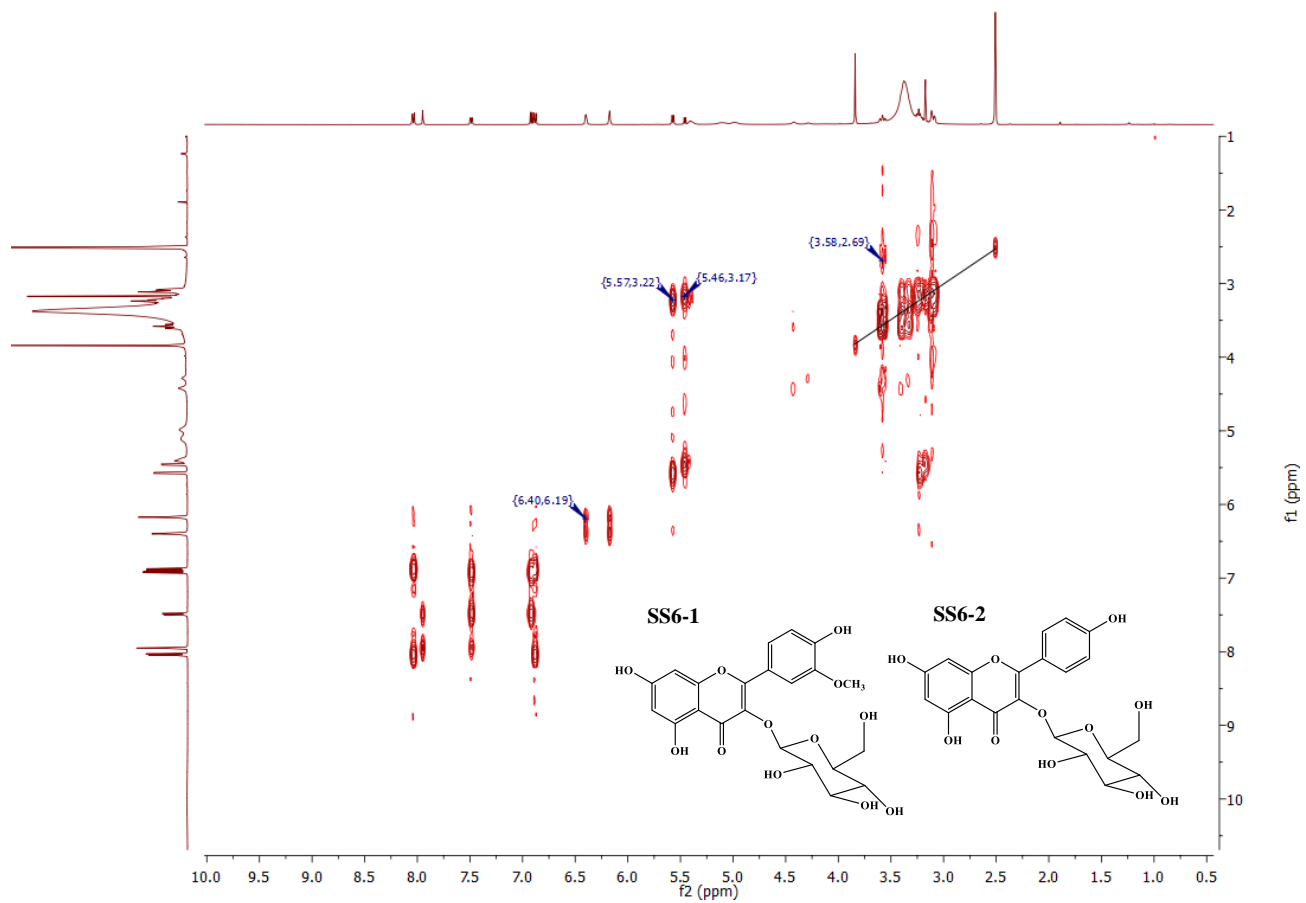
Appendix 30 COSY of SS6 (500 MHz in DMSO-*d₆*)
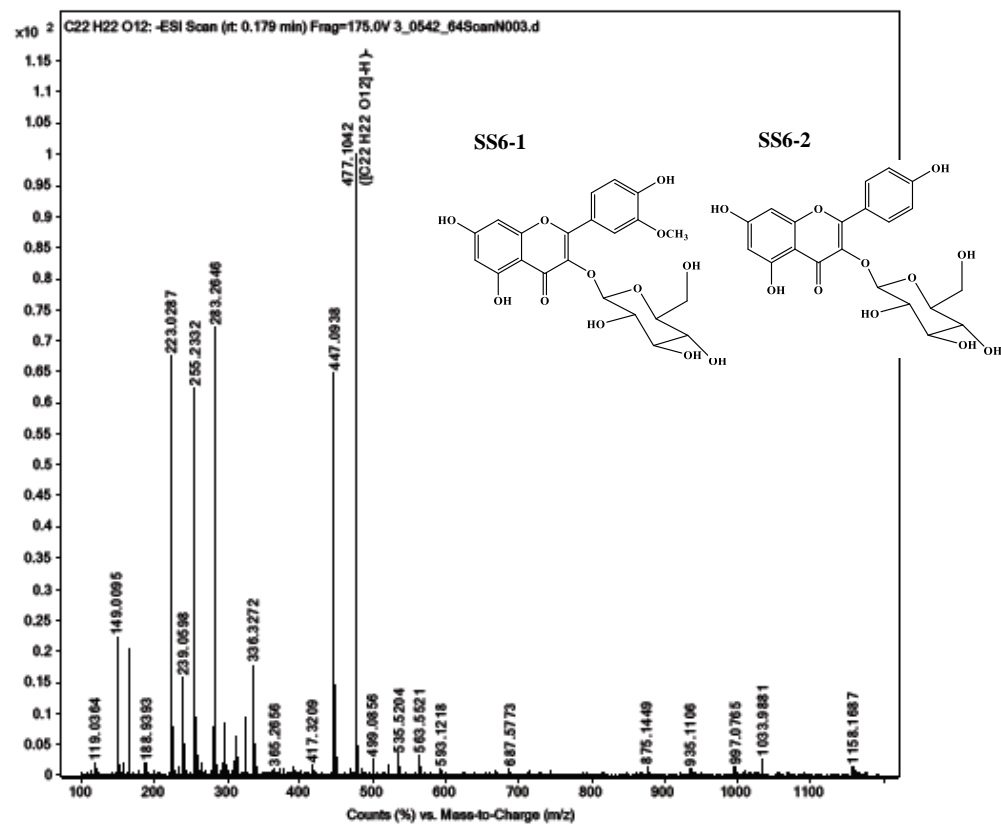
Appendix 31 HRESI-Mass spectrum of SS6
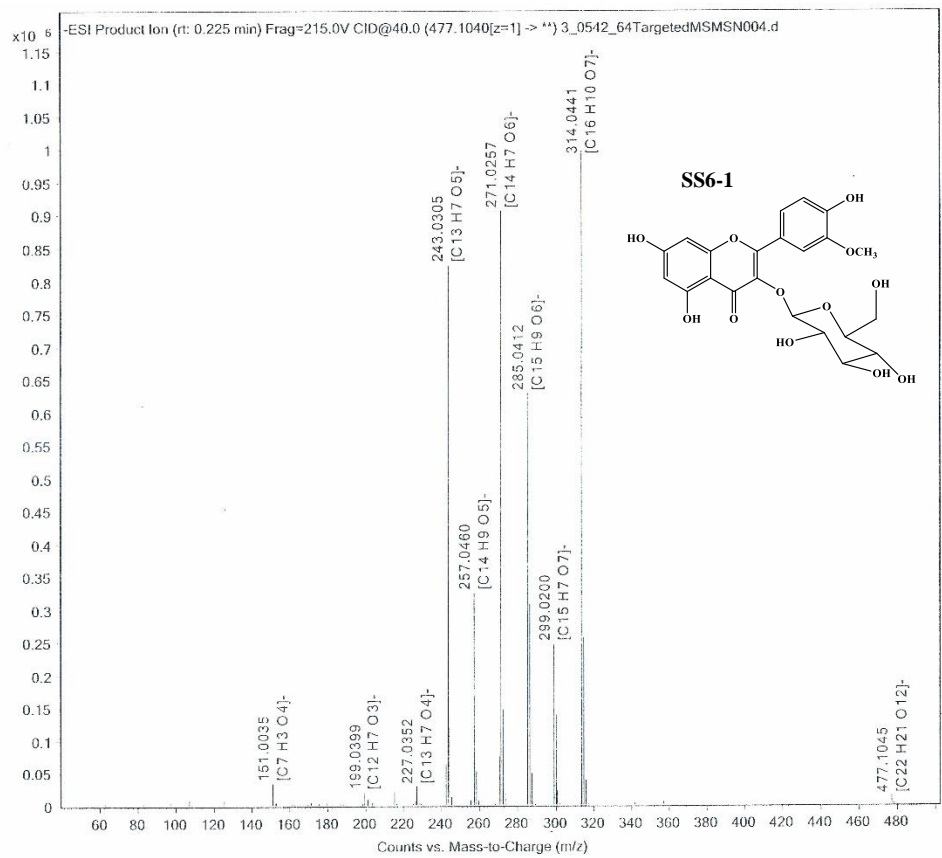
Appendix 32 Quasi-molecular ion fragments of HRESI-Mass spectrum of SS6-1
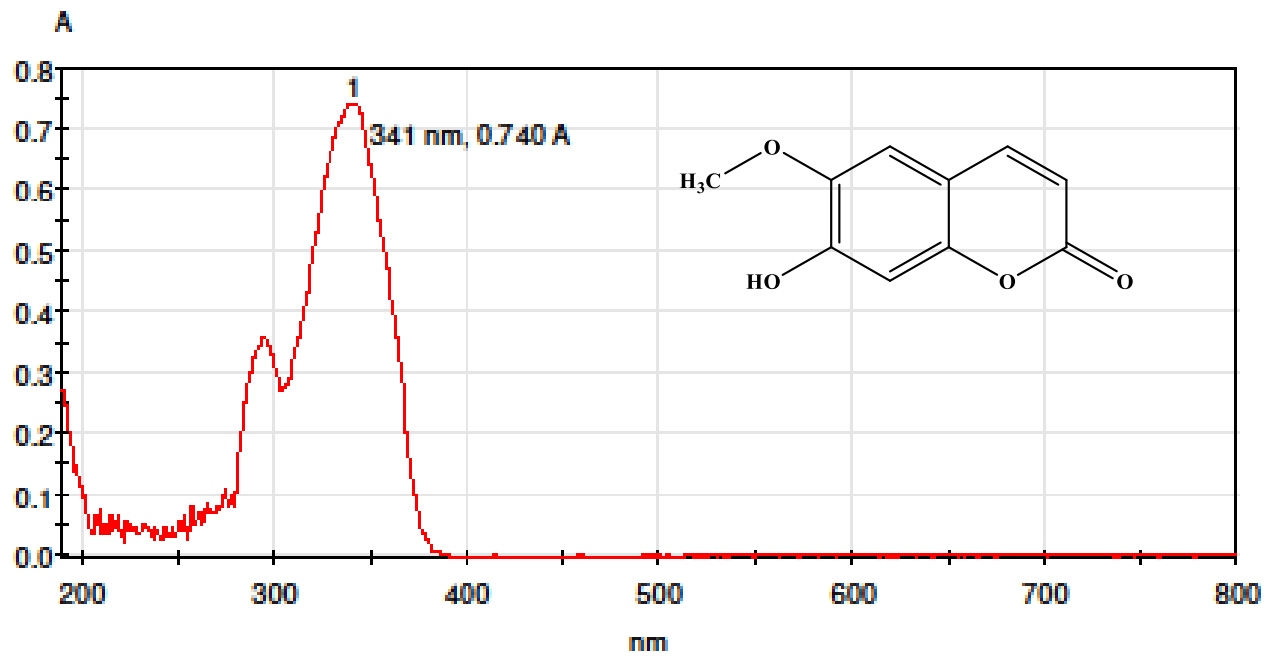
Appendix 33 UV-Visible spectrum of NR1 in chloroform
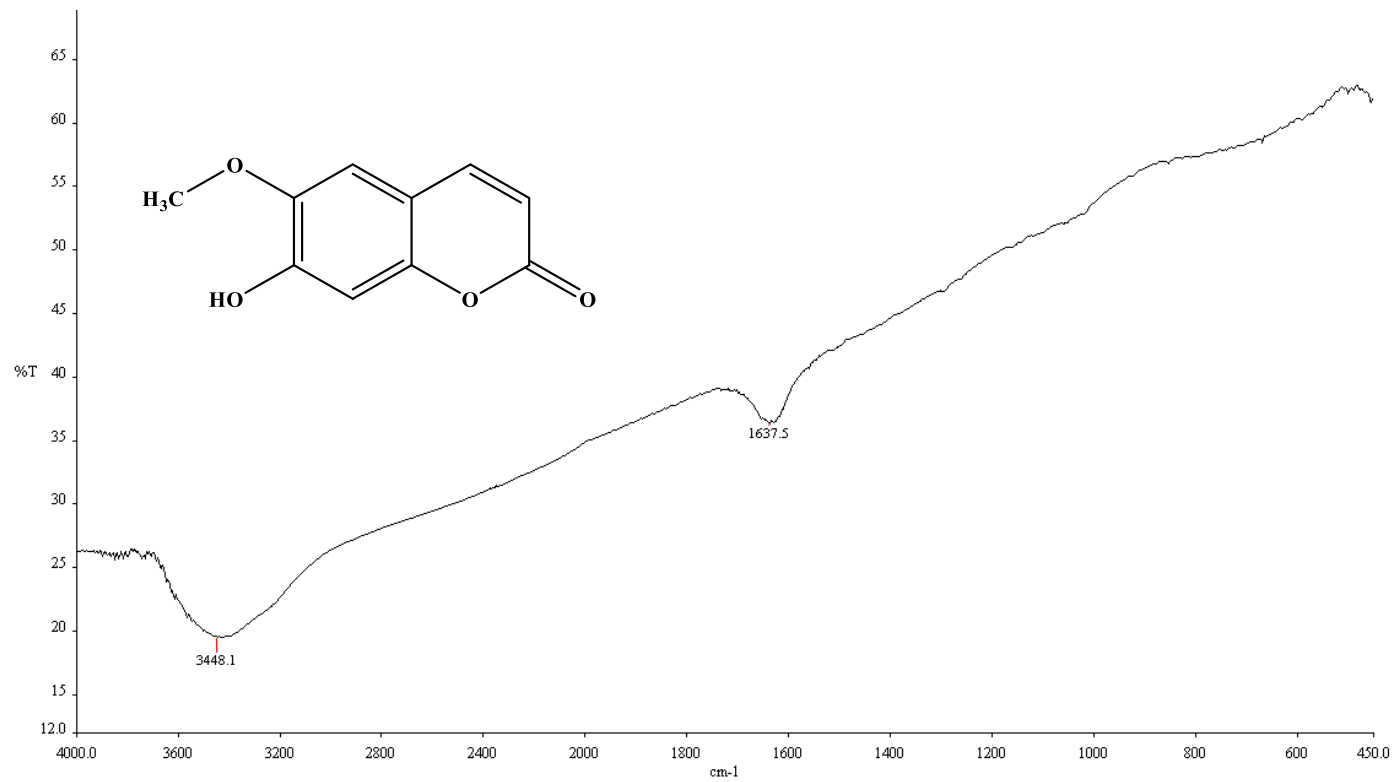
Appendix 34 IR spectrum of NR1 in chloroform
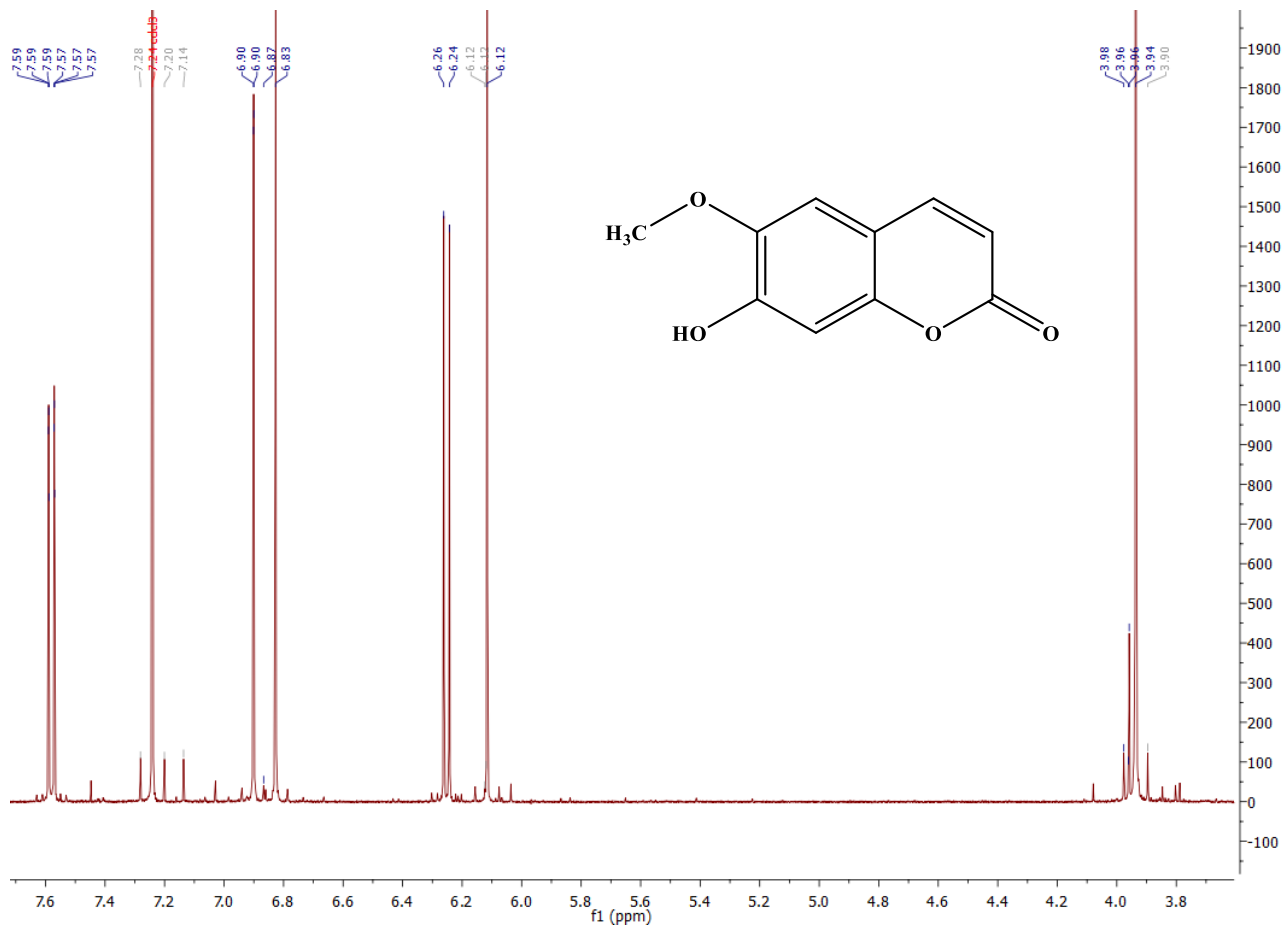
Appendix 35 ^{1}H NMR of NR1 (500 MHz in CDCl$_3$)
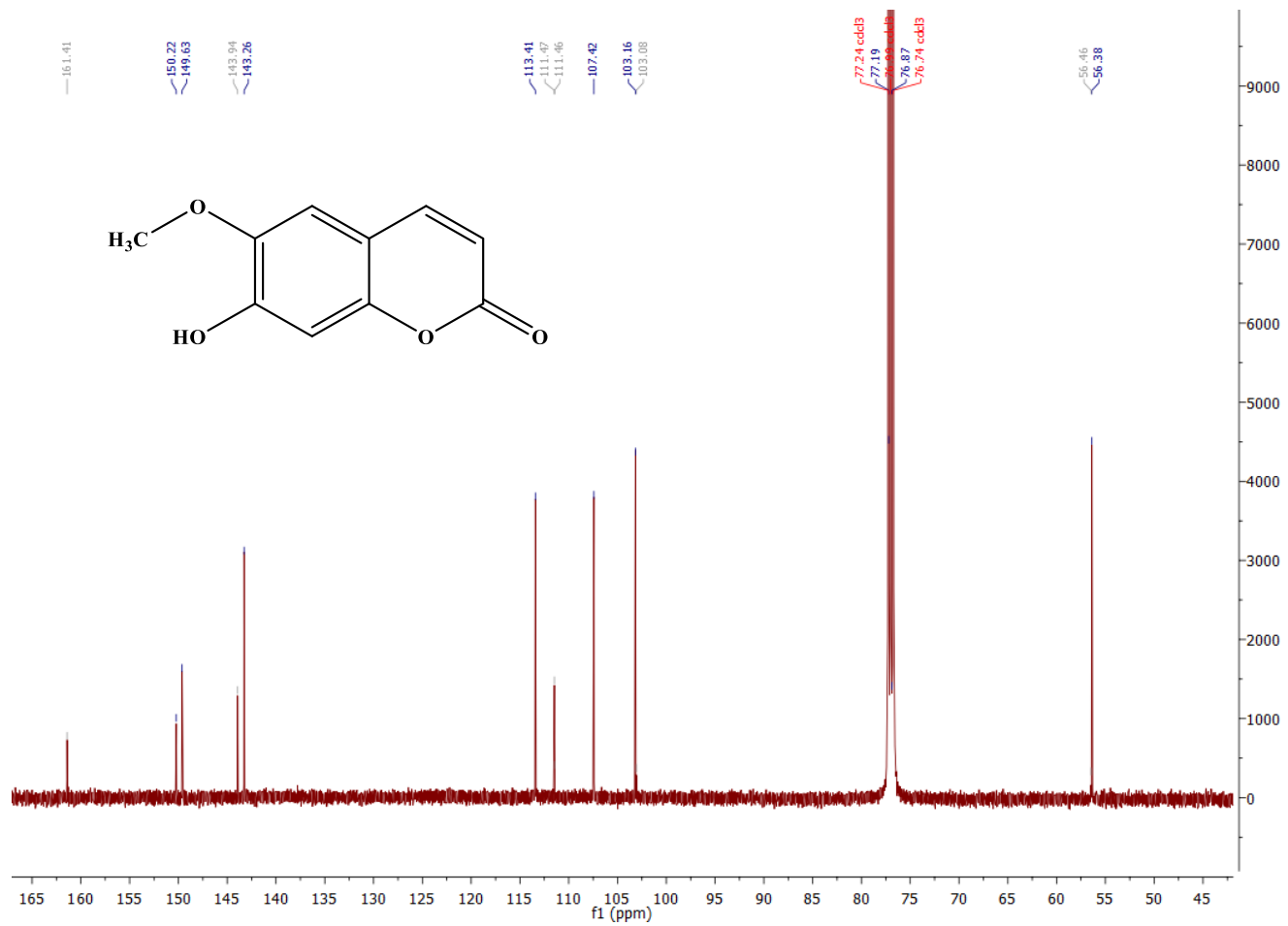
Appendix 36 ^{13}C NMR of NR1 (125 MHz in CDCl$_3$)
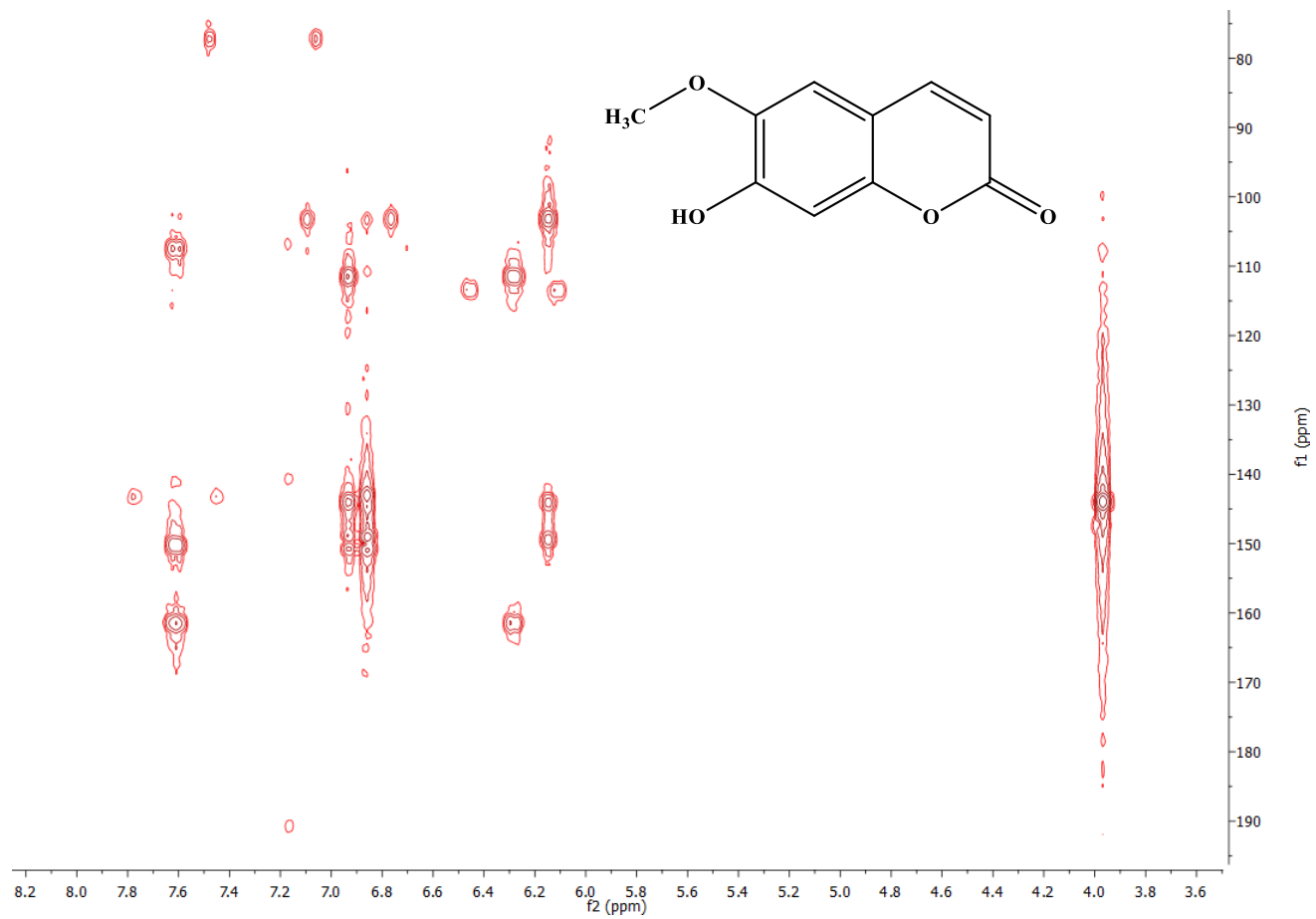
Appendix 37 HMBC of NR1 (500 MHz in CDCl₃)
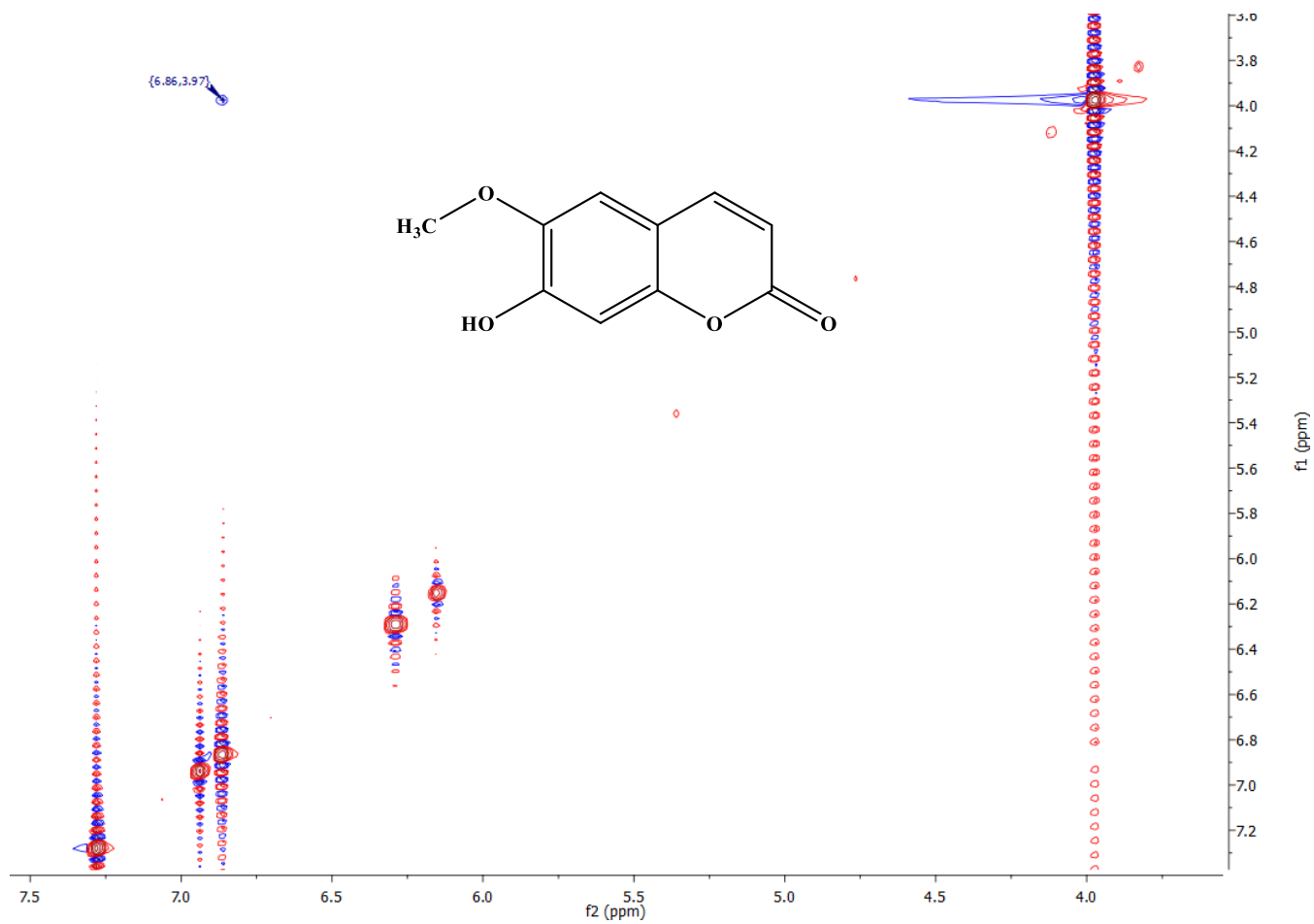
Appendix 38 NOESY of NR1 (500 MHz in CDCl₃)
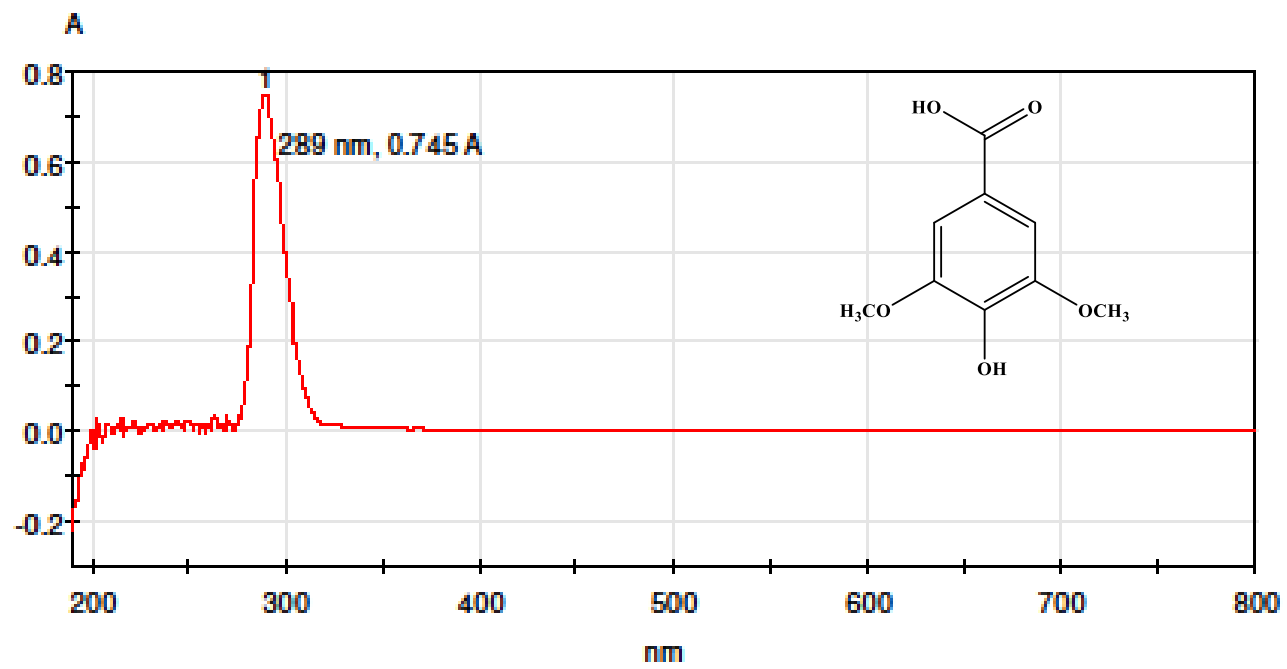
Appendix 39 UV-Visible spectrum of NR2 in methanol
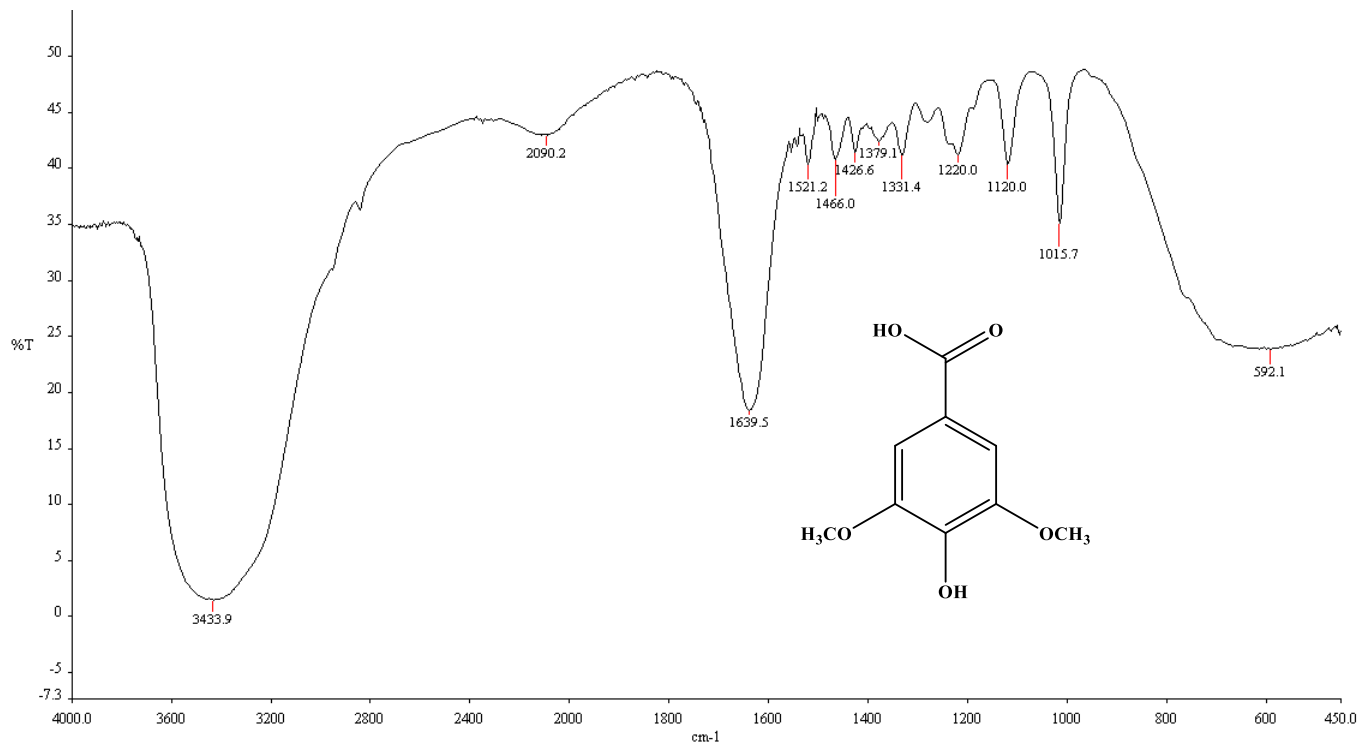
Appendix 40 IR spectrum of NR2 in methanol
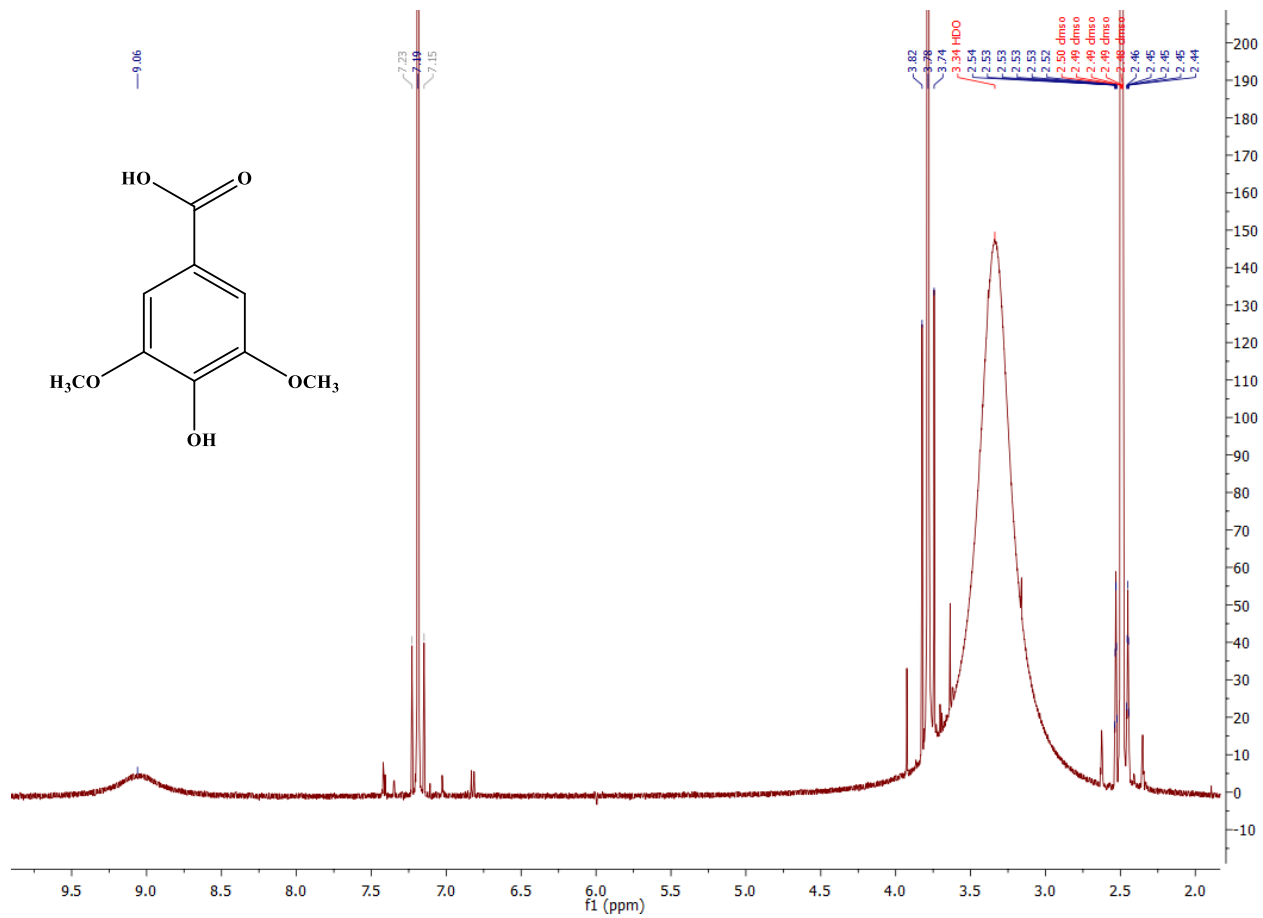
Appendix 41 ^{1}H NMR of NR2 (500 MHz in DMSO-d_6)
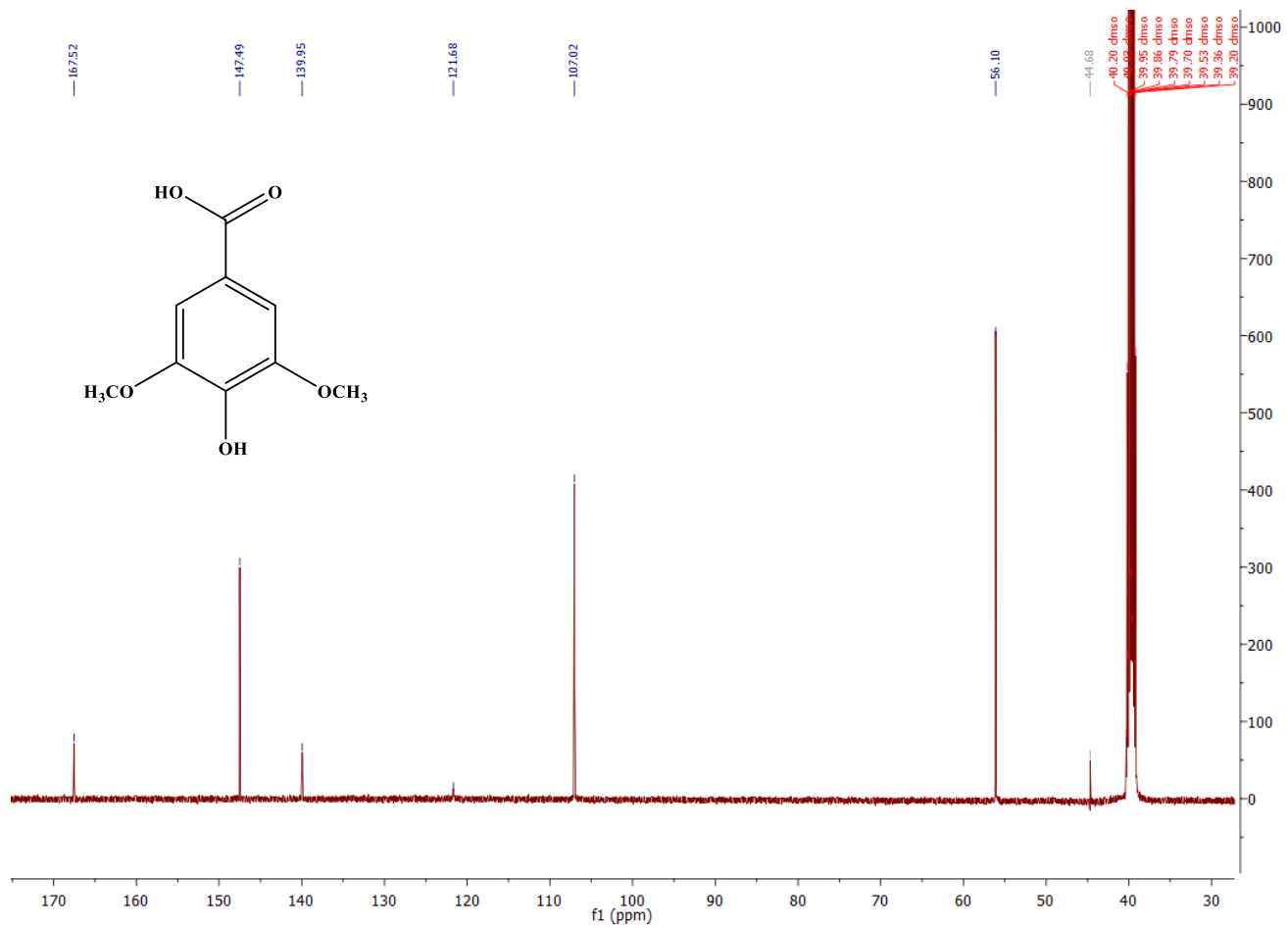
Appendix 42 ^{13}C NMR of NR2 (125 MHz in DMSO-d_6)
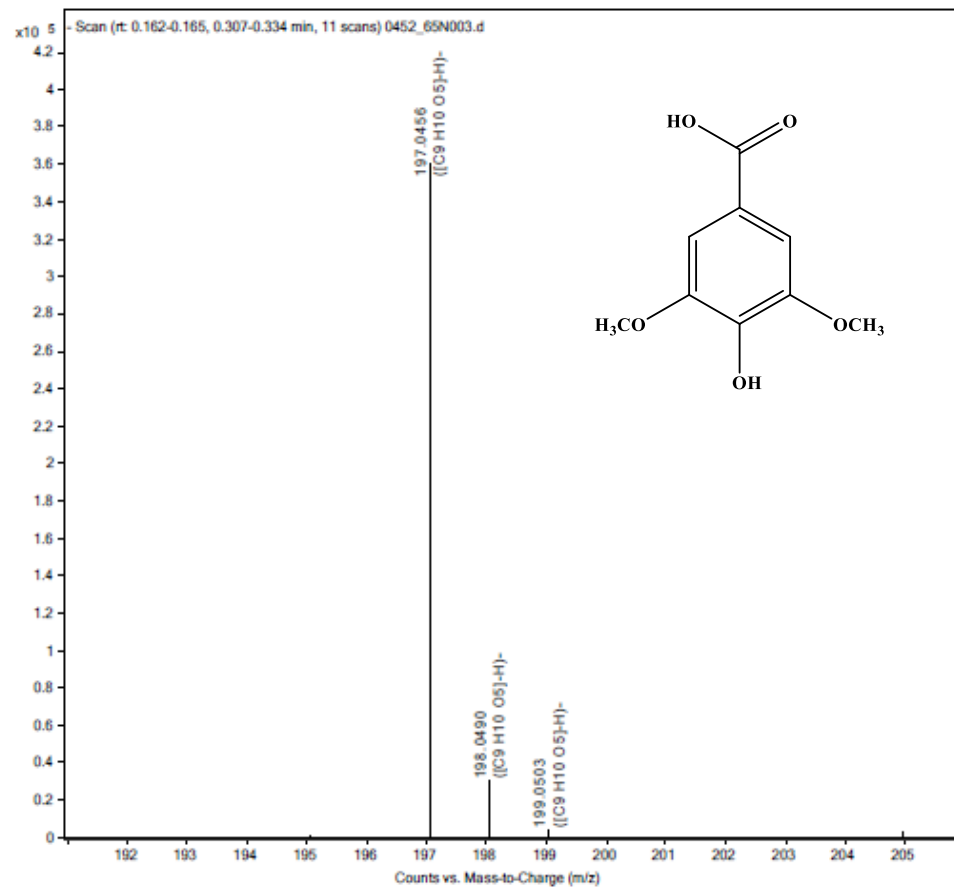
Appendix 43 HRESI-Mass spectrum of NR2
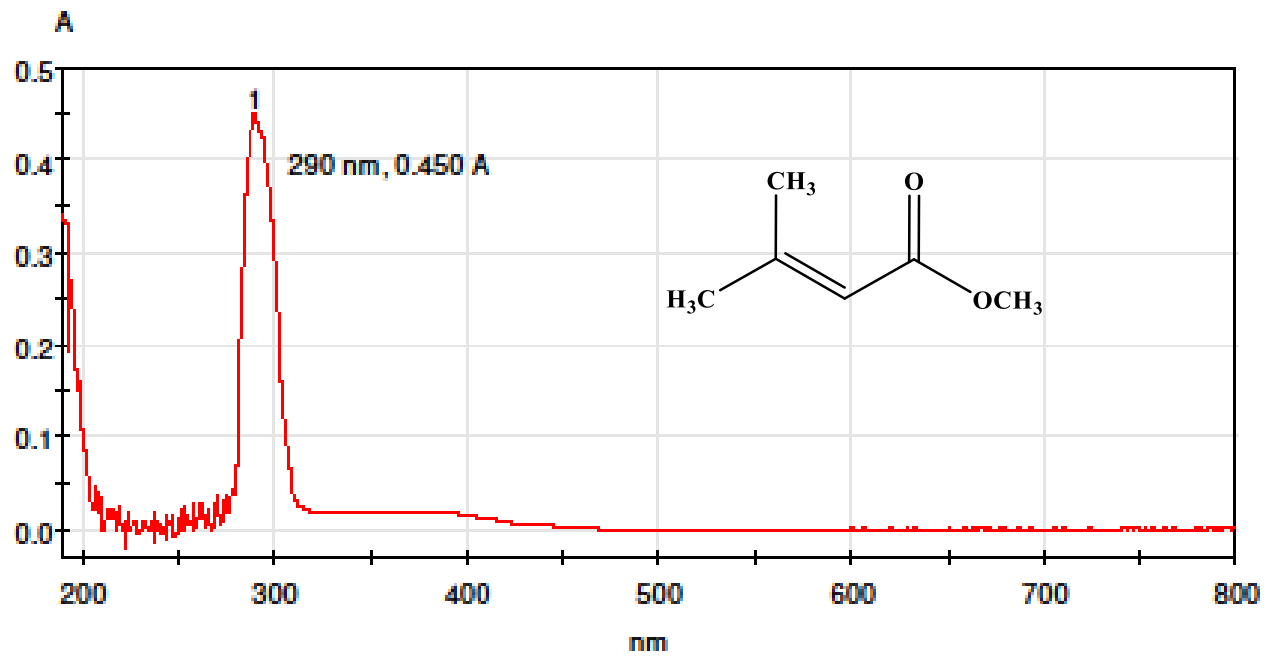
Appendix 44 UV-Visible spectrum of NR3 in chloroform
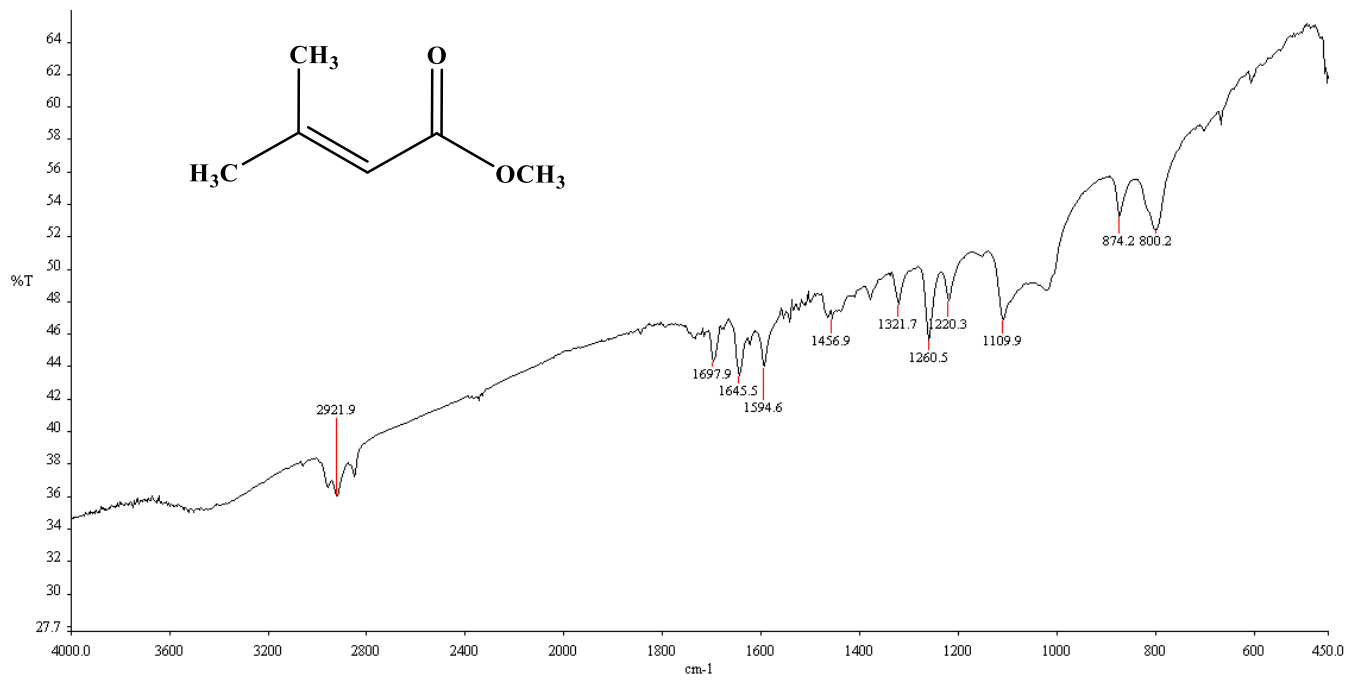
Appendix 45 IR-Visible spectrum of NR3 in chloroform
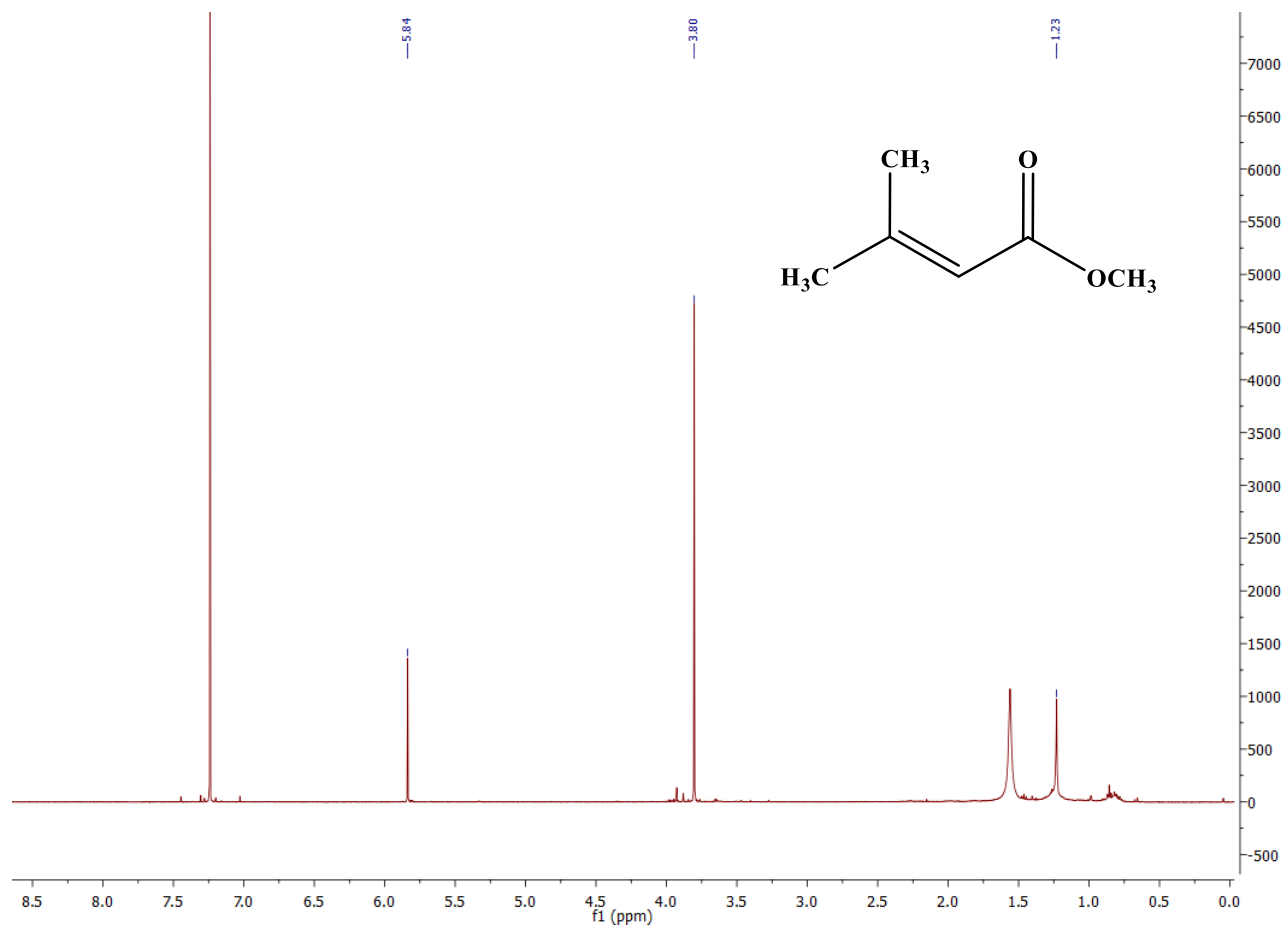
Appendix 46 ^{1}H NMR of NR3 (500 MHz in CDCl$_3$)
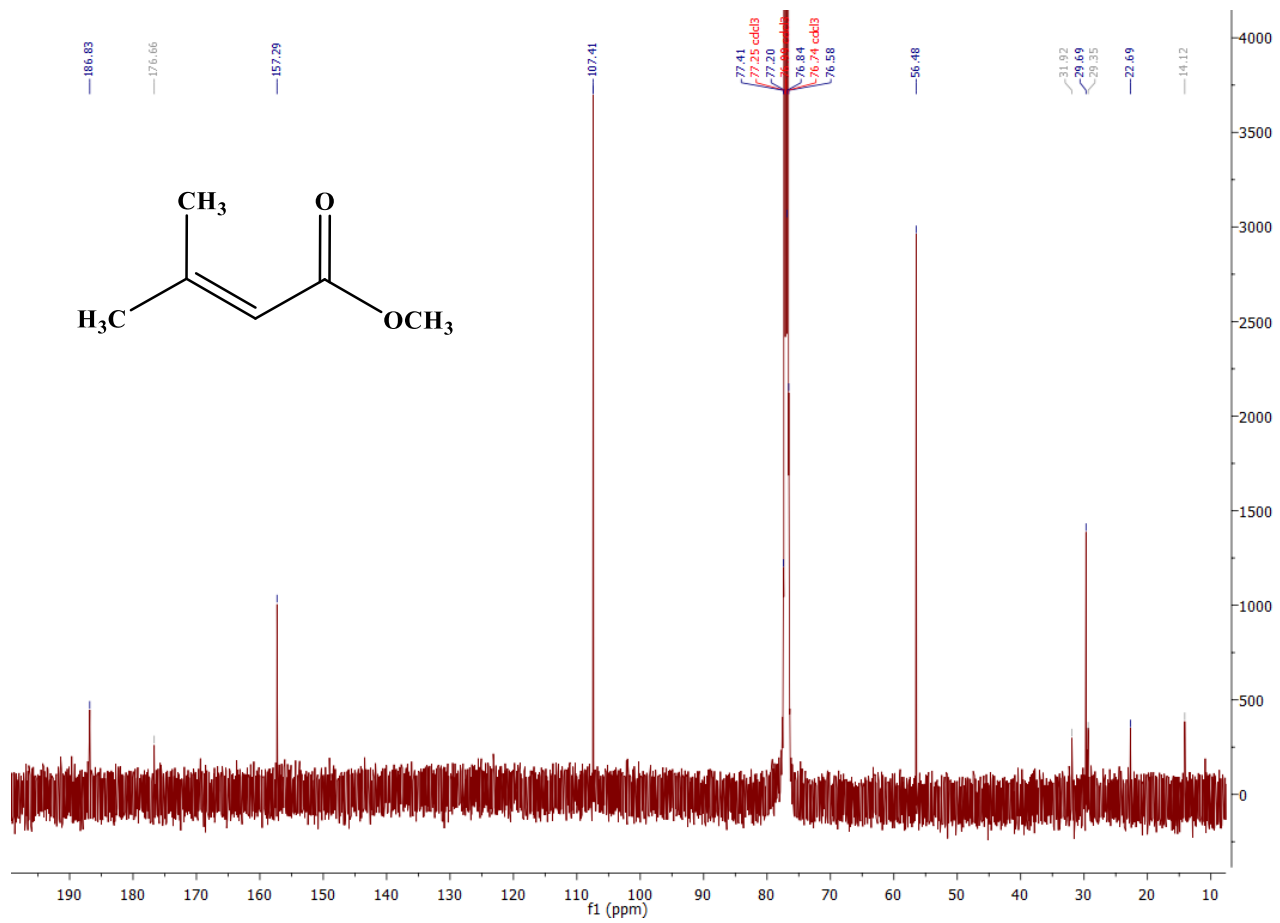
Appendix 47 ^{13}C NMR of NR3 (125 MHz in CDCl$_3$)
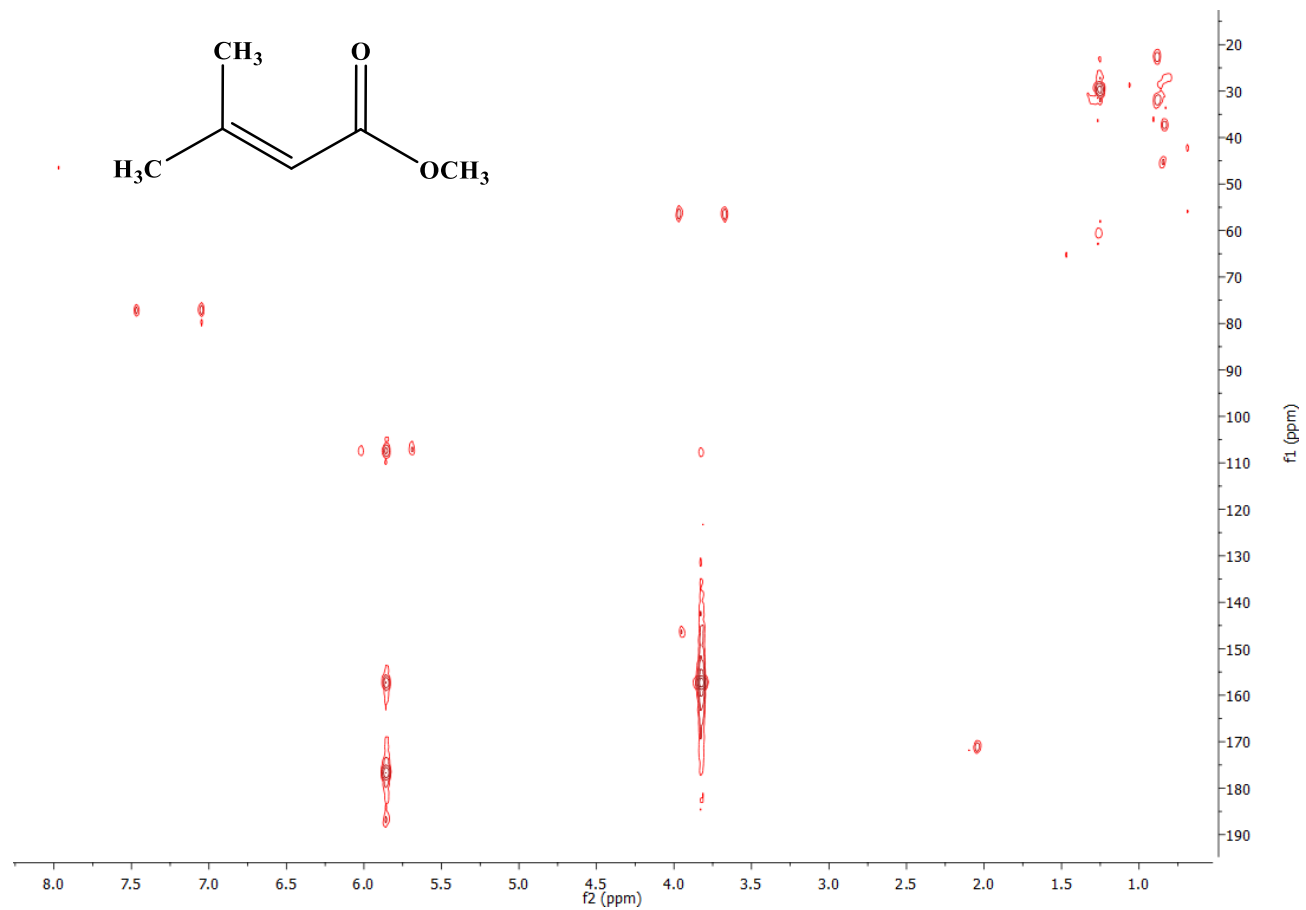
Appendix 48 HMBC of NR3 (500 MHz in CDCl₃)
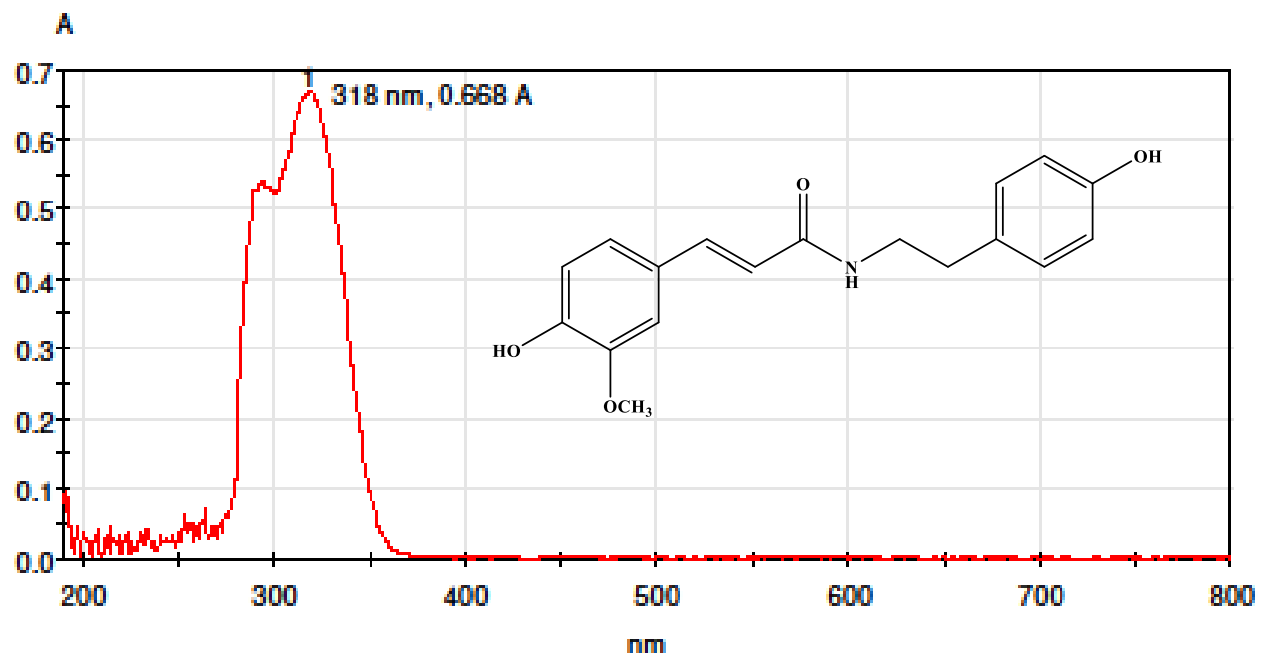
Appendix 49 UV-Visible spectrum of NR4 in methanol
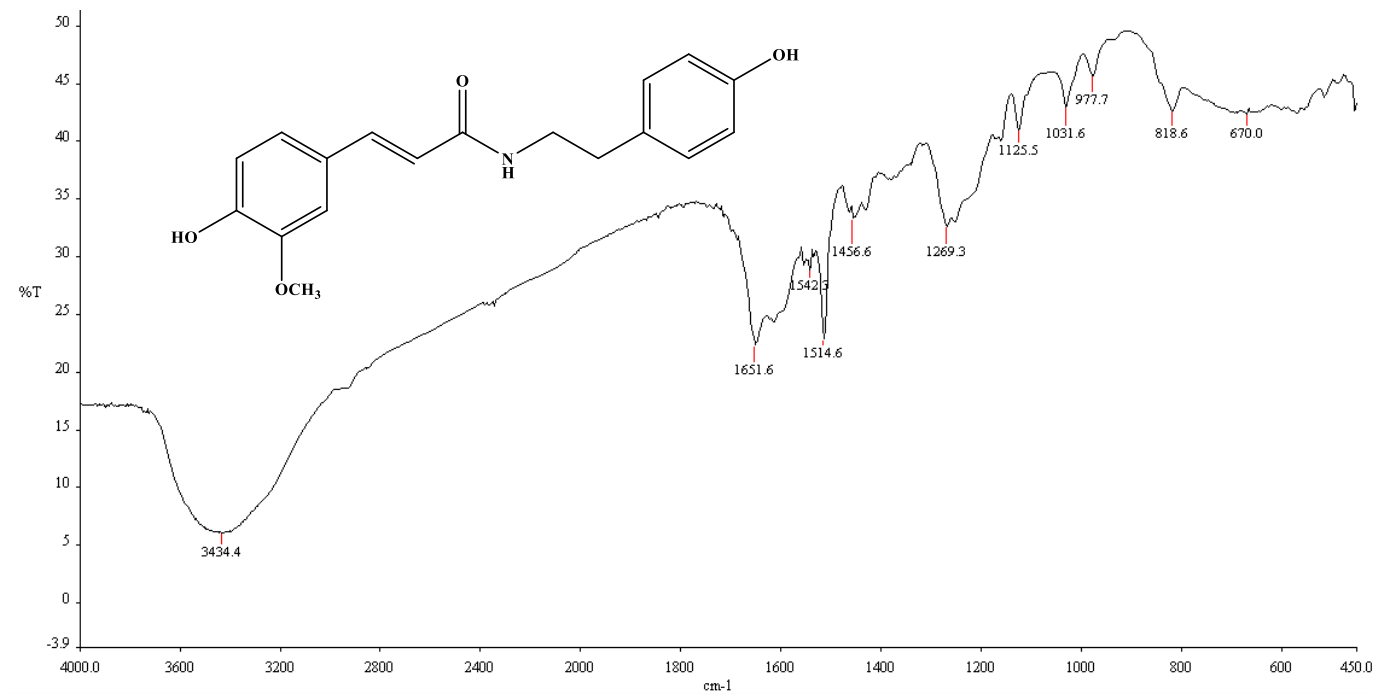
Appendix 50 IR spectrum of NR4 in methanol
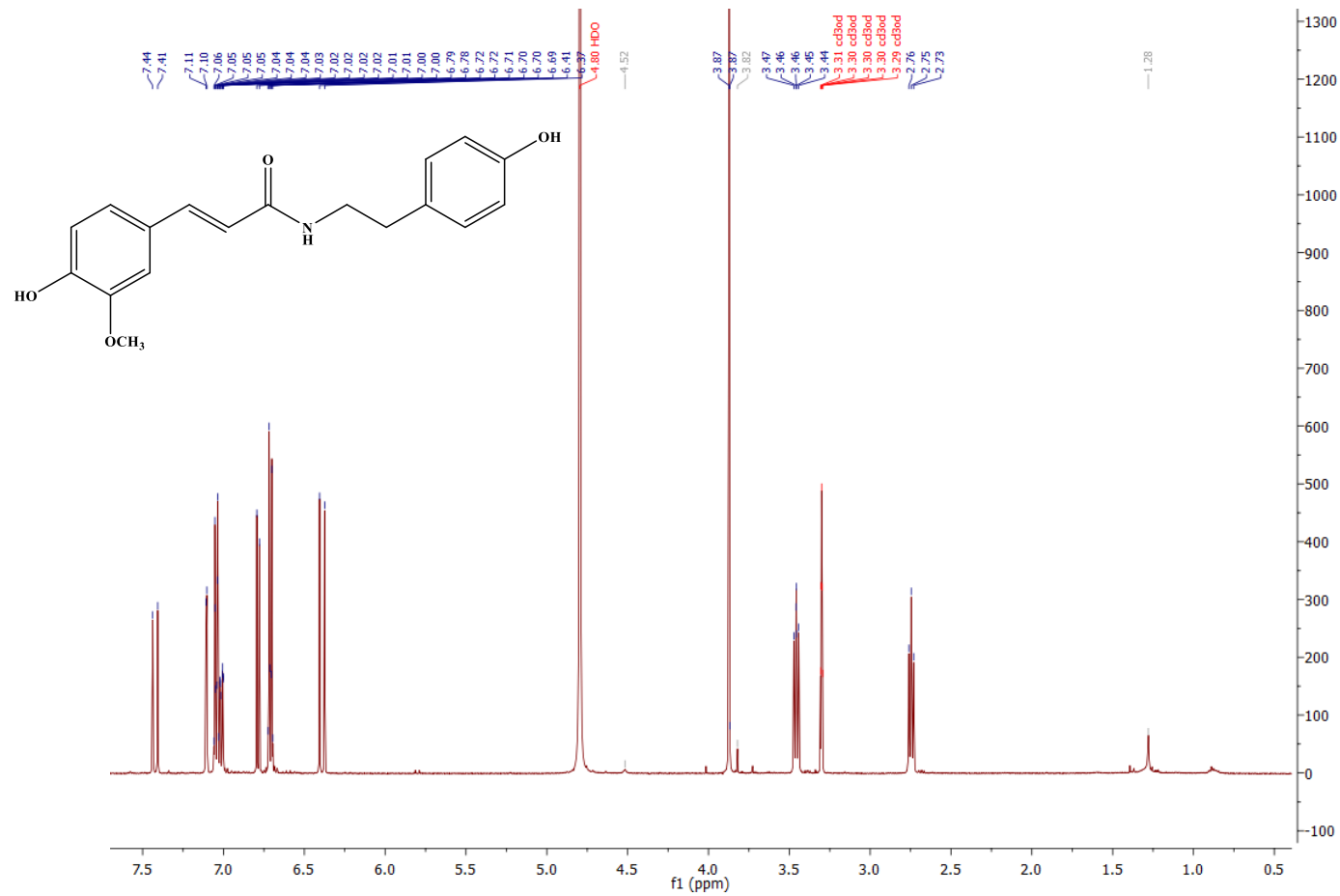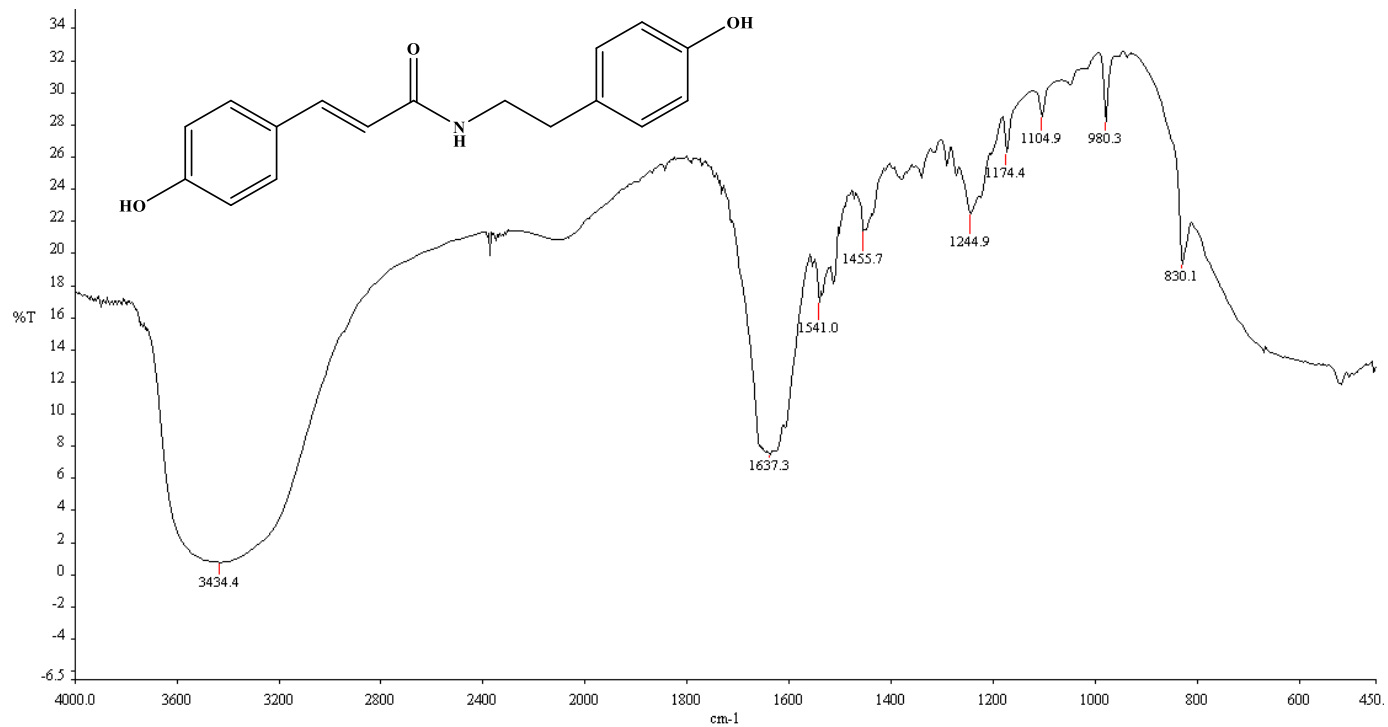
Appendix 51 ^{1}H NMR of NR4 (500 MHz in CD$_3$OD)
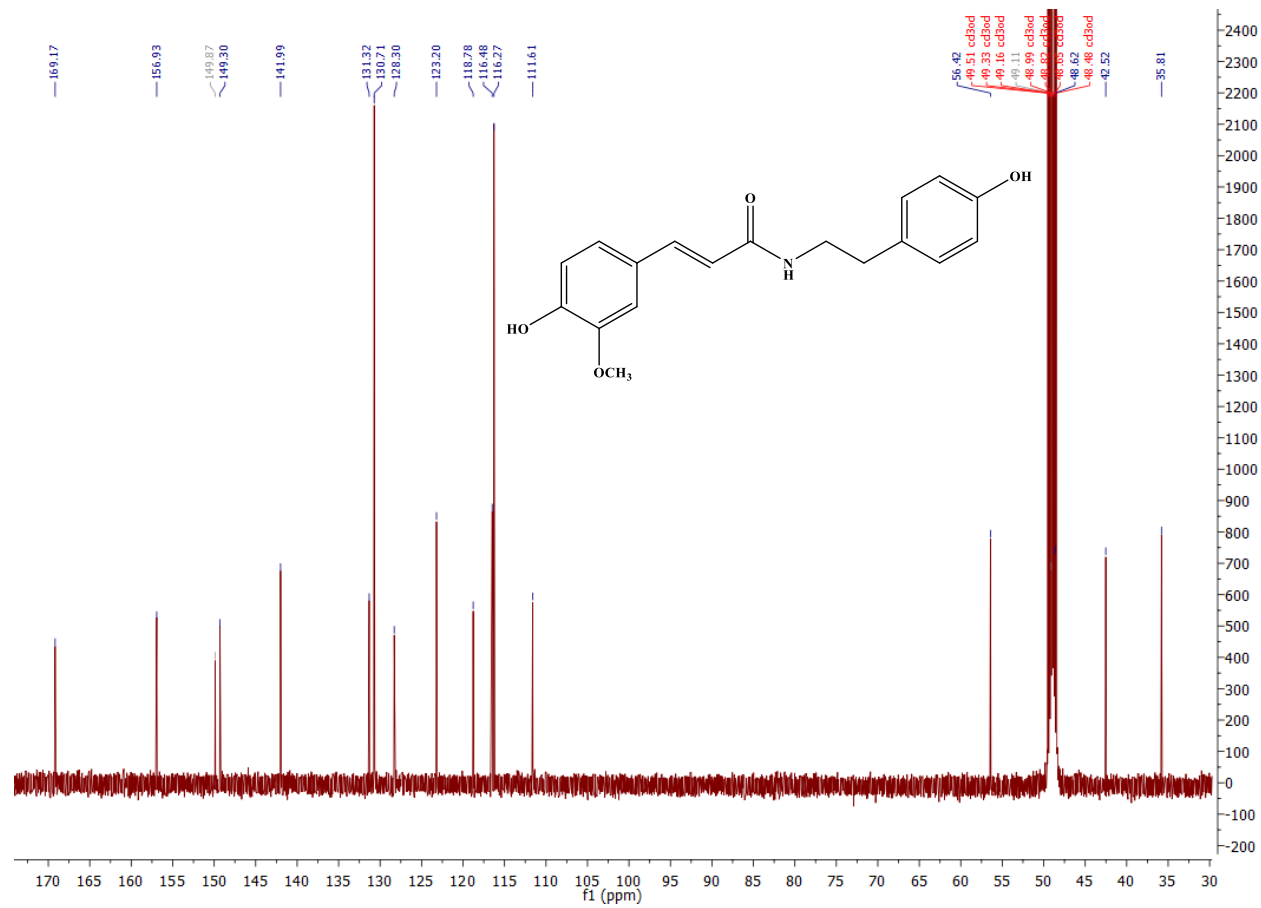
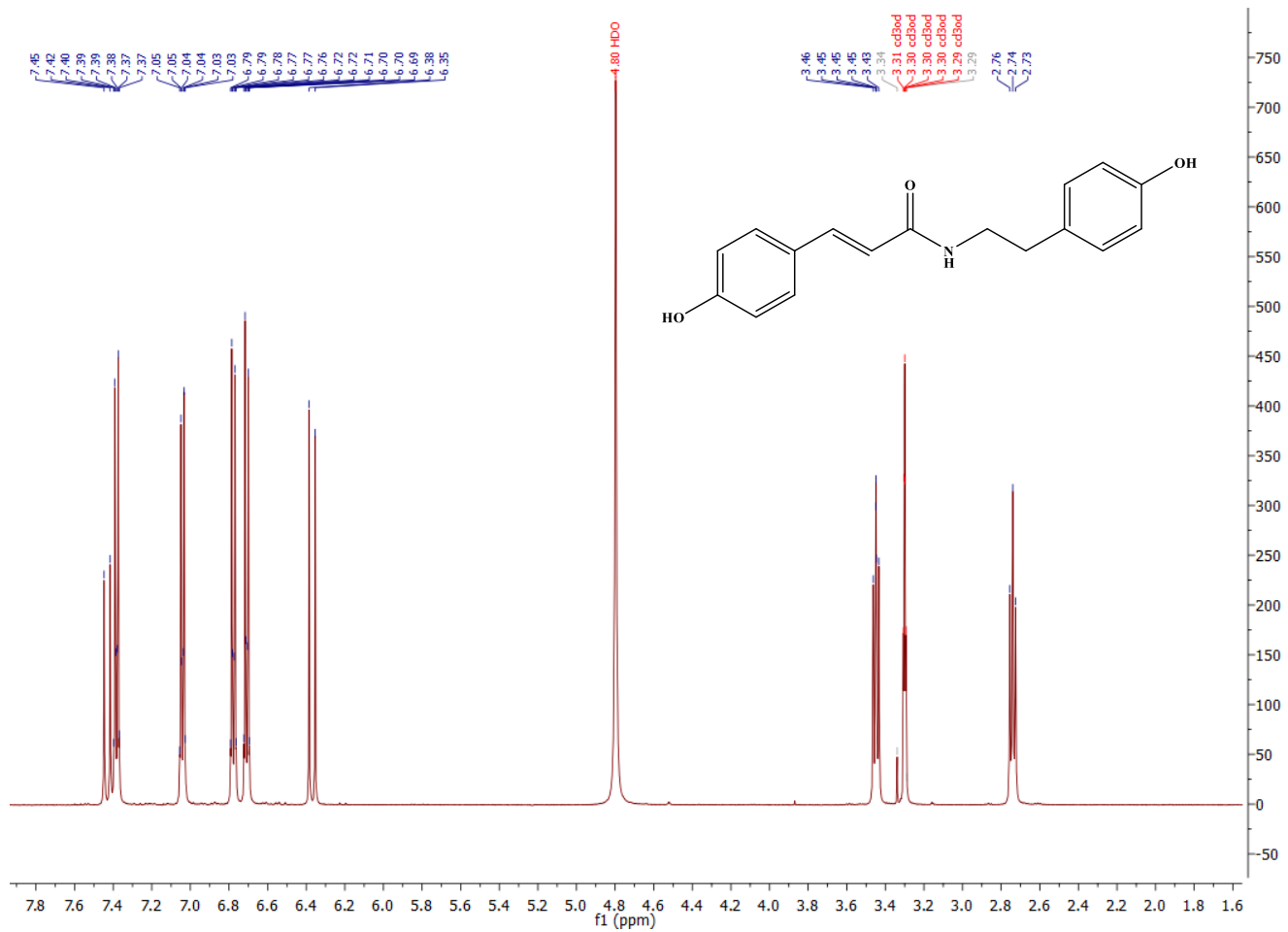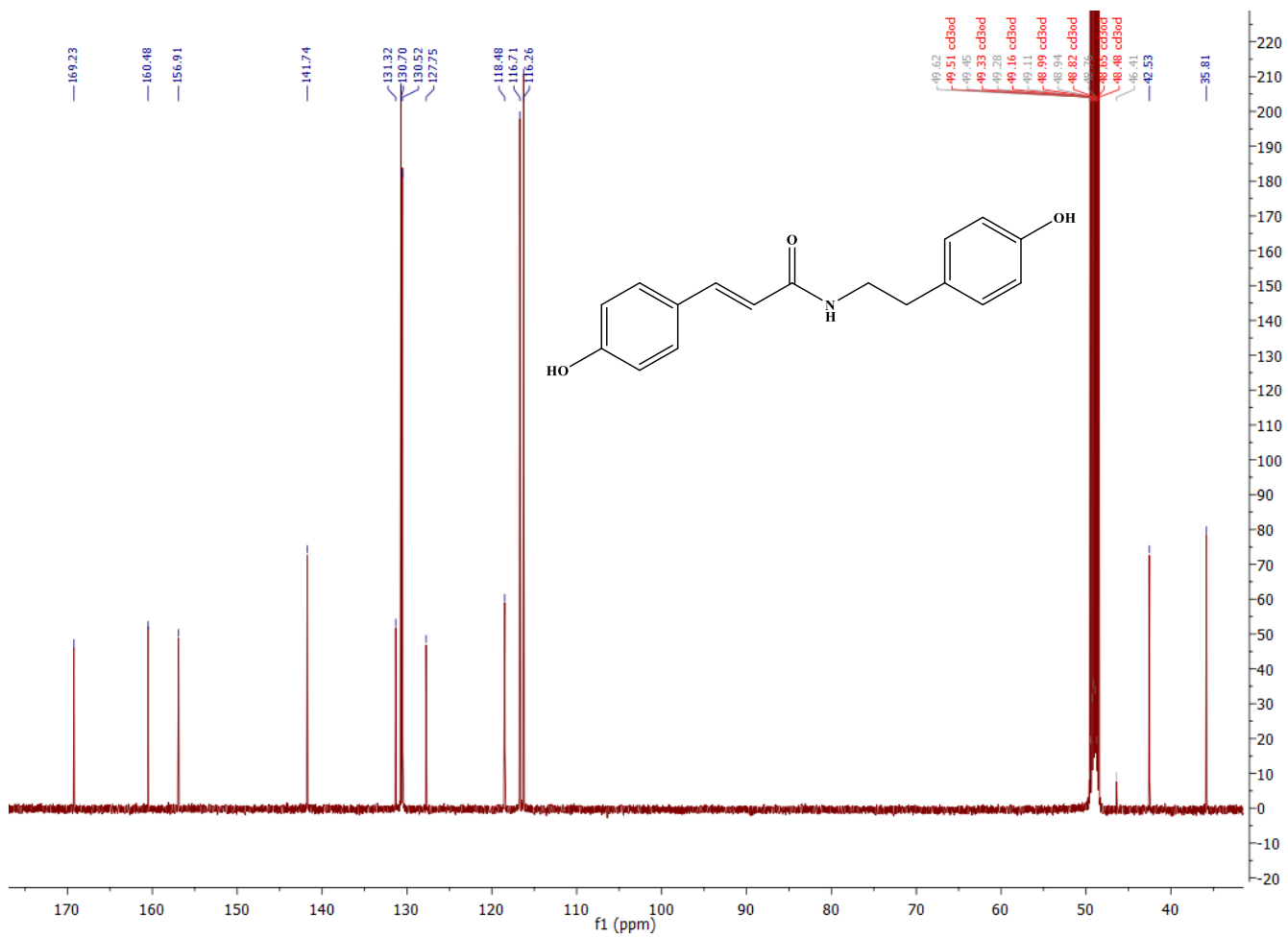**Appendix 52** ^{13}C NMR of NR4 (125 MHz in CD$_3$OD)
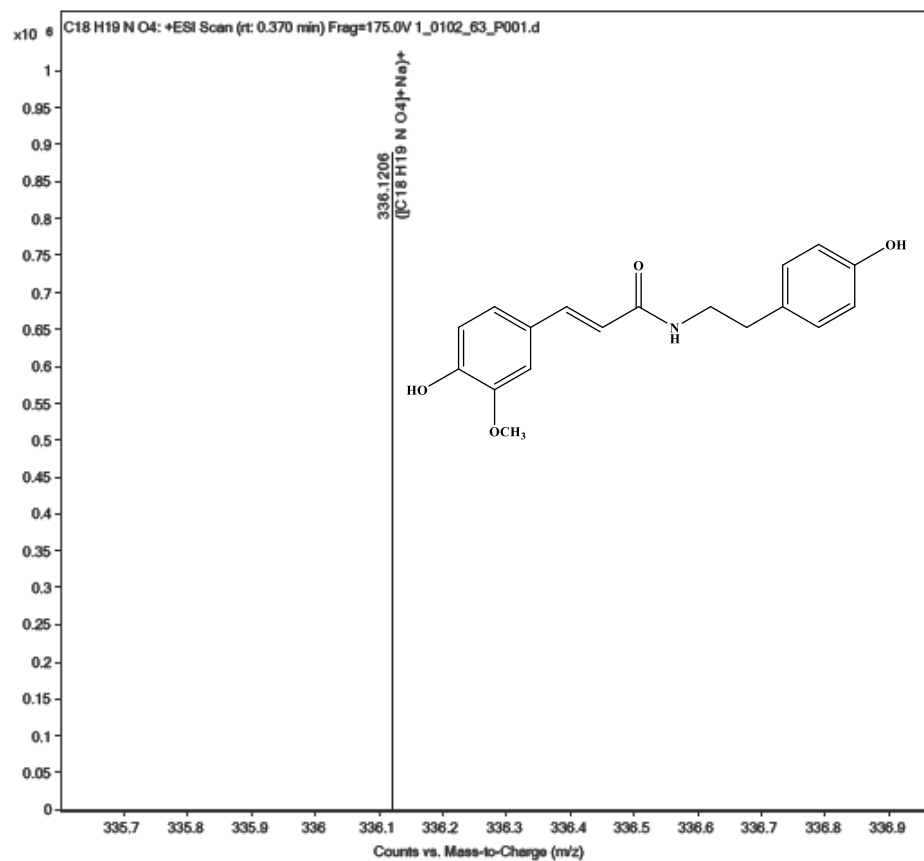
Appendix 53 HRESI-Mass spectrum of NR4
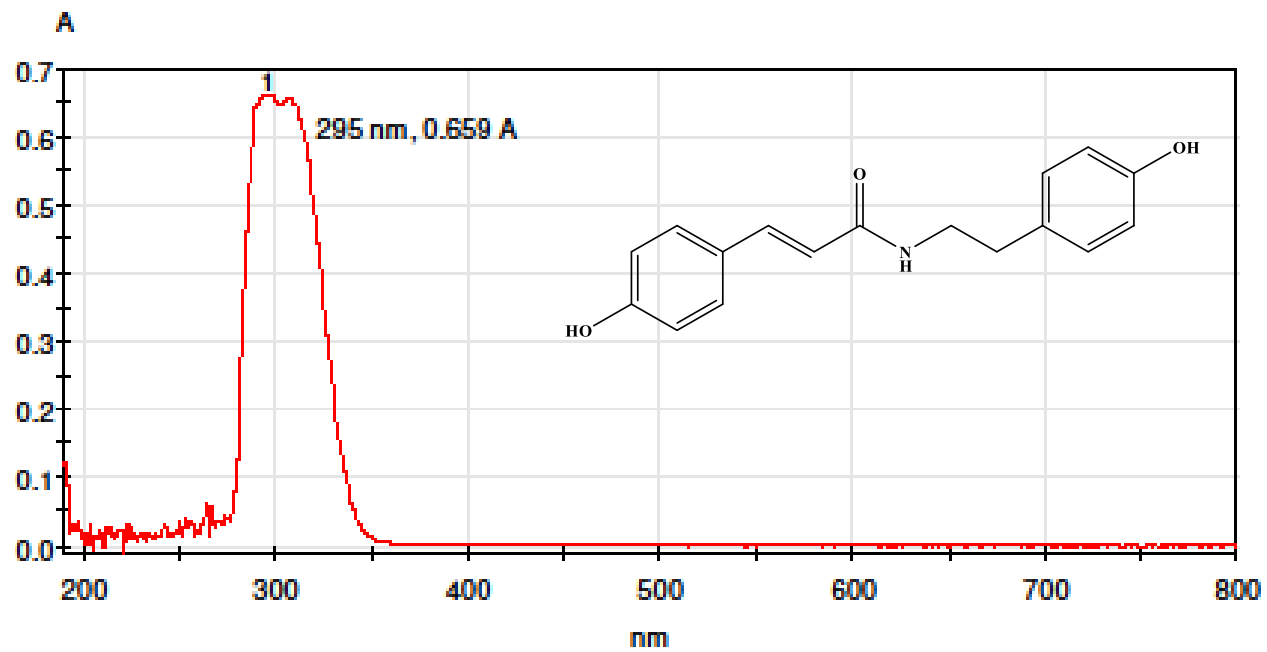
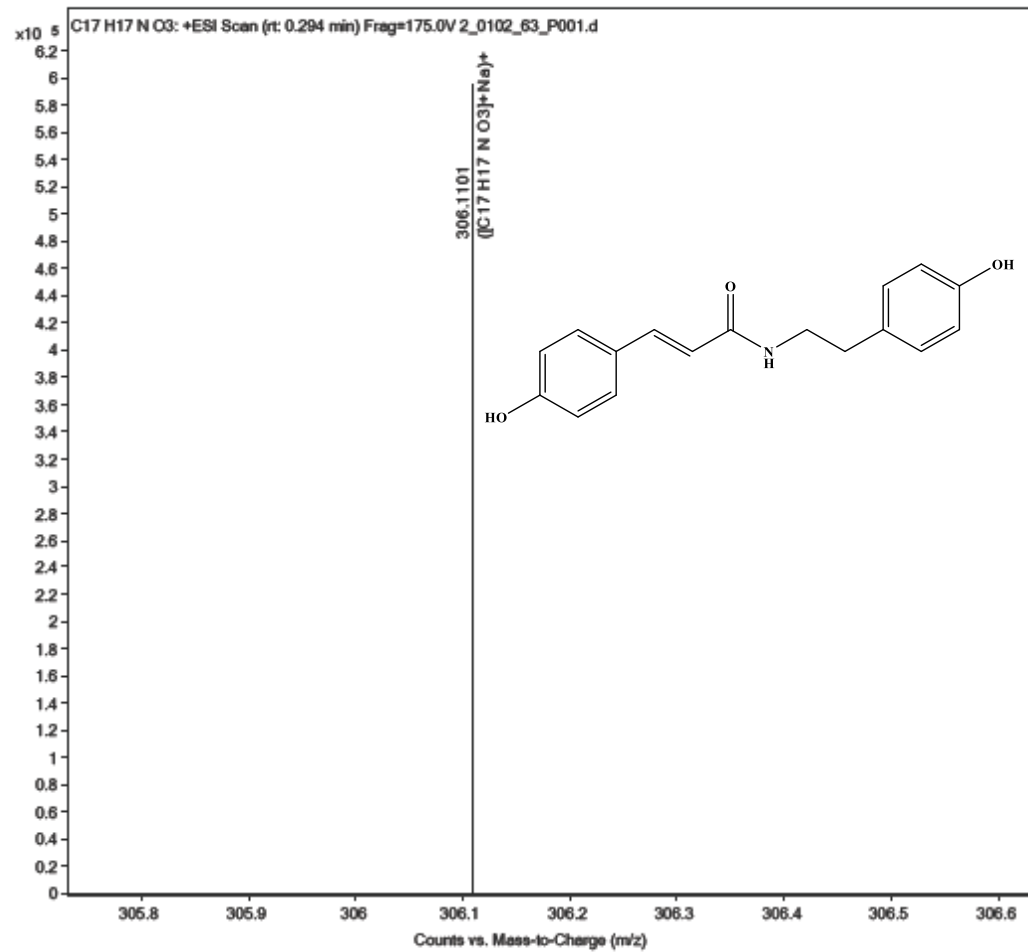**Appendix 54** UV-Visible spectrum of NR5 in methanol
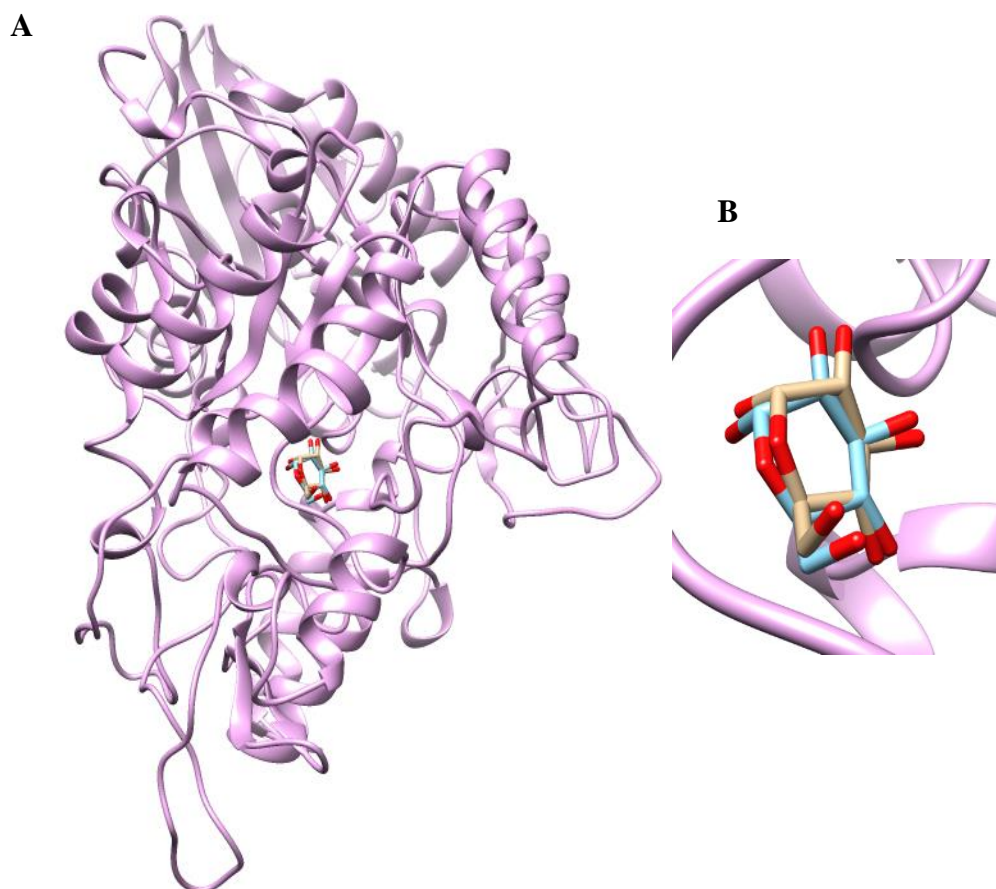
Appendix 55 IR spectrum of NR5 in methanol

Appendix 56 ^{1}H NMR of NR5 (500 MHz in CD$_3$OD)

Appendix 57 ^{13}C NMR of NR5 (125 MHz in CD$_3$OD)

C17 H17 N O3: +ESI Scan (rt: 0.294 min) Frag=175.0V 2_0102_63_P001.d

306.1101 ([C17 H17 N O3]+Na)+

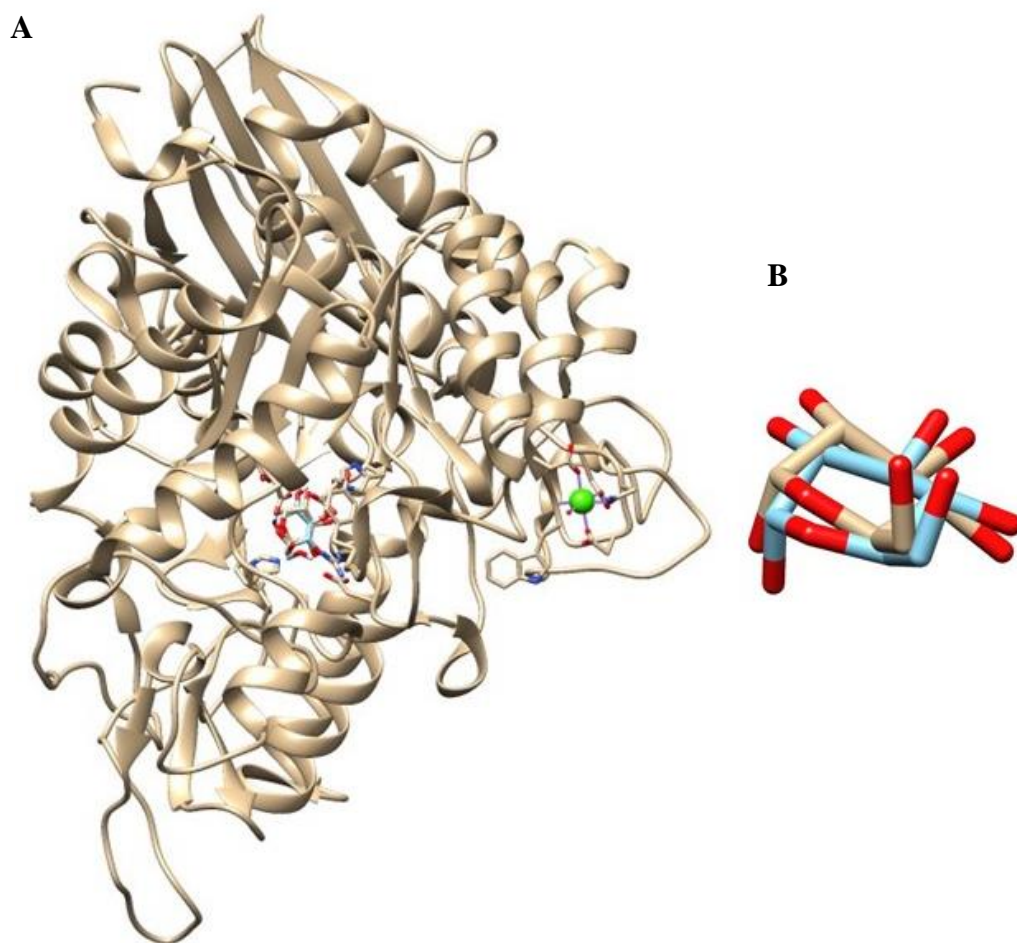Counts vs. Mass-to-Charge (m/z)

Appendix 58 HRESI-Mass spectrum of NR5

A

B

Appendix 59 A) The overlay structures between the native glucose molecule (brown color) and the redock glucose molecule (blue color) at the active site of the α-glucosidase

B) The expanded picture of two ligands, the native glucose molecule (brown color) and the redock glucose molecule (blue color), RMSD = 0.936 Å.

Appendix 60 A) The overlay structures between the native glucose molecule (brown color) and the redock glucose molecule (blue color) at the active site of the α-glucosidase

B) The expanded picture of two ligands, the native glucose molecule (brown color) and the redock glucose molecule (blue color), RMSD = 0.969 Å.

VITAE

Name   Miss Oraphan Sakulkeo

Student ID   6310730001

Educational Attainment

Degree	Name of Institution	Year of Graduation
Bachelor of Pharmacy	Prince of Songkla University	2005
Master of Pharmacy (Pharmaceutical Sciences)	Prince of Songkla University	2007

Scholarship Awards during Enrolment

2014-2016   Scholarship to Support Tuition Fees Discipline of Excellence in Pharmacy Project, Faculty of Pharmaceutical Sciences, Prince of Songkla University.

List of Publication and Proceeding

Sangnoi Y., Sakulkeo O., Yuenyongsawad S., Kanjana-opas A., Ingkaninan K., Plubrukarn A., Suwanborirux K. (2008). Acethylcholinesteres-inhibitory activity of pyrrole derivatives from a novel marine gliding bacterium, *Rapidithirix thailandica*. *Marine Drug. 6*(4), 578-586.

Saeteng S., Sirimahachai P., Rattanaburee P., Jerevilapong S., Sukdang Sukdang K., Ritthong C., Unsiam B., Jarenvilapong P., Sakulkeo O., Subhadhirasakul S. (2010). Standardization of *Piper nigrum* and *Zingiber officinale* from Traditional Thai Drug Store in Hatyai, Songkhla. *Thaksin University Journal. 13*(1), 11-19.

Bakasatae N., Yapa N., Issalamikkun V., Issarachote P., Sakulkeo O., Joycharat N. (2019). Microscopical characters, total phenolic content, and anti oxidant activity of *Albizia myriophylla* Benth. *KKU Science Journal. 47*(1), 69-80.

Ritdet P., Masthong R., Limsuwan S., Sakulkeo O., Joycharat N. (2020). Physical and chemical stability of glycerin formulations containing extracts from *Albizia myriophylla* and Cha-Em-Thang Song. *Isan Journal of Pharmaceutical Sciences. 16*(2), 46-56.

Sakulkeo O., Wattanapiromsakul C.,Pitakbut T., Dej-Adisai S. (2022). Alpha-glucosidase inhibition and molecular docking of isolated compounds from traditional Thai medicinal plant, *Neuropeltis racemosa* Wall. *Molecules. 27*(3), 639.

Saising J., Maneenoon K, Sakulkeo O., Limsuwan S., Götz F., Voravuthikunchai S.P. (2022). Ethnomedicinal plants in herbal remedies used for treatment of skin diseases by traditional healers in Songkhla province, Thailand. *Plants. 11*(7), 880.